Development of Thermally Stable and Moisture Responsive CO_2-Selective Carboxymethyl Chitosan Based Membrane

A Thesis

Submitted in Partial

Fulfilments of the Requirements for the Degree of

DOCTOR OF PHILOSOPHY

by

Rajashree Borgohain

(Roll No.: 146107016)

Department of Chemical Engineering

Indian Institute of Technology Guwahati

Guwahati, Assam 781039

March 2020

Dedicated

To

My Parents and My Mentor

Department of Chemical Engineering
Indian Institute of Technology Guwahati
Guwahati, Assam 781039

STATEMENT

I hereby declare that the content embodied in this thesis entitled "**Development of Thermally Stable and Moisture Responsive CO_2-Selective Carboxymethyl Chitosan Based Membrane**" is the result of investigations carried out by me at the Department of Chemical Engineering, Indian Institute of Technology Guwahati, India, under the guidance of Prof. Bishnupada Mandal. In keeping with the general practice of reporting scientific observations, due acknowledgements have been made wherever the work described is based on the findings of other investigators.

March, 2020 Rajashree Borgohain

Department of Chemical Engineering
Indian Institute of Technology Guwahati
Guwahati, Assam 781039

CERTIFICATE

It is certified that the work described in this thesis, entitled "**Development of Thermally Stable and Moisture Responsive CO_2-Selective Carboxymethyl Chitosan Based Membrane**", done by **Ms. Rajashree Borgohain** (Roll No. 146107016) for the award of degree of Doctor of Philosophy is an authentic record of the results obtained from the research work carried out under my supervision in the Department of Chemical Engineering, Indian Institute of Technology Guwahati, India and this work has not been submitted elsewhere for the award of any other degree or diploma.

This thesis in my opinion, has reached the standard fulfilling the requirements for the award of the degree of Doctor of Philosophy in accordance with the regulations of the institute.

March, 2020

(**Prof. Bishnupada Mandal**)
Professor
Department of Chemical Engineering
Indian Institute of Technology Guwahati
Guwahati 781039, India

ACKNOWLEDGEMENTS

This thesis becomes a reality with the kind support and help of many individuals. It is a genuine pleasure to express my deep sense of thanks and gratitude to them who helped me in the completion of this thesis.

Foremost, I would like to express my sincere thanks to my thesis supervisor ***Prof. Bishnupada Mandal*** *for the continuous support in various stages of my research journey. He provided me an excellent atmosphere to work with freedom of thinking and execution which grew my interest towards the topic. Also, his positive attitude and encouragement helped me to perform and complete the research objectives. His support in doing the experiments, analysis of the data and preparing the manuscripts are invaluable. I am fortunate enough to complete my thesis under his supervision. It has really been a notable working experience with him.*

I would like to extend my sincere gratitude to my doctoral committee chairman ***Prof. G. Pugazhenthi,*** *Department of Chemical Engineering, for his valuable suggestions, evaluation and proper direction during my annual progress seminars. I shall always be obliged to other doctoral committee members,* ***Prof. Chandan das,*** *Department of Chemical Engineering and* ***Dr. Lalmohan Kundu,*** *Department of Chemistry, for their valuable suggestions, time and efforts.*

I am deeply indebted to the ***thesis examiners*** *for their valuable suggestions to improve the quality of the thesis.*

I would like to acknowledge all the centres for providing me various instrument facilities required for characterization during the research work carried out at IIT Guwahati specifically, Analytical Lab Facility (Department of Chemical Engineering), Centre of Excellence for Sustainable Polymers (CoE-SusPol), Central Instrument Facility (CIF), Department of Chemistry for NMR facility and Centre for Nanotechnology for AFM analysis.

Further, I would like to acknowledge North East Institute of Science and Technology, Jorhat, for providing the XPS facility required for the thesis work. Also, I shall be always grateful to Yantrabot Technologies Pvt. Ltd. for helping me in the illustration of the experimental set up.

*I am also grateful to all the **staff and faculty members** of the Department of Chemical Engineering for helping and providing me the necessary facilities.*

*I would like to thank all my **seniors** (Dr. Babul Prasad, Satyannarayan Edubilli, Dr. Sharbani Kaushik**)**, **Colleagues (**Baite, Pradip, Sailesh, Himali, Debarati, Sikha, Mridusmita, Saptarshi, Ramesh, Barnali, Arun, Ankur, Purnima, Lokesh, Hemanta, Geetanjali, Gourhari, Debashish**)**, **friends (**Dharitri, Arun, Ayushman, Chiranjib, Hilly**)** and other **well-wishers** who helped me to complete my research.*

*My final words go to my family whom I want to thank for showering their love, care, sacrifices and encouragement. I am greatly indebted to my **Maa-Deuta** and **Pranjal** whose support made it possible for me to come so far.*

Rajashree Borgohain

Contents

Abstract i

List of Figures iii

List of Tables Viii

CHAPTER 1

CO_2 Capture Overview, Literature Review and Research Objectives 1

1.1 Introduction and CO_2 Emission Overview 1

1.2 CO_2 Capture Approaches 2

1.2.1 Pre- combustion 2

1.2.2 Oxy- combustion 2

1.2.3 Post- combustion 2

1.3 CO_2 Capture Technologies 3

1.3.1 Absorption 3

1.3.2 Adsorption 3

1.3.3 Cryogenic Distillation 3

1.3.4 Membrane Separation Technology 4

1.4 Literature Review 9

1.5 Thesis Objectives 11

1.6 Thesis Outline 12

CHAPTER 2

Synthesis, Characterization and CO_2 Separation Study on Carboxymethyl Chitosan Membrane 15

2.1 Introduction 15

2.2 Experimental Section 16

2.2.1 Materials 16

2.2.2 Synthesis of Carboxymethyl Chitosan (CMC) 16

2.2.3 Development of CMC Membrane 16

2.2.4 Characterization Techniques 17
2.2.5 Gas Permeation Study 20
2.3 Results and Discussion 21
2.3.1 Degree of Substitution and Molecular Weight of CMC 21
2.3.2 Spectroscopic Analysis 23
2.3.3 Microscopic Analysis 26
2.3.4 Moisture Retention Test 26
2.3.5 Thermal Stability 28
2.3.6 Gas Permeation Study 28
2.4 Conclusions 33

CHAPTER 3

Synthesis and Characterization of Small Molecule Carrier Blended Carboxymethyl Chitosan Membrane for CO_2 Separation 35

3.1 Introduction 35
3.2 Experimental Section 36
3.2.1 Materials 36
3.2.2 Membrane Fabrication 36
3.2.3 Characterization Techniques and Gas Permeation Set Up 36
3.3 Results and Discussion 36
3.3.1 Spectroscopic Analysis 36
3.3.2 Moisture Retention Ability 39
3.3.3 Microscopic Analysis 40
3.3.4 Thermal Stability 42
3.3.5 Gas Permeation Study 42
3.3.6 Characterization of the Membrane After Gas Permeation 46
3.3.7 Comparative Study 47
3.4 Conclusions 48

CHAPTER 4

Carboxymethyl Chitosan/Poly (amidoamie) Molecular Gate Membrane for CO_2/N_2 Separation 49

4.1 Introduction 49

4.2 Experimental Section 50

4.2.1 Materials 50

4.2.2 Membrane Fabrication 50

4.2.3 Characterization Techniques and Gas Permeation Set Up 50

4.3 Results and Discussion 51

4.3.1 Spectroscopic Analysis 51

4.3.2 Microscopic Analysis 53

4.3.3 Moisture Retention Ability 55

4.3.4 Temperature Stability 58

4.3.5 Gas Permeation Study 59

4.3.6 Characterization of the Membrane After Gas Permeation 65

4.3.7 Comparative Study 66

4.4 Conclusions 67

CHAPTER 5

Carboxymethyl Chitosan/ Carbon Nanotubes Mixed Matrix Membranes for CO_2 Separation 69

5.1 Introduction 69

5.2 Experimental Section 70

5.2.1 Materials 70

5.2.2 Membrane Fabrication 70

5.2.3 Characterization Techniques and Gas Permeation Set Up 70

5.3 Results and Discussion 71

5.3.1 Dispersion Test for CNTs 71

5.3.2 Spectroscopic and Microscopic Analysis for CNTs 72

5.3.3 Spectroscopic Analysis of Membranes 73

5.3.4 Morphological Analysis of Membranes 77

5.3.5 Water Retention Ability 80

5.3.6 Dynamic Mechanical Analysis (DMA) 82
5.3.7 Gas Permeation Study 84
5.4 Conclusions 89

CHAPTER 6

High Speed CO_2 Transport Channel Assisted Carboxymethyl Chitosan Mixed Matrix Membrane for CO_2 Separation 91

6.1 Introduction 92
6.2 Experimental Section 92
6.2.1 Materials 92
6.2.2 Membrane Fabrication 92
6.2.3 Characterization Techniques and Gas Permeation Set Up 92
6.3 Results and Discussion 92
6.3.1 Elemental and Morphological Analysis 92
6.3.2 Thermal Stability 97
6.3.3 Moisture Retention Ability 98
6.3.4 CO_2 Separation Study 99
6.3.5 Characterization of the Membrane After Gas Permeation 102
6.3.6 Comparative Study 103
6.4 Conclusions 104

CHAPTER 7

Thermally Stable and Moisture Responsive Carboxymethyl Chitosan/Dendrimer/Hydrotalcite Membrane for CO_2 Separation 107

7.1 Introduction 105
7.2 Experimental Section 106
7.2.1 Materials 106
7.2.2 Membrane Fabrication 106
7.2.3 Characterization Techniques and Gas Permeation Set Up 106
7.3 Results and Discussion 107
7.3.1 Morphological Analysis 107

7.3.2 Structural Aspect 108
7.3.3 Thermal Stability 112
7.3.4 Moisture Retention Ability 114
7.3.5 CO_2 Separation Study 116
7.3.6 Characterization of the Membrane After Gas Permeation 119
7.3.7 Comparative Study 121
7.4 Conclusions 122

CHAPTER 8

Overall Conclusions and Recommendation for Future Work 123
8.1 Major Conclusions 123
8.2 Recommendation for Future Research 127
References 128
Appendix 1 144
Appendix 2 146
Research Output 158
Awards and Achievements 160

Abstract

The primary focus of the thesis is to develop a thermally stable and moisture responsive biopolymer-based membrane for CO_2 separation. Among various biopolymers, chitosan possesses CO_2 transport site as its structure consists of amine group. Moreover, chitosan has very good film forming ability and thermal stability without crosslinking. However, the limited solubility of chitosan in neutral and basic medium drives towards an alteration. Also, the unmodified chitin present in the chitosan solution may hinder the gas permeation through membrane. Therefore, carboxymethyl chitosan (CMC), a water soluble derivative of chitosan has come into picture. The optimum performance of CO_2 separation was obtained for CMC membrane at 80 °C with supplied sweep/feed water flow ratio of 1.67 and feed pressure of 2/1.2 bar (feed/sweep) presenting a significant increase of CO_2 permeance (~35 GPU) and CO_2/N_2 selectivity (~39) as compared to that of chitosan membrane. The membrane showed its thermal stability at the operating temperatures. Hence, CMC membrane was further explored for CO_2 separation application by incorporation of different amines and fillers. In order to increase the amine content in the membrane matrix, piperazine (PZ), a small molecule amine was blended with CMC and utilised for CO_2/N_2 separation. Improved performance of CO_2 separation was obtained for 20 wt. % PZ containing membrane at the same operating conditions as CMC membrane and exhibited more than two times increase in CO_2 permeance (89 GPU) and CO_2/N_2 selectivity (103) as compared to that of pure CMC membrane. The membrane performance was found stable up to 3 days. Then poly (amidoamine) (PAMAM), a large molecule amine was blended with CMC which remarkably enhanced the CO_2/N_2 separation performance than pure CMC membrane. The membrane containing 10 wt. % PAMAM and 90 wt. % CMC showed the overall CO_2 permeance of ~ 101 GPU with the CO_2/N_2 selectivity ~137 on maintenance of sweep/feed water flow ratio 2.33 at 90 °C. However, the amine blended polymeric membranes possess the drawback of performance stability for a longer duration. Hence, the incorporation of filler was deliberated. Accordingly, multiwall carbon nanotubes (CNTs) were incorporated to CMC matrix which presented the optimum CO_2 permeance of ~ 43 GPU and CO_2/N_2 selectivity ~ 45 at water flow ratio 3 and temperature 80 °C. Although, the CNTs (1 wt. %) loaded CMC membrane showed slight improvement in CO_2 permeance and CO_2/N_2 selectivity as compared to CMC, the membrane stability retained even after 10 days. In a similar experiment, 1 wt. % of hydrotalcite (HT) was incorporated to CMC matrix as filler and the CMC/HT membrane

displayed remarkable CO_2 permeance (70 GPU) but inferior CO_2/N_2 selectivity (13) than that of CMC at 90 °C and water flow ratio of 2.33. Well ahead, based on the above-mentioned studies, a goal has set to work on the improvement of CO_2/N_2 selectivity as well as CO_2 permeance simultaneously. In view of that, CMC/PAMAM/HT membrane was fabricated and obtained the significant augmentation of CO_2 permeance up to 123 GPU and CO_2/N_2 selectivity of 67 at 90 °C pertaining a constant water flow ratio of 2.33 (sweep/feed). Hence, among all the tested membranes (CMC, CMC/PZ, CMC/PAMAM, CMC/CNT and CMC/HT), CMC/PAMAM/HT membrane showed the best CO_2 permeance which substantiated the efficiency of the membrane for CO_2 separation application. In this way this work encourages us to envision the utilization of carboxymethyl chitosan-based mixed matrix membranes for CO_2 separation from flue gas.

List of Figures

Figure No.	Figure Caption	Page No.
Figure 1.1	Schematic representation of facilitated transport in fixed carrier containing membrane.	7
Figure 1.2	Robeson upper bound (2008) plot for a few chitosan based membrane system.	11
Figure 2.1	Fabrication of flat sheet membrane for CO_2 separation study	17
Figure 2.2	Laboratory scale set up for (a) moisture retention test (b) pH metric titration.	19
Figure 2.3	Schematic representation of gas permeation set up.	21
Figure 2.4	pH-metric titration curve of CMC sample (a) volume of NaOH consumed vs pH (b) Differential graph of titration curve.	22
Figure 2.5	^{1}H NMR spectrum of CMC powder in D_2O at room temperature.	23
Figure 2.6	The high resolution XPS spectra of CMC (a) O1s (b) C1s (c) N1s (d) Na1s.	24
Figure 2.7	(a) FTIR and (b) XRD spectra of CMC membrane.	25
Figure 2.8	FESEM images of (a) PES top surface (b) PES cross- section (c) CMC top surface (d) CMC cross section.	26
Figure 2.9	Moisture retention behavior of CMC membrane at different RH (%).	27
Figure 2.10	TGA graph of CMC membrane (preliminary drying at 100 °C).	28
Figure 2.11	Effect of temperature on (a) CO_2 and N_2 permeance and (b) CO_2 /N_2 selectivity for CMC membrane at sweep/feed water flow ratio =1.67.	30
Figure 2.12	Effect of water flow ratio on (a) CO_2 and N_2 permeance and (c) CO_2 /N_2 selectivity for CMC membrane at 90 °C.	32
Figure 3.1	The high resolution XPS spectra of PZ20 (a) O1s (b) C1s (c) N1s (d) Na1s.	38
Figure 3.2	FTIR spectra of CMC and CMC/PZ blend membranes.	38

Figure 3.3	Water retention behavior of CMC, PZ20, PZ30 and PZ40 membranes at different RH % at room temperature.	39
Figure 3.4	FESEM images for the cross sectional view of the membranes before gas permeation test (a) CMC (b) PZ20 (c) PZ30 and (d) PZ40.	40
Figure 3.5	FESEM analysis of top surface of the membranes before gas permeation (a) CMC (b) PZ20 (c) PZ30 and (d) PZ40.	41
Figure 3.6	AFM analysis of the membranes before gas permeation (a) CMC (b) PZ20 (c) PZ30 and (d) PZ40.	41
Figure 3.7	TGA graph of CMC and PZ20 active layer.	42
Figure 3.8	Effect of sweep water flow rate on (a) CO_2 and N_2 flux (b) CO_2 and N_2 permeance and (c) CO_2/N_2 selectivity of CMC and PZ20 at 80 °C.	45
Figure 3.9	TGA isotherm for PZ20 membrane at 80 °C, 100 °C and 120 °C.	46
Figure 3.10	Characterization of PZ20 membrane after gas permeation study (a) FTIR spectra (b) AFM image (2D view).	47
Figure 4.1	(a) FTIR spectrum (b) XPS survey spectrum of PAMAM blended CMC membrane.	52
Figure 4.2	Deconvoluted XPS spectra of PAMAM10 membrane (a) C1s, (b) N1s (c) O1s (d) Na1s.	53
Figure 4.3	FESEM image obtained for the cross section and top surface of (a, b) PAMAM10 (c, d) PAMAM20 (e, f) PAMAM30, respectively.	54
Figure 4.4	AFM analysis of the membranes before gas permeation (a) PAMAM10 (b) PAMAM20 (c) PAMAM30.	55
Figure 4.5	Moisture retention behavior of PAMAM blended membranes under different relative humidity (%) at room temperature (Inset image shows the chain opening conformation happening in PAMAM10, PAMAM20 and PAMAM30).	57
Figure 4.6	(a) TGA graph for the active layer of PAMAM10 (inset image indicates the zoomed graph for TGA isotherm at temperatures	58

	80 °C, 90 °C, 100 °C and 110 °C) (b) XPS spectra at 80 °C and 90 °C.	
Figure 4.7	Overall CO_2 transport mechanism in CMC/PAMAM membrane.	61
Figure 4.8	Effect of temperature on (a) CO_2 and N_2 permeance (b) CO_2/N_2 selectivity of PAMAM10 at sweep/feed water flow ratio =1.67.	63
Figure 4.9	Effect of sweep/feed water flow ratio on (a) CO_2 and N_2 permeance and (c) CO_2/N_2 selectivity of PAMAM10 at 90 °C.	64
Figure 4.10	CO_2/N_2 separation performance stability of PAMAM10 membrane at the operating conditions, temperature = 90 °C and sweep/feed water flow ratio =2.33.	65
Figure 4.11	Characterization of PAMAM10 membrane after gas .permeation study (a) FTIR spectra and (b-d) AFM image.	66
Figure 5.1	Photographs of raw CNTs and CMC-w-CNTs dispersed in CMC solution, (a) day zero and (b) day one.	71
Figure 5.2	(a) Raman spectra of raw CNTs and CMC-w-CNTs. The inset represents the FETEM image of raw CNTs and CMC-w-CNTs (b) Energy dispersive X- ray analysis of CMC wrapped CNTs	73
Figure 5.3	(a) FTIR spectra (b) XPS survey spectra for CMC and CNT1 membranes	75
Figure 5.4	Deconvoluted XPS spectra for C1s in (a) CMC (b) CNT1 membranes.	76
Figure 5.5	Deconvoluted XPS spectra for CMC and CNT1 membranes (a) CMC/O1s, (b) CMC/N1s, (c) CMC/Na1s, (d) CNT1/N1s, (e) CNT1/O1s, (f) CNT1/Na1s.	77
Figure 5.6	FESEM analysis of the top surface of the membranes (a) CMC, (b) CNT0.5, (c) CNT1, (d) CNT1.5.	79
Figure 5.7	FESEM analysis of the cross section of the membranes (a) pure CMC membrane, (b) CNT1 membrane (5kx).	79
Figure 5.8	AFM images (2D image, height profile and 3D image) of the membranes (a) CMC, (b) CNT0.5, (c) CNT1, (d) CNT1.5.	80
Figure 5.9	(a) Moisture retention behavior and (b) rate of moisture intake in CMC, CNT0.5, CNT1 and CNT1.5 membranes.	82

Figure 5.10	DMA curves for the active layers of CMC, CNT0.5, CNT1, and CNT1.5.	83
Figure 5.11	(a) Effect of temperature on CO_2 and N_2 permeance and CO_2/N_2 selectivity in CNT1 membrane at feed absolute pressure = 2 bar, sweep absolute pressure = 1.21 bar, sweep/feed water flow ratio = 1.67 (b) DSC graph of CMC and CNT1 membranes.	85
Figure 5.12	CO_2 Permeance and CO_2/N_2 selectivity of membranes having different composition of CNTs at temperature = 80 °C, sweep/feed absolute pressure = 2/1.21 bar, sweep/feed side water flow ratio = 1.67.	86
Figure 5.13	Effect of sweep water flow ratio on CO_2 and N_2 permeance and CO_2/N_2 selectivity of CNT1 at 80 °C, feed absolute pressure = 2 bar, sweep absolute pressure = 1.21 bar.	88
Figure 6.1	(a) EDX analysis of HT (inset image corresponds to the FESEM image of HT powder)(b) XRD spectrum obtained for HT powder.	94
Figure 6.2	(a) FTIR spectra and (b) XRD of CMC and CMC/HT membrane.	95
Figure 6.3	FESEM and EDX mapping on the top surface of CMC membrane (a) FESEM image (10kX) (b) elemental mapping.	96
Figure 6.4	FESEM and EDX mapping on the top surface of CMC/HT membrane (a) FESEM image (10kX) (b) elemental mapping.	97
Figure 6.5	(a) FESEM cross section and (b) AFM image (3D) of CMC/HT membrane.	97
Figure 6.6	TGA graph obtained for CMC/HT active layer (a) dynamic (b) isotherm.	98
Figure 6.7	Effect of (a) temperature (b) water flow ratio on CO_2 separation performance of CMC/HT membrane.	101
Figure 6.8	Performance stability of CMC/HT membrane at temperature = 90 °C, sweep/feed water flow ratio = 2.33.	102
Figure 6.9	FTIR of CMC/HT membrane (with PES support) before and after gas permeation study.	103

Figure 7.1	FESEM (a) top surface (b) cross section and AFM image (c) 2D view (d) height profiling (e) 3D view of CMC/PAMAM/HT membrane.	108
Figure 7.2	(a) FTIR spectrum (b) XPS survey spectrum of CMC/PAMAM/HT active layer.	110
Figure 7.3	XPS narrow scan of CMC/PAMAM/HT for (a) O1s, (b) N1s, (c) C1s, (d) Na1s, (e) Mg2p and (f) Al2p.	111
Figure 7.4	EDX mapping analysis of the top surface CMC/PAMAM/HT membrane.	112
Figure 7.5	TGA isotherm for CMC/PAMAM/HT membrane at 80 °C, 90 °C, 100 °C and 110 °C.	113
Figure 7.6	XPS analysis of CMC/PAMAM/HT membrane at different temperatures (a) survey spectra (b) deconvulated O1s spectra corresponding to H_2O molecule.	114
Figure 7.7	Moisture uptake behavior of CMC/PAMAM/HT membrane at different temperatures.	115
Figure 7.8	FESEM image (cross section) of CMC/PAMAM/HT with different active layer thickness.	116
Figure 7.9	(a) Effect of temperature on CO_2 separation performance of CMC/PAMAM/HT membrane (b) Robson upper bound (2008) plot for CO_2/N_2 separation at different temperature.	119
Figure 7.10	(a) FTIR analysis of the membrane before and after gas permeation (b) UV analysis of the water knockout obtained from feed and sweep side.	119
Figure 7.11	AFM analysis of the membrane after gas permeation test.	120
Figure 7.12	EDX mapping for the cross section of CMC/PAMAM/HT membrane (a) before gas permeation (b) after gas permeation.	120
Figure A1.1	Chemical structure of (a) CMC, (b) PZ and (c) PAMAM.	144
Figure A1.2	Structure of (a) multiwalled carbon nanotubes (b) hydrotalcite.	145
Figure A2.1	GC peaks of PAMAM10 membrane at 80 °C and absolute pressure = 2/1.21 bar (feed/sweep) having sweep/feed water flow ratio of 1.67.	156

List of Tables

Table No.	Table Caption	Page No.
Table 3.1	Effect of PZ concentration on CO_2 permeance and CO_2/N_2 selectivity at 80 °C	43
Table 4.1	Moisture retention ability of different chitosan based membranes at 100 % RH	57
Table 4.2	Elemental analysis of PAMAM10 membrane at 30 °C, 80 °C and 90 °C using XPS	59
Table 4.3	Effect of PAMAM concentration on CO_2 permeance and CO_2/N_2 selectivity at 90 °C, sweep/feed water flow ratio = 1.67 and feed side absolute pressure = 2 bar	61
Table 5.1	CO_2 Permeance and CO_2/N_2 selectivity of CNTs loaded membranes	89
Table 6.1	Moisture retention behaviour of CMC/HT membrane at different RH %	99
Table 6.2	Gas separation performance of recently developed various membranes systems	104
Table 7.1	Elemental analysis of CMC/PAMAM/HT active layer at different temperatures	114
Table 7.2	Influence of active layer thickness on CO_2 separation with the supplied water flow ratio (sweep/feed = 2.33), feed absolute pressure = 2 bar and operating temperature = 90 °C	117
Table 8.1	Optimum CO_2 separation performance exhibited by the membranes studied in this research work	126

CHAPTER 1

CO_2 Capture Overview, Literature Review and Research Objectives

CHAPTER 1

CO_2 Capture Overview, Literature Review and Research Objectives

In this particular chapter, the adverse effects owing to the continuous escalation of CO_2 in the atmosphere and the remedial methods for CO_2 mitigation have been discussed in brief. The membrane based technology has been highlighted on the basis of its advantages and elaborated its suitability towards CO_2 capture approach. In depth study has been done on various CO_2 transport mechanisms corresponding to different membrane configurations. Finally, on the basis of the gaps and challenges, the research objectives have been defined.

1.1 Introduction and CO_2 Emission Overview

Energy consumption is indispensable to the growth of economic development, but at the same time massive use of non-renewable fossil fuels as the primary source of energy contributes largely to the global warming due to the emission of CO_2 [1]. Various scientific reports disclose that the concentration of CO_2 in the atmosphere is increasing at a rate exceeding 1 ppmv per year [2]. Consequently, the earth's surface temperature has increased by 0.4–0.8 °C above the reference line of 14 °C [3]. As per the latest statistics, the fossil fuel thermal power plants supply 85% of entire world demanded energy [4]. Generally, the flue gas emitted by the natural gas fired plant and coal fired power plants contains 4-8 % CO_2 and 12-15 % of CO_2 by volume, respectively. As per the statement made by the intergovernmental panel on climate change (IPCC), the atmospheric CO_2 concentration has been projected to cross 750 ppmv by the year 2100 if no action is taken to reduce its continuous emissions [5]. Therefore, the regulation of CO_2 emission is very vital at this point of time although it is a complex task.

There are basically three routes to reduce the emission of industrial CO_2 into the atmosphere [6]: (a) Reduction of energy intensity, (b) Reduction of carbon intensity, and (c) Enhancement of CO_2 sequestration. The first option requires limited use of energy which is a challenging job in today's era. The second option suggests the limited use of fossil fuels or switching to the use of non-fossil fuels such as hydrogen and renewable

energy. The third option involves the development of technologies to capture and sequester CO_2.

1.2 CO_2 Capture Approaches

Depending on the type of plant, following CO_2 capture technologies have been adopted: pre-combustion, post-combustion and oxy-fuel combustion [3].

1.2.1 Pre-combustion

Pre-combustion technique, aims the removal of all or some portion of the carbon from fuel before burning it [7]. This is done by transforming the fuel into a synthetic gas comprising mainly carbon monoxide and hydrogen. Then water vapour is added, which reacts with the carbon monoxide converting it into CO_2. In this process, the molar concentration of CO_2 is very high (~ 25–40 %) coming out at a total pressure of 25- 50 bar [8]. The CO_2 and the hydrogen are then separated using an amine-type solvent or gas hydrate formation.

1.2.2 Oxy-combustion

Oxy combustion is combustion in pure oxygen rather than air. In a conventional combustion scheme air is used, but this generates a large volume of smoke and fumes, where the CO_2 is much diluted [9]. In a technique called chemical looping combustion, the oxygen needed for combustion is transferred from the combustion air to the fuel by the use of an oxygen carrier; most commonly an oxidized metal. In this system, the metal oxide is transported between two fluidized bed reactor- air and a fuel reactor. Thus a system is created in which the fuel and combustion air never comes into contact with one another, creating a CO_2 exhaust gas stream not diluted with N_2, which is made for relatively easy CO_2 capture [10].

1.2.3 Post-combustion

In this technique, CO_2 is removed from the flue gas after the combustion [11]. This technique is important mainly due to its flexibility and retrofit option. In post combustion, there are four separation technologies, namely, absorption, adsorption, cryogenic distillation and membrane separation which are discussed below.

1.3 CO_2 Capture Technologies

1.3.1 Absorption

In absorption process, the gaseous stream is brought into contact with a solvent in which CO_2 is soluble. This process takes place in a counter-current absorption tower, where the solvent (downward flow) is in counter-flow with the gaseous stream (upward flow). The solvent is supposed to be highly selective for CO_2 absorption and CO_2 must have high solubility in the solvent. Besides, the solvent should be volatile, chemically stable, low cost, available, non-corrosive, less viscous, non-flammable and environment friendly. CO_2 is separated from the gaseous stream by absorption in the solvent and later in stripping section it get desorbed from the solvent [12]. The absorption mechanism can either be physical or chemical. In physical absorption, CO_2 gas has higher solubility in the solvent than the other gaseous species, by which it gets selectively absorbed in the solvent. No chemical reaction takes place between CO_2 and the solvent here. On the other hand, the chemical absorption technique is based on the principles of reaction equilibria and reaction kinetics, and is employed for CO_2 separation from streams having low to moderate CO_2 partial pressure.

Although the absorption process is a mature technology, which has been extensively used in industries for decades, it has certain major disadvantages like equipment corrosion, high energy consumption and solvent degradation [12-14].

1.3.2 Adsorption

The adsorption process is described by the adhesion of a specific component of the gas mixture selectively on an adsorbent surface due to the surface forces, thereby separating the component from the gas mixture. This step is followed by desorption of the adsorbed component. The desirable characteristics of an adsorbent are: High selectivity for the component to be separated, good capacity and long service life. Adsorption is categorised into two types – physical adsorption and chemical adsorption. In physical adsorption, the gas molecules are adsorbed and are attached to the adsorbent surface by weak forces – van der Waals forces and electrostatic forces. Regeneration of the adsorbent surface with desorption of the adsorbed gas is simple as these forces are weak. Along with van der Waals forces, CO_2 can be adsorbed through interactions with a polar adsorbent surface due to the quadrupolar nature of CO_2. In case of chemical adsorption, the gas molecules

undergo chemical reactions with reactive sites on the adsorbent surface. The chemical bonds formed are much stronger than the interactions exhibited in physical adsorption. Reactive sites for CO_2 adsorption can be obtained by incorporating amine groups in the adsorbent. CO_2 will react with the amine groups to form ammonium carbamate groups, which, in the presence of water will form ammonium bicarbonate species. The adsorption process can be categorised based on regeneration techniques: temperature swing adsorption (TSA), pressure swing adsorption (PSA) and electrical swing adsorption (ESA). However, the adsorption process suffers from the limitations such as it can achieve low CO_2 selectivity and can deal with very less concentration of CO_2 (0.04% – 1.5%) [15].

1.3.3 Cryogenic Distillation

In this technique, CO_2 is separated from N_2 by introducing the gas mixture to a cryogenic chamber which is at an extremely low temperature. The temperature and pressure of the chamber are manipulated such that CO_2 is liquefied, while N_2 remains in the gaseous state, thereby separating CO_2 from N_2 [15]. Commercially, this method is employed to separate CO_2 from gas mixtures containing CO_2 concentrations greater than 50-70% [12]. This method requires the usage of mature technologies such as compression, refrigeration and separation, making them feasible for application in chemical industries [16]. Additionally, this technique does not require the usage of chemical agents which prevents secondary pollution [16] and the liquid CO_2 produced offers ease of transport through pipelines. However, despite the advantages offered, cryogenic distillation and separation suffers from the following limitations such as requirement of high energy to get cryogenic temperatures and large cost [15]. Also, the water molecule present in the stream can freeze and clog pipes resulting corrosion of the equipment, hence it requires pre-treatment.

1.3.4 Membrane Separation Technology

The principle of gas separation using membranes is the difference in the rates of permeation of the individual feed stream components through the membrane. This difference causes one component to have higher selectivity of transport through the membrane over other components, thereby separating them [17]. The driving force for gas permeation through the membrane is the partial pressure gradient across the membrane of the component being transported [18]. The performance of a gas separation membrane is described in terms of two quantities: the permeability and the selectivity [19, 20]. The

permeability is defined as the transport flux of the gas component through the membrane per unit driving force for a given membrane thickness. A common unit for permeability is Barrer, where 1 Barrer = 10^{-10} (cm^3 (STP).cm)/ (cm^2.s.cm-Hg) [21]. The permeance of a gas separation membrane is defined as the permeability per unit thickness. Its unit is GPU (Gas Permeation Unit), where 1 GPU = 10^{-6} (cm^3 (STP))/ (cm^2.s.cm-Hg). The membrane selectivity of one component over the other is given by the ratio between the permeabilities of the respective components. The ideal membrane selectivity is obtained from the ratio of the pure gas permeabilities. Membrane technology offers us a variety of advantages such as: low cost, high energy efficiency, operational simplicity, reliability, compactness, and modularity.

1.3.4.1 Types of membranes and fabrication methods

Efforts to study membranes for CO_2 separation have generally focused on a few different classes of materials such as polymeric [22], ceramic [23] and mixed matrix [24]. The ceramic membranes are a type of artificial membranes made from inorganic materials such as alumina, titania, zirconia oxides, silicon carbide etc. They also have excellent thermal stability which makes them usable in high-temperature membrane operations. The polymeric membranes can be either synthetic or natural. Natural polymers are widely appreciated due to its abundance, low cost and biocompatibility. The recent development of polymeric and inorganic materials has seemingly reached a limit in trade-off between selectivity and permeability. The deficiencies of these materials have in turn switched the focus of researches towards the realization of a new class of membrane material, namely mixed matrix membrane (MMM). Mixed matrix membranes are considered as a class of composite membranes that comprise of inorganic materials embedded in a polymer matrix. Several inorganic materials such as zeolites, carbon molecular sieves (CMS), metal peroxides (MOs), carbon nanotubes (CNTs) and metal organic frameworks (MOFs) have been incorporated in different polymers. Generally, the inorganic dispersed phase has permeability superior to the neat polymer. The fabrication of polymeric and mixed matrix membranes can be done either by phase inversion or solvent evaporation method. In phase inversion, a homogeneous polymer solution is cast onto a suitable support as a thin film and then immersed into a coagulation bath containing a suitable non-solvent. The polymer film solidifies to form a membrane with a symmetric or asymmetric structure through the exchange between the solvent inside the cast film and the nonsolvent outside the cast film

in the coagulation bath. In this process of solidification, the film goes through complicated phase changes which include liquid–liquid phase separation, solid–liquid phase separation, or both, depending on polymer properties and coagulation conditions. On the other hand, in solvent evaporation method, the cast films are allowed to dry under an ambient condition or at a higher temperature. The evaporation of the solvents from the fabricated membrane leads the formation of the desired solid membrane. Hence, the solvent evaporation method is preferred over phase inversion due to its simplicity.

1.3.4.2 Membrane based gas transport mechanism

The transfer of gas molecules involves several processes, depending on the nature of the pore structure and the solid. There are three different mechanisms for separation of a gas mixture through membrane: Knudsen diffusion, molecular sieving and solution diffusion. Knudsen diffusion mechanism occurs in porous membranes where the pore size is less than the mean free path of the gas molecules. The collisions of the gas molecules with the pore walls is more frequent than the collisions with other gas molecules, allowing lighter molecules to preferentially transport through the pores [25]. The molecular sieving mechanism describes the ideal condition for the separation of vapour compounds of different molecular sizes through a porous membrane. Smaller molecules have the highest diffusion rate and this process happens with sufficient driving force. The main limitation of this is that condensable gases may cause fouling and can alter the structure of the membrane. Solution diffusion mechanism is based on both solubility and mobility factors. In this model gas permeation can be seen as a three stage process;

- Adsorption and dissolution of gas at the polymer membrane interface
- Diffusion of gas in and through the bulk polymer
- Desorption of gas into the external phase

In post-combustion CO_2 capture, the solution-diffusion mechanism exhibits reduced performance due to low CO_2 partial pressure in flue gas and alteration in membrane structure because of plasticization by water vapour [26-28]. These membranes show low selectivity governed by Robeson's upper bound, suffering a trade-off between permeability and selectivity [29-32]. To overcome these limitations, the researchers welcomed facilitated transport membranes as they offer improved CO_2 performance beyond the upper bound limit [33]. Facilitated transport membranes are described by the selective and reversible reaction of CO_2 [29] with the reactive carriers forming complexes,

which facilitate the transport of CO_2 through the membrane. These carriers can be mobile or fixed. Mobile carriers react with CO_2 on the upstream side, forming complexes which freely move through the membrane, releasing CO_2 on the downstream side. Although they offer high separation performance, they have an inherent lack of stability due to carrier loss and degradation [34-36]. The use of fixed carriers, which are covalently bonded to the membrane polymer chains, thereby having limited mobility around the equilibrium position, overcomes these problems [37, 38]. CO_2 reacts with the fixed carrier forming the complex, from which it hops to the adjacent carrier along the direction of the driving force till the downstream side, where it is released [39, 40]. A schematic representation of a fixed amine based facilitated transport mechanism of CO_2 is shown in **Figure 1.1**.

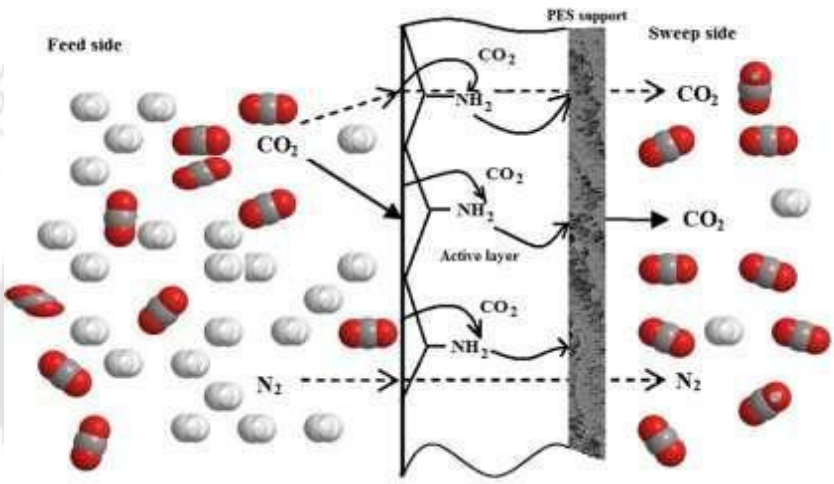

Figure1.1 Schematic representation of facilitated transport in fixed carrier containing membrane

The amine carrier serves the facilitated transport mechanism by reacting with CO_2 that can be described by the following equations. CO_2 reacts with primary or secondary amines (RR′NH, where R is a functional group and R′ is a hydrogen for primary amine whereas R, R′ are functional group in case of secondary amine) to form zwitterions (**Reaction 1.1**) as an intermediate and then the zwitterion is deprotonated by bases such as, the amine itself (**Reaction 1.2**) and formed a protonated amine or carbamate ion and overall reaction is shown in **Reaction 1.3**, which suggest that 2 moles of amine is required to capture one mole of CO_2 [41, 42].

$$CO_2 + RR'NH \rightleftharpoons RR'NH^+COO^- \qquad \text{(Reaction 1.1)}$$

$$RR'NH^+COO^- + RR'NH \rightleftharpoons RR'NCOO^- + RR'NH_2^+ \qquad \text{(Reaction 1.2)}$$

$$CO_2 + 2RR'NH \rightleftharpoons RR'NCOO^- + RR'NH_2^+ \quad \text{(Reaction 1.3)}$$

The zwitterion then is deprotonated by bases such as H_2O to form the carbamate ion.

$$RR'NH^+COO^- + H_2O \rightleftharpoons RR'NCOO^- + H_3^+O \quad \text{(Reaction 1.4)}$$

If the carbamate ion of the amine carrier is not stable which is the case of satirically hindered amine then it will react with H_2O to form bicarbonate.

$$RR'NCOO^- + H_2O \rightleftharpoons RR'NH + HCO_3^- \quad \text{(Reaction 1.5)}$$

Similarly, for tertiary amine bicarbonate is formed following the base catalyzed mechanism [43].

$$R_3N + CO_2 + H_2O \rightleftharpoons R_3N^+H + HCO_3^- \quad \text{(Reaction 1.6)}$$

In the above reactions, water plays major role by promoting ion transfer. Water and CO_2 react reversibly with amines in the active layers forming carbamate and bicarbonate that diffuses rapidly across the membrane and finally dissociates in the permeate side, releasing the CO_2 [44]. Hence, membranes following facilitated transport mechanism have high CO_2 flux along with CO_2/gas selectivity. Also, water improves polymer chain mobility and reduces the gas diffusion resistance [35, 37, 45]. The CO_2 separation efficiency of a membrane is highly dependent on CO_2-carrier reaction kinetic. The strong affinity between the CO_2 molecule and amine provides irreversible reaction resulting no liberation of CO_2 at the permeate side [46]. On the other hand, a slow reaction rate forms a very unstable CO_2-carrier complex and no facilitated transport occurs as the membrane turns saturated very easily [46]. Hence, the mild reaction rate is the prime requisite for facilitated transport, especially at the decomposition step with moderate equilibrium constants [3]. Also, the fractional free volume (FFV) of the polymer helps the CO_2 molecules to achieve reversible reaction more comfortably [47]. The high density and small size of the carrier provides more number of active sites for fast facilitated transport [46, 48]. Additionally, the water content in the matrix is very important as water induces swelling and creates additional free volume for gas diffusion [49]. It was also revealed that the presence of salts in water swollen membrane can decrease the solubility of non-condensable gases like N_2, and CH_4. This is an appealing way to increase the selectivity of CO_2 over N_2 and the process is referred to as "salting out effect" [50]. Humidified membranes with high salt have both enhanced permeability and selectivity. The state of water (free water or bound

water) which is present in the membrane affects the overall CO_2 separation performance [51]. The gas solubility is higher in bound water, whereas gas diffusivity is higher in free water [52]. It was reported that the CO_2/N_2 selectivity increases with increasing bound water [53].

1.4 Literature Review

The focus of my research work is on CO_2 separation from gas mixtures using membrane technology. Extensive works have been reported for membrane-based CO_2 separation technology by using pristine [35, 37] or amine blended [54] polymeric membranes. The blending of the amines with polymer enriches the carrier content in the membrane matrices which enhance the facilitated transport of CO_2. Among various works, the experiment performed by Matsuyama's group [55] using poly (ethylene amine)/poly (vinyl alcohol) showed the CO_2 permeance ~ 4 GPU with the CO_2/N_2 selectivity ~160. Deng et al. [49] synthesized a poly (vinylamine)-poly(vinyl alcohol) blend membrane and reported a CO_2 permeance of ~ 215 GPU and CO_2/N_2 separation factor of 174 at a feed pressure of 2 bars and 25 °C. However, the synthesis process of poly(vinyl alcohol) (PVA) membranes is complex and time consuming, as PVA dissolves in water at temperatures greater than 70 °C, and must be crosslinked [33] to ensure its thermal stability. The biopolymer chitosan has recently captivated researchers due to its film-forming ability, temperature stability, and a fixed carrier site to interact with CO_2 [27]. Ito et al. [56] studied on swollen chitosan membrane for CO_2/N_2 separation at room temperature and achieved CO_2 permeance of 35.71 GPU and CO_2/N_2 selectivity of 70. Further, El-Azami [57] group worked on swollen chitosan membrane varying the temperature from 20 to 150 °C and attained a permeance of 7.4 GPU at 110 °C. In this context, Liu et al. [58] prepared a membrane using chitosan and poly ether-block-amide (Pebax®) and found that the blending of Pebax into chitosan generates more gas passage networks in polymer system, which directly enhances the CO_2 permeability. In a previous study carried out in our research group, Prasad et al. [59] reported CO_2 permeance of 24.7 GPU for TEPA blended chitosan membrane at 90 °C, whereas pure chitosan displayed 12.5 GPU and selectivity of 54 at the same temperature. Yu et al. [60] prepared a membrane by blending chitosan and triethanolamine (TEA). With the addition of 15 % TEA, the membrane exhibited improved mechanical stability and contributed to a CO_2/N_2 selectivity of 63. Similarly, Shen et al. [61] obtained the CO_2 permeance of 0.36 GPU and a CO_2/N_2 selectivity of 33 at 0.293 psi feed pressure and room

temperature for chitosan modified to CMC. Other than these amine carriers, monoethanolamine (MEA), diethanolamine (DEA), ethylenediamine (EDA), etc. were also introduced into different membrane systems [16–18]. However, these membranes were found to be unstable due to the high volatility of the amines [19]. In contrast, piperazine (PZ) has lower volatility and it acts as amine promoter. Later, Wang et al. studied the effect of EDA and PZ incorporated to polyvinyl amine matrix separately and observed the superior performance of PZ over EDA [20]. They suggested that the presence of two secondary amine groups reduce the crystallinity of these membranes and improves permeation performance. Lately, dendrimers, the large molecule amines have proved its proficiency as a carrier for CO_2 facilitation. Dendrimers possess exceptional properties such as, multiple valency, water solubility, consistent nanosize and suitable approach for synthesis [62-64]. Studies conducted on PAMAM dendrimer-based membranes have shown high CO_2 selectivities [65]. Later, the hybrid membrane containing PAMAM/poly(vinyl alcohol) showed CO_2 permeance of 1.6 GPU and a CO_2/N_2 selectivity of 42 at 60 °C [66]. Duan et al. prepared a PAMAM dendrimer composite membrane with chitosan forming gutter layer and reported a CO_2 permeance of 61 GPU and CO_2/N_2 selectivity of 230 at 40 °C [67]. After the extensive study on amine blended membranes, mixed matrix membranes (MMMs) have come into picture which are the promising membranes having significant potential in gas separation applications [68]. Various filler materials such as zeolite, silica nanoparticle, graphene oxide, etc. have been studied so far. However, the study of carbon nanotubes (CNTs) have been of a special interest [69, 70]. CNTs fused in membranes basically provides one-dimensional nano-channels that act as alternate paths for CO_2 transport through membranes [71]. However, various studies have been performed using CNTs-incorporated composite films. Deng and Hägg studied the PVAm and PVA membranes reinforced with CNTs for the CO_2 separation application from CO_2/CH_4 gas mixture [72]. Similarly, a membrane comprising of single-walled CNTs loaded in a poly(imide siloxane) copolymer has been fabricated and evaluated the gas transport properties [73]. CNTs embedded N-isopropyl acrylamide hydrogel [71] and amino-functionalized CNT embedded crosslinking polyvinylalcohol–polysiloxane/amine blend membrane have also been studied for high-pressure gas separation application [74]. Recently, cellulose acetate/MWCNT MMMs have been used for CO_2 separation [75]. Another inorganic filler Hydrotalcite (HT) also outshined as CO_2 capture material similar to CNTs. HT consists of brucite-like host sheets (positively charged) and hydrated carbonate anions sailed freely in the interlayer corridor [76]. The hydrated carbonate

anions sailing in the interlayer of HT works as the carrier for CO_2 facilitated transport [77]. In one work, Mg-Al hydrotalcite (HT) nanosheets has been added in to aqueous polyetheramine in order to rise the permeability of CO_2 and achieved the permeance of 90 GPU and selectivity as 40 [78]. Later, Liao et al. [79] developed the polyvinyl amine – HT membrane and reached the CO_2 permeance of 3187 GPU and the CO_2/N_2 selectivity of 296 at 1.1 bar. Although, various studies have been performed on sole amine blended and filler incorporated membranes, few literatures have been found regarding the cumulative role of both amine and filler in CO_2 separation performance [80, 81]. Among all the membrane systems, the chitosan based membranes have been chosen as the system of our interest and a Robeson plot has been presented in **Figure 1.2** including the data obtained from a few chitosan- based membranes.

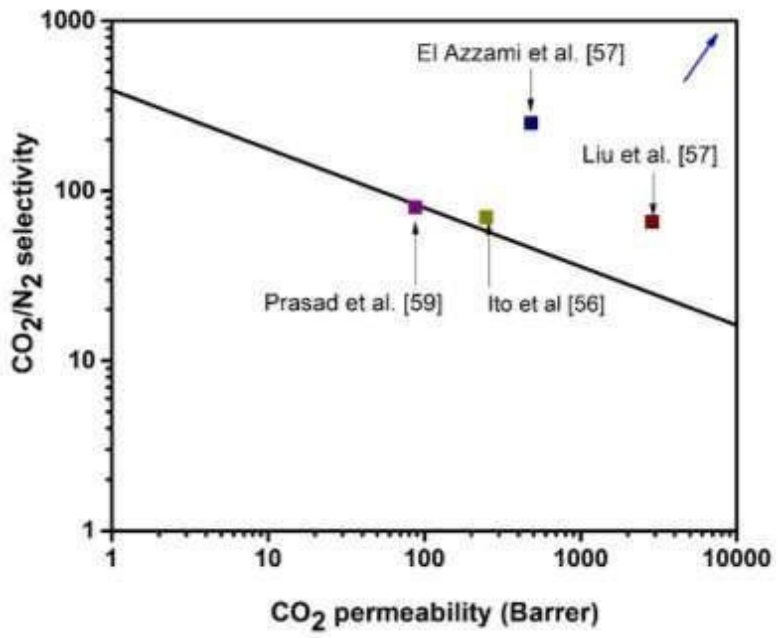

Figure 1.2 Robeson upper bound (2008) plot for a few chitosan based membrane system.

On the basis of the above discussion, the CMC membrane based CO_2 separation approach was scheduled. Here, the thermal stability, film forming ability and moisture responsive nature of CMC were discussed elaborately in terms of CO_2 separation. In this study, small and large molecule amines were exploited as carriers in CMC membranes for facilitated transport of CO_2. However, this study also embodies the use of fillers to improve various properties of membrane along with gas permeation activity. The objectives of our research work have been summarized as below.

1.5 Thesis Objectives

The primary objectives of the thesis are

1. Selection and preparation of the bio based polymeric membrane efficient for CO_2 separation by means of facilitated transport mechanism.
2. Further improvement of the CO_2 facilitated transport by blending with different amines and fillers

The following research works have been undertaken on the basis of the above objectives:

a) Preparation of the CO_2 selective membrane using biopolymer that possesses high thermal stability and sufficient moisture retention ability without crosslinking. Here CMC has been chosen as the control polymer.
b) Development of CMC membrane for CO_2 separation by blending with small molecule amine (PZ) and large molecule amine (PAMAM).
c) Enhancement of various physical properties of membrane and CO_2 separation performance by incorporating carbon nanotubes and hydrotalcite.
d) Study on the synergistic effect of both amine and filler in order to get high speed CO_2 transport membrane.
e) Optimization of the operating temperature and moisture content during gas permeation along with the detailed gas transport mechanism.
f) Characterization and material study corresponding to the synthesis and gas permeation study.

1.6 Thesis Outline

On the basis of the above discussion, thesis work has been divided into eight chapters. A brief overview of each chapter is presented below.

Chapter 1: This chapter focused on the importance of the CO_2 separation as it is one of the major greenhouse gases responsible for the global warming problem. Also, discussed the available technologies designed for CO_2 capture along with their pros and cons. The membrane separation technology has been emphasized on the basis of its characteristic advantages. Also, this chapter comprises the detailed literature review on CO_2 – selective thin-film polymeric membranes mainly focusing the chitosan based membrane activities.

Finally, this chapter listed the research objectives and scheduled the plan of work to accomplish the research goal.

Chapter 2: This chapter contains the synthesis and characterization of the control polymer carboxymethyl chitosan (CMC) along with the detailed gas permeation study investigating the temperature and water flow effect on the separation performance. The schematic diagram of gas permeation set up and laboratory scale set up for moisture retention study has been demonstrated which has been used to complete the objectives of this thesis. Various characterizations like FTIR, XRD, NMR, XPS and FESEM have been carried out to investigate the successful formation of CMC polymer and CMC membrane. Alongside, the thermal and moisture retention behaviour has been determined with the help of TGA-DSC and moisture retention test. The eeffects of temperature and water flow rate on the CO_2 permeance and CO_2/N_2 selectivity were studied on CMC membrane by sending the gas mixture of CO_2/N_2.

Chapter 3: This chapter discusses the role of piperazine (PZ), a small molecule amine as a CO_2 carrier. FTIR, XPS, FESEM and TGA have been utilized to characterize the prepared membranes. The moisture holding behaviour of the membranes at different relative humidity has been assessed by water retention test. The combined role of fixed carrier of CMC and mobile carrier PZ has been evaluated from the gas permeation test. The CO_2 separation study was executed at different sweep side water flow ratio (0.33 to 3). Also, various characterizations have been performed to check if the tested membrane has lost its originality during CO_2 separation.

Chapter 4: This chapter deliberated the mechanism of poly (amidoamine) (PAMAM), a large molecule amine as CO_2 transporter. Additionally, this chapter engaged with the versatile aspects of carboxymethyl chitosan and dendrimer in terms of CO_2 separation. A comprehensive study has been accomplished to inspect the physico - chemical properties of the prepared membrane. The mixed gas (CO_2/N_2) separation performances have been measured varying the temperature (60 - 110 °C) and sweep/feed water flow ratio (0.33-3). It is expected that CMC/PAMAM membrane will take part in CO_2 separation event by ensuring its role as semi mobile carrier, polyionic salt and hydrogel membrane. The combined advantages of both CMC and PAMAM will accomplish this novel approach.

Chapter 5: In this study, the improvement of gas separation activity has been investigated after incorporation of carbon nanotubes (CNTs) to CMC matrix. Herein, the amine groups

present in CMC serve as CO_2 carrier and CNTs provide alternate pathway to the gas molecules. Also, it has been identified that the wrapping of CNT improves the dispersion of CNT in CMC matrix. Various spectroscopic and microscopic analyses have been used to confirm the successful wrapping of CNTs. Further, the prepared mixed matrix membranes were characterized using FESEM, AFM, XPS and DMA. The moisture holding ability of the membranes which is essential for the facilitated transport reaction has been measured at different humid conditions.

Chapter 6: This chapter demonstrates the role of hydrotalcite (HT) in CO_2 separation when incorporated in to CMC matrix. The synthesis of HT has been verified by XRD and EDX analysis. Later, the homogeneous incorporation of HT in CMC matrix has been characterized with the help of FTIR, TGA and EDX coupled FESEM instruments. Also, the moisture holding behaviour of CMC/HT membrane at different relative humidity has been evaluated. The CO_2 separation study was performed at different temperatures (60-110 °C) and water flow ratio (0.33 to 3).

Chapter 7: This chapter comprehends the appreciable effect offered by the synergistic combination of poly (amidoamine) dendrimer (PAMAM) and hydrotalcite (HT) towards CO_2 separation performance. PAMAM and HT have been loaded to carboxymethyl chitosan (CMC) to fabricate a thermally stable MMM which was assessed by TGA isotherm. Further, using various spectroscopic and microscopic techniques the membrane has been characterized. The moisture retention behaviour of the membrane at different temperature has been investigated. Later, the CO_2 separation study was accomplished for the MMM varying the temperature (60-110 °C) and analysed the data by comparing with Robeson upper bound (2008) curve.

Chapter 8: This chapter draws appropriate overall conclusions based on the investigation in the present study. This chapter also provides some useful recommendations for future research in the relevant field.

CHAPTER 2

Synthesis, Characterization and CO_2 Separation Study on Carboxymethyl Chitosan Membrane

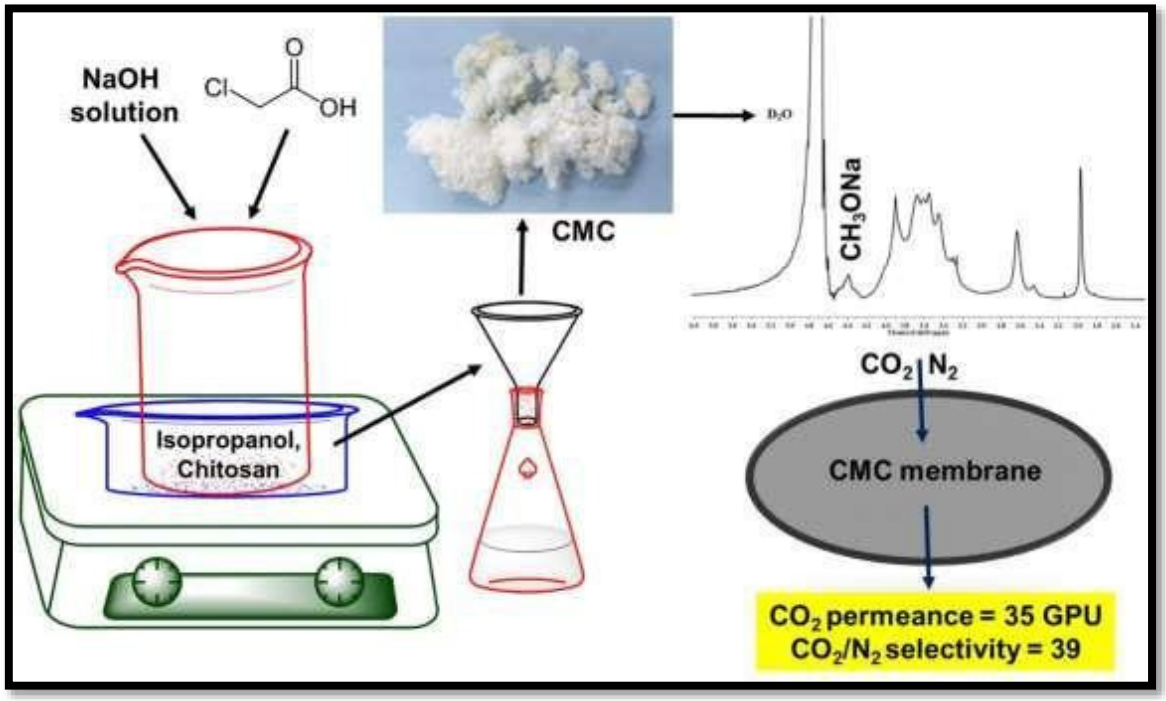

Synthesis of CMC and CO_2 separation performance by CMC membranes.

CHAPTER 2

Synthesis, Characterization and CO_2 Separation Study on Carboxymethyl Chitosan Membrane

*Chitosan, the amine containing biopolymer has recently excelled in the CO_2 separation field. However, the limited solubility of chitosan and the presence of unconverted chitin during membrane formation reduce CO_2 separation performance. This chapter discusses the solution key to the above-mentioned limitations by developing carboxymethyl chitosan (CMC) membrane. Additionally, the relevant characterizations and CO_2 separation performances using CMC membrane have been explained. This work is scientifically acknowledged in "**Separation and Purification Technology**".*

2.1 Introduction

Chitosan has fascinated researchers due to its film-forming ability, temperature stability without crosslinking, and a fixed carrier site to interact with CO_2 [82, 83]. However, certain downsides of chitosan limit the application of chitosan as a membrane matrix for CO_2 separation. Chitosan dissolves only in moderately acidic solution (pH < 6.5) and it precipitates on the addition of basic compound [84]. Also, some chitin retain in chitosan solution depending upon the degree of deacetylation, which impedes the gas flow. Thus, the carboxylation is adopted to overcome the problem of limited solubility of both chitin and chitosan [85]. The presence of bulky methyl group weakens the intra H-bond of chitosan and it helps carboxymethyl chitosan (CMC) to swell in water [86]. The presence of this additional carboxymethyl group other than the primary amine group in the CMC membrane also takes part in the gas permeation mechanisms (**Figure A1.1a, Appendix 1**) [61]. These groups generate an environment for water retention which enhances the CO_2 permeation through the membrane. The CMC membrane follows both facilitated and solution - diffusion mechanism.

Although, CMC has been utilized in various applications, very limited work has been performed in terms of gas permeation application. In the present work, the synthesis and characterization of CMC membrane has been extensively studied. The CO_2 separation study has been carried out on the membrane at different temperature and water flow ratio.

2.2 Experimental Section

2.2.1 Materials

The coarse ground flakes of chitosan (310,000-375,000 Da) was procured from Sigma Aldrich and monochloroacetic acid, sodium hydroxide (NaOH) pellets, isopropyl alcohol (≥ 99 % purity), glycerol (≥ 99.5 % purity) and methanol (≥ 99 % purity) were obtained from Merck. Polyethersulfone (PES) membrane (pore size 0.1µm diameter) supplied by sterlitech, USA was used as the porous support. Millipore water® was used throughout the experiment. The feed gas containing CO_2/N_2 (20/80) and sweep gas Argon (99.99 % purity) were taken from Vadilal Chemicals Ltd. The Helium gas used in gas chromatography analysis was purchased from Jainex Gases Company, India.

2.2.2 Synthesis of Carboxymethyl Chitosan (CMC)

The synthesis procedure of CMC has been adopted from elsewhere [87]. Briefly, chitosan (10 g) was dispersed in isopropyl alcohol (300 ml) and NaOH (25 M) was added for alkalization. Further, monochloroacetic acid was added and stirred for 24 hours. A white precipitate was formed and washed by soxhlet method using methanol as the solvent. The final mass was dried in a vacuum oven at 40 °C to obtain dry CMC.

2.2.3 Development of CMC Membrane

CMC was dissolved (5 wt. %) in water at room temperature to prepare the casting solution. The undissolved particles and bubbles were removed from the solution using a centrifuge. The homogeneous solution was poured on a PES support and cast using a micron film applicator (GARDCO, Paul N. Gardner, USA). The cast membrane was kept inside a laminar air flow for evaporation of solvents for 12 hours and finally dried at 110 °C for 6 hours. The prepared membrane was then cut into a circular size of 45 mm diameter to fit in membrane module for CO_2 separation test as shown in **Figure 2.1**.

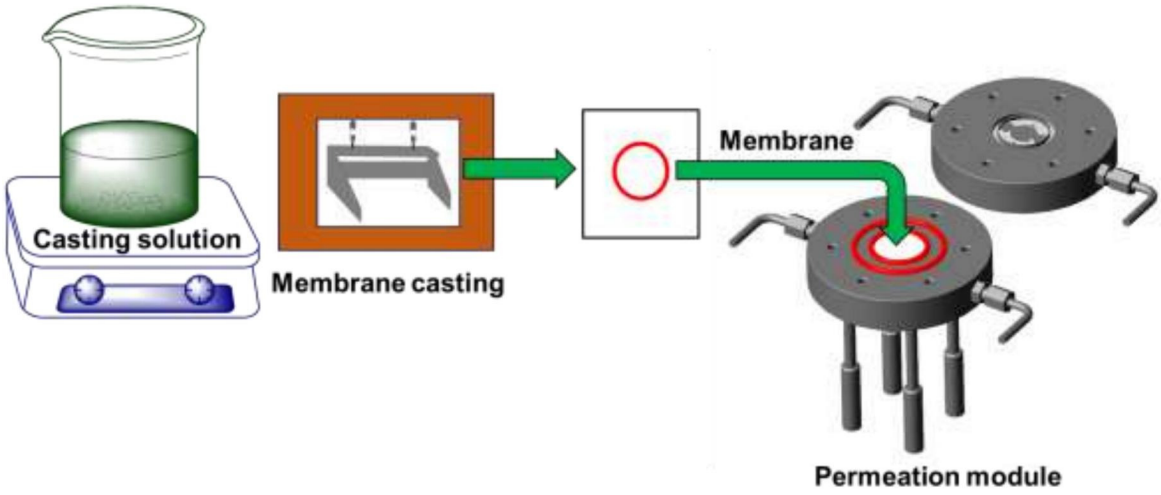

Figure 2.1 Fabrication of flat sheet membrane for CO_2 separation study.

2.2.4 Characterization Techniques

The efficient synthesis of CMC has been investigated by the proton nuclear magnetic resonance (NMR) spectrophotometer. The sample was first dissolved in D_2O and piped into the NMR tube so that it can be analyzed in the Bruker AM 400 spectrophotometer instrument. X-ray photoelectron spectroscopy (XPS) has been used to detect the elemental composition present in CMC membranes. XPS measurements were performed using a Thermo-Scientific ESCALAB Xi+ spectrometer equipped with a monochromatic Al Kα X-ray source (1486.6 eV) and a spherical energy analyser. The spherical energy analyser operates in the constant analyser energy (CAE) mode via the electromagnetic lens. The CAE for survey spectra is 100 eV and that for high-resolution spectra is 50 eV. Fourier transform Infra-red spectroscopy (FTIR) analysis was accomplished using attenuated total reflectance (ATR) mode (SHIMADZU, IR Affinity 1, Japan) to investigate the functional groups present in the membrane. The FTIR spectra were recorded by ranging the wave number range from 4000 to 1000 cm^{-1} with a 30 scan per sample. The top surface and cross-sectional view of the blend membrane were examined using field emission scanning electron microscope (FESEM), Zeiss, Germany, Model Sigma. The samples were coated with gold before loading into the FESEM instrument to avoid the charging effect. The images were then recorded at the voltage of 2-3 kV using in lens detector. The thermal stability of blended membranes was characterized by TGA/DTA, TG209 F1 Libra (Netzsch, Germany). The samples were analyzed from 30 °C to 450 °C at the heating rate of 10 °C per min under N_2 environment.

Moisture retention test was performed on a setup designed on a flat 3- neck round bottom flask as shown in **Figure 2.2a**. The glycerol-water mixtures of different compositions are used to maintain the relative humidity. The membrane samples were clinched above the solution and kept for 12 hours so that the membranes get saturated by holding moisture. Later, it was dried at 110 °C until it achieves constant weight. The % moisture retention (% W_R) by the membranes has been calculated using the relation:

$$\% W_R = (W_{wet} - W_{dry}) \times 100/W_{dry} \quad 2.1$$

Where W_{wet} = weight of the swelled membrane, W_{dry} = weight of the dried membrane. The degree of substitution of CMC was determined using the pH-metric titration setup as shown in **Figure 2.2b.** The equation used for the calculation purpose is mentioned below.

$$\text{Degree of substitution} = \frac{161 \times V_{NaOH} \times C_{NaOH}}{m_{CMC} - 58 \times V_{NaOH} \times C_{NaOH}} \quad 2.2$$

Where m_{CMC}, V_{NaOH} and C_{NaOH} are mass of CMC (g), volume and molarity of aqueous NaOH respectively. The respective molecular weights of glucosamine (chitosan skeleton unit) and carboxymethyl group are 161 and 58. Ostwald method was used to measure the viscosity of casting solutions by comparing the viscosity with water. The intrinsic viscosity [η] of the unknown solution will be obtained from the following relation [88].

$$[\eta] = \frac{4\eta_{sp}^{1.02} \ln \eta_r}{c^{1.01}(3\eta_{sp} + ln\eta_r)} \quad 2.3$$

Where η_{sp} is the specific viscosity and η_r is the relative viscosity obtained from

$$\eta_r = t/t_0 \quad 2.4$$

$$\text{and } \eta_{sp} = (1-\eta_r) \quad 2.5$$

Here, t, t_0 and c are the flow time of CMC solution, flow time of water and the concentration (g/mL) of CMC, respectively. Viscosity average molecular weight of CMC can be determined from Mark–Houwink–Sakurada (MHS) equation:

$$[\eta] = KM^{\alpha} \quad 2.6$$

Here, *K* and *α* are constants given for CMC as 7.92×10^{-5} and 1, respectively [89].

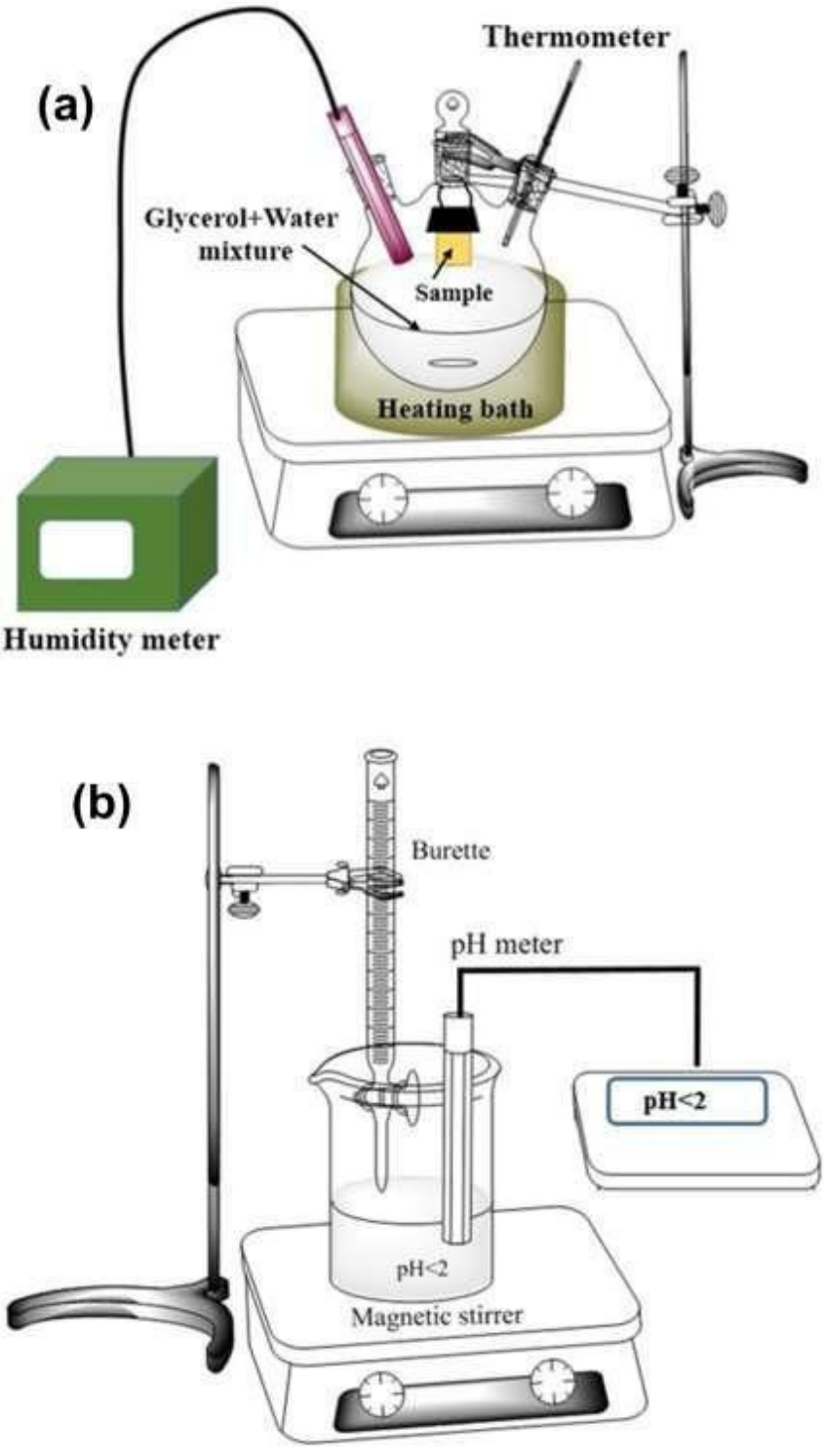

Figure 2.2 Laboratory scale set up for (a) moisture retention test (b) pH metric titration.

2.2.5 Gas Permeation Study

The membranes were positioned in a counter-current circular flat sheet module made of stainless steel to perform the gas permeation test. The membrane fitted module was housed inside a programmable temperature controlled hot air oven to study the temperature effect. The feed (20 % CO_2 and 80 % N_2) and sweep (Ar) gases were directed to the module in counter flow direction using two mass flow controllers (AALBORG) as presented in **Figure 2.3**. The gas flow rate were maintained at 40 mL/min and 35 mL/min for feed and sweep gas, respectively. The pressure inside the module was maintained with the help of two different back-pressure regulators. The different humidity of the feed and sweep side gas were maintained by providing controlled water flow rate via the HPLC pumps (Shimadzu, LC 20AD, Japan). The humidified gases were dehumidified again when they came out from the module as well as from oven through water knockout. The flow rates of retentate and permeate gases released from the module were measured by bubble flow meter. The compositions of permeate and retentate were studied by Varian 450 Gas Chromatograph (GC) having thermal conductivity detector (TCD). The individual readings of the permeation through membrane were recorded after 8 hours at a specific pressure, temperature, and water flow rate. Throughout the experiment the absolute pressure exerted was maintained constant at 2 bar and 1.21 bar on the feed gas side and sweep gas side, respectively. Similarly, the water supplied rate to the feed side was set fixed at 0.03 mL/min. The gas permeance can be defined as follows [90]

$$\frac{P_i}{l} = \frac{F_i}{\Delta p_i} \qquad 2.7$$

Where, permeability is denoted by P_i [Barrer, 1 Barrer = 10^{-10} cm^3 (STP) cm/ (cm^2s cmHg)] and i corresponds to the molecule CO_2. 'l' is the active layer thickness (cm). Pi/l is the permeance [GPU, 1 GPU = 10^{-6} cm^3 (STP)/(cm^2s cmHg)] of i, F_i is the flux [10^{-6} cm^3(STP)/cm^2s] of i and Δp_i is the differential partial pressure. Similarly, selectivity is given by $\propto_{ij} = \frac{y_i/y_j}{x_i/x_j}$ where, x and y represent the mole fractions in the retentate and permeate, respectively. Here, CO_2 and N_2 are represented by i and j, respectively. The details calculation procedures of CO_2 and N_2 flux, permeability and permeance along with CO_2/N_2 selectivity were discussed in appendix section (**Appendix 2**).

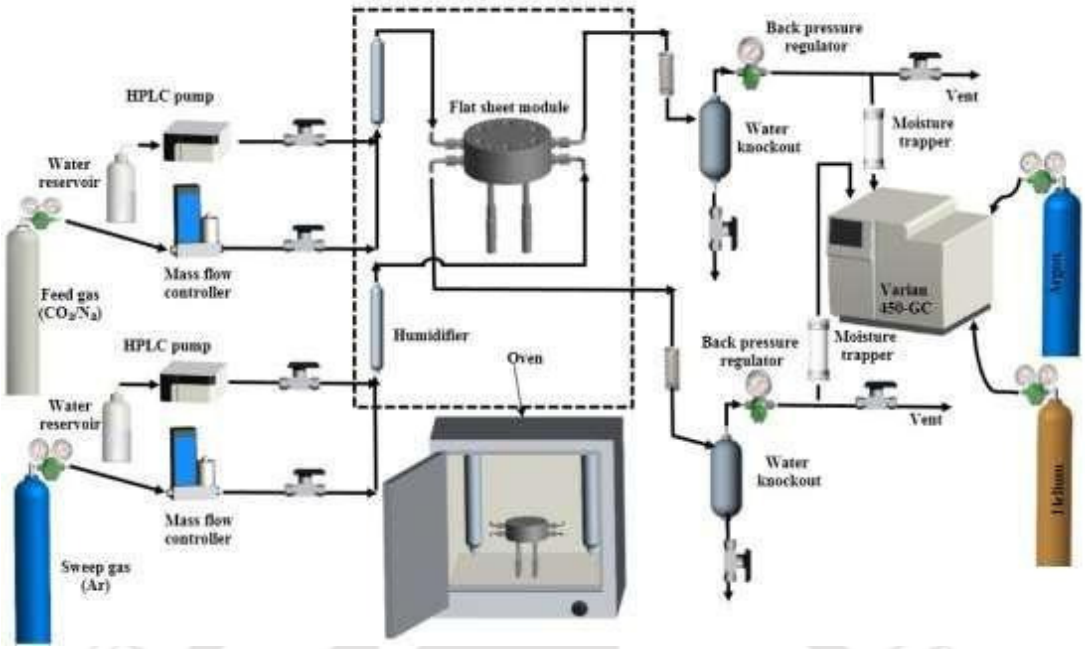

Figure 2.3 Schematic representation of gas permeation set up.

2.3 Results and Discussion

2.3.1 Degree of Substitution and Molecular Weight of CMC

The degree of substitution in CMC was determined by the pH-metric titration performed at room temperature. The pH value recorded is shown in **Figure 2.4** with respect to the different volumes of 0.1 M NaOH consumed. Putting the values of V_{NaOH}, C_{NaOH} and m_{CMC} as 0.0074 L, 0.1M and 0.2 g, respectively we obtained the degree of substitution as 75.84 %. MHS equation was then used to determine the viscosity average molecular weight of the prepared CMC. Taking an aqueous solution of 0.5 weight percent concentrations a flow time of 1456 s was obtained from Ostwald viscometer. Using the MHS equation the viscosity average molecular weight for the prepared CMC was obtained as 3.54×10^3 KDa.

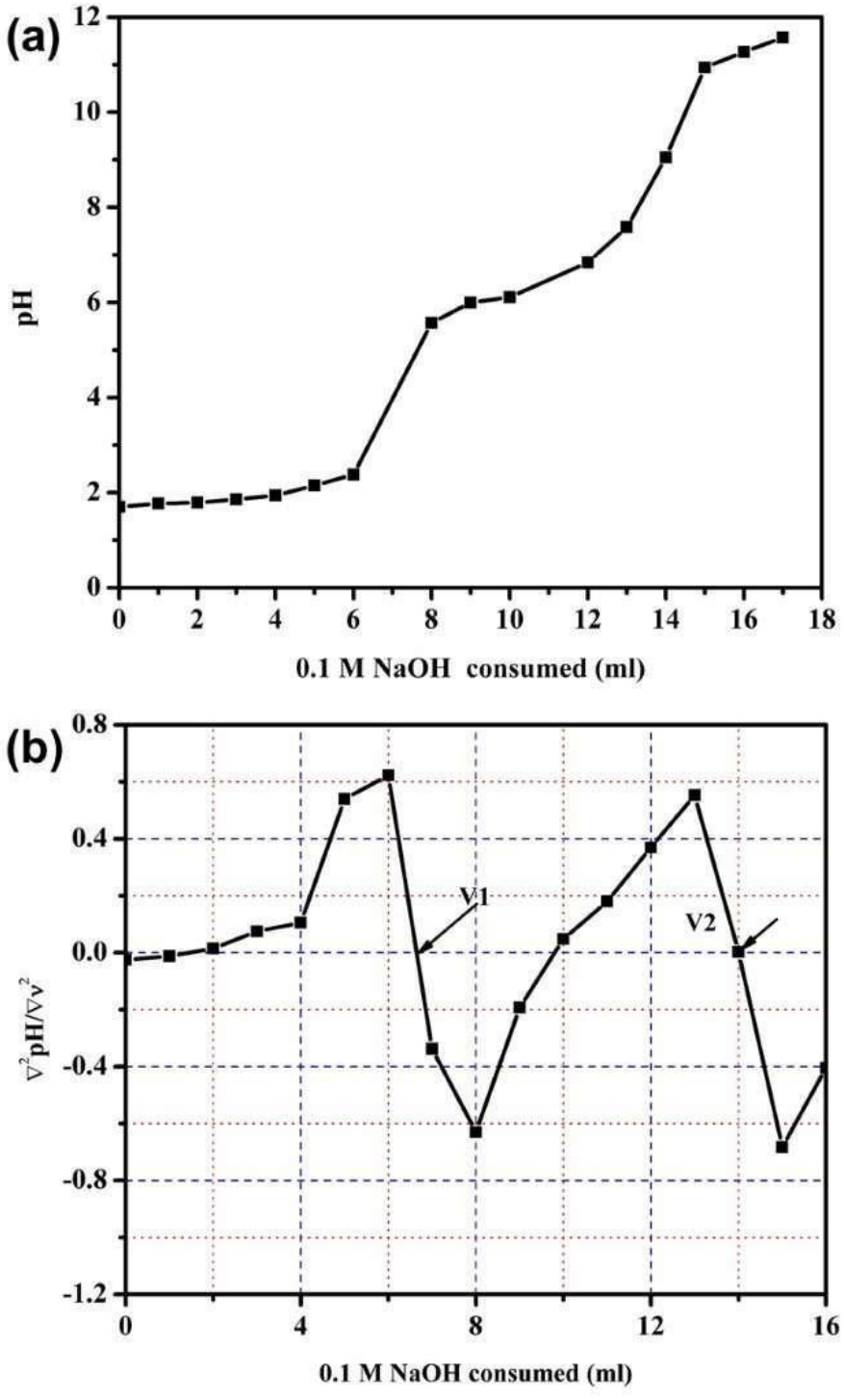

Figure 2.4 pH-metric titration curve of CMC sample (a) volume of NaOH consumed vs pH (b) Differential graph of titration curve

2.3.2 Spectroscopic Analysis

The ^{1}H-NMR spectra as shown in **Figure 2.5** validates the successful synthesis of CMC which matches available literature as well. The signal at 1.97 ppm (d) indicates the CH_3 of acetamide groups [87]. The signals at 2.63 ppm can be ascribed to the H-atoms of C2 of the glucosamine ring which is shown as peak c in the spectrum. The signals in the range of 3.26–3.90 ppm point to H-atoms of C3, C4, C5 and C6 of the glucosamine ring; and the signal at 4.34 ppm is due to the CH_2 of OCH_2COONa groups. From the integrals of NMR peaks we obtained the degree of substitution as 76.45 % which is nearly similar to the value obtained from pH-metric titration.

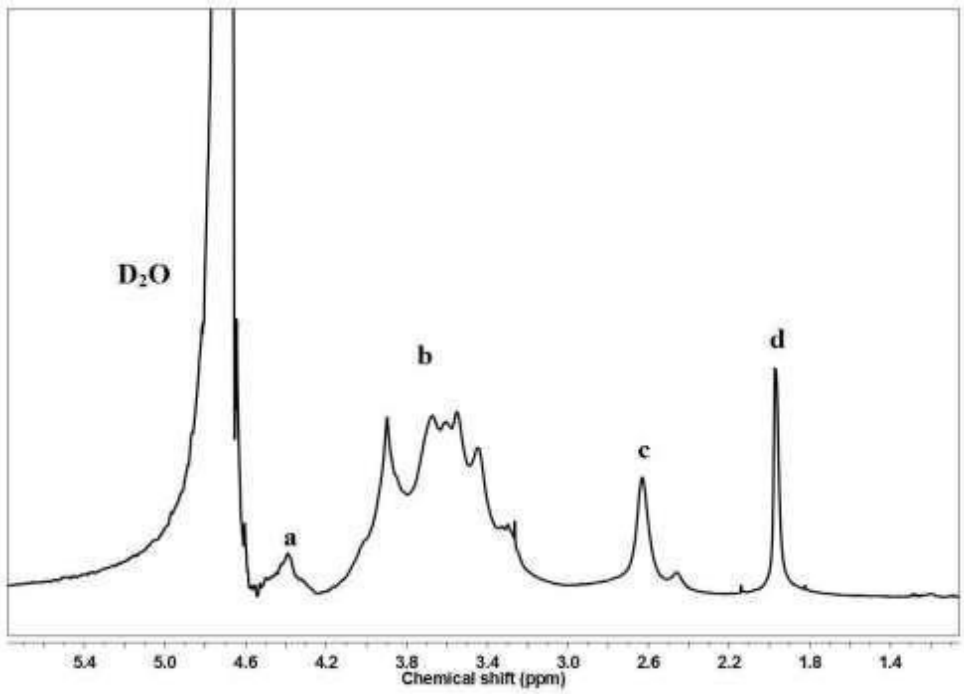

Figure 2.5 ^{1}H NMR spectrum of CMC powder in D_2O at room temperature.

XPS analysis was implemented to investigate the chemical composition of CMC film as shown in **Figure 2.6**. The deconvolution of carbon peak (C1s) showed the major peak at binding energy 284.6 eV which was due to the presence of C-C or C-H bond of fundamental structure of CMC and the peaks at binding energies 286.5, 287.6 and 288.6 attributed to the presence of C-N, C-O-C of carboxymethyl group and O-C=O of carboxylate, respectively. The presence of C-O-C and O-C=O bonds were also confirmed by the deconvolution of oxygen peaks. The peak fitting of O1s indicated the two peaks at binding energies 531.3 and 532.5 eV. Similarly the peak at 1071.3 eV indicated the

presence of sodium. The deconvoluted nitrogen (N1s) peak of CMC ascribed the presence of primary and secondary amine at the binding energies 400.3 and 399.1 eV. The major peak at 400.3 eV indicated the synthesis of O-substituted CMC positively.

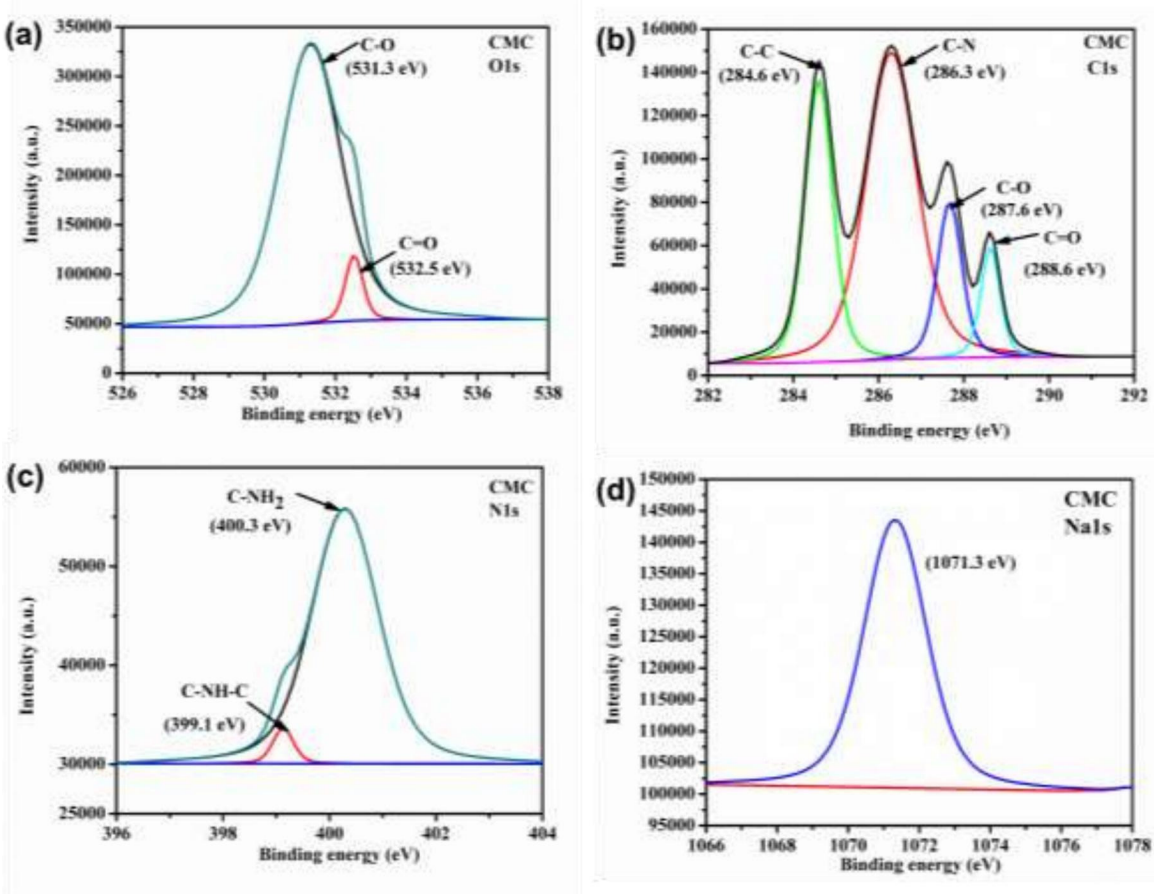

Figure 2.6 The high resolution XPS spectra of CMC (a) O1s (b) C1s (c) N1s (d) Na1s.

FTIR analysis was performed to detect the functional groups present in the blend membranes (**Figure 2.7a**). The wide and weak peaks detected at 3320 cm^{-1} was due to the stretching vibration of the N-H group of CMC. The peak noticed at 1412 and 1377 attributed to the C=O of –COONa symmetric stretching and C-N stretching of CMC.

XRD gives the idea about crystalline behavior of a membrane which is an important component related to gas permeation. The crystallinity increases the resistance of the membrane and restricts the gas sorption rate of the membrane. There are three forms of chitosan structure namely, noncrystalline, hydrated crystalline, and anhydrous (”annealed”) crystalline. Among all, the presence of hydrated crystalline structure has been

identified in the prepared CMC membrane as the XRD spectra of CMC membrane showed a characteristic peaks around 2θ = 9.8°. Besides, the broad peak (**Figure 2.7b**) at around 2θ= 20° indicated the existence of an amorphous structure. Whenever moisture is supplied to the membrane, primitively it interacts with the amorphous region of the membranes and forms H-bonding causing swelling with which membrane performance is associated.

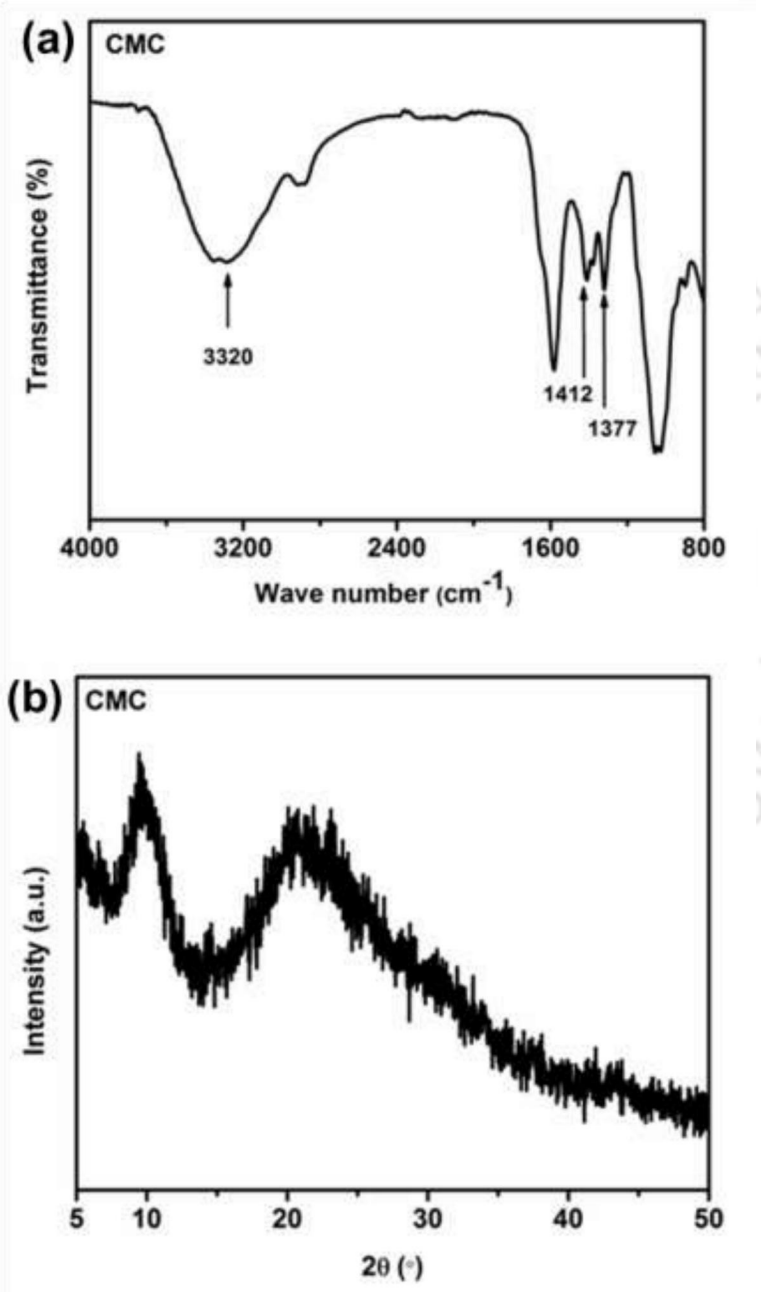

Figure 2.7 (a) FTIR and (b) XRD spectra of CMC membrane.

2.3.3 Microscopic Analysis

The surface morphologies of the membranes were observed by (FESEM) images as shown in **Figure 2.8 (a-d)**. The polyethersulfone (PES) is a porous membrane (**Figure 2.8a**) having 0.1-micron pore diameter which gives mechanical support to the active layer. The formation of a dense CMC skin on the PES support is shown in **Figure 2.8c**. The magnified cross sectional view suggested that there was no seepage of the polymer solution through the support pores (**Figure 2.8d**). The pore filling by the casting material causes increase of active layer thickness which directly affects the gas permeation.

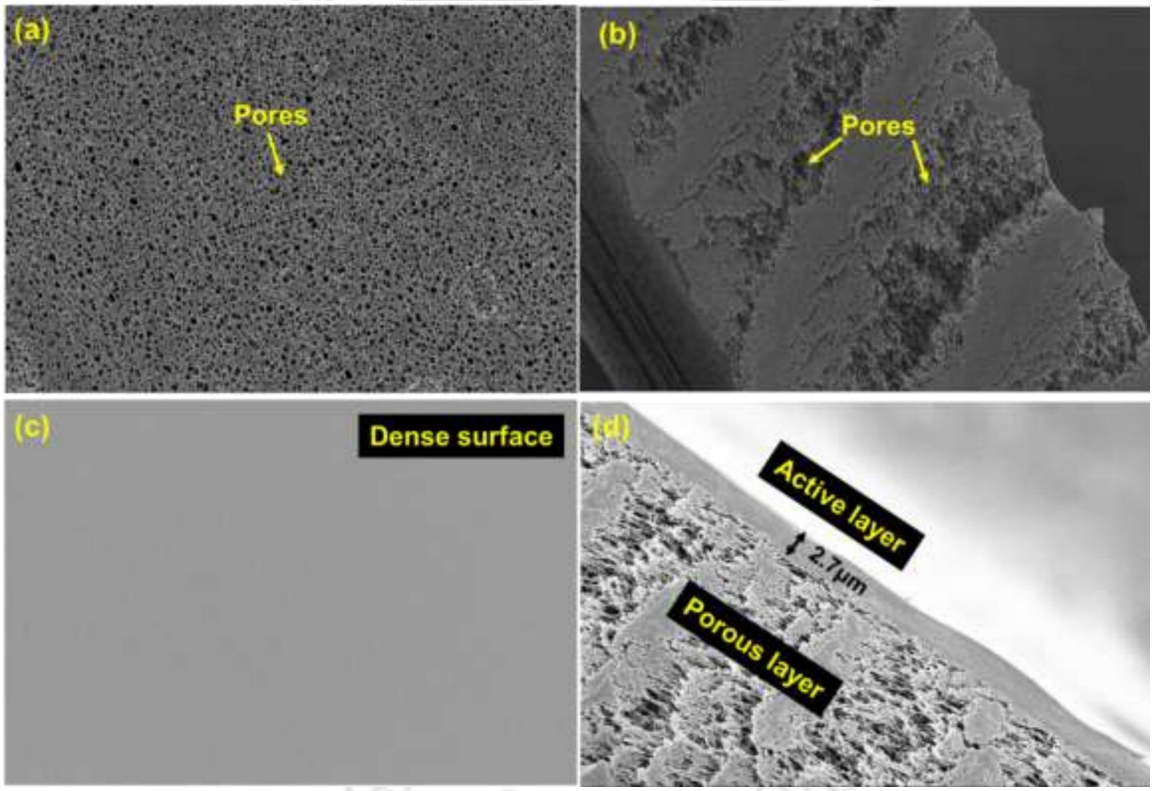

Figure 2.8 FESEM images of (a) PES top surface (b) PES cross- section (c) CMC top surface (d) CMC cross section

2.3.4 Moisture Retention Test

Water plays an important role in CO_2 separation which can be described in three aspects (1) Swelling increases the flexibility of the membrane and allows more gas to pass through by reducing the mass transfer resistance, (2) CO_2 reacts with amine of CMC in presence of moisture due to which high CO_2 flux is achieved and (3) CO_2 can pass through the water

molecule present in the matrix. The water molecule hydrolyses the zwitterion and carbamate ion during CO_2 - amine reaction and accelerates the formation of carbamate ion and redevelopment of amine carrier. Varying the relative humidity (RH), the water retention percentage is plotted for CMC membrane (**Figure 2.9**). The hydrophilic CMC membrane showed 10 % water retention at 20 % RH which was sparingly increased up to 60 % RH. As it reached 80 % RH, the water holding capacity increased to 44 %. Subsequently, a sharp upswing of % W_R was observed beyond 80 % RH and it displayed 345 % W_R at 100 % RH. The % W_R phenomenon can be explained on the basis of Flory-Huggins theory which suggests that the swelling free energy of mixing is associated with two basic entropy factors; the conformation of polymer chains and the contact between polymer chains and the solvent. At low relative humidity, swelling occurs due to polymer conformation. At this point, the chain relaxation starts and swelling starts by holding some moisture in its matrix. Later the polymer-solvent interaction becomes significant at higher relative humidity and the water retention capacity drastically increases after crossing a critical relative humidity.

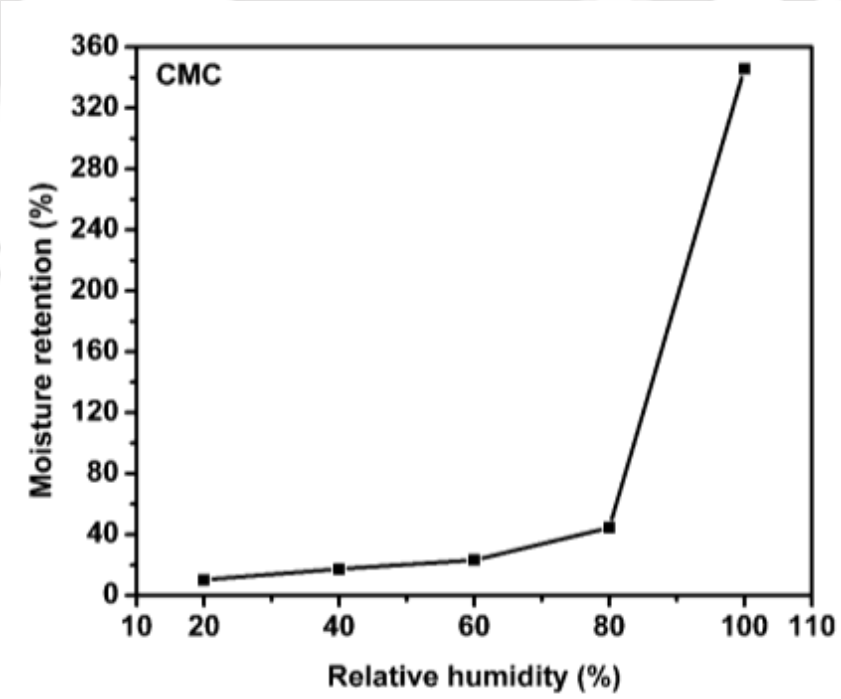

Figure 2.9 Moisture retention behavior of CMC membrane at different RH (%)

2.3.5 Thermal Stability

The thermal stability of CMC membrane was analysed through the TGA graph shown in **Figure 2.10**. The CMC membrane showed three stages mass loss and initial stage weight loss was recorded in the range of 30 to 100 °C indicating the loss of the moisture held by the matrix. The second stage weight loss witnessed in the range of 248-284 °C was due to the dehydration of saccharide ring and breakage of glycosidic bond present in the main polymer chain. The slight downturn observed after 340 °C corresponds to the complete degradation of polymer matrix.

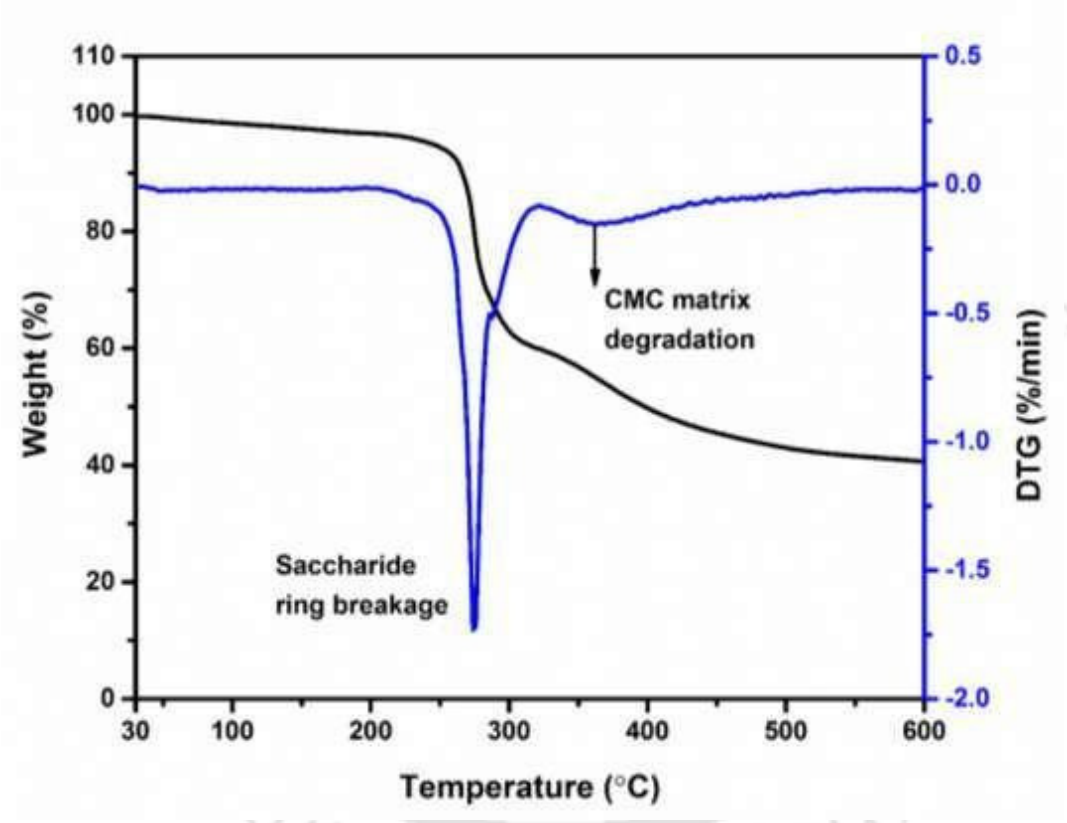

Figure 2.10 TGA graph of CMC membrane (preliminary drying at 100 °C)

2.3.6 Gas Permeation Study

2.3.6.1 Effect of temperature

The effect of temperature on CO_2 separation performance has been studied in the range of 60 to 120 °C for CMC membrane at sweep/feed water flow ratio of 1.67 and feed absolute pressure of 2 bar. The CO_2 permeance continuously increased from 60 to 80 °C as shown in **Figure 2.11**. This may be due to the fact that rise in temperature enhances the reaction

rate between CO_2 and amines in the presence of moisture, resulting prompted overall CO_2 facilitated transport. As the temperature reached 90 °C, a minor decrease in CO_2 permeance was observed. However, further increase in temperature drastically reduced the CO_2 separation performance due to decreased water retention ability of the membrane which lessens the facilitated transport mechanism [41]. Also, the membrane becomes stiffer with increase in temperature as water molecule evaporates from the active layer and reduces the membrane flexibility. The reduced membrane flexibility hinders the gas molecules to pass through the membrane which resulted in a drop in the overall permeance. The CO_2 permeance at 120 °C was 2.9 GPU which is 91.7 % lower than the CO_2 permeance at 80 °C. Although the CO_2 permeance was maximum at 80 °C, CMC membrane showed the highest CO_2/N_2 selectivity at 90 °C. The CO_2/N_2 selectivity at 60 °C was 29 and improved by 70 % when the temperature reached to 90 °C. Both CO_2 and N_2 permeance start decreasing after 80 °C, but the decrease in N_2 permeance is more than the CO_2 permeance which resulted in an increase in CO_2/N_2 selectivity at 90 °C. Therefore, it can be noted that CMC membrane contributes to better separation performance when the temperature ranges from 80 and 90 °C in terms of permeance and selectivity.

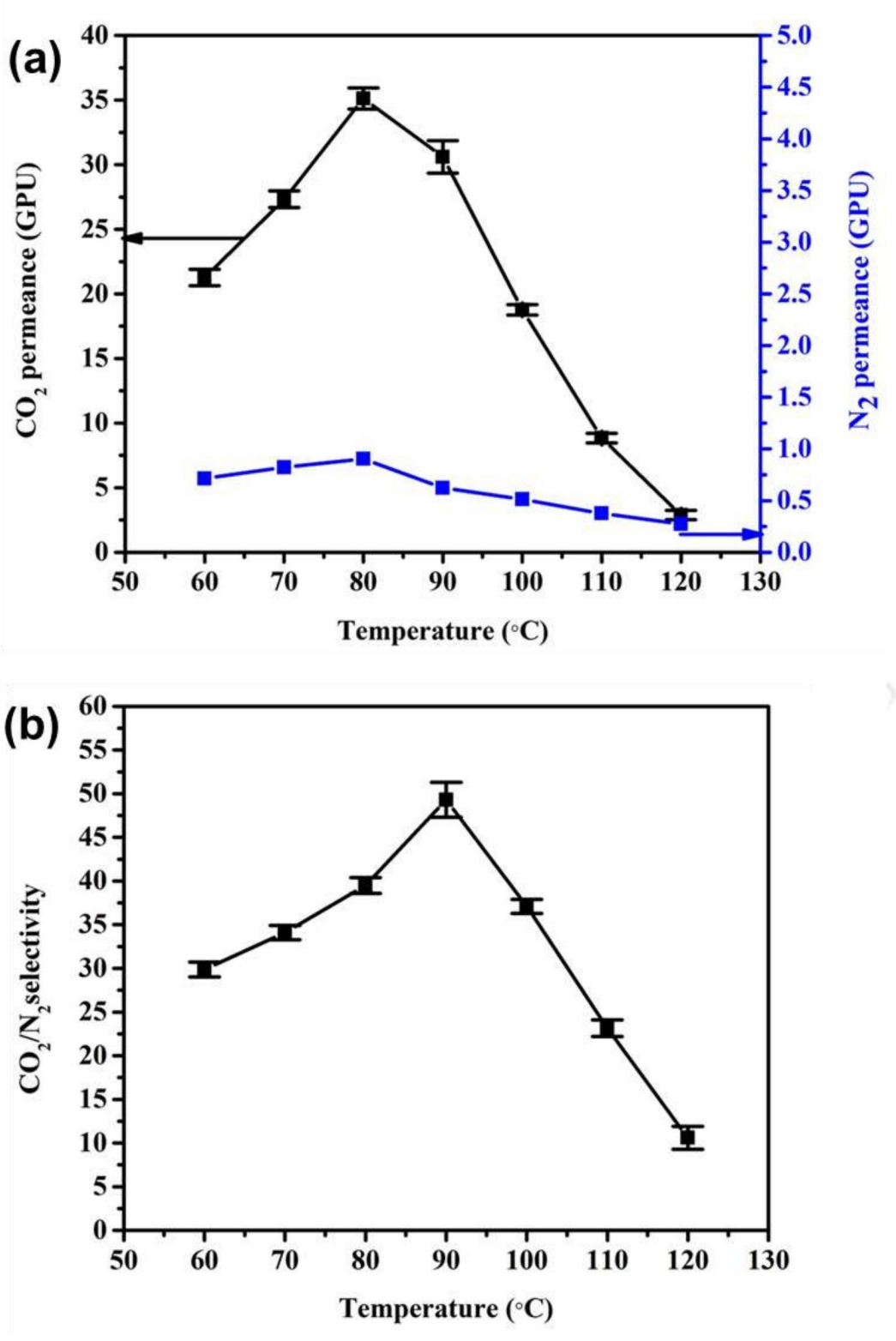

Figure 2.11 Effect of temperature on (a) CO_2 and N_2 permeance and (b) CO_2 /N_2 selectivity for CMC membrane at sweep/feed water flow ratio =1.67

2.3.6.2. Effect of water flow ratio

The effect of sweep/feed water flow ratio on CO_2 separation performance for CMC membrane is shown in **Figure 2.12**. The sweep water flow ratios were varied from 0.33 to 3 at temperature 80 °C and an absolute pressure of 2/1.21 bar (feed/sweep).

The CO_2 permeance increased with an increase in water flow amount from 0.33 to 1.67. The CO_2 permeance obtained at 0.33 sweep/feed water flow ratio was 12.3 GPU. A steep increase in the performance was observed after the sweep/feed water flow ratio reached 1. The increase in the water flow ratio from 0.33 to 1.67 offered 195 % increase in CO_2 flux for CMC membrane. This indicates that the higher flow rate in sweep side than feed side provides a positive contribution towards CO_2 separation. The adequate supply of water from the sweep side helps in holding of moisture inside the membrane matrix. In addition, the increased quantity of moisture improves flexibility of the membrane. The water retained by the membranes induce flexibility by plasticization effect and the flexibility reduces the mass transfer resistance of the membrane. This directly takes part in upgrading of CO_2 permeance. Moreover, the higher sweep side water content dilutes the concentration of permeated CO_2 and increases the driving force for the CO_2 transport. After 1.67 sweep/feed water flow ratio, no further rise in CO_2 permeance is observed. This may be due to the carrier saturation and competitive sorption of N_2 gas into the active layer. Since N_2 molecules follow solution diffusion mechanism, the N_2 permeance increases continuously with the increase in water flow rate. This resulted in the decrease in CO_2/N_2 selectivity after 1.67 water flow ratio.

The gas permeation performance of CMC membrane was compared with some other similar works. The CMC membrane showed two times better performance than the pure chitosan membrane. Previously the pure CMC membrane was studied at room temperature. In this work, the membrane was examined at different temperatures and exhibited a pretty good performance than the available literature.

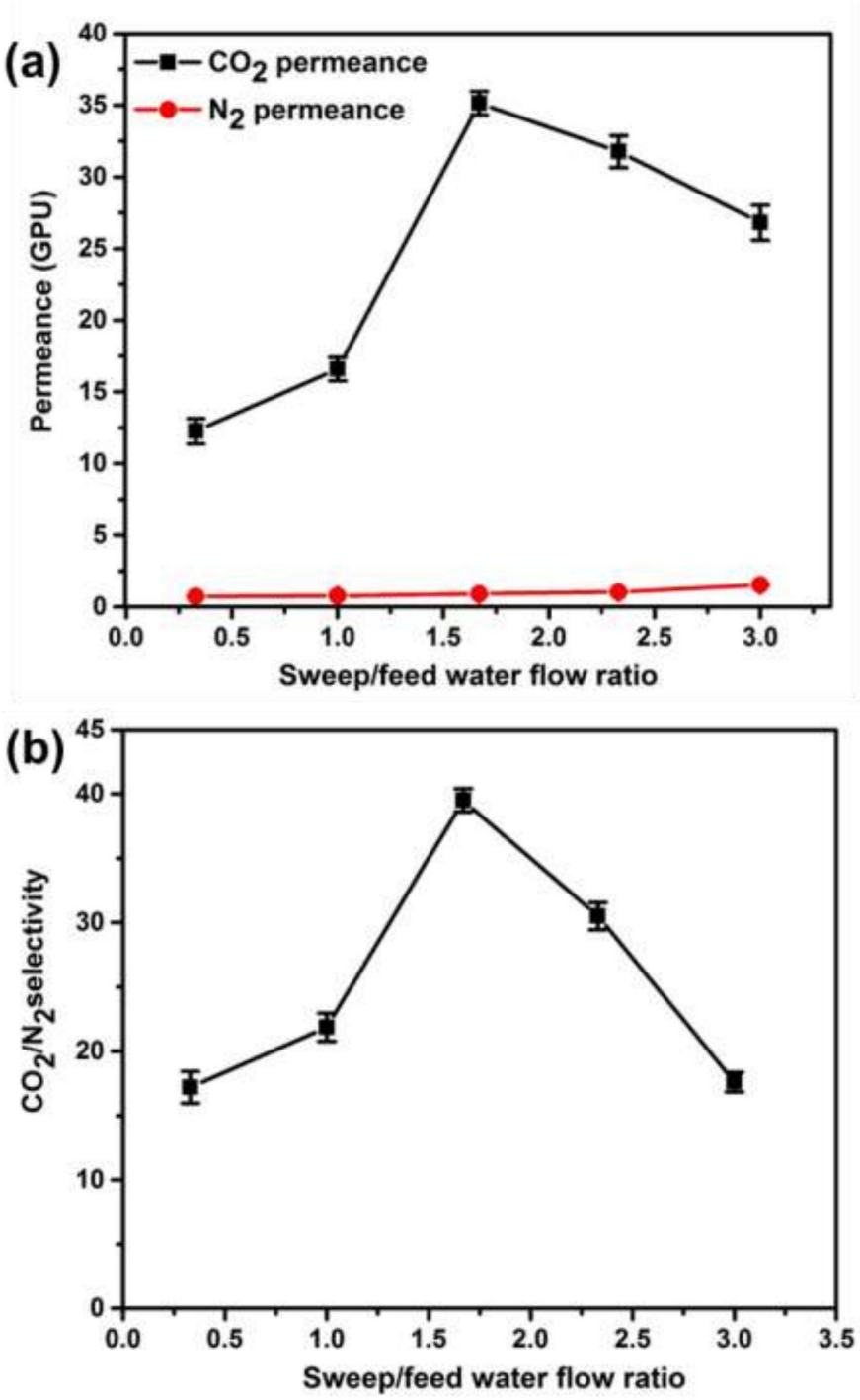

Figure 2.12 Effect of water flow ratio on (a) CO_2 and N_2 permeance and (c) CO_2 /N_2 selectivity for CMC membrane at 90 °C

2.4 Conclusions

The successful synthesis of CMC was established by the NMR analysis. The development of CMC membrane was verified with the help of XPS, FTIR and XRD spectra. The CMC membrane was fabricated by solvent evaporation method and the defect free morphology of the membrane was investigated with the help of microscopic analysis. The % W_R of CMC membrane was found ~ 345 % at 100 % RH which indicated the abundant moisture retention ability of the active layer. The thermal behaviour shown by CMC active layer implies that it can be an effective CO_2 selective membrane. The optimum performance of CO_2 separation was obtained for CMC membrane at 80 °C with supplied sweep/feed water flow ratio of 1.67 and feed pressure of 2/1.2 bar (feed/sweep) presenting a significant increase of CO_2 permeance (~35 GPU) and CO_2/N_2 selectivity (~39) as compared to that of chitosan membrane.

CHAPTER 3

Synthesis and Characterization of Small Molecule Carrier Blended Carboxymethyl Chitosan Membrane for CO_2 Separation

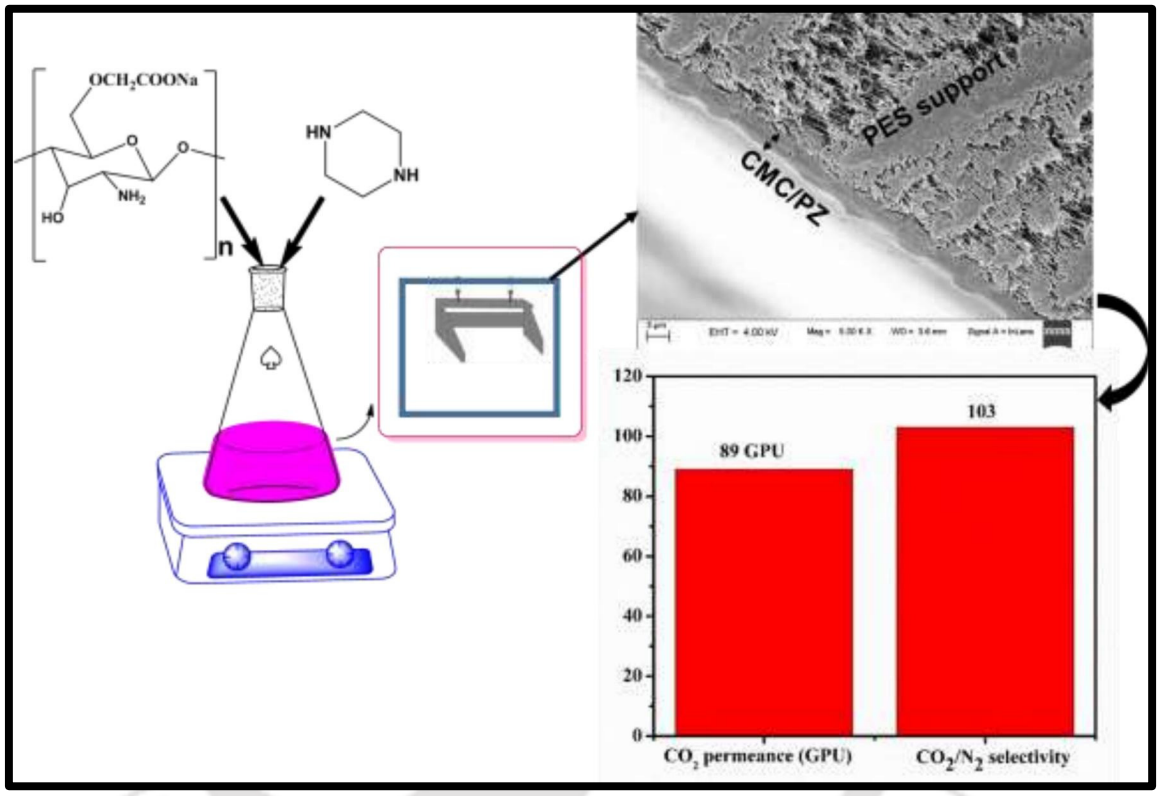

Overall representation of CMC/PZ membrane fabrication and gas permeation result.

CHAPTER 3

Synthesis and Characterization of Small Molecule Carrier Blended Carboxymethyl Chitosan Membrane for CO_2 Separation

*In this study, CMC has been blended with a mobile carrier, piperazine (PZ), to improve the facilitated transport of CO_2 by increasing the carrier content. Here, PZ plays the role of mobile carrier, amine promoter as well as physical cross-linker for CMC. PZ blended membranes can hold surplus moisture inside the matrix which directly helps in getting better CO_2 permeance and selectivity as compared to pristine CMC. This work is scientifically acknowledged in "**Separation and Purification Technology**".*

3.1 Introduction

The enrichment of carrier content in the membrane can be done by adopting various mechanisms namely, copolymerization, crosslinking, blending, etc., amongst which, the blending of the amines with polymers is an easy, simple and cost-effective way to increase the amine content in the matrix. Mobile carriers like monoethanolamine (MEA) [45], diethanolamine (DEA) [91], ethylenediamine (EDA) [92], etc. were introduced in the CO_2 selective membranes. However, these membranes were found to be unstable due to the high volatility of the amines. In contrast, piperazine (PZ) has lower volatility and it acts as amine promoter. The presence of two secondary amine groups reduce the crystallinity of these membranes and improves permeation performance [93]. The structure of PZ has been included in **Figure A1.1b, Appendix 1.**

Nevertheless, limited work has been reported so far on CO_2 separation using CMC membrane at temperature higher than the room temperature. In a novel approach, we have made an effort to improve the facilitated transport of CO_2 by increasing the carrier content by adding the small amine molecule such as PZ with CMC. The CO_2 molecule first reacts with amine (RR′NH) to form zwitterions as intermediates which are then deprotonated by another amine or water by forming carbamate ion as discussed in **Chapter 1**. Thus in CMC/PZ system CO_2 transports via formation of carbamate and bicarbonate complexes.

3.2 Experimental Section

3.2.1 Materials

Carboxymethyl chitosan is prepared in our laboratory as described in **Chapter 2**. Piperazine (PZ) was purchased from Merck and polyethersulfone (PES) membrane (pore size 0.1μ) supplied by Sterlitech, USA was used as porous support. Millipore water® obtained from the analytical laboratory of the department of Chemical Engineering, IITG was used throughout the experiment. The feed gas containing CO_2/N_2 (20/80) and sweep gas Argon (99.99 % purity) were taken from Vadilal Chemicals Ltd. The Helium gas used in gas chromatography analysis was purchased from Jainex Gases Company, India.

3.2.2 Membrane Fabrication

The CMC powder was dissolved (5 wt. %) in water at room temperature to prepare the control solution. The undissolved particles and bubbles were removed from the solution with the help of a centrifuge. Desired membranes were prepared by blending PZ with CMC varying the PZ wt. % like 80 % CMC + 20 % PZ (PZ20), 70 % CMC + 30 % PZ (PZ30) and 60 % CMC + 40 % PZ (PZ40). The homogeneous solutions were fabricated onto the PES support to get the required membranes as discussed in **Chapter 2**.

3.2.3 Characterization Techniques and Gas Permeation Set Up

The instruments used for FTIR, XPS, FESEM and TGA analysis are same as mentioned in **Chapter 2**. Similarly, the moisture retention test set up and gas permeation set up have been elaborated in the same chapter. Additionally, the atomic force microscopy (AFM) analysis was done to record the high resolution images of the membrane top surface in Innova AFM (Innova, Bruker). The tapping mode is used at a scan rate 0.8 Hz.

3.3 Results and Discussion

3.3.1 Spectroscopic Analysis

The formation of PZ blended CMC active layer was investigated with the help of XPS spectra as shown in **Figure 3.1 (a, b, c, d)**. The nitrogen peak deconvolution of PZ20 membrane showed three significant peaks at 400.3, 399.1 and 401.0 eV which specified the presence of tertiary amine along with the primary and secondary amines, respectively

(**Figure 3.1b**). The leading N1s deconvoluted peak was found at 399.1 eV corresponded to the secondary amine of PZ [42]. The peak obtained for tertiary amine is may be due to the formation of weak H-bond between PZ and amine of CMC. The deconvolution of C1s, O1s and Na1s peaks of PZ20 membrane shows the similar nature as CMC membrane (**Figure 3.1. a,c,d**).

FTIR analysis was performed to detect the functional groups present in the blend membranes. The PZ blended membranes possess few extra peaks along with the peaks corresponding to the functional groups of CMC indicating the presence of PZ with CMC as shown in **Figure 3.2**. The symmetrical stretching frequency of the CH_2 group in PZ observed at 2853 and 2914 cm^{-1} [47]. The symmetric and asymmetric N-H stretching vibrations of PZ are assigned to 3360 and 3288 cm^{-1}. These two peaks are not distinct in PZ20 whereas in PZ30 and PZ40 it is clearly visible. This result attributes that all the PZ molecules of PZ20 formed H-bonds with the primary amine of CMC but in PZ30 and PZ40 excess molecules remain as free PZ [93]. The symmetric CNH deformation vibration and the asymmetric C-N stretching band of PZ are assigned to 1475 $cm^{-1}$and 1253 cm^{-1}, respectively [47].

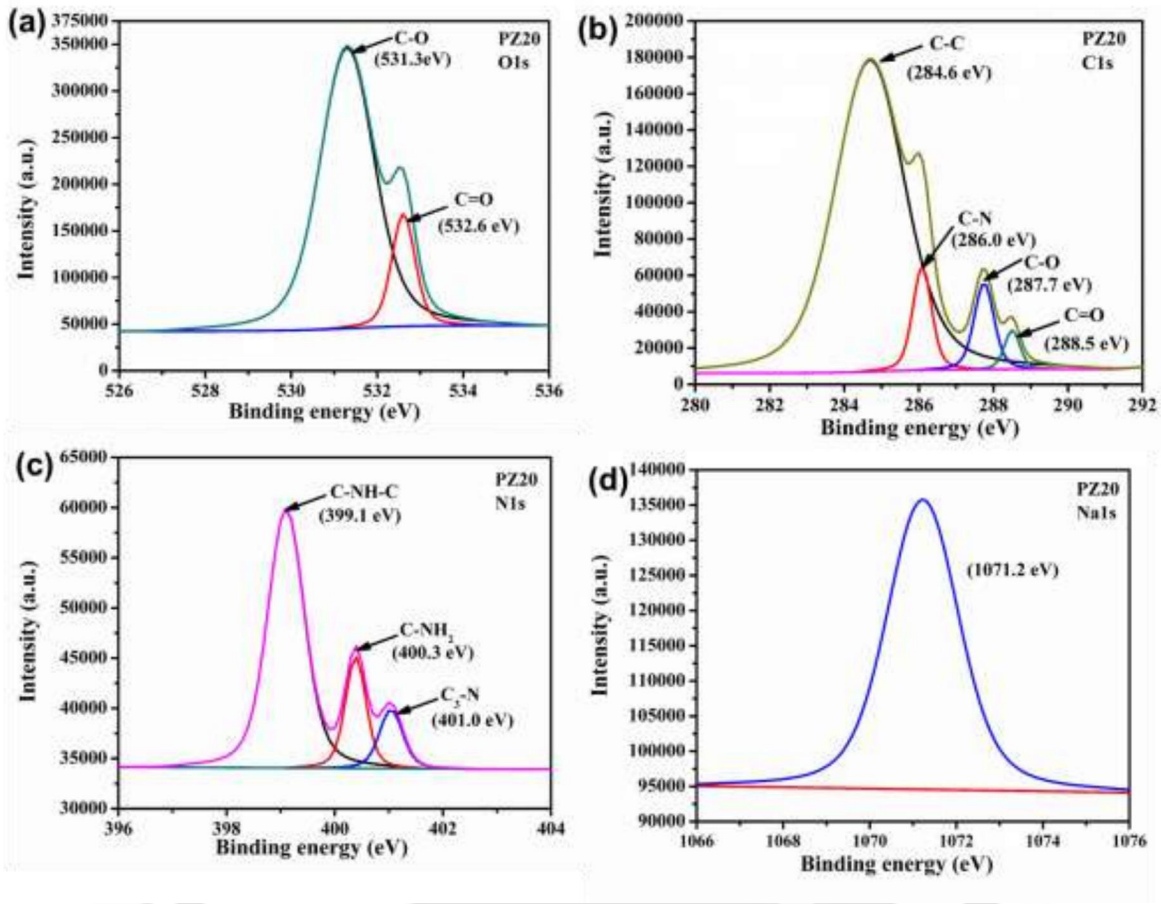

Figure 3.1 The high resolution XPS spectra of PZ20 (a) O1s (b) C1s (c) N1s (d) Na1s.

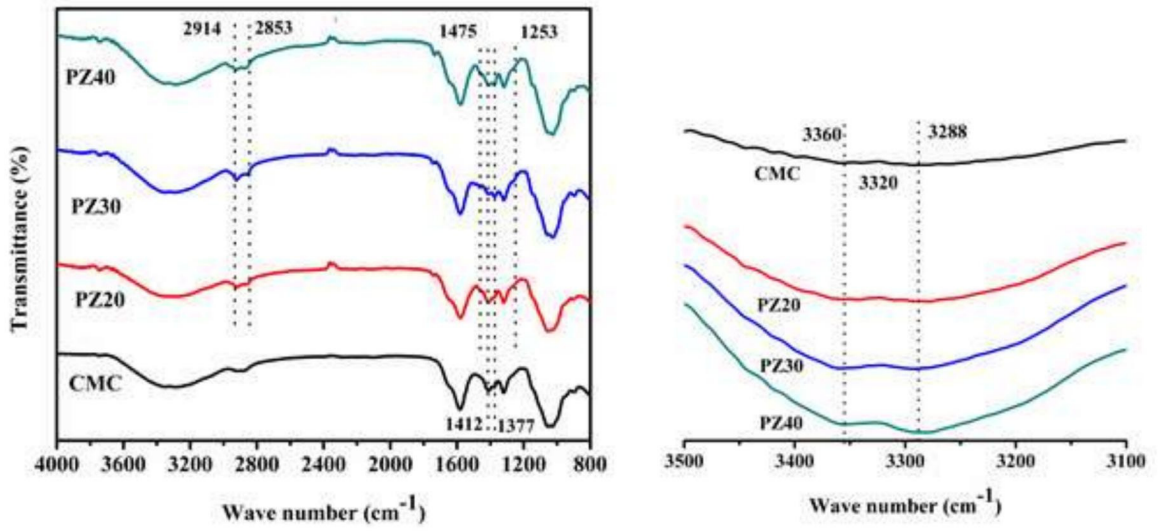

Figure 3.2 FTIR spectra of CMC and CMC/PZ blend membranes.

3.3.2. Moisture Retention Ability

Varying the relative humidity (RH), the water retention percentage is plotted for the membranes (**Figure 3.3**). The hydrophilic CMC membrane showed 10 % water retention at 20 % RH which was sparingly increased up to 60 % RH. As it reached 80 % RH, the water holding capacity was increased to 44 %. Subsequently, a sharp upswing of water retention % was observed beyond 80 % RH and it displayed 345 % water retention at 100 % RH. Similarly, the PZ blended membranes also followed the identical trend as CMC. The membranes showed 384 % (PZ20), 423 % (PZ30) and 444 % (PZ40) water retention at 100 % RH. Since, the PZ present in the matrix increases the polymer-solvent interaction, the water holding capacity also increases as compared to the CMC membrane. The water retention capacity of the membranes pursue the trend CMC < PZ20 < PZ30 < PZ40 which indicates that swelling increases with an increment of PZ content.

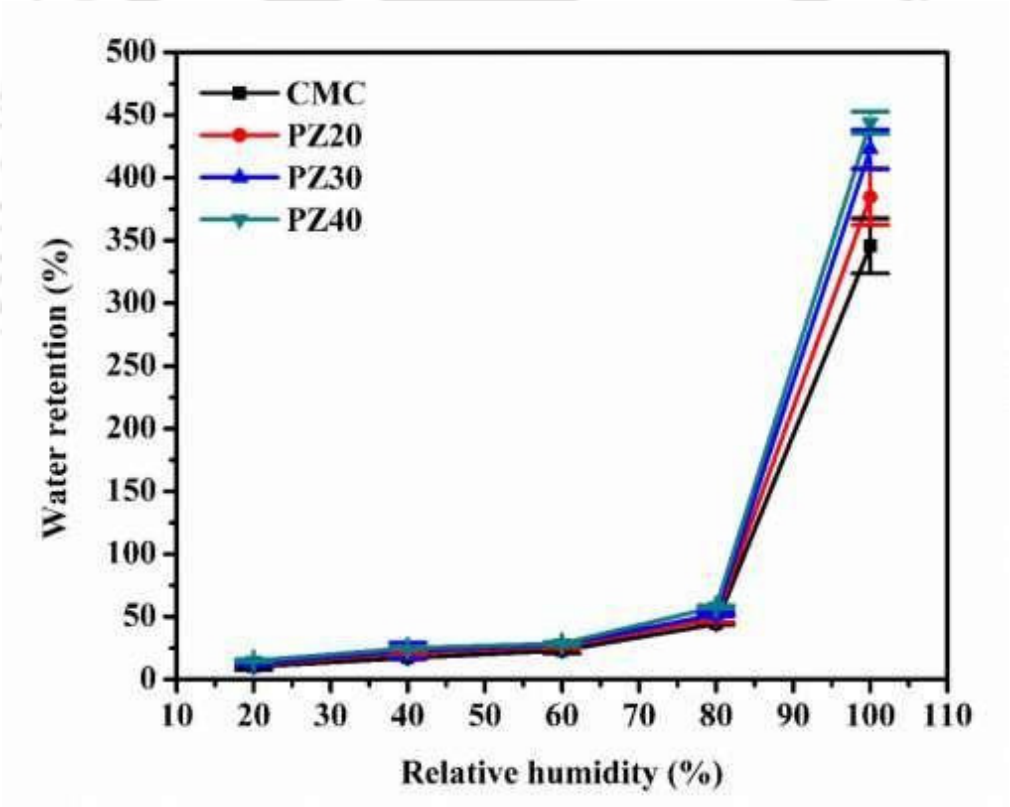

Figure 3.3 Water retention behavior of CMC, PZ20, PZ30 and PZ40 membranes at different RH % at room temperature.

3.3.3 Microscopic Analysis

The surface morphologies of the membranes were observed by (FESEM) images as shown in **Figure 3.4** and **Figure 3.5**. The image obtained for the top surfaces of the prepared membranes, provides the information of smooth dense layer formation for CMC and rough surfaces for PZ blended CMC membranes. The membrane roughness is also clearly visible in AFM images as shown in **Figure 3.6**. PZ being a smaller molecule it diffuses into the polymer entanglements easily and forms H-bond with the amino group of CMC. The top surface took for PZ20 denotes the appropriate distribution of PZ in the matrix. The excess blending of PZ with CMC supplements an accumulated PZ layer on the membrane surface as spotted in the FESEM images. The aggregated PZ particles instead of improving the CO_2 separation, it hampers the movement of the gas molecules.

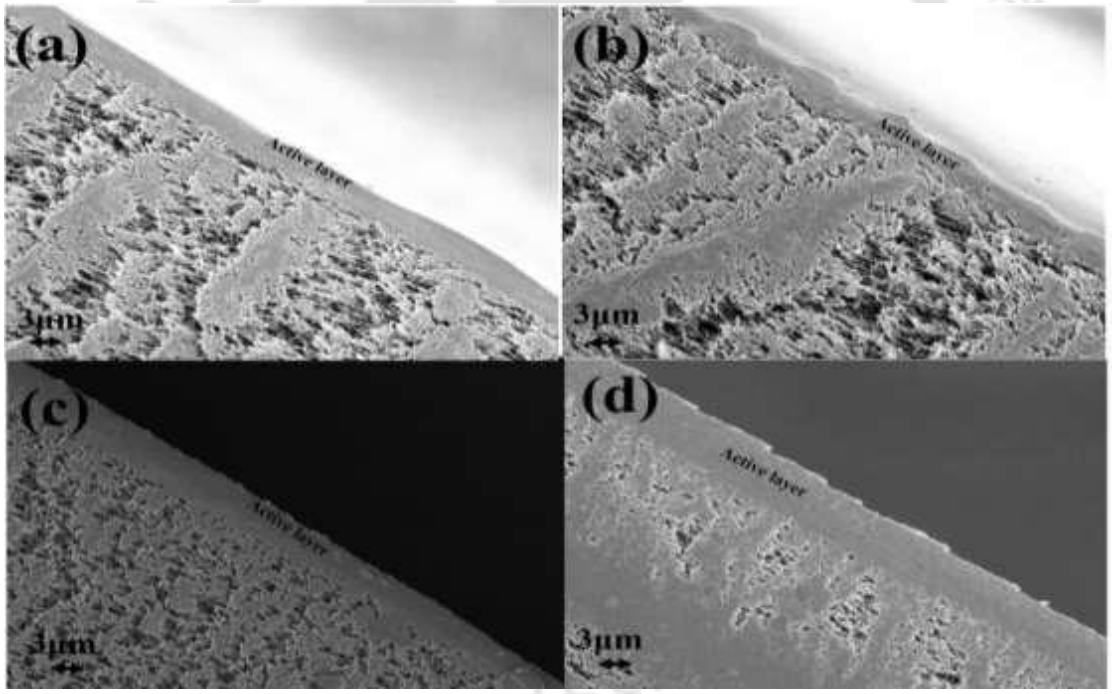

Figure 3.4 FESEM images for the cross sectional view of the membranes before gas permeation test (a) CMC (b) PZ20 (c) PZ30 and (d) PZ40.

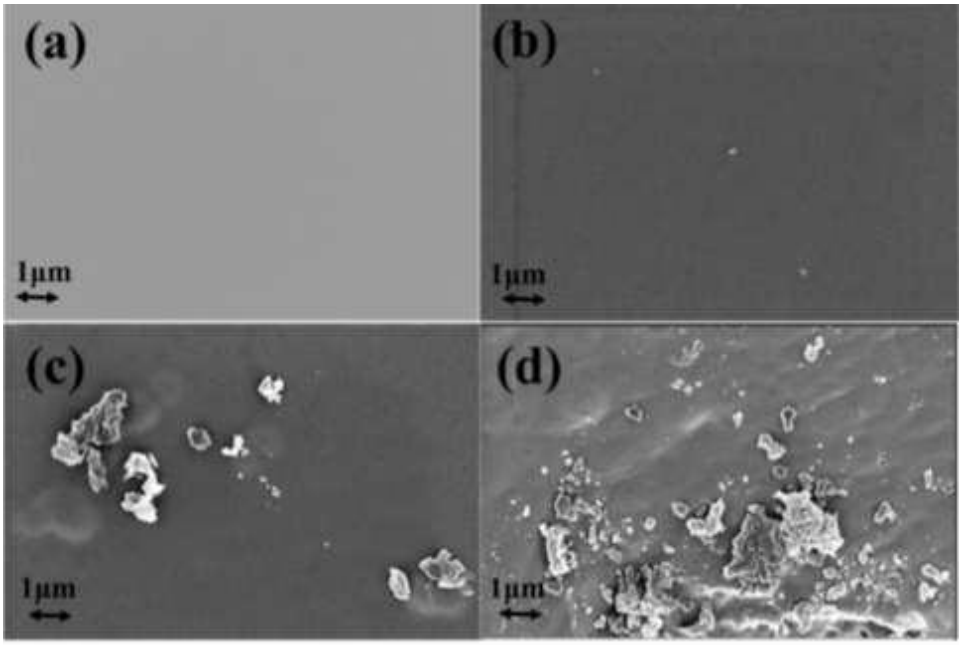

Figure 3.5 FESEM analysis of top surface of the membranes before gas permeation (a) CMC (b) PZ20 (c) PZ30 and (d) PZ40.

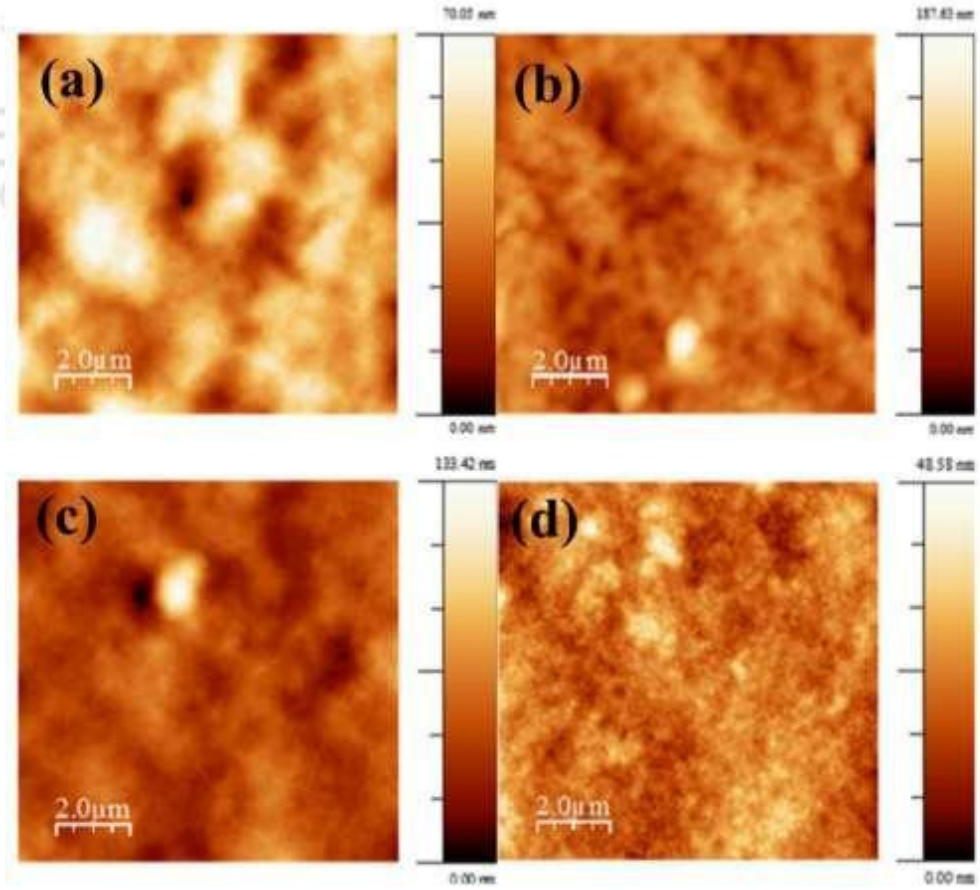

Figure 3.6 AFM analysis of the membranes before gas permeation (a) CMC (b) PZ20 (c) PZ30 and (d) PZ40

3.3.4 Thermal Stability

The thermal stability of PZ20 membrane can be explained on the basis of the TGA isotherm graph shown in **Figure 3.7**. The PZ blended membranes showed 3-4 % weight loss up to 100 °C. This loss was spotted may be due to the enormous water retention capacity by the PZ blended hydrogel membranes. A significant loss was observed at 105 °C in the PZ blended membranes which were predicted to be due to the melting of PZ.

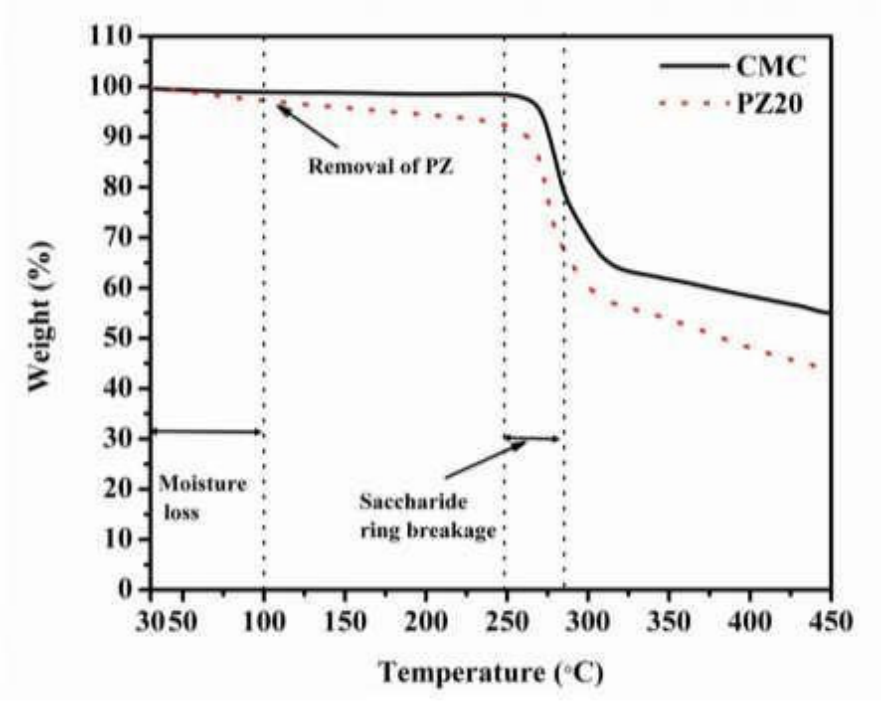

Figure 3.7 TGA graph of CMC and PZ20 active layer

3.3.5 Gas Permeation Study

3.3.5.1 Effect of PZ content

The PZ was added to the CMC membrane at different wt. % from 20-40 wt. % to increase the carrier in the active layer. The gas permeation results indicated that blending of PZ improves the CO_2 permeance and selectivity by increasing facilitated transport of CO_2 at 80 °C having a constant sweep/feed water flow ratio of 1.67 at an absolute pressure of 2/1.21 bar (feed/sweep). The addition of 20 wt. % PZ leads to an increment in CO_2 permeance and CO_2/N_2 selectivity by 103 % and 158.9 % compared to the pure CMC membrane, respectively. However, further increasing PZ content in the dense layer did not

enhance the CO_2 separation performance, on the contrary slight reduce in the CO_2 permeance was perceived.

The CO_2 permeance of 58 GPU and 47 GPU were seen with the separation factors 72 and 55 for PZ30 and PZ40, respectively (**Table 3.1**). The results suggest that more than 20 wt. % PZ reduce the CO_2 performance by agglomerating PZ and this agglomeration hinder the CO_2 molecules to interact with the amine present in the PZ. The reduction in the effective carrier influences the overall CO_2 separation performance. The agglomeration of PZ beyond 20 wt. % can also be validated by FESEM images (**Figure 3.5**). The CMC and PZ20 displayed smooth surface while PZ30 and PZ40 surfaces were seen with some cluster-like structure. Based on the gas permeation results, PZ20 membrane was chosen to study the gas permeation behaviour with the change in water flow rate at a given temperature and pressure.

Table 3.1 Effect of PZ concentration on CO_2 permeance and CO_2/N_2 selectivity at 80 °C

Membrane	PZ wt. (%)	CO_2 permeance (GPU)	CO_2/N_2 selectivity
CMC	0	34.6 ± 0.6	39 ± 0.7
PZ20	20	72 ± 0.9	102 ± 1.4
PZ30	30	58 ± 1.5	72 ± 1.3
PZ40	40	47 ± 0.5	55 ± 0.6

3.3.5.2 Effect of sweep side water flow rate

The effect of sweep water flow rate on CO_2 separation performance for both CMC and PZ20 membranes are shown in **Figure 3.8**. The sweep/feed water flow ratios were varied from 0.33 to 3 keeping the feed side water flow rate constant at 0.03 mL/min with temperature 80 °C and an absolute pressure of 2/1.21 bar (feed/sweep).

The CO_2 flux and permeance increase with an increase in water flow amount from 0.33 to 1.67. The CO_2 flux and CO_2 permeance obtained at 0.33 sweep/feed water flow ratio were 201×10^{-6} cm^3(STP)/cm^2sec and 12.26 GPU for CMC membrane while for PZ20 membrane it was found as 351×10^{-6} cm^3 (STP)/cm^2sec and 22.3 GPU, respectively. The improvement occurred for PZ20 membrane was mainly due to the enhancement of facilitated transport mechanism. The steep increase in the performance was observed for

both the membranes after sweep/feed water flow ratio = 1. The increase in the sweep/feed water flow ratio from 0.33 to 1.67 offered 195 % and 240 % increase in CO_2 flux for CMC and PZ20 membranes, respectively. This indicates that the higher flow rate in sweep side than feed side provides a positive contribution towards CO_2 separation. The adequate supply of water from the sweep side helps in holding of moisture content inside the membrane matrix. In addition, the increased quantity of moisture improves flexibility of the membrane. The water retained by the membranes induce flexibility by plasticization effect and the flexibility reduces the mass transfer resistance of the membrane. This directly takes part in upgrading of CO_2 permeance. Moreover, the higher sweep side water content dilutes the concentration of permeated CO_2 and increases the driving force for the CO_2 transport. Other than these factors PZ20 membrane possess more roughness than the CMC membrane as shown in the AFM images of **Figure 3.6**. The average roughness for CMC membrane was found to be 10.78 which were increased to 19.59 in PZ20 membrane. The increment of roughness enhances the effective surface area for CO_2 molecules to be absorbed and thereby dissolve into the polymer easily and further permeate through the bulk of the membrane. After 1.67 sweep/feed water flow ratio, no further rise in CO_2 flux and permeance is observed. The membrane was stable at the particular temperature of 80 °C and was not damaged during gas separation experiment. The TGA isotherm recorded for PZ20 membrane evidenced the thermal stability at the experimental temperature condition. The loss of 1.97 % was witnessed at 80 °C when the membrane was hold for 30 minutes at that temperature as presented in **Figure 3.9**. This negligible loss corresponded to the elimination of moisture from the membrane matrix. Another loss of 0.8 % and 1.10 % was viewed when the membrane was heated for 30 minutes at 100 °C and 120 °C, respectively. The minor loss at 100 °C was may be due to the removal of complete moisture present in the membrane. Later, the weight loss occurred by the reason of melting of PZ present in the active layer. Therefore, it can be assured that the membrane was stable up to 100 °C.

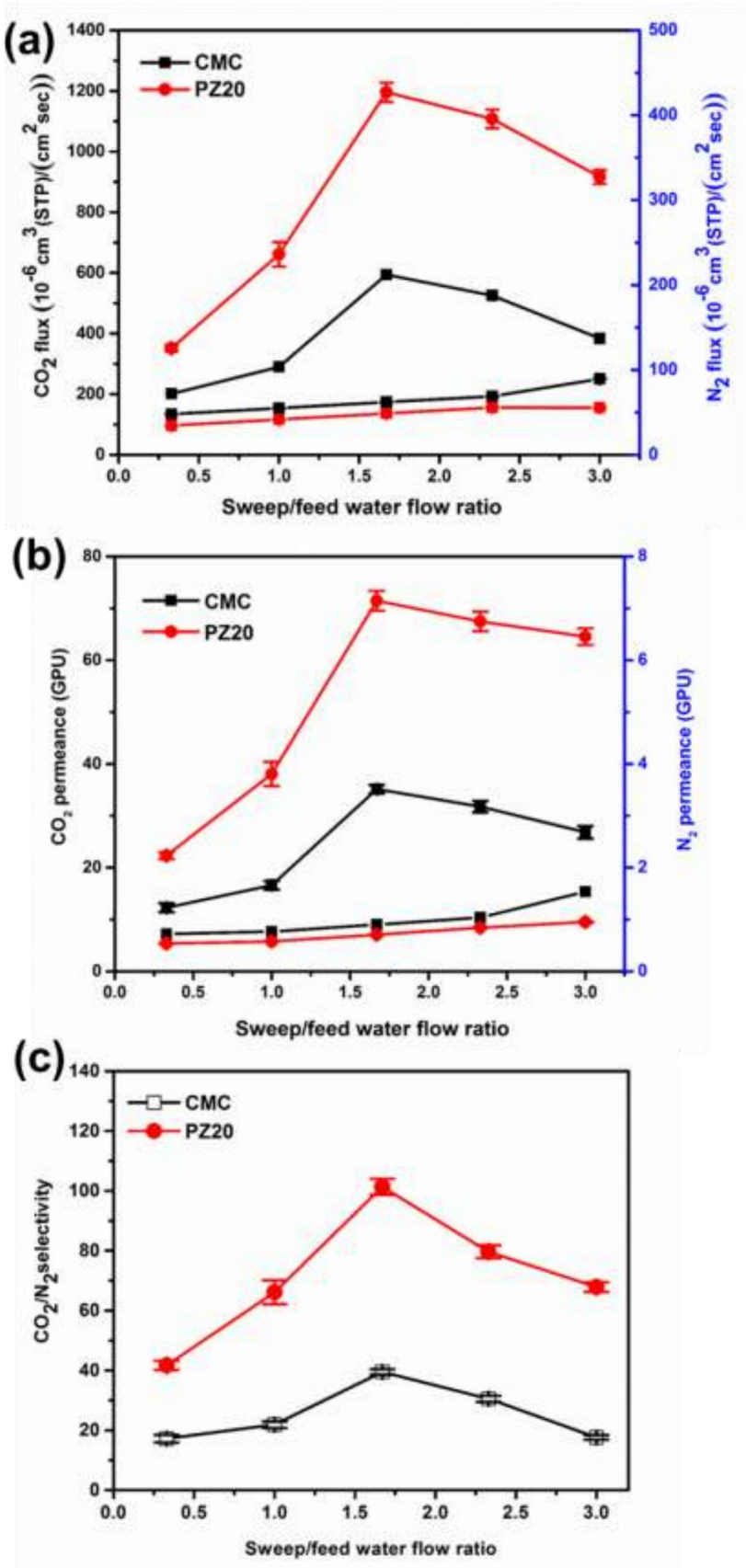

Figure 3.8 Effect of sweep water flow rate on (a) CO_2 and N_2 flux (b) CO_2 and N_2 permeance and (c) CO_2/N_2 selectivity of CMC and PZ20 at 80 °C

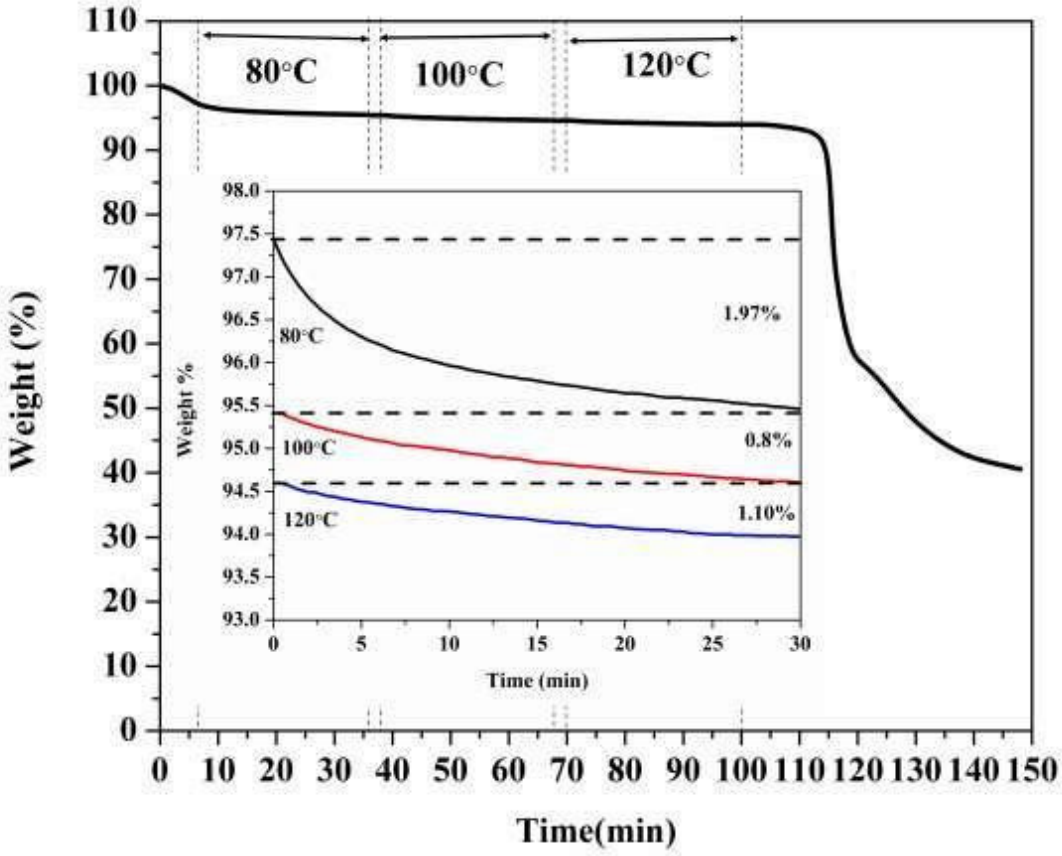

Figure 3.9 TGA isotherm for PZ20 membrane at 80 °C, 100 °C and 120 °C.

3.3.6 Characterization of the Membrane After Gas Permeation

The FTIR spectra obtained for PZ20 membrane after gas permeation study shown in **Figure 3.10** also indicated the unaltered functional groups in the membrane. Although, a peak was detected at 3410 cm^{-1} which may be due to O-H stretch of water present in the membrane after gas permeation test. Moreover, the average roughness value obtained from AFM image of PZ20 after gas permeation study (15.05 nm) was nearly similar to that of the membrane before gas permeation study (15.71 nm). In this way, the PZ blended membrane gave four times higher permeance than the pure CMC membrane. The selectivity was also quite improved compared to the pristine CMC membrane. The membrane performance was found stable up to 3 days.

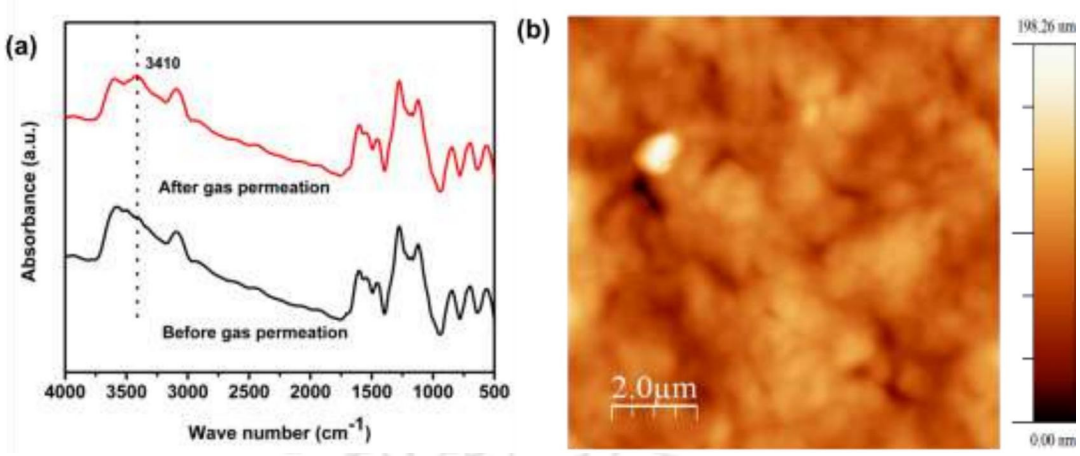

Figure 3.10 Characterization of PZ20 membrane after gas permeation study (a) FTIR spectra (b) AFM image (2D view)

3.3.7 Comparative Study

The gas permeation performance of our membrane can be compared with some other similar works [59–61]. Santos et al. [94] worked on hybrid ionic liquid (IL) - chitosan membrane and studied the permeation behavior in the temperature range 298-323 K. Further, Casado-coterillo et al. [95] investigated that the incorporation of metal organic framework (MOF) can enhance the selectivity of IL-chitosan membrane. Similarly, Prasad et al. [59] reported CO_2 permeation data for chitosan composite membrane. On comparison to that result, the CMC membrane showed two times better performance than the pure chitosan membrane [59]. Previously the pure CMC membrane was studied at room temperature. In this work, the membrane was examined at different temperatures and exhibited a pretty good performance than the available literature. The PZ blended membrane gave four times higher permeance than the pure CMC membrane. The selectivity was also quite improved compared to the pristine CMC membrane.

3.4 Conclusions

The thermally stable hydrophilic membranes of PZ20, PZ30 and PZ40 were successfully prepared and implemented in the GC set up for CO_2 separation. The XPS analysis confirmed the successful synthesis of PZ20 membranes. The microscopic analysis established the formation of defect free active layer over the porous support. The water retention test revealed the high moisture holding capacity of the PZ blended membranes over the CMC membrane, which positively influenced the CO_2 separation. Excellent performance of CO_2 separation was obtained for PZ20 membrane at 80 °C with supplied sweep/feed water flow ratio of 1.67 and feed pressure of 2/1.2 bar (feed/sweep) exhibiting a remarkable increase of CO_2 permeance (89 GPU) and CO_2/N_2 selectivity (103) as compared to that of pure CMC membrane.

CHAPTER 4

Carboxymethyl Chitosan/Poly (amidoamine) Molecular Gate Membrane for CO_2/N_2 Separation

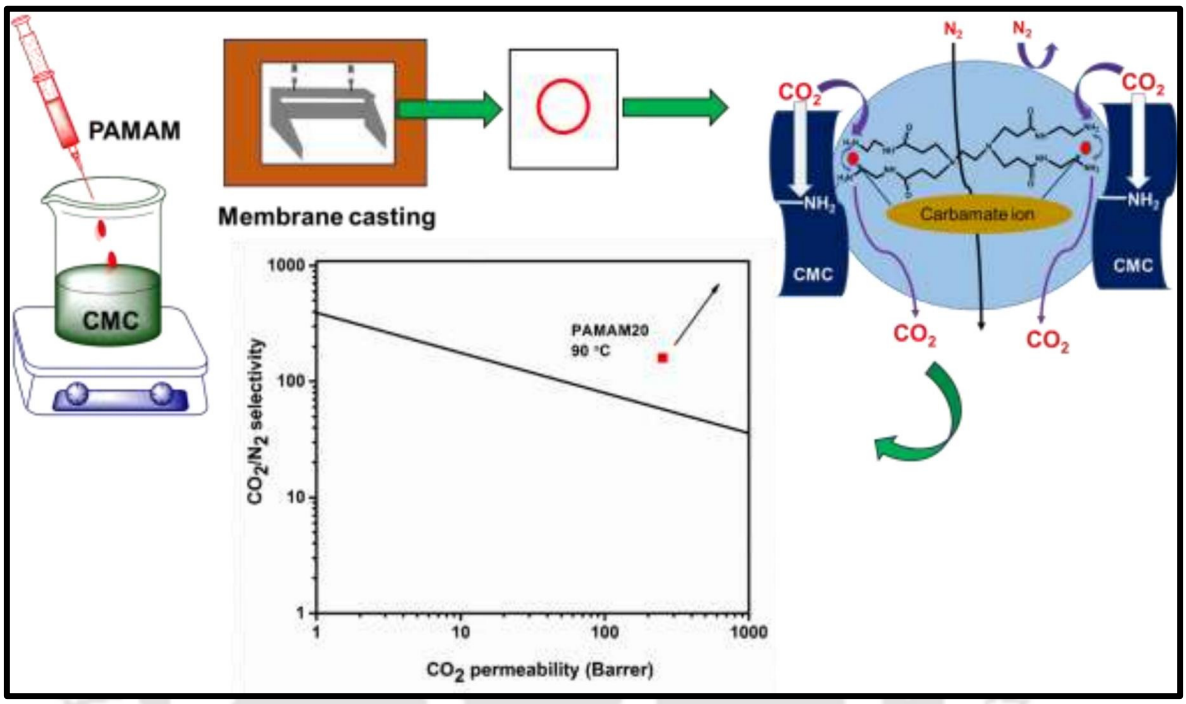

Schematic representation of CMC/PAMAM membrane preparation and obtained gas permeation result.

CHAPTER 4

Carboxymethyl Chitosan/Poly (amidoamine) Molecular Gate Membrane for CO_2/N_2 Separation

In this study, poly (amidoamine) (PAMAM) has been blended with CMC to enhance the amine carrier content and investigate the CO_2 separation performance. Elucidating the limitations of small molecule amines, PAMAM, being a large molecule amine, has rested as fixed carrier in the system. In the swollen state, CMC/PAMAM membrane functioned as semi mobile carrier and hydrogel membrane. Additionally, PAMAM and CMC individually follow molecular gate and salting out mechanism, respectively. The combined advantages of both CMC and PAMAM helped to accomplish this novel approach towards CO_2 separation. This work is published in ***ACS Applied Materials & Interfaces****.*

4.1 Introduction

Lately, the addition of dendrimers as the carrier for CO_2 facilitation proves to be a potential method to enhance the CO_2 separation performance. Dendrimers possess exceptional properties such as, multiple valency, water solubility, consistent nanosize and suitable approach for synthesis [62-64]. Non-volatile polyamidoamine (PAMAM) dendrimers are particularly of interest as they offer a large concentration of primary and tertiary amine groups. The tertiary amine groups too can contribute to CO_2 facilitation in the presence of water by reacting with CO_2 forming bicarbonate ions as described by the base-catalysis reaction mechanism [96].

$$CO_2 + R_3N + H_2O \rightleftharpoons HCO_3^- + R_3NH^+ \qquad \text{(Reaction 4.1)}$$

The carbamates formed by the reaction of CO_2 with dendrimer amine crosslink the dendrimer and thereby inhibit the permeation of other feed gas species and in turn increase CO_2 selectivity by the molecular gate effect, while CO_2 transport is accomplished by the bicarbonate ions [97]. The chemical structure of PAMAM has been shown in **Figure A1.1c, Appendix A1**.

Although, various application based studies have been done on PAMAM and CMC separately or together, but their behaviour on CO_2 separation application is yet to be explored. Various analyses performed on the membrane established the correlation

between the structure of the matrix and gas separation performance. It is expected that CMC/PAMAM membrane will take part in CO_2 separation event by ensuring its role as semi mobile carrier, polyionic salt and hydrogel membrane. The combined advantages of both CMC and PAMAM will accomplish this novel approach.

4.2 Experimental Section

4.2.1 Materials

Carboxymethyl chitosan is prepared in our laboratory as mentioned in **Chapter 2**. PAMAM generation 0.0 with ethylenediamine core (20% in methanol) and glycerol anhydrous (≥ 99.5 % purity) were obtained from sigma Aldrich and Merck, respectively. Polyethersulfone (PES) sheet (pore size 0.1μ) provided by Sterlitech, USA. The materials have been used without further purification. The cylinders containing CO_2/N_2 (1:4) and Ar (99.99 % pure) have been procured from Vadilal Chemicals Ltd. The cylinder containing He was purchased from Jainex Gases Company, India. Millipore water® obtained from analytical laboratory has been used throughout the experiment.

4.2.2 Membrane Fabrication

Aqueous CMC solution was prepared at 27 °C and the bubbles formed due to stirring have been removed via centrifugation. Desired PAMAM blended membranes were prepared by adding various wt. % of PAMAM to clear CMC solution following the same procedure as discussed in **Chapter 2**. The membranes have named as: PAMAM10 (90 wt. % CMC + 10 wt. % PAMAM), PAMAM20 (80 wt. % CMC + 20 wt. % PAMAM) and PAMAM30 (70 wt. % CMC + 30 wt. % PAMAM).

4.2.3 Characterization Techniques and Gas Permeation Set Up

The instruments used for FTIR, XPS, FESEM, AFM and TGA analysis are same as mentioned in **Chapter 2**. Here, FTIR and XPS was used to investigate the presence of functional groups and elemental composition of the prepared membrane. FESEM and AFM images showed the morphology of the membranes. TGA was used to know the thermal stability of the membrane at the operating conditions. Similarly, the moisture retention test set up and gas permeation set up used in this chapter has been elaborated in the **Chapter 2**.

4.3 Results and Discussion

4.3.1 Spectroscopic Analysis

The FTIR spectrum shown in **Figure 4.1a** indicates the presence of functional groups in membrane which verifies the successful blending of CMC and PAMAM. The peak at 1658 cm^{-1} is associated with the C=O bond of PAMAM [98, 99]. The peak from 3580 to 3100 corresponds to N-H and O-H stretching vibration of CMC and PAMAM, respectively. The broadness of the peak can be associated with the large number of N-H groups present in the membrane due to the addition of PAMAM. Another band at 1640 cm^{-1} corresponds to the N-H bending vibration of PAMAM and CMC. The minor peak at 2930 cm^{-1} corresponds to C-H alkane stretching vibration of CMC and PAMAM [99]. Also, the transmittance frequencies at 1150 (bridge O of CMC [100]), 1071, 1028, and 897 cm^{-1} are assigned to the saccharide structure of CMC. The peak observed between 1188 cm^{-1} and 967 cm^{-1} correspond to C-N bonds in PAMAM. The peak at 1421 cm^{-1} corresponds to the COO^- symmetric stretch in CMC which indicates the ionic salt nature of CMC [99-101]. The peak lying in the range 1900-1550 cm^{-1} corresponds to the asymmetrical stretching vibration of COO^- in CMC [101]. The band found in the region 1680-1630 cm^{-1} and 3300 cm^{-1} correspond to the C=O and N-H stretch of amide in PAMAM, respectively. Another band between 1640-1550 cm^{-1} attributes the bending vibration of N-H of secondary amide in PAMAM [99]. The broad band at 2170 cm^{-1} is associated with the stretching vibration of protonated amine groups [99]. The band at 1610 cm^{-1} denotes the asymmetric stretching vibration of protonated primary amine, and the band near 1500 cm^{-1} represents the symmetric stretch of this group [99]. Further, the XPS analysis (**Figure 4.1b and Figure 4.2**) supports the above mentioned FTIR analysis. The deconvoluted narrow scan of carbon peak (C1s) shows peaks at binding energies 284.6 eV, 286.0, 287.7 and 288.5 are attributed to the presence of C-C or C-H, C-N, C-O-C and O-C=O bond in CMC, respectively. Here, the major peak is observed for C-N bond which is mainly due to the loading of PAMAM. Similarly, the narrow scans for O1s, N1s and Na1s have been shown in **Figure 4.2 (b-d)**. The presence of primary, secondary and tertiary amine has been indicated by the significant peaks observed at 400.3, 399.1 and 401.0 eV.

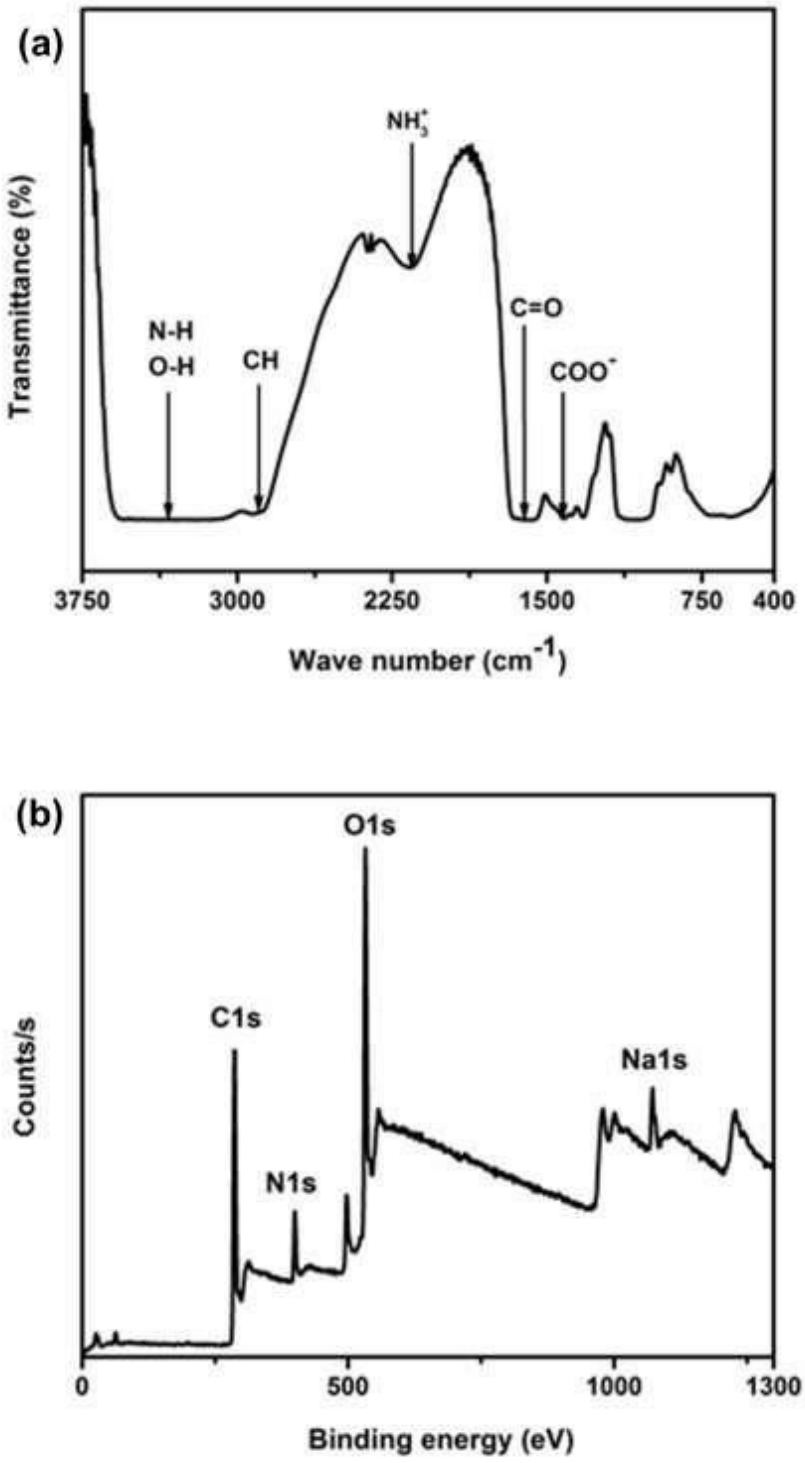

Figure 4.1 (a) FTIR spectrum (b) XPS survey spectrum of PAMAM blended CMC membrane.

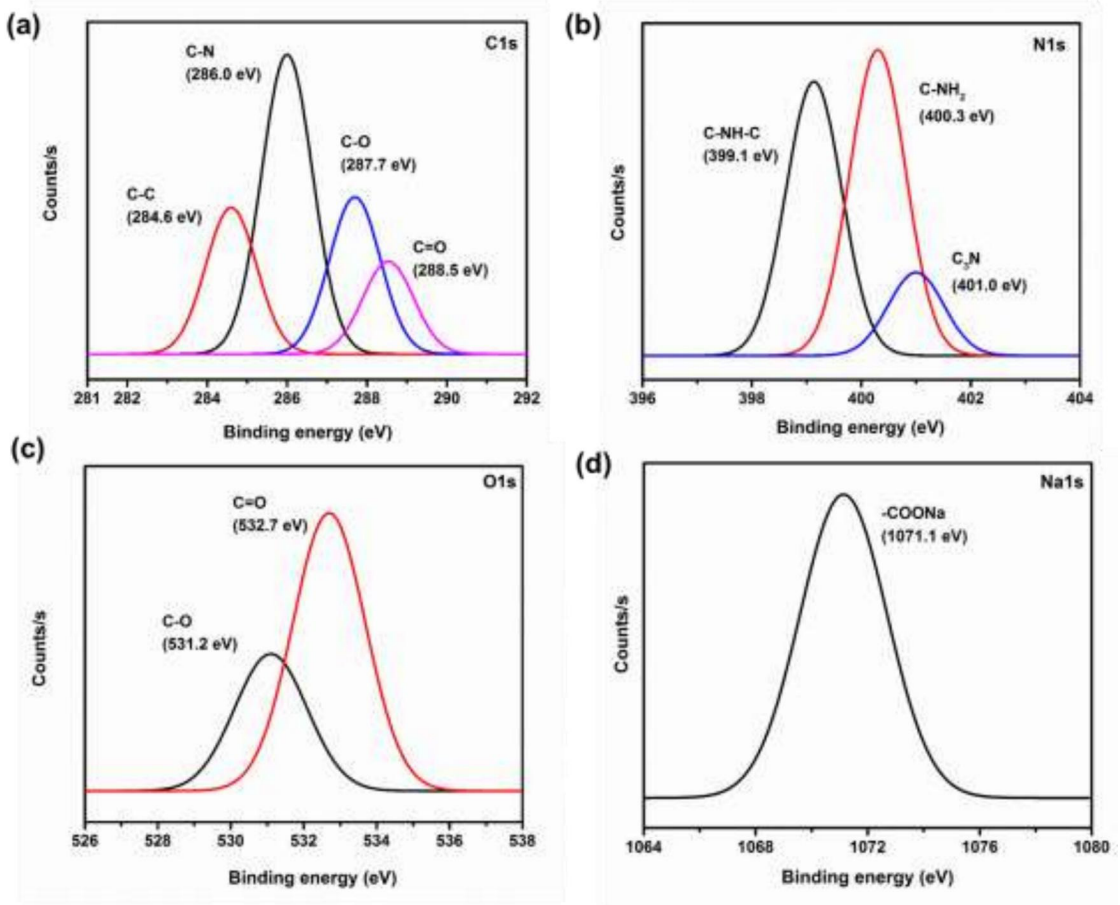

Figure 4.2 Deconvoluted XPS spectra of PAMAM10 membrane (a) C1s, (b) N1s (c) O1s (d) Na1s.

4.3.2 Microscopic Analysis

The FESEM images obtain for PAMAM10, PAMAM20 and PAMAM30 show the variation in morphology of the membrane with different percentage of PAMAM loading **(Figure 4.3 a-f)**. Usually, it is necessary to obtain a defect free dense layer for CO_2 separation application. Accordingly, the membrane comprising 10 % PAMAM formed distinct dense layer over PES with a thickness of 2.64 μm (**Figure 4.3a**). Also, the **Figure 4.3b** indicates the development of even dense surface. The higher percentage of PAMAM loading may form intramolecular H-bonding among the amine groups resulting the formation of compact chain [102]. The casting solution viscosities have been observed as 1360 cp, 1070 cp and 892 cp for PAMAM10, PAMAM20 and PAMAM30, respectively. The reduced viscosity of the casting solution causes penetration of solution into the pores of the substrate layer. The pore infiltration increases the active layer thickness as shown

in **Figure 4.3c** and **Figure 4.3e**. The higher thickness causes lowering of permeability. Moreover, the greater fraction of PAMAM can cause self-aggregation on the membrane surface and over deposition of particles can suppress the active sites for gas transport. Consequently, CO_2 separation performance will be affected. The images obtained from AFM instrument also corroborate the FESEM results (**Figure 4.4a, b, and c**). The average roughness obtained from PAMAM10, PAMAM20 and PAMAM30 are 2.81 nm, 3.25 nm and 4.21 nm, respectively.

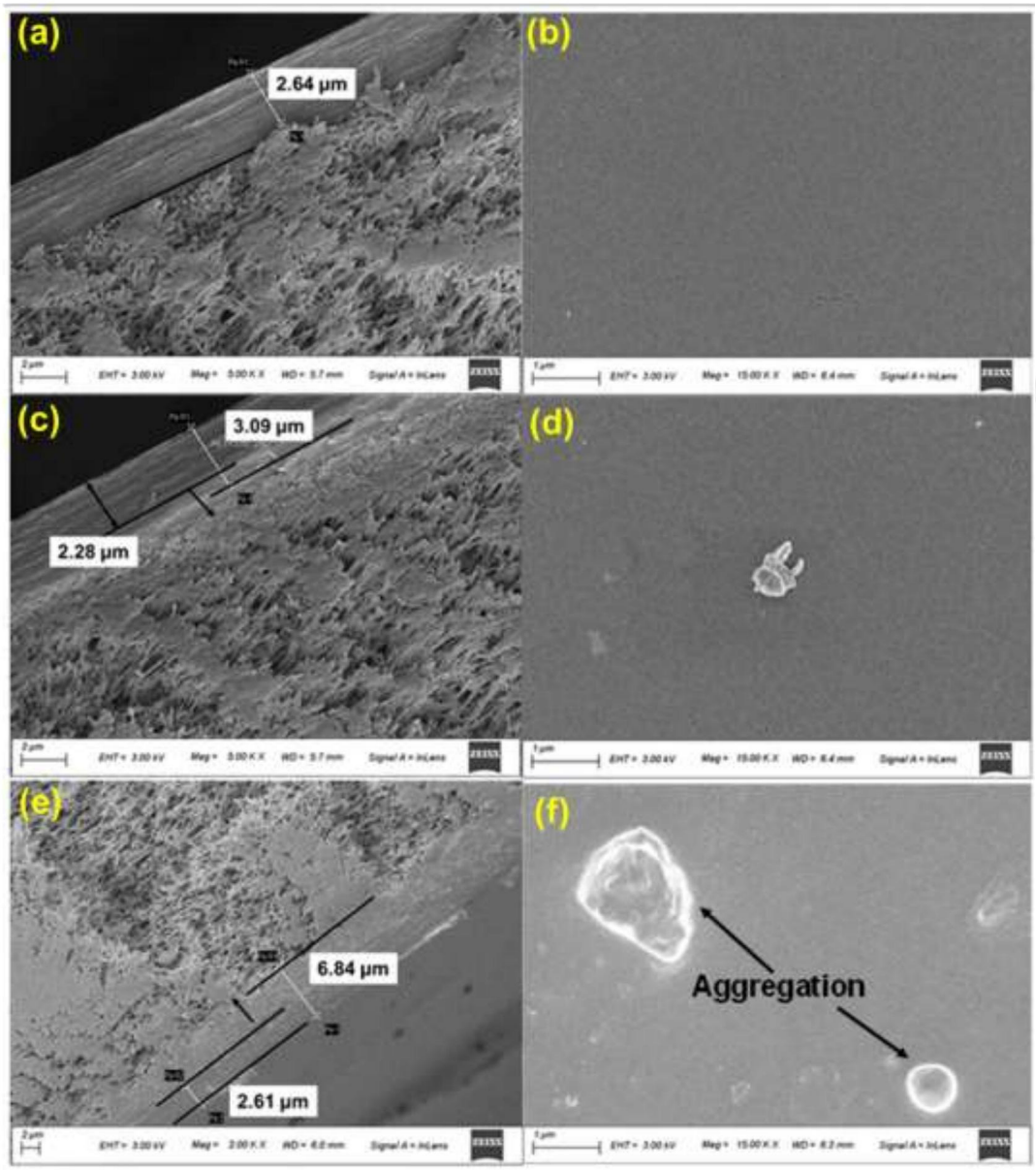

Figure 4.3 FESEM image obtained for the cross section and top surface of (a, b) PAMAM10 (c, d) PAMAM20 (e, f) PAMAM30, respectively.

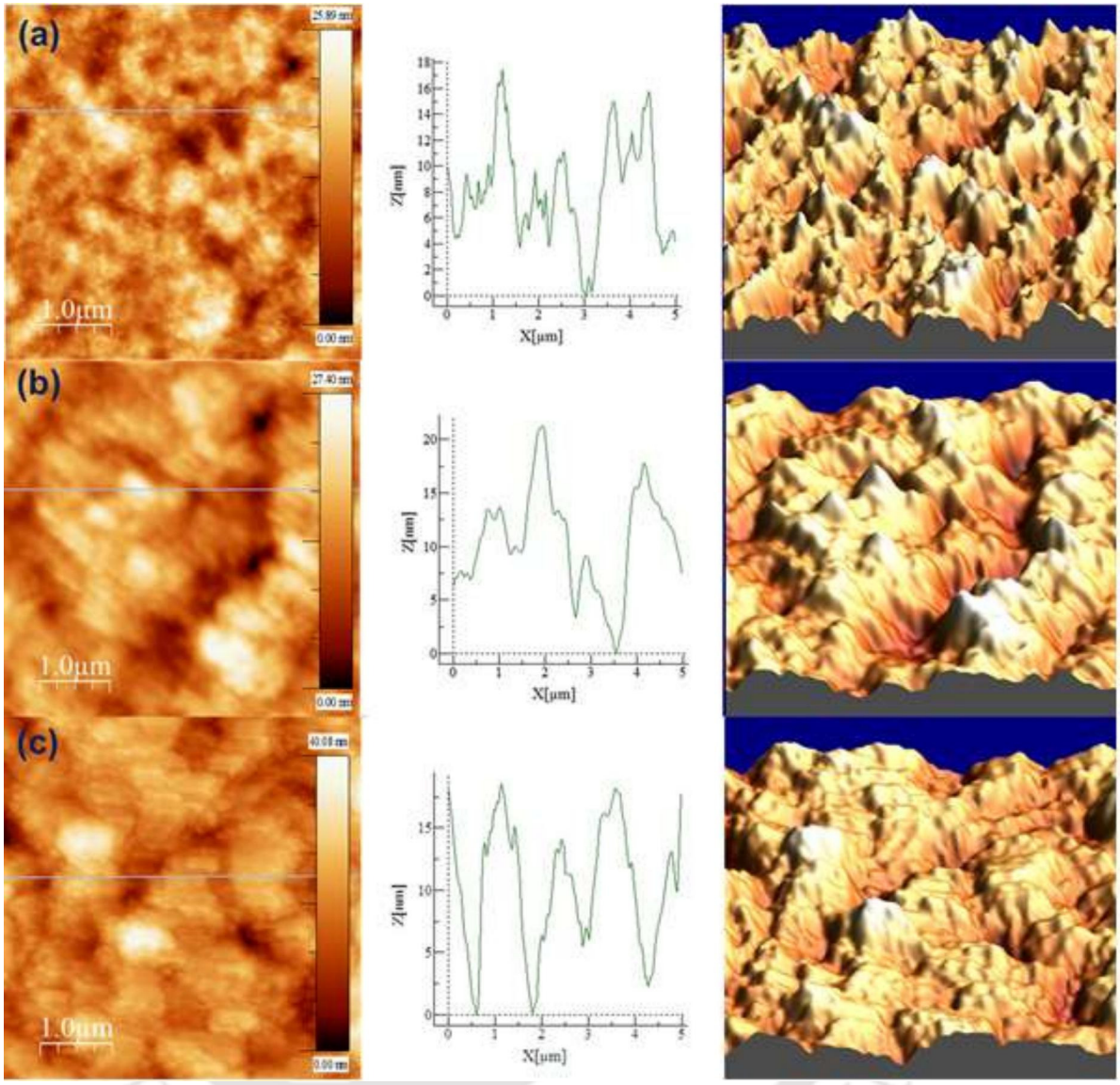

Figure 4.4 AFM analysis of the membranes before gas permeation (a) PAMAM10 (b) PAMAM20 (c) PAMAM30.

4.3.3 Moisture Retention Ability

Moisture plays significant role in CO_2 separation application by taking part in facilitated transport reaction and offering flexibility to the membrane. The moisture retention behaviour of CMC/PAMAM membrane was investigated at different relative humidity percentage (RH %) at room temperature. These membranes basically followed the Flory Hugging's [103] theory and exhibited two segmented exponential growth as shown in **Figure 4.5.** However, the PAMAM20 showed higher water retention ability than PAMAM10 and PAMAM30. This attributed to the radially symmetrical and loose

structure of PAMAM [104] accompanied by inherent hydrophilic sites of CMC. Far along, when the PAMAM percentage was increased, a surprisingly different trend came into picture. When the loading of PAMAM was increased, the pH of PAMAM10, PAMAM20 and PAMAM30 became 7.5, 9.2 and 10, respectively. With increase in pH the amino groups of CMC got deprotonated and imbalanced the intra and inter chain interaction between the carboxyl and amino groups resulting repulsion between polymer chains. That drove CMC to adopt an extended open-chain conformation as shown in the inset image of **Figure 4.5** [84]. In the meantime, the excess amino groups of PAMAM formed intramolecular H-bond among them and started accumulating on the membrane surface as observed in **Figure 4.3f**. As a result, the expected H-bond forming sites between water molecule and matrix were found preoccupied. Thus, the moisture retention ability of PAMAM30 membrane was found very less as compared to PAMAM10 and PAMAM20. Although, surplus water retention by the membrane offered excesses flexibility to the membrane which might adversely affect the CO_2 separation performance. If the moisture retention ability of the PAMAM blended membranes are compared with other competing membranes used for CO_2/N_2 separation, a variety of trends come into picture (**Table 4.1**). However, pristine CMC membrane [105] acquire higher moisture retention ability than the pure chitosan [106] and chitosan/polyallylamine [33] membrane. Therefore, it is expected that the lower CO_2 permeance offered by these membrane may be resolved in CMC membrane. Another membrane system composed of CMC/piperazine [105] showed higher moisture retention ability than CMC membrane. Accordingly, the CMC/piperazine membrane showed two times better CO_2 permeance than CMC membrane. On the other hand, PAMAM blended membrane is showing lower moisture retention ability than CMC membrane which is similar to another membrane system comprising of chitosan and silk fibroin (~ 130 %) [106]. The chitosan/15 % silk fibroin membrane showed the CO_2 permeance of ~ 97 GPU with the CO_2/N_2 selectivity ~ 62. Similarly, it is presumed that the PAMAM10 membrane may show better CO_2 permeance than CMC/piperazine membrane.

Table 4.1 Moisture retention ability of different chitosan based membranes at 100 % RH

Membrane system	Moisture uptake %
Chitosan **[106]**	~ 165
Chitosan/ PAA 15 % **[33]**	~ 100
Chitosan/Silk fibroin 15% **[106]**	~ 135
CMC **[105]**	~ 345
CMC/PZ 20 % **[105]**	~ 380
CMC/PAMAM 10 %	~ 125

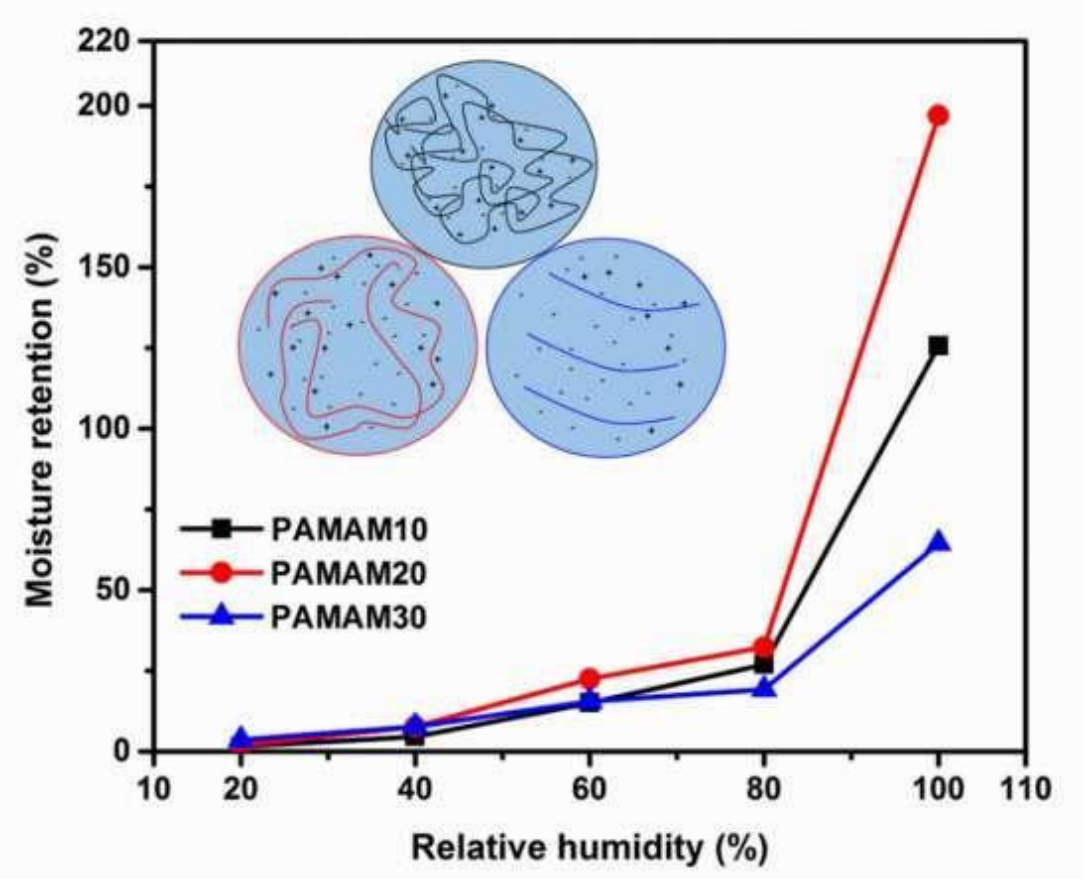

Figure 4.5 Moisture retention behavior of PAMAM blended membranes under different relative humidity (%) at room temperature (Inset image shows the chain opening conformation happening in PAMAM10, PAMAM20 and PAMAM30).

4.3.4 Temperature Stability

The temperature stability of PAMAM10 was investigated by TGA isothermal analysis and heating assisted XPS analysis as shown in **Figure 4.6a, b**.

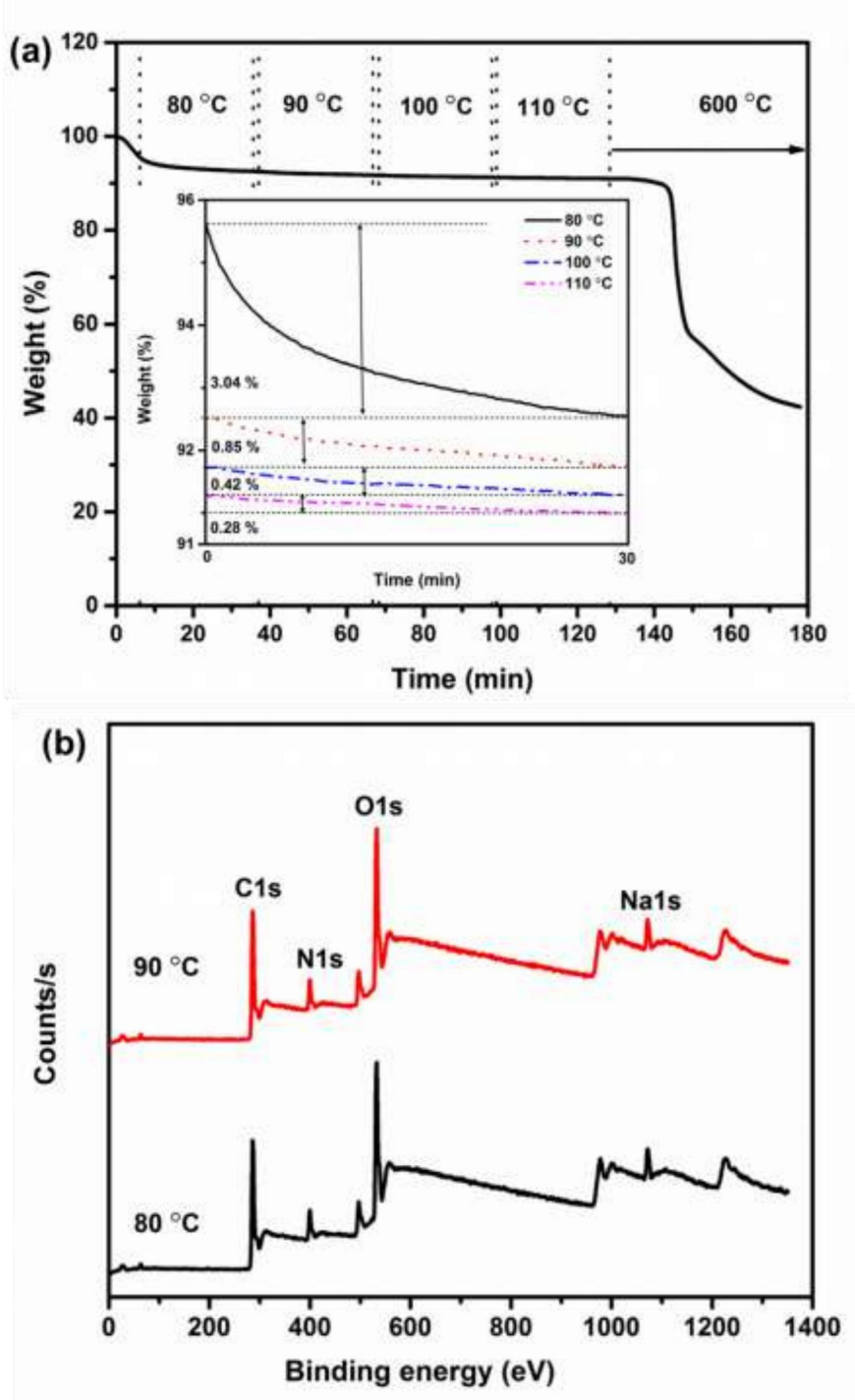

Figure 4.6 (a) TGA graph for the active layer of PAMAM10 (inset image indicates the zoomed graph for TGA isotherm at temperatures 80 °C, 90 °C, 100 °C and 110 °C) (b) XPS spectra at 80 °C and 90 °C.

The distinct loss of 3.04 % at 80 °C was due to the moisture loss from the membrane. Other minor weight losses were witnessed at 90 °C (0.85%), 100 °C (0.42%) and 110 °C (0.28%) as presented in the inset image of **Figure 4.6a**. These negligible losses corresponded to the complete elimination of the moisture present in the matrix. Notably, these moisture loss events were directly involved in the gas separation activity as water is the essential entity for facilitated transport and solution diffusion mechanism. Other than the loss of water from the membrane, no significant change was observed in the operating temperature range. Later, when the temperature was increased till 600 °C a major weight loss had been perceived at on set temperature 248 °C ascribing the breakage of saccharide ring in CMC. The TGA graph obtained for CMC membrane also showed the similar degradation temperature at 248 °C [105]. The elemental composition obtained from XPS spectra taken at 80 °C and 90 °C also supported the TGA isotherm (**Figure 4.6b**). No substantial compositional change was observed for PAMAM10 membrane at both the temperatures (80 °C and 90 °C) as compared to the spectrum obtained at room temperature (**Figure 4.1b**). Although, a minor change was observed in **Table 4.2** which might be due to the selection of different scan areas.

Table 4.2 Elemental analysis of PAMAM10 membrane at 30 °C, 80 °C and 90 °C using XPS

Temperature	O1s	C1s	N1s	Na1s
30 °C	30.08	58.42	8.13	3.38
80 °C	31.63	56.35	8.88	3.15
90 °C	31.75	56.83	8.44	2.99

4.3.5 Gas Permeation Study

The gas permeation test was operated for the CMC/PAMAM membrane to study (a) the effect of PAMAM percentage (b) the effect of temperature (60-110 °C) and (c) the effect of sweep/feed water flow ratio (0.33 to 3). In all these cases, the absolute pressures were fixed at 2 bar on feed side and 1.21 bar on sweep side.

4.3.5.1 *Effect of PAMAM content*

The PAMAM was added to the CMC membrane at different wt. % from 10-30 wt. % to increase the carrier content in the active layer. The CO_2 separation performance presented by the PAMAM blended membranes have been tabulated in **Table 4.3**. PAMAM10 showed the highest CO_2 permeance and CO_2/N_2 selectivity over other membranes (PAMAM20 and PAMAM30). Therefore, another membrane comprising 5 wt. % PAMAM (PAMAM5) was tested under the same operating condition to investigate the optimum percentage of PAMAM to be loaded in CMC matrix. The PAMAM5 membrane exhibited lower CO_2 permeance and CO_2/N_2 selectivity than PAMAM10, PAMAM20 and PAMAM30 membrane. This might happen due to the presence of lower carrier percentage in PAMAM5 than the other membranes.

The CMC/PAMAM membrane basically follows four mechanisms (**Figure 4.7**): (a) molecular gate mechanism of PAMAM [65] (b) salting out phenomenon of CMC [53] and (c) facilitated transport by semi mobile carriers and (d) solution diffusion mechanism offered by the moisture retention capability of the hydrophilic matrix. In molecular gate mechanism, the carbamate formed in the reaction between CO_2 and amines crosslink the dendrimer and thereby inhibit the permeation of N_2 and in turn increase CO_2 selectivity and the CO_2 transport is accomplished by the bicarbonate ions. In salting out event, CMC being a polyelectrolyte, may enhance the CO_2/N_2 selectivity by preventing dissolution of N_2 molecule on the membrane matrix. Moreover, in alkaline medium, the carboxyl groups of CMC turn into carbonates[107] which directly takes part in CO_2 transport mechanism. In swollen state, the primary amine of CMC and large molecule of PAMAM act as semi mobile carriers which speed up the CO_2 transport via hopping mechanism. Winding up the above analyses, we would like to propose that CMC/PAMAM system may follow all four CO_2 transport mechanisms cooperatively. Hence, it showed improved CO_2 separation performance as compared to that of pristine CMC (**Table 4.3**). Although, the self-aggregation of PAMAM beyond 10 wt. % (**Figure 4.3**) evidently affected the gas separation results of PAMAM20 and PAMAM30 membrane. The increased active layer thickness acquired due to the casting solution infiltration to porous support in PAMAM20 and PAMAM30, negatively influences CO_2 permeance. Also, the cluster formation of amines owing to excessive PAMAM loading to CMC suppresses the active amine sites

and directly restricts the gas molecule movement resulting reduced gas permeance and CO_2 selectivity. Therefore, PAMAM10 has been picked for further gas permeation evaluation.

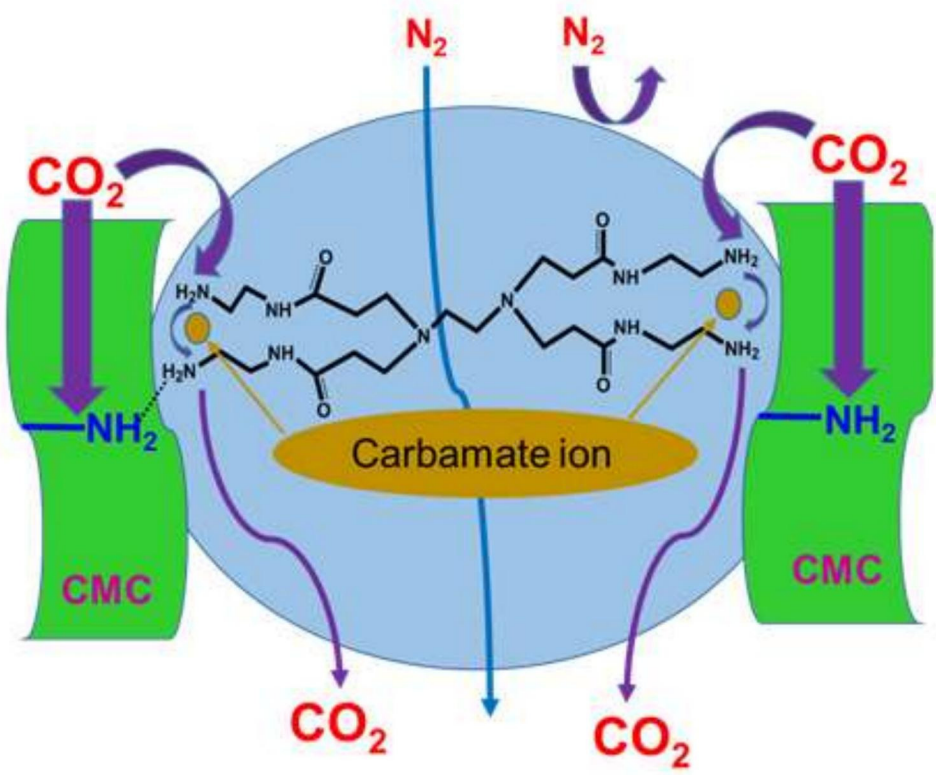

Figure 4.7 Overall CO_2 transport mechanism in CMC/PAMAM membrane.

Table 4.3 Effect of PAMAM concentration on CO_2 permeance and CO_2/N_2 selectivity at 90 °C, sweep/feed water flow ratio = 1.67 and feed side absolute pressure = 2 bar

Membrane name	PAMAM wt (%)	CO_2 permeance (GPU)	CO_2/N_2 selectivity
CMC **[105]**	0	34.6 ± 0.6	39 ± 0.7
PAMAM5	5	43 ± 0.6	82 ± 1
PAMAM10	10	98 ± 1.4	149 ± 1.7
PAMAM20	20	61.4 ± 1.7	102 ± 1
PAMAM30	30	55 ± 0.6	79 ± 1

4.3.5.2 *Effect of temperature and water flow ratio*

The variation in gas permeation parameters were investigated in the temperature range of 60 – 110 °C (**Figure 4.8**). An increase in the CO_2 permeance from ~68 GPU to ~97 GPU was observed (**Figure 4.8a**) on increasing the temperature from 60 °C to 90 °C. This attributed to the enhanced rate of reaction between CO_2 and the amine carriers with increase in temperature (Arrhenius equation). At 60 °C, CO_2 permeation was taking place through both solution-diffusion and facilitated transport mechanism. Meanwhile, N_2 also traversed through the flexible matrix showing a N_2 permeance of 1.33 GPU. Gradually, the N_2 permeance reduced to 0.99 GPU, 0.67 GPU, 0.66 GPU, 0.52 GPU and 0.33 GPU at 70 °C, 80 °C, 90 °C, 100 °C and 110 °C, respectively. Similarly, CO_2 permeance began to decrease at the temperatures beyond 90 °C. This declining trend obtained for both CO_2 and N_2 permeance corresponded to the gradual loss of free water content from the membrane matrix with rising temperature [108]. Eventually, a steep up pattern for CO_2/N_2 selectivity occurred in the range 60 - 90 °C.

The effect of the sweep/feed water flow ratio on the CO_2 permeance, N_2 permeance and CO_2/N_2 selectivity have been illustrated in **Figure 4.9**. The CO_2 permeance started increasing as the sweep/feed water flow ratio was augmented from 0.33 to 2.33. Upon a further increase of the ratio up till 3, a drop in CO_2 permeance was noticed. The initial upturn of the CO_2 permeance was attributed to the facilitated transport reaction under sufficient moisture environment. Later, the transport of CO_2 was troubled by the co-sorption of N_2 and water molecules. The increased trend obtained for N_2 permeance clearly indicated the race between both CO_2 and N_2 for transportation. As a result of this, the CO_2 selectivity over N_2 got reduced. The performance stability of PAMAM10 membrane was investigated by maintaining the temperature at 90 °C and sweep/feed water flow ratio = 2.33. The membrane didn't show drastic variation in CO_2 permeance and CO_2/N_2 selectivity. The data recorded up to 168 hours have been shown in **Figure 4.10** which clearly indicates the long term performance constancy of the membrane.

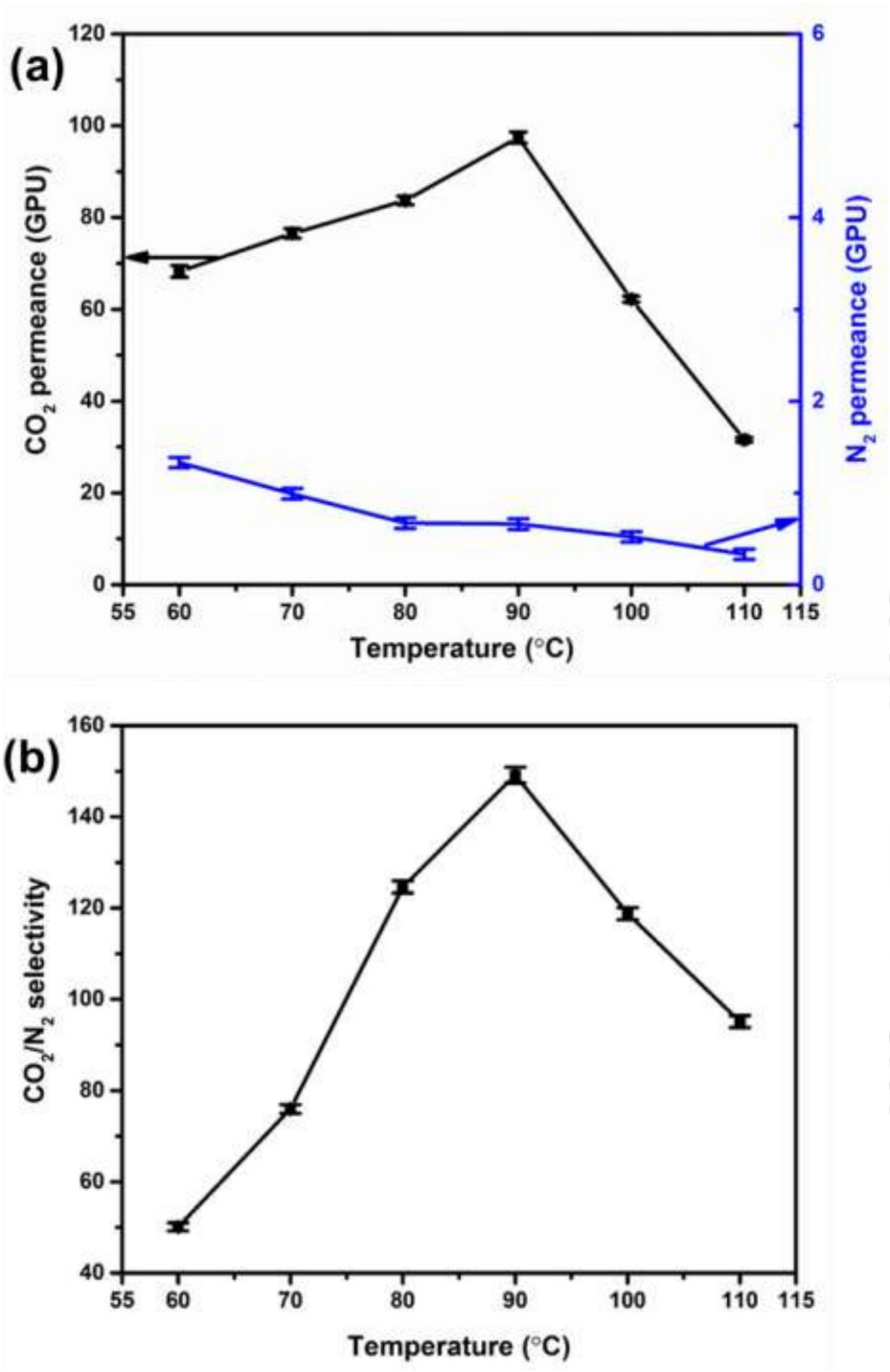

Figure 4.8 Effect of temperature on (a) CO_2 and N_2 permeance (b) CO_2/N_2 selectivity of PAMAM10 at sweep/feed water flow ratio =1.67.

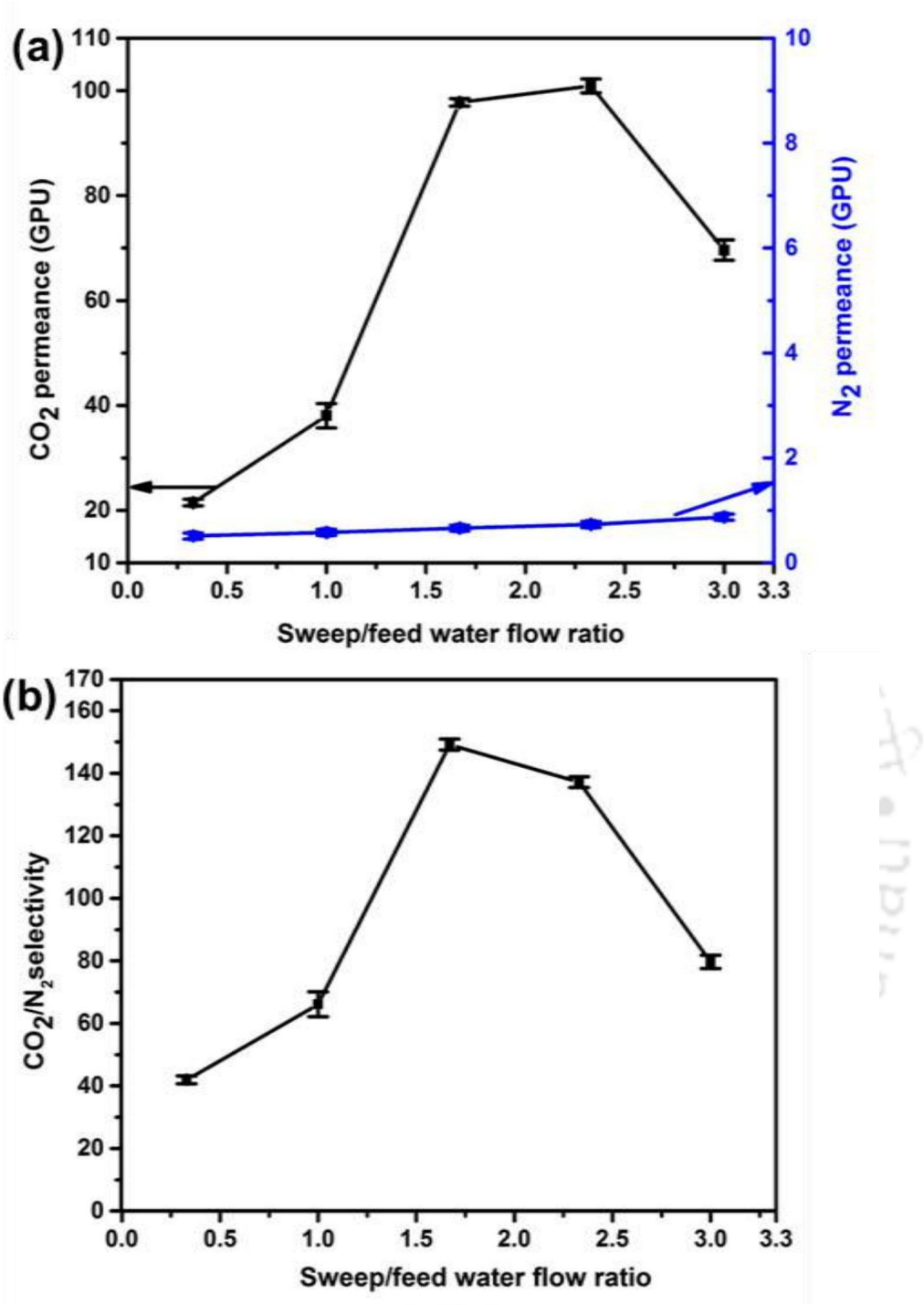

Figure 4.9 Effect of sweep/feed water flow ratio on (a) CO_2 and N_2 permeance and (c) CO_2/N_2 selectivity of PAMAM10 at 90 °C

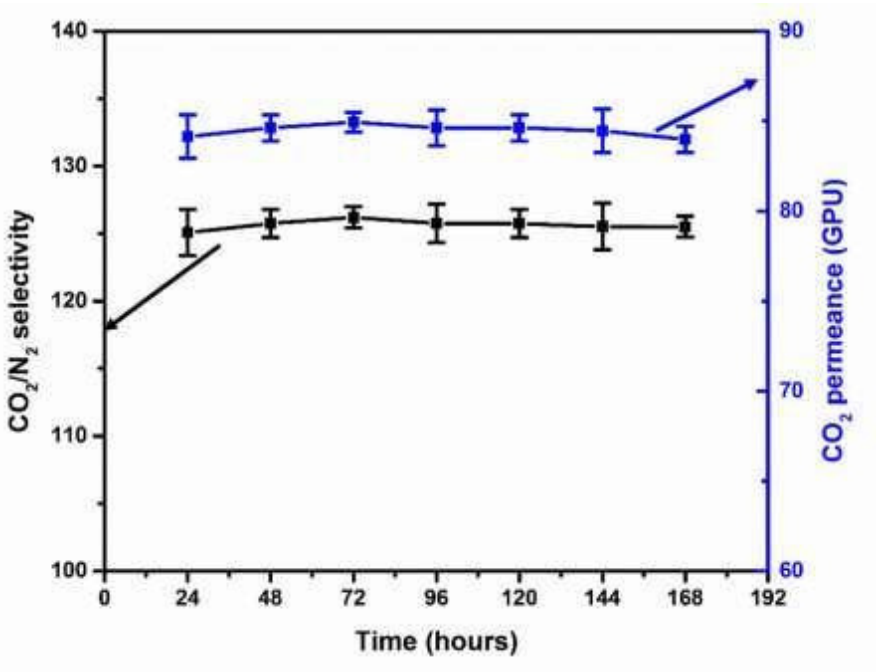

Figure 4.10 CO_2/N_2 separation performance stability of PAMAM10 membrane at the operating conditions, temperature = 90 °C and sweep/feed water flow ratio =2.33

4.3.6 Characterization of the Membrane After Gas Permeation

The FTIR absorbance spectra collected for PAMAM10 also indicated the unaltered functional groups of the membrane after gas permeation test (**Figure 4.11a**). A distinct absorbance peak was perceived at 3374 cm^{-1} in the membrane before gas permeation which featured the NH stretch of the primary amine group of PAMAM. Later, the peak was found merged with OH stretch band in the membrane after gas permeation. Since the gas permeation test was performed under humid condition, most of the water molecules might get reserved in the matrix during the experiment. Therefore, a cumulative effect of OH and NH stretch was visible in the spectrum obtained after gas permeation test. The AFM images of PAMAM10 surface after gas permeation test signposted the unchanged top layer of the membrane (**Figure 4.11b, c, d**). The average roughness achieved for the membrane after gas permeation study was 2.99 nm which was almost similar to that of the membrane before gas permeation study (2.81 nm).

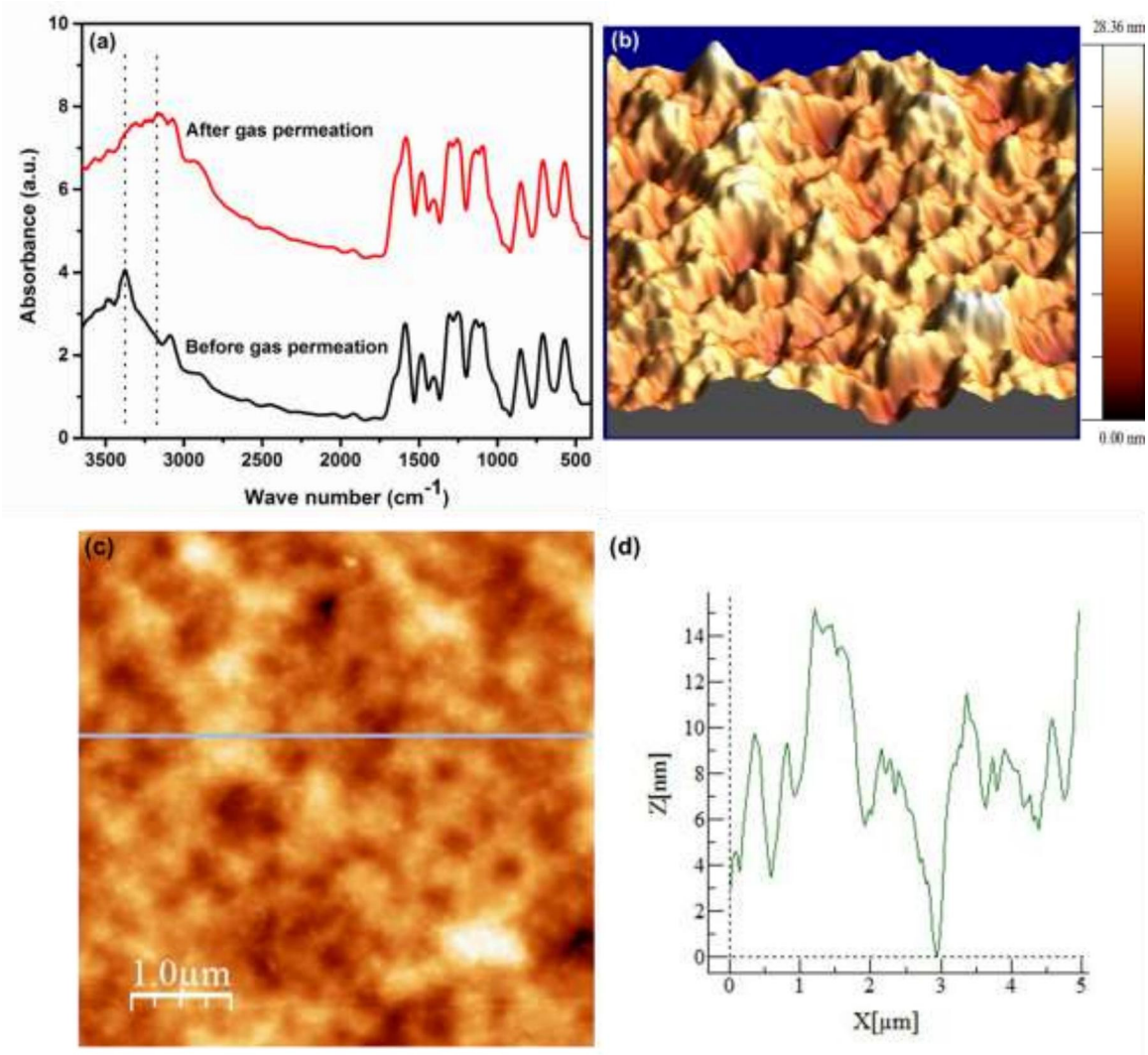

Figure 4.11 Characterization of PAMAM10 membrane after gas permeation study (a) FTIR spectra and (b, c, d) AFM image

4.3.7 Comparative Study

So far, a number of amine blended composite membranes have been utilized for CO_2/N_2 separation where researchers used single amine or amine blends [49, 109, 110]. Out of those, Francisco et al. reported CO_2/N_2 separation result obtained for different alkanolamines loaded polyvinyl alcohol (PVA) membranes [45]. The diethanolamine blended PVA membrane showed a CO_2/N_2 selectivity more than 100 along with CO_2 permeance ~ 8 GPU. Later, Cai et al. achieved CO_2 permeance 24 GPU and CO_2/N_2 selectivity as 80 for the PVA/polyallylamine membrane [39]. Other than PVA, chitosan was also utilized as the base polymer for amine loading [80, 111, 112]. The membrane comprising of chitosan/tetraethylenepentamine [59] exhibited the optimum CO_2

permeance of 24.7 GPU with the CO_2/N_2 selectivity 80. On the other hand the chitosan/ poly(allylamine) [33] membrane showed more than ~1.5 times better CO_2/N_2 separation performance than the chitosan/tetraethylenepentamine membrane. The large number of amines in poly (allylamine) improved the CO_2 permeance to 39 GPU with CO_2/N_2 selectivity ~260. Similarly, PAMAM provided abundant facilitated transport sites for CO_2 in CMC/PAMAM resulting almost three times higher CO_2 permeance than pristine CMC. Moreover, the thermal stability and moisture responsive nature of CMC based membranes encourage researchers to pick out CMC/PAMAM as CO_2 separation membrane.

4.4 Conclusions

PAMAM can be conjectured as the very effective CO_2 selective molecular gate after blending with CMC owing to its various tunable properties. The spectroscopic and microscopic analyses have established the formation of flawless thin layered CMC/PAMAM composite membrane. The increased percentages of PAMAM contribute aggregated molecules on the membrane surface which hinder gas permeation. Temperature stability and the moisture retention ability of the CMC/PAMAM have driven the membrane towards high temperature CO_2 separation application. The detailed study on mixed gas permeation have recognized the engagement of the membrane in facilitated transport, solution - diffusion and salting out phenomena. In conclusion, the membrane exposed an overall CO_2 permeance of ~98 GPU with the CO_2/N_2 selectivity ~149 on maintenance of sweep/feed water flow ratio 1.67 at 90 °C. Thus, CMC/PAMAM membrane set forth itself to be an impending candidate for large scale CO_2 separation application.

CHAPTER 5

Carboxymethyl Chitosan /Carbon Nanotubes Mixed Matrix Membranes for CO_2 Separation

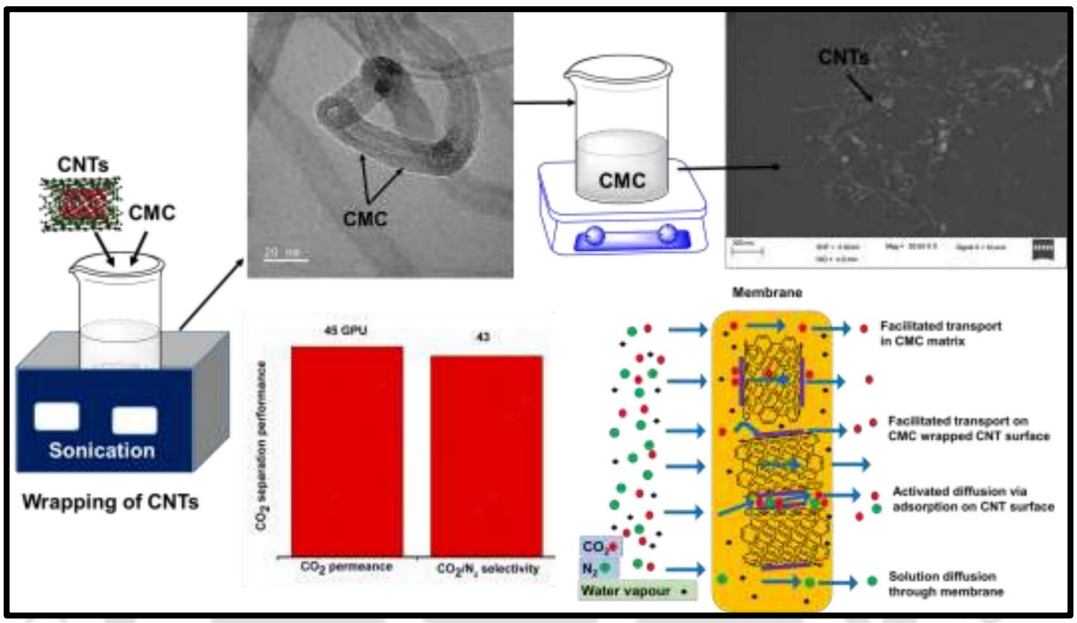

Overall graphical representation of fabrication of CMC/CNT membrane and CO_2 transport mechanism.

CHAPTER 5

Carboxymethyl Chitosan /Carbon Nanotubes Mixed Matrix Membranes for CO_2 Separation

*This work elaborates the stability issue confronted by conventional polymeric membranes in high temperature flue gas separation application. The multiwalled carbon nanotubes (CNTs) have been loaded to CMC matrix to improve its various physical properties which are relatively associated with CO_2/N_2 separation events. Herein, the amine groups present in CMC serve as CO_2 carrier and CNTs provide alternate pathway to the gas molecules. CNT regulated the moisture retention ability of CMC membrane which helps in upgradation of CO_2 selectivity. This work is scientifically acknowledged in "**Reactive and Functional Polymers**".*

5.1 Introduction

The pristine CNTs are hydrophobic in nature and hence they could reduce the extremely wetting tendency of hydrophilic membranes. The structure of CNTs has been shown in **Figure A1.2a**, **Appendix 1**. Additionally, incorporation of CNTs upgrades the mechanical properties of the polymeric membranes [113, 114]. CNTs fused in membranes basically provides one-dimensional nano-channels that act as alternate paths for CO_2 transport through membranes [71]. However, the pristine CNTs cannot disperse in polymeric matrix due to hydrophobic nature of the CNT surface. Therefore, functionalization of CNTs is required either by chemical or physical treatment. Chemical treatment process might lead to degradation of the walls of CNTs [115]. The dispersion of CNTs can be improved without chemical treatment through substantial wrapping by polymers such as carboxymethyl chitosan (CMC), which has emulsifying capacity and unique solubility [116]. The CNTs wrapping method not only preserves the inherent sp2 structure of CNTs, but also sustains the electronic structure of CNTs in a nondestructive manner [117]. The CMC wrapped CNTs (CMC-w-CNT) also show homogeneous dispersion in the membrane matrix due to the intermolecular interaction between matrix and the wrapping material [118]. Briefly, the mechanism of CO_2 transport through CMC/CNT membrane mainly follows (a) solution-diffusion and (b) facilitated transport mechanism.

This work emphasizes the simultaneous improvement of CO_2 permeance and CO_2/N_2 selectivity due to the alternate paths provided by CNTs. Moreover, the effect of temperature, moisture and filler percentage on the CO_2 separation performance of the prepared MMMs have been extensively investigated in the present study.

5.2 Experimental Section

5.2.1 Materials

Multiwalled carbon nanotubes (CNTs) containing > 95 % carbon (O.D. × L, 6-9 nm × 5 μm) and chitosan (310,000-375,000 Da) were procured from Sigma Aldrich. Methanol (≥ 99 % purity), monochloroacetitic acid, sodium hydroxide (NaOH) pellets and isopropyl alcohol (≥ 99 % purity) obtained from Merck were used to prepare CMC. The CMC was prepared using an already existing method as discussed in **Chapter 2** [87]. The polyethersulfone (PES) membrane (typical pore diameter = 0.1 μm, thickness = 0.015 cm) was supplied by Sterlitech, USA. The feed gas comprising CO_2/N_2 (20/80) were bought from Vadilal Chemicals Ltd. The Argon (99.99 % purity) gas used in sweep side and helium gas used in gas chromatography analysis were purchased from Jainex Gases Company, India. Millipore water® (>18 MΩ cm^{-1}) was used all through the experiments.

5.2.2 Membrane Fabrication

The CNTs were wrapped by CMC using wet grinding assisted sonication method [119]. An aqueous solution of 5 wt. % CMC was prepared by stirring the mixture at room temperature and centrifuged to eliminate the bubbles created during stirring. Calculated percentages of CMC wrapped CNTs (CMC-w-CNT) suspension (0.5 % (CNT0.5), 1 % (CNT1) and 1.5 % (CNT1.5)) were mixed to the CMC. The viscous solution was cast over the PES support using the casting blade and stored inside a laminar airflow for drying at room temperature. The dried membrane was further kept at 110 °C for 6 h and then was fixed in a flat sheet membrane module for gas separation test. The detail experimental set up for gas permeation study has been reported in **Chapter 2**.

5.2.3 Characterization Techniques and Gas Permeation Set Up

Field emission transmission electron microscope (FETEM, 2100F, JEOL) was used to visualize the magnified the magnified image of CMC wrapped CNTs. The CNTs wrapping

was validated using laser micro Raman system (Horiba Jobin Vyon, Model LabRam HR). The thermo mechanical behavior of the membranes were studied using dynamic mechanical analysis (DMA) (Netzsch DMA 242EArtemis1). The membranes were studied at the temperature range of 30-120 °C at 2.5 °C/min heating rate. The DMA was operated under N_2 environment in tensile mode (frequency = 1 Hz, dynamic force = 1 N). However, the instruments used for XPS, FESEM, AFM and TGA analysis are same as mentioned in **Chapter 2**. Similarly, the moisture retention test set up and gas permeation set up have been elaborated in the same chapter.

5.3 Results and Discussion

5.3.1 Dispersion Test for CNTs

The pristine CNTs are hydrophobic in nature which cause aggregation instead of dispersion [120]. The unsuccessful dispersion of CNTs leads to formation of ineffective CO_2 transport sites inside the membrane. The dispersion test was performed for raw CNTs and CMC-w-CNT obtained via wet grinding assisted sonication. The suspensions attained after stirring the raw and modified filler in polymer solution are shown in **Figure 5.1a.** The black shade of the suspension obtained from raw CNTs is lighter than that of the wrapped CNTs. Both the suspensions were kept for one day and no sediment was observed in CMC-w-CNTs suspension **(Figure 5.1b)**. This is the signposted of wrapping the CMC with CNTs that significantly improved the dispersion.

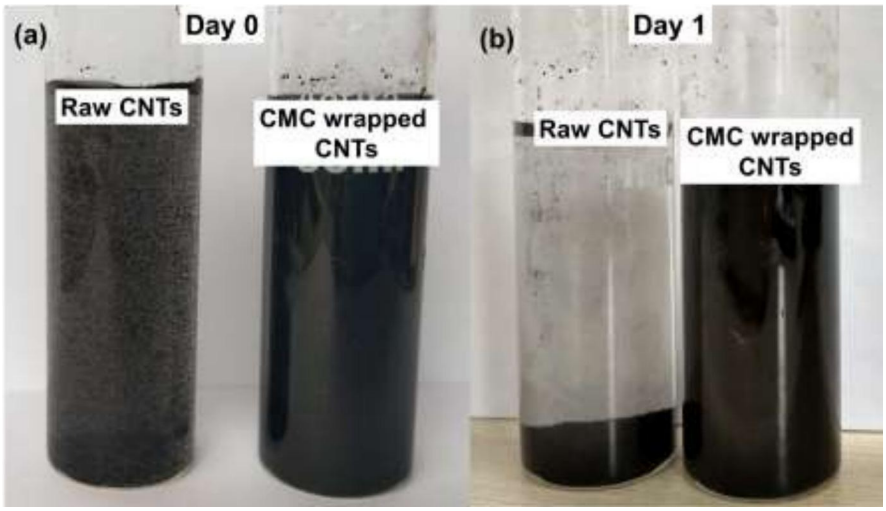

Figure 5.1 Photographs of raw CNTs and CMC-w-CNTs dispersed in CMC solution, (a) day zero and (b) day one.

5.3.2 Spectroscopic and Microscopic Analysis for CNTs

Raman spectroscopy provides strong evidence for the adherence of the polymer to the CNT surface. The CMC wrapping influences the vibrational frequencies that occur due to tangential movement of the carbon atoms. This indicates the presence of a strong attractive force between the graphite sheet and CMC. The G-band observed in the range of 1500–1600 cm^{-1} attributed to the tangential C-C stretching vibrations in both longitudinal and transverse direction on CNTs axis (**Figure 5.2**). The D-band perceived at 1300–1400 cm^{-1} corresponds to the disordered nanotube construction [121, 122]. It has been observed that the G-band has shifted to a greater wavenumber to 1590 from 1575 cm^{-1} after wrapping with CMC, whereas the D-band spectral shift is trivial. The un-altered position seen in D-band implies that CMC has not chemically attached to CNTs. The increase of the wave number of G-band is due to the field disturbance created by CMC coating in the graphite skeleton. This indicates the strong interaction between CMC and CNTs [119]. Moreover, D-band intensity to G-band intensity ratio (ID/IG) was obtained as 1.08 and 1.26 for raw CNTs and wrapped CNTs, respectively, which suggested the decrease of crystalline perfection in CNTs after CMC wrapping [123]. These results indicate the successful wrapping of CNTs with CMC.

The wrapping of the CNTs were further demonstrated from FETEM analysis. The FETEM images of the CMC-w-CNTs (**inset Figure 5.2**), depicted the non-destructive walls of CNTs. The polymer wrapping did not alter the integral architecture of CNTs due to the formation of bridge between CMC and CNTs. Some distinct layers were observed on the outer walls of the CNTs which may be due to CMC adherence. The elemental analysis of

those layers indicated that the aggregation was due to the CMC wrapping only, as presented in **Figure 5.2b**.

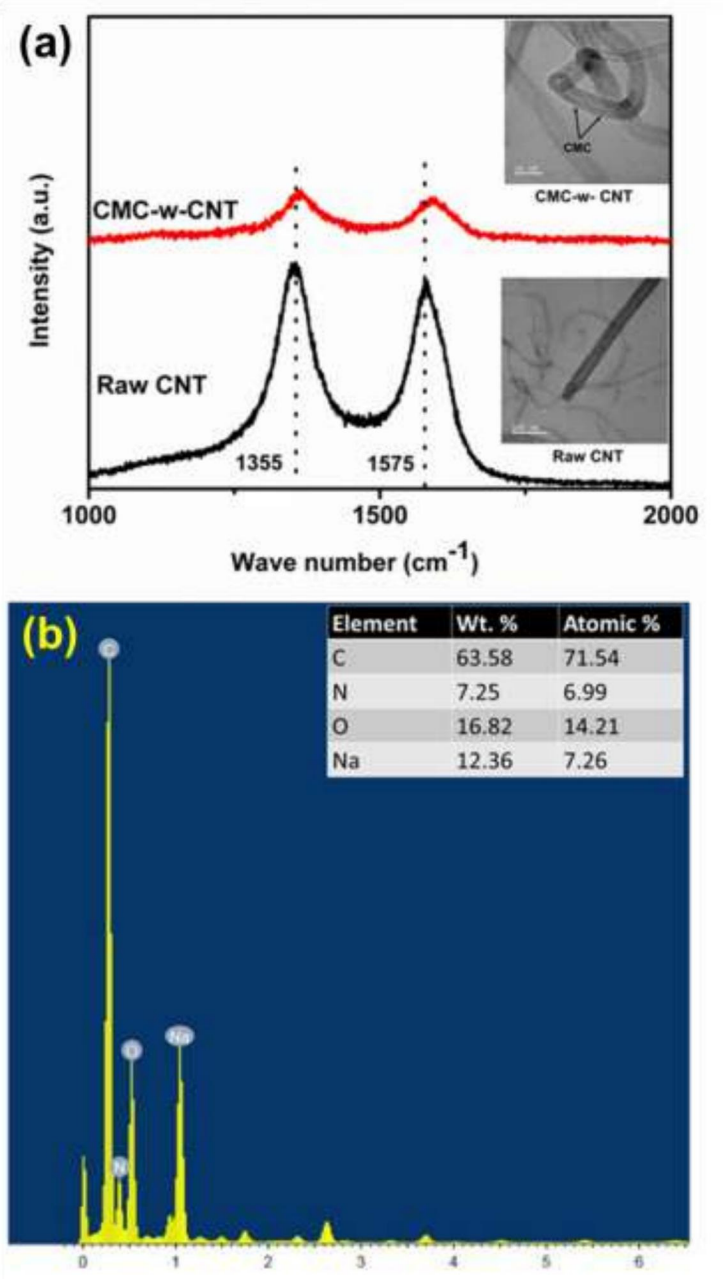

Figure 5.2 (a) Raman spectra of raw CNTs and CMC-w-CNTs. The inset represents the FETEM image of raw CNTs and CMC-w-CNTs (b) Energy dispersive X- ray analysis of CMC wrapped CNTs

5.3.3 Spectroscopic Analysis of Membranes

The functional groups present in the MMMs have been identified using FTIR analysis (**Figure 5.3a**). The wide peak detected at wave number range 3200-3500 cm^{-1} is due to the combined effect of N-H and -OH groups of CMC which was observed more broadened in CNTs incorporated membranes [56, 124]. The peaks noticed at 1412 and 1377 cm^{-1} are attributed to the C=O of –COONa symmetric stretching and C-N stretching of CMC. The CNTs incorporated membranes possess few extra peaks, indicating the presence of CNTs in CMC, as shown in **Figure 5.3a.** The weak peak at 1880 cm^{-1} assigned to the ring substitution pattern of CNTs.

The XPS has been utilized to comprehend the successful loading of CMC-w-CNTs in the CMC membranes. The deconvoluted peak obtained for CMC and CNT1 membranes indicated the characteristic bonds present in the membranes. The XPS survey spectra indicated the presence of C, N, O and Na in the prepared membranes (**Figure 5.3b**). The deconvoluted peak for C1s of CMC membrane signposted the presence of C-C, C-N, C-O and C=O bonds at binding energies of 284.6 eV, 286.3 eV, 287.6 eV and 288.6 eV, respectively (**Figure 5.4a, b**) [125]. The existence of C-O-C and O-C=O bonds are also established by the deconvolution of O1s peak showed at binding energies of 531.3 and 532.5 eV (**Figure 5.5**). Likewise, the peak at 1071.3 eV indicated the presence of sodium (**Figure 5.5**). The deconvoluted nitrogen (N1s) peak at 400.3 eV of CMC recognized the primary amine present in the CMC unit structure. The additional peak obtained at 399.1 eV ascribed the secondary amine formed due to intra polymer hydrogen bonding. Similarly, the deconvolution of C1s of CNT1 recognized the occurrence of C-C, C-N, C-O and C=O bonds at the binding energies of 284.6 eV, 286.06 eV, 287.77 eV and 288.5 eV, respectively (**Figure 5.5**). The C-C peak in CNT1 was found as the major peak whereas in CMC the C-C and C-N peaks were perceived as the leading peaks. The CNTs structure mostly comprises of C-C bonds which contributed to the major peak at 284.6 eV for CNT1 membrane. The atomic percentage of C has been obtained as 62.2 % in CNT1 whereas the C atomic percentage in CMC membranes is 61.19 %. This increase of atomic percentage of C occurred may be due to the loading of CNTs in CMC.

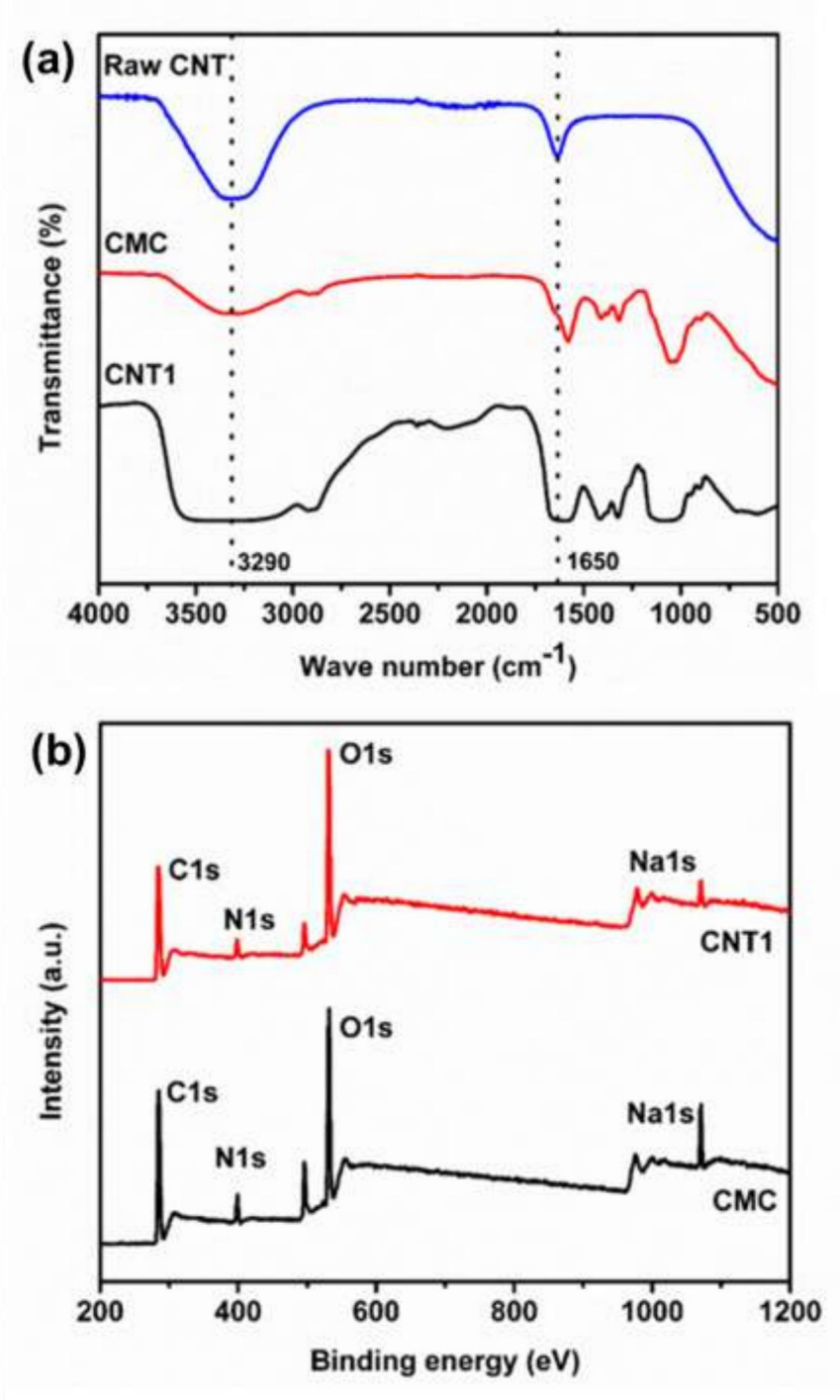

Figure 5.3 (a) FTIR spectra (b) XPS survey spectra for CMC and CNT1 membranes

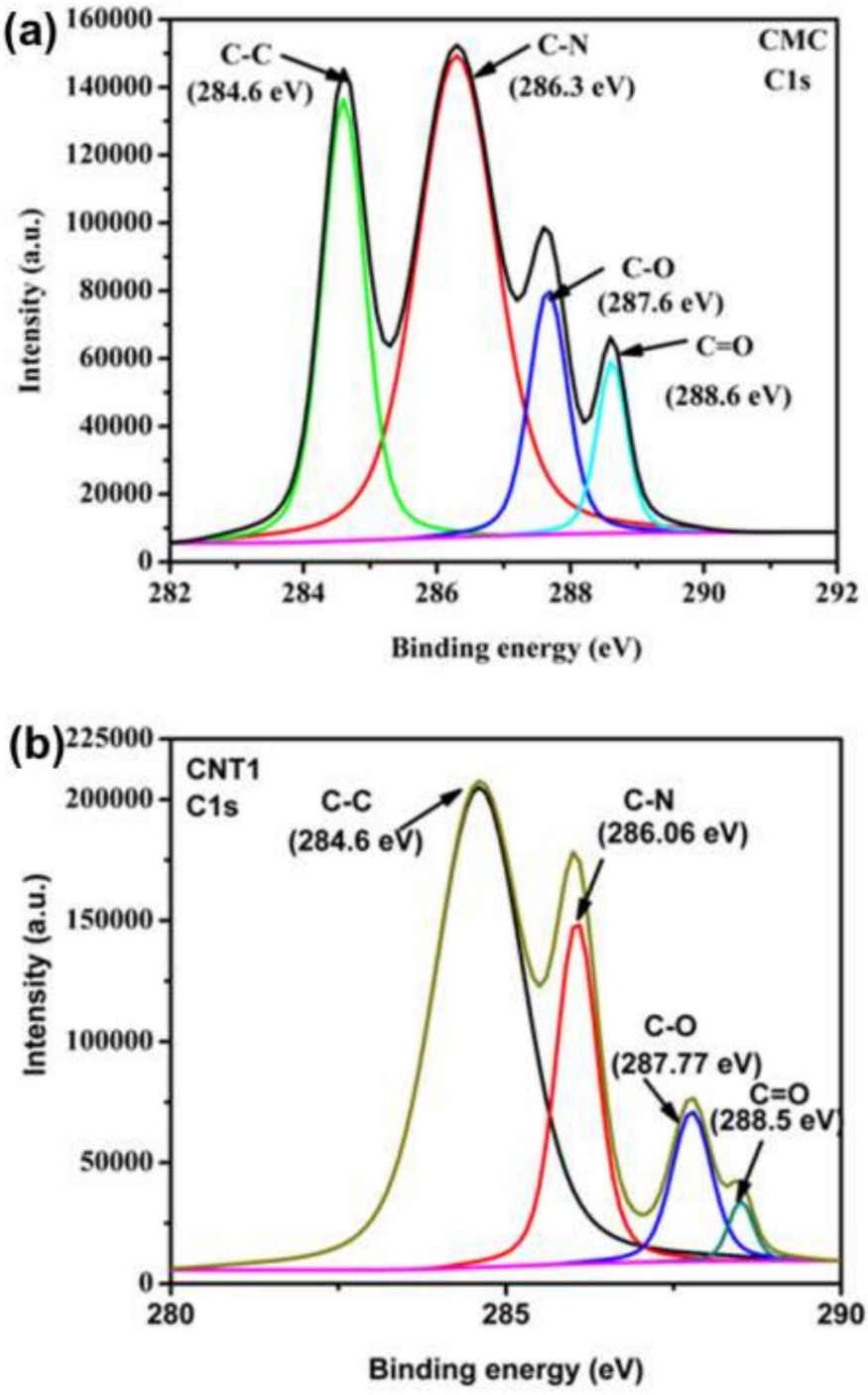

Figure 5.4 Deconvoluted XPS spectra for C1s in (a) CMC (b) CNT1 membranes.

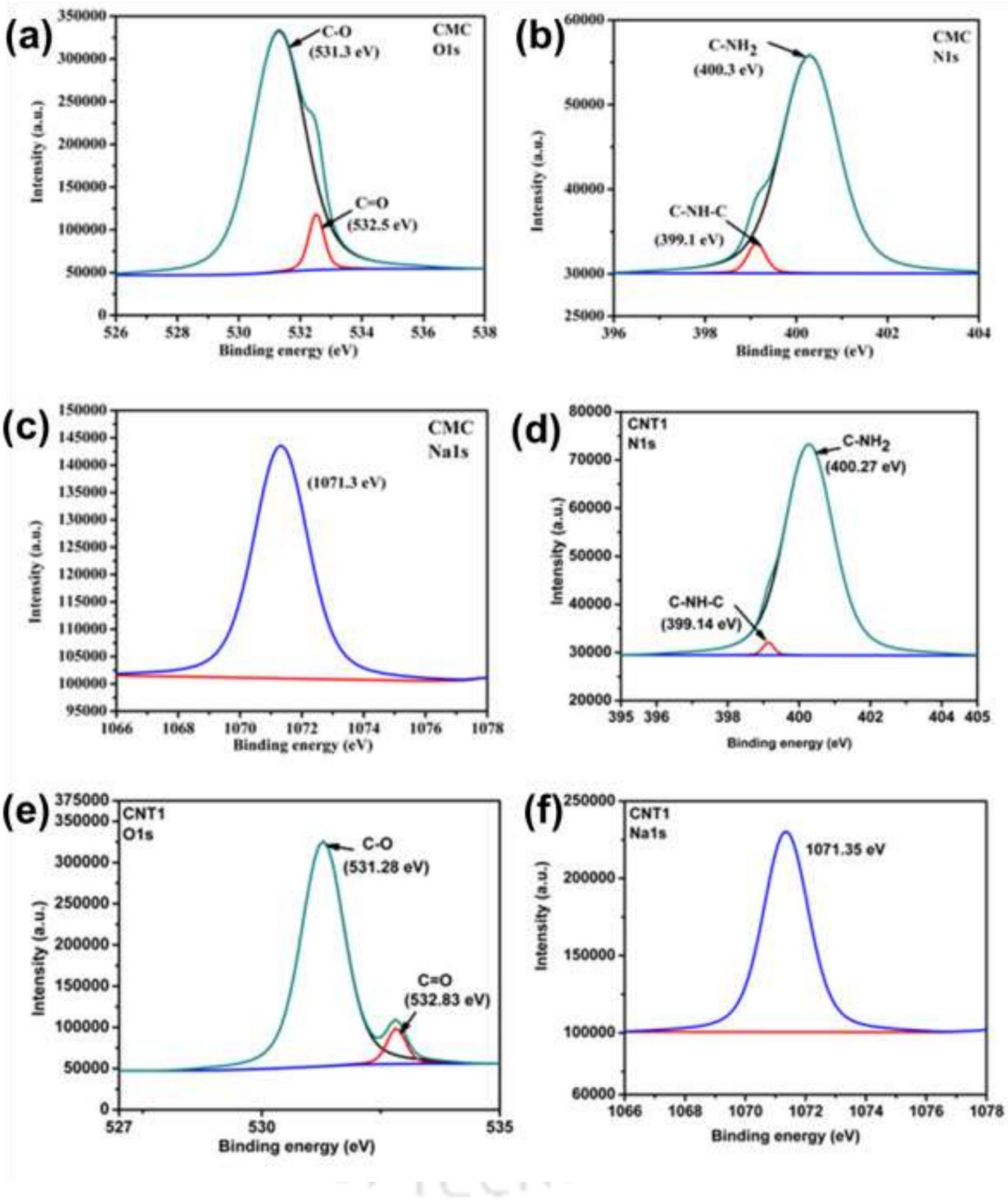

Figure 5.5 Deconvoluted XPS spectra for CMC and CNT1 membranes (a) CMC/O1s, (b) CMC/N1s, (c) CMC/Na1s, (d) CNT1/N1s, (e) CNT1/O1s, (f) CNT1/Na1s

5.3.4 Morphological Analysis of Membranes

The top surface and cross-sectional morphologies of the membranes for different CNT loadings were investigated using FESEM at 45-50 kx magnification. From the images shown in **Figure 5.6**, it was clear that the pure CMC membrane top surface was smooth and

homogeneous without defects. Tube-like structures were observed with the loading of CNTs. The surface of the CNTs loaded membranes were uniform, depicting the good interface compatibility of CNTs with the membrane polymer. The loading of 1.5 % CNTs lead to agglomeration of nanotubes on the matrix of the membrane. The accumulated CNTs might restrict the movement of gas molecules through the membrane instead of providing an alternate way for gas flow.

The cross-section of the membranes displayed perfectly differentiated dense and porous layers (**Figure 5.7**). The finger-like structured part is due to the pores present in the PES support and the thin dense layer consisted of the CNTs blended CMC. The PES support provides mechanical strength to the thin active layer (~ 2.7 micron). Since the casting solution viscosity was maintained above 1200 cp, the active layer has not penetrated into the pores of the PES support. Moreover, when pressure is applied during the permeation test, the pure CMC active layer penetrates into the pores and increases the active layer thickness [126]. Hence the permeability of the membrane drops. The CNTs incorporated membranes are free from this problem as CNTs induces the mechanical stability of the membranes. Some randomly distributed tube-like structures were evident in the dense layer of CNTs embedded membranes. The typical 3D image obtained from the AFM analysis of CMC, CNT0.5, CNT1, CNT1.5 membranes clearly showed distinct peak and valley regions (**Figure 5.8**). The topographical images were taken in the area of 10×10 micron of all the membranes. The membrane containing 0.5 wt. % CNTs showed an average roughness of 15.7 nm which is due to the random scattering of CNTs in the matrix. A few small spikes were observed along with the bulky peaks of CMC, indicating the presence of CNTs in the membranes (CNT0.5, CNT1 and CNT1.5). Average roughness of the CNT1.5 membrane is 30.16 nm, evidenced the agglomeration of fillers on the membrane surface instead of homogeneous dispersion in the matrix.

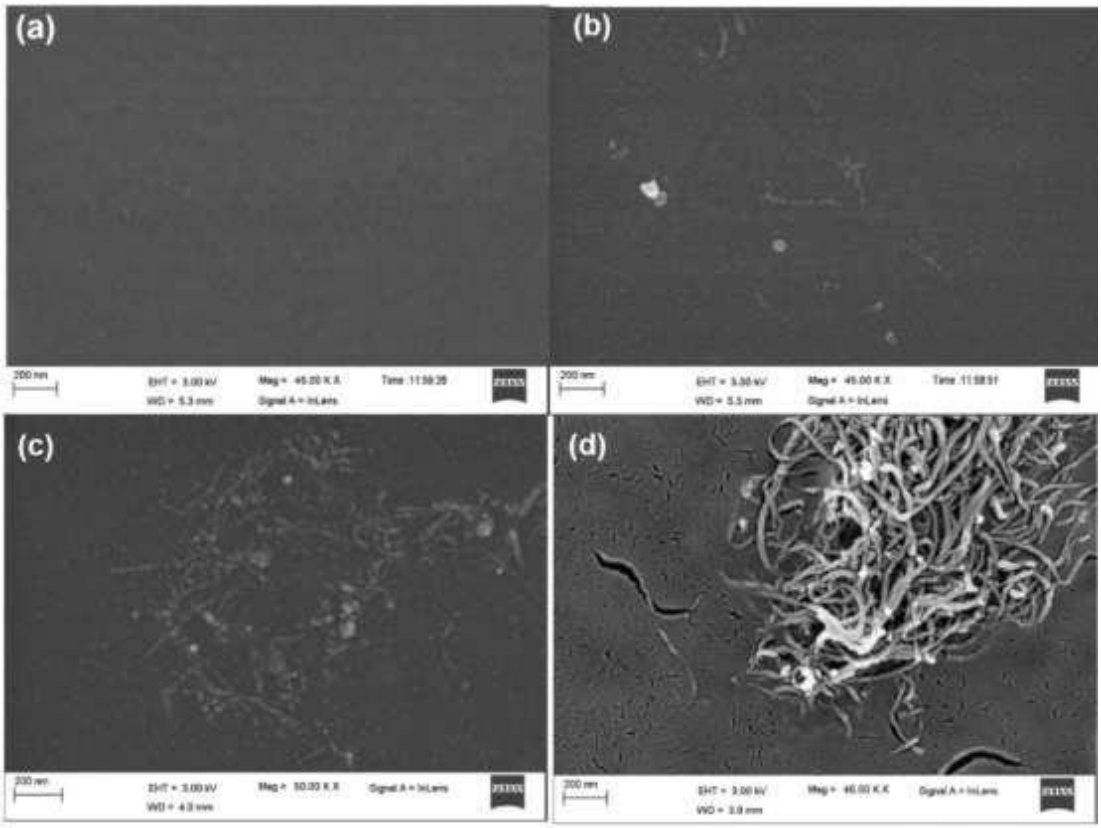

Figure 5.6 FESEM analysis of the top surface of the membranes (a) CMC, (b) CNT0.5, (c) CNT1, (d) CNT1.5.

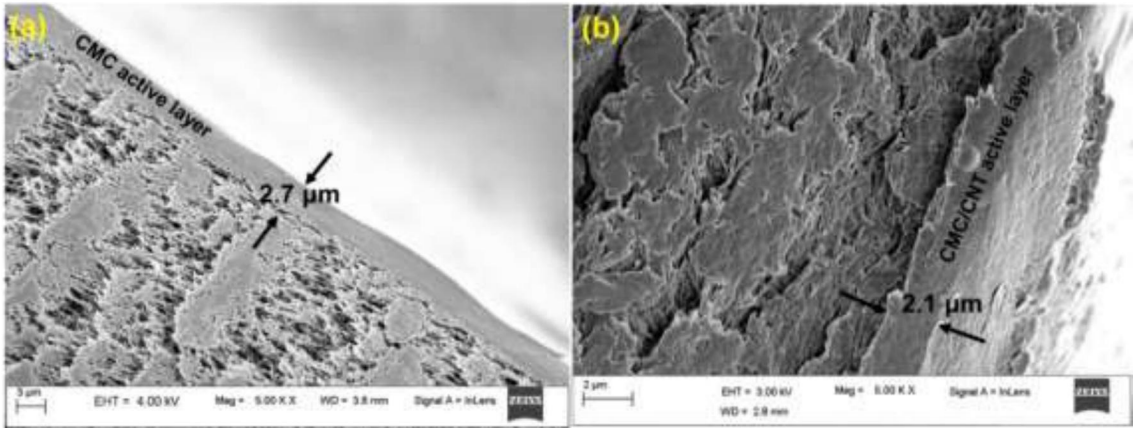

Figure 5.7 FESEM analysis of the cross section of the membranes (a) pure CMC membrane, (b) CNT1 membrane (5kx).

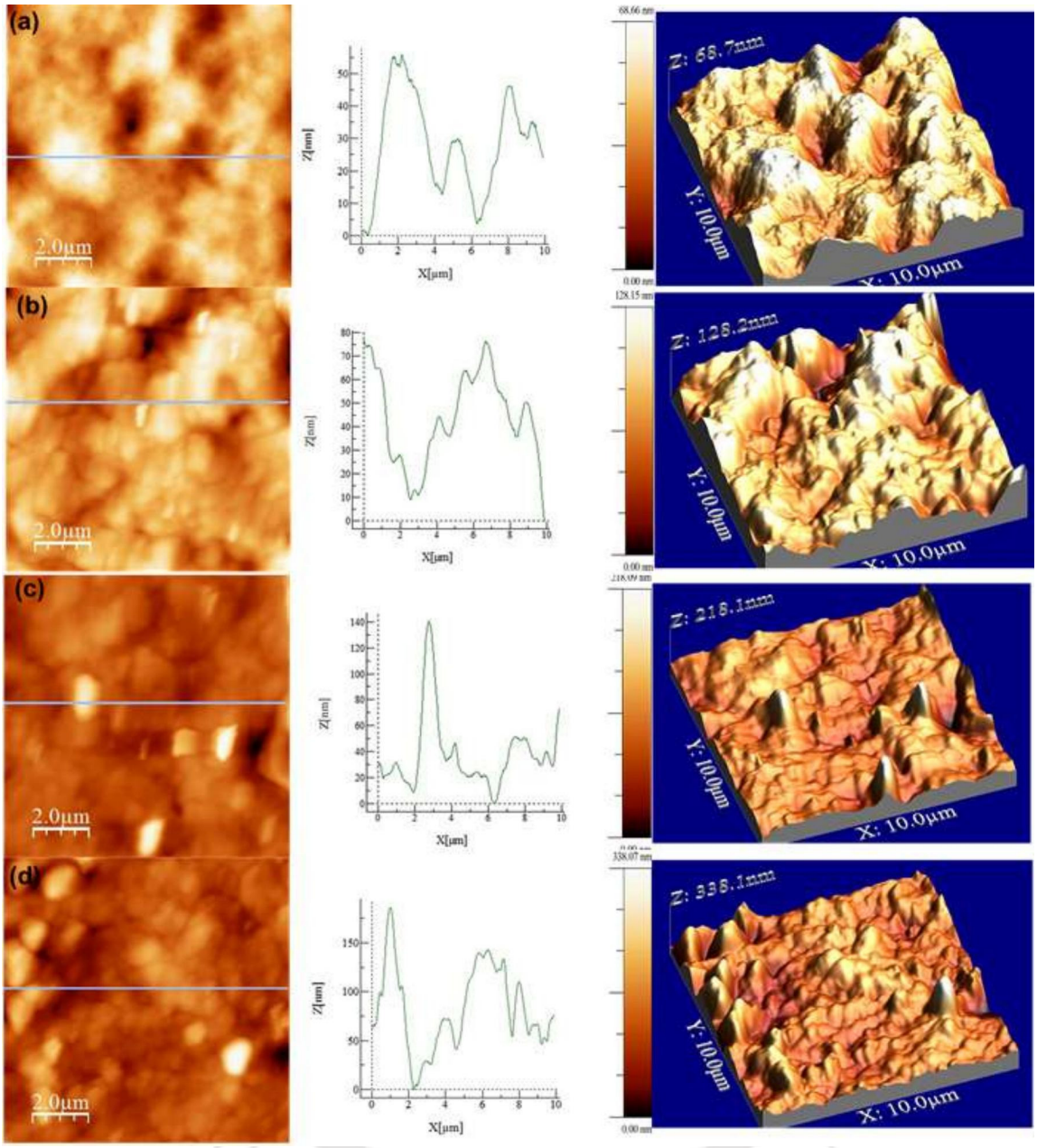

Figure 5.8 AFM images (2D image, height profile and 3D image) of the membranes (a) CMC, (b) CNT0.5, (c) CNT1, (d) CNT1.5.

5.3.5 Water Retention Ability

Water retention capacity of membrane has dominant role in CO_2 separation [127]. In hydrophilic polymers the state of water are found as (a) bound water in non-freezable form having tight interaction between water and polymer, (b) bound water in freezable form having loose interaction between water and polymer and, (c) free water is free from water-polymer interaction [128]. The water molecules take part in facilitated transport mechanism.

Further, water molecules induce the membrane flexible that reduce the mass transfer resistance for the gas molecule. The free water molecules present on the membrane matrix increases the CO_2 solubility [58]. Most importantly, the diffusion coefficient of ions in water is usually four times superior to gas molecules in solid [49]. Therefore, the bicarbonate ion (HCO_3^-) formed due to CO_2 - NH_2 reaction in presence of water diffuses swiftly (Eq. 5.1).

$$CO_2 + 2RNH_2 + H_2O \rightleftharpoons RHNCOOH + RNH_3^+ + HCO_3^- \qquad \text{(Reaction 5.1)}$$

The excess membrane swelling directly affects the selectivity of the membrane [51]. Therefore, the limited swelling of the membrane shows perfect CO_2 separation performance. Varying the relative humidity (RH), the swelling percentage for CMC, CNT0.5, CNT1 and CNT1.5 at room temperature has been recorded, as presented in **Figure 5.9**. Initially, at lower RH the water held up by the membranes are very less. Later, at 80 % relative humidity, the water uptake capacity increased up to 44 %, 24 %, 17 % and 16 % for CMC, CNT0.5, CNT1, CNT1.5, respectively. Afterwards, the membranes achieved remarkably higher water holding capacity at 100 % RH. The swelling process occurs in two stages which can be explained by Flory Huggin's theory. According to this theory, the free energy of mixing (G_{mixing}) is ascribed to the conformation of polymers ($\Delta G_{conformation}$) and polymer-solvent interaction ($\Delta G_{contact}$) [106]. These two entropy factors can be expressed as:

$$\Delta G_{\text{conformation}} = RT\,[\ln \Phi w + \Phi p] \qquad 5.1$$

$$\text{and } \Delta G_{\text{contact}} = RT\chi\,\Phi_p^2 \qquad 5.2$$

Where, R = gas constant, Φ = volume fraction of polymer (p) and water (w), T = absolute temperature, and χ = polymer- solvent interaction parameter. $\Delta G_{conformation}$ is predominant in the low RH region and the chain relaxation of the polymer takes place as soon as polymer comes in contact with water. In this stage, the water uptake by the membrane is limited depending on the amount of water in the gas phase. Once the RH reaches the critical point, $\Delta G_{contact}$ becomes the main controlling factor of the swelling phenomenon and the overall swelling has been affected by both $\Delta G_{conformation}$ and $\Delta G_{contact}$. Thus, the water uptake by the membranes increases drastically even with the slight increase of RH.

Moreover, the water intake behaviour of membranes have been noted at different time period. The water absorption capacity of the CMC membrane is very high. Initially it absorbs water continuously up to 10 h and gradually it reached the saturation point. The

achievement of the equilibrium point occurs if G_{mixing} equals to the free energy for polymer network deformation (ΔG_e) which can be expressed as:

$$\Delta G_e = RT \left(\frac{\rho_p / \breve{V}_s}{\overline{M_c}} \right) \varphi_p^{1/3} \qquad 5.3$$

Where, $\breve{V}_s$ = molar volume of solvent and $\overline{M_c}$ = molecular mass of the network chain. This expression for ΔG_e specifies the influence of the polymer property and environment on the water uptake behaviour of the membranes [49].

The incorporation of hydrophobic entities to CMC reduces the water intake rate of the membrane [129]. This action reduces the solution-diffusion of bigger gas molecules and as a result CO_2 selectivity increases substantially.

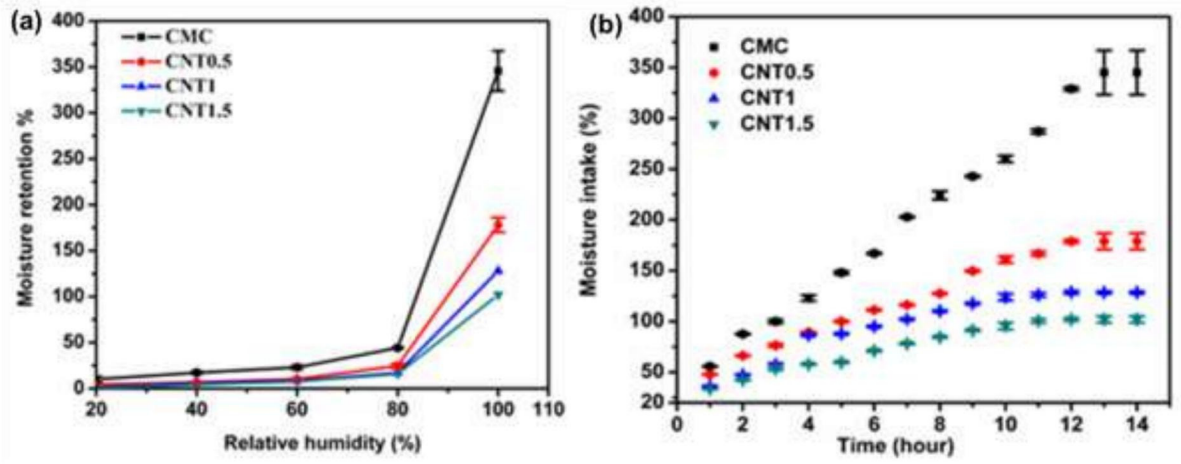

Figure 5.9 (a) Moisture retention behavior and (b) rate of moisture intake in CMC, CNT0.5, CNT1 and CNT1.5 membranes.

5.3.6 Dynamic Mechanical Analysis (DMA)

DMA is a very useful technique for describing the thermal changes of the polymer membranes [130]. The upturning pattern of the storage modulus versus temperature curve as shown in **Figure 5.10** indicates the increasing stiffness of the membranes with rising of temperature. The increased stiffness may restrict the gas flow through the membrane at higher temperature. The increment of CNTs percentage also showed higher storage modulus than the CMC membrane which increased the anti-plasticization of the membranes. This is because the free volume present in the CMC molecules have been occupied by CNTs and

thus the chain molecular movement of CMC has restricted [131]. However, the hydrogel membranes contain some amount of absorbed moisture in the matrix and the elevation of temperature prompts desorption [132]. Thus the membrane eventually acquires embrittlement with rise in temperature. Furthermore, CMC membrane has more swelling tendency whenever gas molecules come inside the membrane. Thus, the gas diffusion coefficient increases and the gas diffusion selectivity decreases [133]. On the contrary, the improvement of antiplasticization phenomenon in the CNTs incorporated membranes helps in enhancement of CO_2/N_2 selectivity of the membrane. Nevertheless, excessive incorporation of CNTs can completely hinder the gas transportation and decline the CO_2 flux as well.

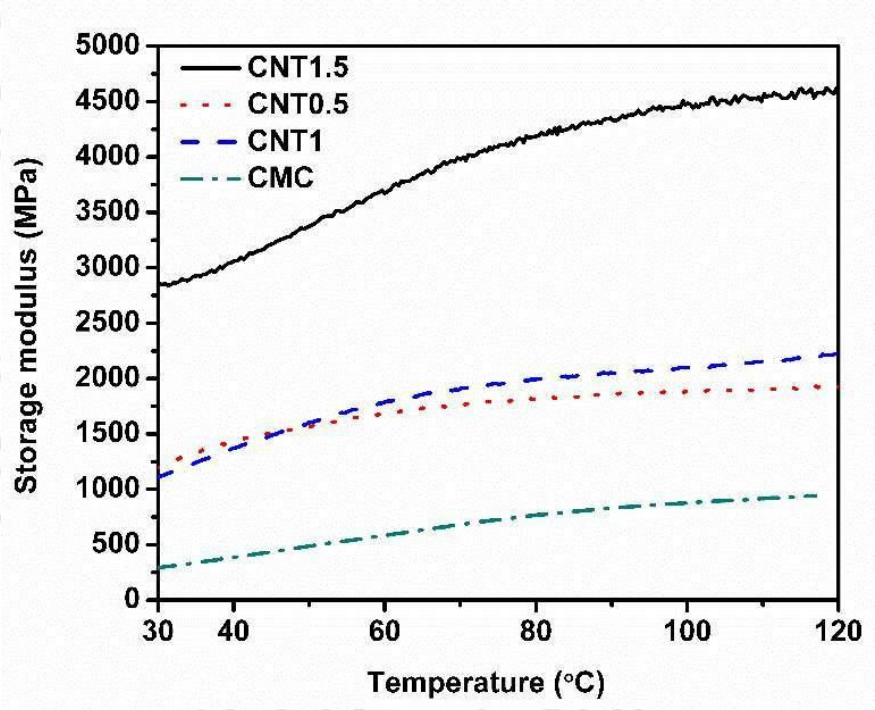

Figure 5.10 DMA curves for the active layers of CMC, CNT0.5, CNT1, and CNT1.5.

5.3.7 Gas Permeation Study

The gas permeation study was executed for CMC, CNT0.5, CNT1 and CNT1.5 membranes to see the effect of CNTs loading on the separation performance. Additionally, the effect of temperature was studied on the membrane containing 1 wt. % CNTs by changing the temperature from 60-120 °C. Later, the sweep/feed water flow ratio was varied from 0.33 to 3.

5.3.7.1 Effect of operating temperature

The temperature influence on CO_2 separation performance of CNT1 membrane has been studied at different temperatures (60-120 °C) keeping the absolute pressure constant at 2 and 1.21 bar in the feed and permeate side, respectively. The moisture environment was maintained at 1.67 sweep/feed water flow ratio. **Figure 5.11a** evidenced the reduction of CO_2 permeance in CNT1 membrane (from 45 GPU to 21 GPU) with rising of the temperature from 60 to 120 °C. The permeance drops were found as 13 % at 70 °C and 10 % at 80 °C, respectively. Later, as the temperature reached to 90 °C a minor permeance drop was observed as 2 % only. This may happen due to increased facilitated transport reaction at higher temperature. Also, CO_2 solubility increases with increase in temperature [134]. Well along, a 17 % reduction of CO_2 permeance was witnessed at 100 °C when the temperature was increased from 90 °C. After that, it started decreasing drastically at 110 °C. This change may be due to the stiffness gained by the membranes and reduced moisture content within the matrix [135]. The free and bound moisture release event has been identified in the DSC graph, as shown in **Figure 5.11b**. On the other hand, the CO_2/N_2 selectivity of the CNT membrane was found increasing from ~34 to ~47 when the temperature was varied from 60 to 90 °C. Although, the CO_2 permeance of the membrane at 90 °C (34 GPU) and 100 °C (28 GPU) has significant difference, the CO_2/N_2 selectivities were almost alike at both the temperatures. The CO_2/N_2 selectivity was dropped down to 38 at 110 °C.

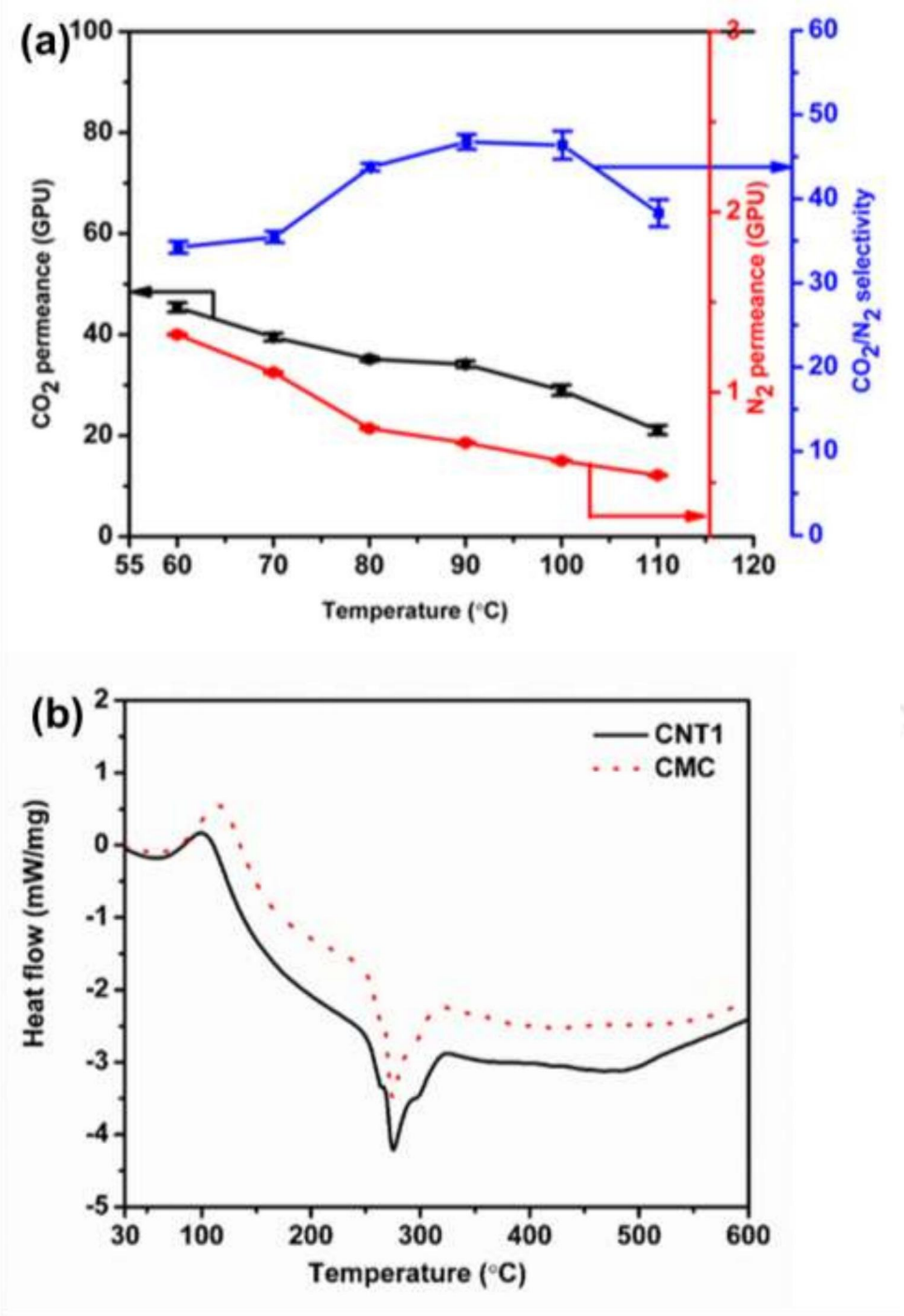

Figure 5.11 (a) Effect of temperature on CO_2 and N_2 permeance and CO_2/N_2 selectivity in CNT1 membrane at feed absolute pressure = 2 bar, sweep absolute pressure = 1.21 bar, sweep/feed water flow ratio = 1.67 (b) DSC graph of CMC and CNT1 membranes.

5.3.7.2 Effect of CNTs content

Gas permeation study has been performed on the prepared membranes using binary gas mixture of CO_2/N_2. All membranes were tested at 80 °C with the sweep to feed water supply ratio of 1.67. The absolute pressure was maintained at 2 bar on the feed side. **Figure 5.12** displays the gas transport behavior of the membranes with different CNTs content. The graph obtained from water intake capacity test clearly indicates that the water intake ability decreased for the CNTs blended membranes which directly affect the flexibility of the membrane. The thickness of the pristine CMC active layer increases when we apply pressure on the membrane as the layer starts penetrating to the pores of the support layer [136]. The loading of CNT resolves this problem by providing mechanical strength to the membrane. The thin active layer helps in getting higher flux and permeability as compared to a thick membrane. Besides, the porous structure of the CNTs increases the CO_2 transporting channels in the matrix. However, the higher CNTs content may cause agglomeration of the particles on the membrane surface, which affects the membrane separation performance as clustered fillers may block the CO_2 passage paths. Besides, more CNTs loading reduces the water intake ability of the membrane, as seen in **Figure 5.9**, which lowers the solution-diffusion and facilitated transport of CO_2.

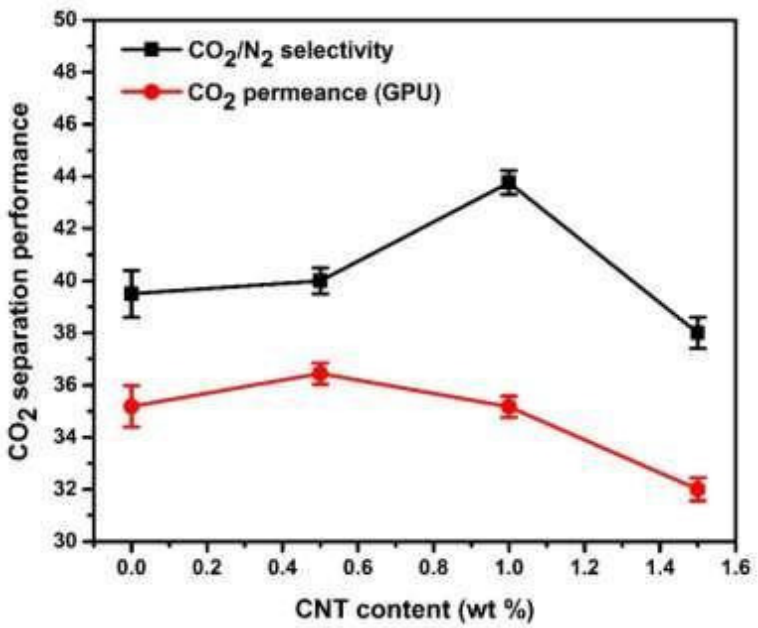

Figure 5.12 CO_2 Permeance and CO_2/N_2 selectivity of membranes having different composition of CNTs at temperature = 80 °C, sweep/feed absolute pressure = 2/1.21 bar, sweep/feed side water flow ratio = 1.67.

5.3.7.4 Effect of sweep/feed water flow rate ratio

The influence of sweep side water flow rate on the gas separation performance has been studied. The operating conditions for this test have been set as: sweep/feed water ratio = 0.3, 1, 1.67, 2.44 and 3; feed / sweep side absolute pressure = 2 bar / 1.21 bar, respectively and temperature = 80 °C. The CO_2 permeance for the CNT1 membrane increased from 15 GPU to 43 GPU when the sweep/feed water flow rate ratio was changed from 0.33 to 3. Correspondingly, the CO_2/N_2 selectivity followed the similar trend as shown in **Figure 5.13**. Initially, at low sweep/feed water flow ratio, the CO_2/N_2 selectivity was less due to the less flexibility of the membrane and minimum facilitated transport reaction inside the membrane. As soon as the water flow ratio was increased to 1.67, the permeance and the CO_2/N_2 selectivity reached to 35 and 44, respectively. The following reasons can be attributed to the observed trend of CO_2 permeance and CO_2/N_2 selectivity behaviour when the sweep/feed water flow ratio is greater than one: (a) the water vapour permeation has been obstructed from sweep side which enhances the water retention in the membrane system. This in turn helps in the formation of more CO_2- carrier complex for CO_2 facilitated transport. (b) Higher water retention increases the flexibility of the membrane and supports the transport of gas molecules via solution diffusion. Besides, water leads to plasticization of the membrane that increases the gas diffusivity through it [137]. Further, the water flow ratio was increased to 2.33 and obtained a CO_2/N_2 selectivity of 43 and CO_2 permeance as 36 GPU. However, the ratio was increased up to 3 for further investigation and a slight change is witnessed in CO_2/N_2 selectivity (45) and CO_2 permeance (43 GPU). The saturated trend of CO_2/N_2 selectivity is due to the competitive sorption between CO_2 and N_2 molecules [138]. The increased moisture supply resulted in excessive swelling of the membrane matrix which induces the flexibility of the membrane and hence encourages N_2 passage. Additionally, the performance stability of CNT1 membrane has found more than 160 hours whereas the bare CMC membrane exhibited fluctuation after 96 hours.

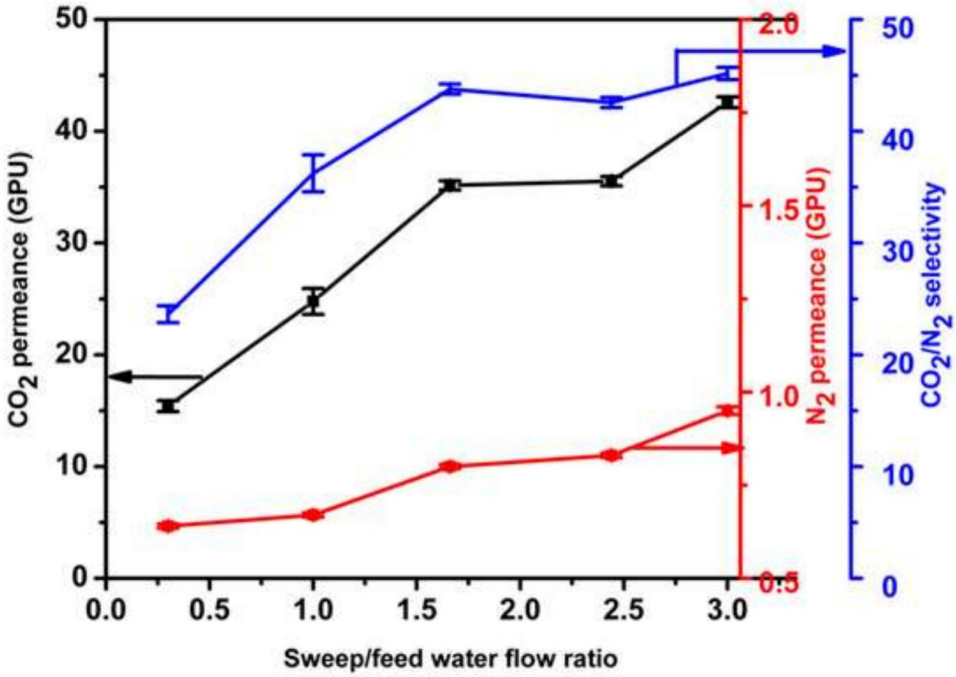

Figure 5.13 Effect of sweep water flow ratio on CO_2 and N_2 permeance and CO_2/N_2 selectivity of CNT1 at 80 °C, feed absolute pressure = 2 bar, sweep absolute pressure = 1.21 bar.

The CO_2 separation result obtained for CMC-w-CNT incorporated CMC membrane has been compared in **Table 5.1** with a few literatures reported on CNTs based membranes. The CNTs had been loaded with various matrix materials and utilized for CO_2 separation application. However, the membrane discussed in our work showed explicit improvement in CO_2 selectivity as well as permeability compared to other membranes. The significant improvement has been observed presumably due to the synergistic effect of CNTs and CMC. Hence, this combination can flourish as the promising material to be used in enhanced CO_2 separation.

Table 5.1 CO_2 Permeance and CO_2/N_2 selectivity of CNTs loaded membranes

Polymer matrix and CNTs percentage	Operation condition			CO_2/N_2 Selectivity	Permeance (GPU)	Ref.
	Pressure bar	Temp. (°C)	Thickness (micron)			
Pebax1657/2 % CNTs	10	Room temp.	15-20*	78.6	18.8	[139]
Cellulose acetate/0.1 wt. % pure CNTs	3	-	250	5.5	146.9	[75]
brominated poly(2,6- diphenyl-1,4-phenylene oxide)/ 5% CNTs	0.67	Room temp.	50-90*	31	2.1	[140]
Polyimide/CNTs (25:1)	1	Room temp.	3-4*	4.1	247.6	[141]
Pebax-PEG/ 2% CNTs	10	Room temp.	80-100*	108	8.2	[142]
CMC/1 wt. % CNTs	2	80	2.7	45	43 GPU	This work

*Average values are considered for calculation of premeance (GPU)

5.4 Conclusions

The CNTs are dispersed in CMC successfully and a series of CMC membranes with different CNTs content were prepared using solution casting method. The Raman and FETEM techniques verified the formation of CMC wrapped CNTs on application of wet grinding assisted sonication. The development of defect-free thin layer of CMC/CNTs over the porous support has been spotted in the FESEM images. The AFM images signposted the surface roughness of the membranes increases with increased percentage of CNTs. The XPS and FTIR analyses confirmed the development of CNTs incorporated membranes. The water uptake ability of the matrix layers was also investigated under different humid environment and the moisture holding capacity was decreased with the increasing of CNTs loading in the CMC membrane. Optimal CO_2 permeance (~ 43 GPU) and CO_2/N_2 selectivity (~ 45) were achieved with the incorporation of 1 wt. % CNTs at water flow ratio 3 and temperature 80 °C. The CNTs loaded membrane in our work showed explicit improvement in CO_2 selectivity and permeability compared to other membranes reported in the literature.

CHAPTER 6

High Speed CO_2 Transport Channel Assisted Carboxymethyl Chitosan Mixed Matrix Membrane for CO_2 Separation

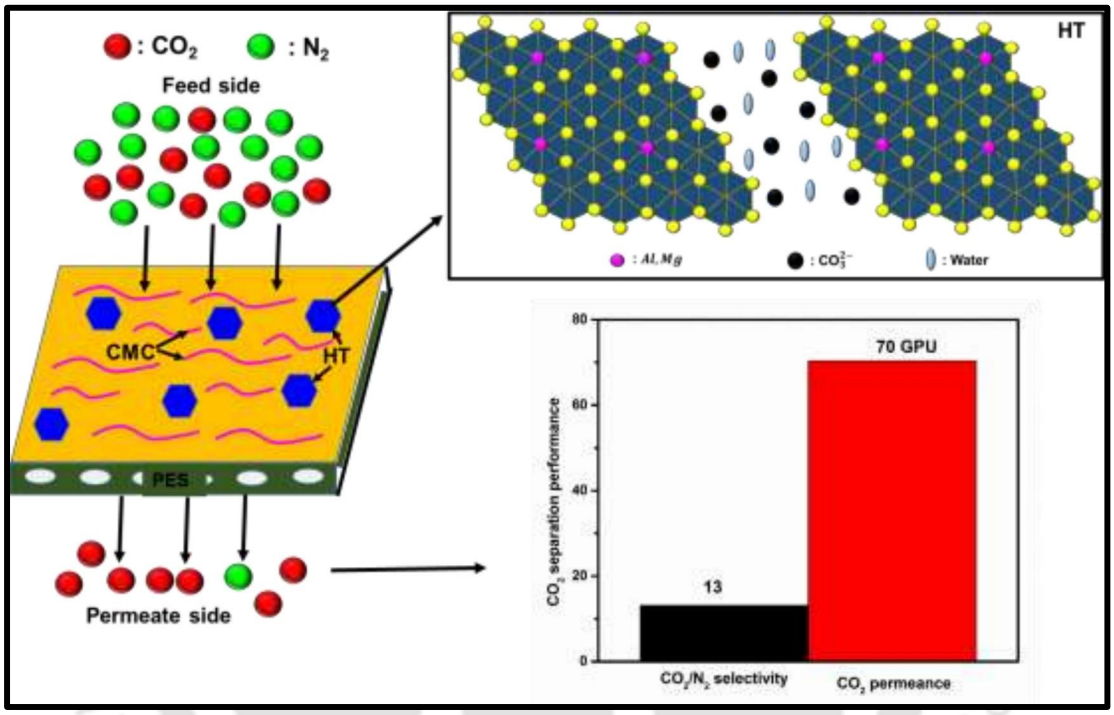

Overall representation of CMC/HT membrane in terms of CO_2 separation.

CHAPTER 6

High Speed CO_2 Transport Channel Assisted Carboxymethyl Chitosan Mixed Matrix Membrane for CO_2 Separation

The present work elaborates the contribution of hydrotalcite (HT) and CMC in CO_2 separation application. This chapter is an attempt to rectify the compatibility issue observed in CNT loaded membranes as discussed in the previous chapter. In CMC/HT system, a better empathy between polymer matrix and filler has been noticed and the alternate pathways provided by HT directly improve the CO_2 permeance. This work is scientifically acknowledged in ***Journal of Applied Polymer Science****.*

6.1 Introduction

Hydrotalcites (HT) are the layered double hydroxides which consist of brucite-like host sheets (positively charged) and hydrated carbonate anions sailed freely in the interlayer corridor (**Figure A1.2b**, **Appendix 1**) [76]. The hydrated carbonate anions sailing in the interlayer of HT works as the carrier for CO_2 facilitation which could be described by the following reaction [77].

$$CO_2 + CO_3^{2-} + H_2O \rightleftharpoons 2HCO_3^- \qquad \text{(Reaction 6.1)}$$

Moreover, the HT channel can increase the polymer chain spacing which enhances the gas permeance. The present study demonstrates the incorporation of hydrotalcite (HT) in to CMC matrix provides better CO_2 permeance. The CMC/HT membrane generally follows the solution - diffusion and facilitated transport mechanism. In solution - diffusion mechanism CO_2 possesses higher solubility than N_2 due to its higher critical temperature which results in better solubility selectivity of CO_2. CO_2 also has a smaller kinetic diameter than N_2 resulting in a favorable diffusivity selectivity [143]. On the other hand, in facilitated transport mechanism, CO_2 transfer occurs by the reversible reaction between the CO_2 and reactive carriers, i.e. amine of CMC and carbonate of HT. CMC modified filler was used in CO_2 separation application by Shamsabadi's group [87]; but CMC as a matrix material for fillers in gas separation application is not yet explored.

6.2 Experimental Section

6.2.1 Materials

Carboxymethyl chitosan (CMC) and hydrotalcite (HT) were synthesized in our laboratory following the already existing procedures.[79, 87] The materials used for HT synthesis i.e. Na_2CO_3, Al $(NO_3)_3.9H_2O$, NaOH and Mg $(NO_3)_2.6H_2O$ were purchased from Merck. Sterlitech, USA provided polyethersulfone (PES) porous membrane support having a pore diameter of 0.1µ. Millipore water® was used during the course of the experiment. Certified CO_2/N_2 (20/80) and Ar gas were brought from Vadilal Chemicals Ltd. and Jainex Gases Company, India, respectively.

6.2.2 Membrane Fabrication

Initially, 1 wt. % of HT (dry solid basis) has been properly dispersed in water. Later, CMC has been added to the solution and stirred at room temperature until the formation of a homogeneous mixture and the membrane was prepared as described in **Chapter 2**.

6.2.3 Characterization Techniques and Gas Permeation Setup

The instruments used for FTIR, XPS, FESEM, AFM and TGA analysis are same as mentioned in **Chapter 2**. Similarly, the moisture retention test set up and gas permeation set up have been elaborated in the same chapter.

6.3 Results and Discussion

6.3.1 Elemental and Morphological Analysis

The desired formation of HT has been scrutinized with the help of FESEM coupled EDX and XRD analysis as shown in **Figure 6.1a, b**. The EDX analysis showed the elemental compositions of the synthesized filler (**Figure 6.1a**) which clearly indicated the presence of O, Mg, Al and C in the powdered sample of HT. The XRD peaks obtained at 2θ = 11.35°, 23.23°, 34.54°, 39.30°, 46.82°, 60.65° and 62.22° verified the formation of HT (**Figure 6.1b)**. Also, the 2θ positions of the diffraction peaks were in agreement with available literature.[79] The corresponding Miller indices were (003), (006), (009), (015), (018), (110) and (113) at the respective 2θ positions as shown in **Figure 6.1b**.

Later, FTIR analysis was performed on the active layers to investigate the presence of desired functional groups in the system as shown in **Figure 6.2a**. The band observed at 3498–3467 cm^{-1} corresponded to OH, caused by the interlayer water molecules, hydroxyl groups in the brucite-like layers and bound water molecule present in CMC/HT system. The medium peak around 1646 cm^{-1} in the infrared spectrum was credited to the H_2O in the interlayer. Another peak around 1377 cm^{-1} related to the band of carbonate [144]. The spectra obtained in the low energy region 557 cm^{-1} attributed to the presence of Mg–O and Al–O bands [145]. The additional peaks obtained in CMC/HT indicated the successful loading of HT in the selective layer matrix. The XRD spectra obtained for CMC/HT (**Figure 6.2b**) indicates that the regular structure of CMC and HT was interrupted due to the interpenetration of each other, and their crystallinity is reduced accordingly. The CMC film showed crystalline peaks at $2\theta = 8°$ and $20.2°$ which was verified with reported literature [146]. On the other hand, CMC/HT active layer retained the peak at $2\theta = 20.28°$ and the peak at $2\theta = 8°$ disappeared which indicated that CMC was intercalated into a monolayer arrangement.

The FESEM image recorded for CMC and CMC/HT membranes have evidenced the development of dense layer on PES support (**Figure 6.3a, Fig. 6.4a**). EDX mapping records taken on the surfaces of both the membranes showed the presence of C, O, N and Na which are the essential elements of CMC. In CMC/HT membrane additional Al and Mg was perceived indicating the successful loading of HT into the CMC matrix. The cross - section of the CMC/HT membrane has been presented in **Figure 6.5a**. The dense active layer achieved a thickness of 1.22 μm after final stage drying. The porous morphology was due to the PES substrate on which the active layer was developed. The AFM image taken on the top surface of the CMC/HT membrane showed an average roughness of 23.9 μm.

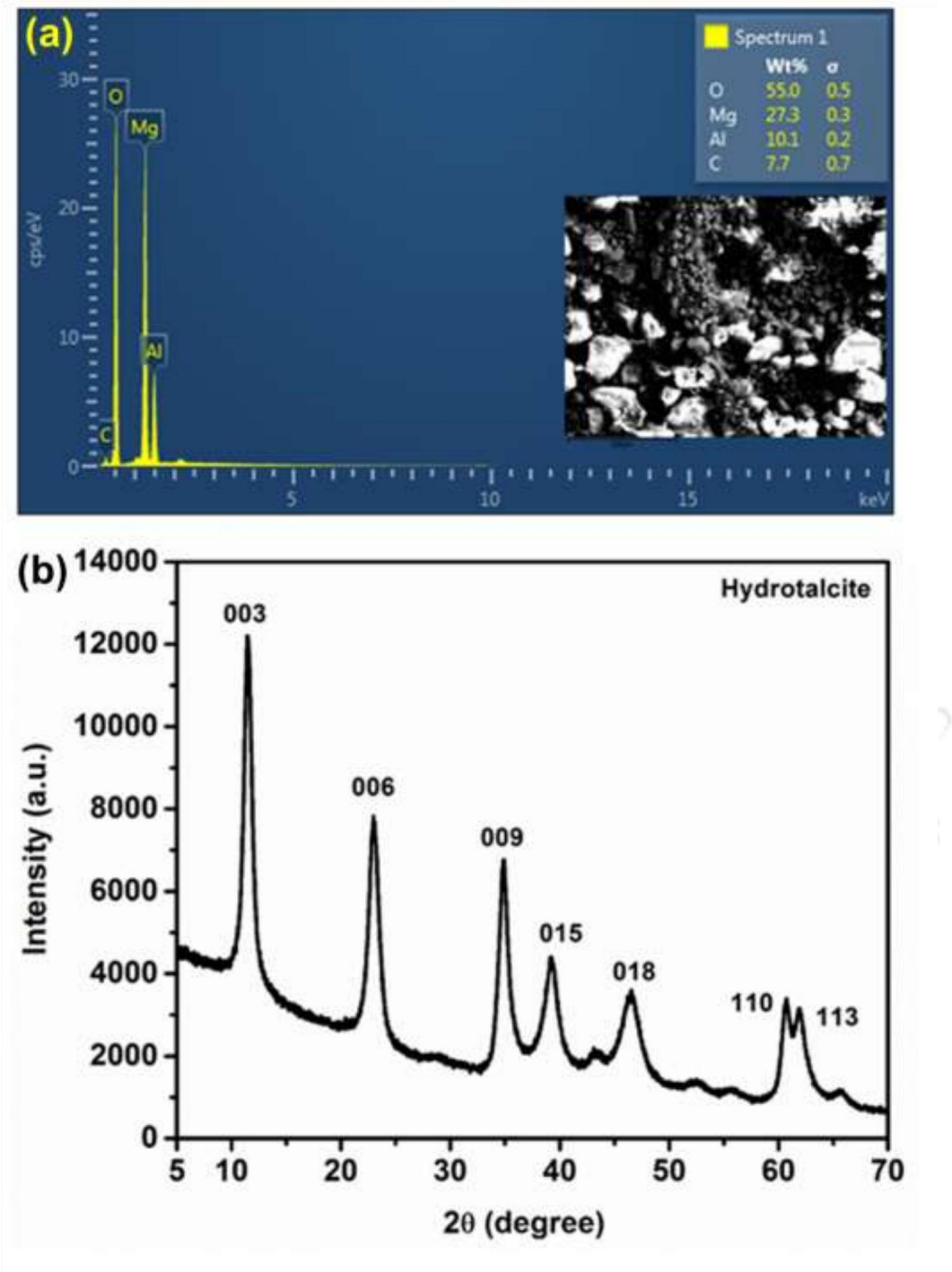

Figure 6.1 (a) EDX analysis of HT (inset image corresponds to the FESEM image of HT powder)(b) XRD spectrum obtained for HT powder.

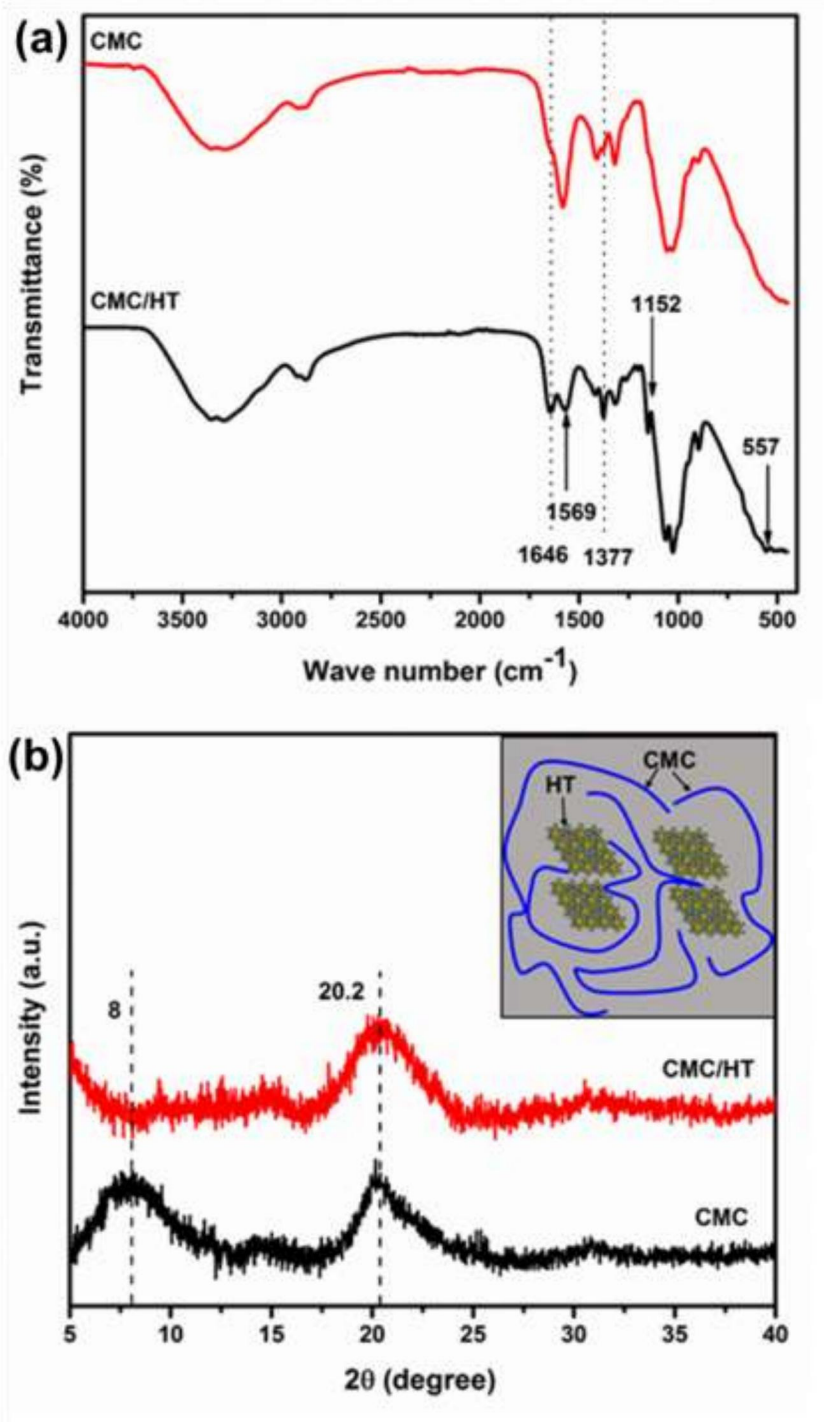

Figure 6.2 (a) FTIR spectra and (b) XRD of CMC and CMC/HT membrane.

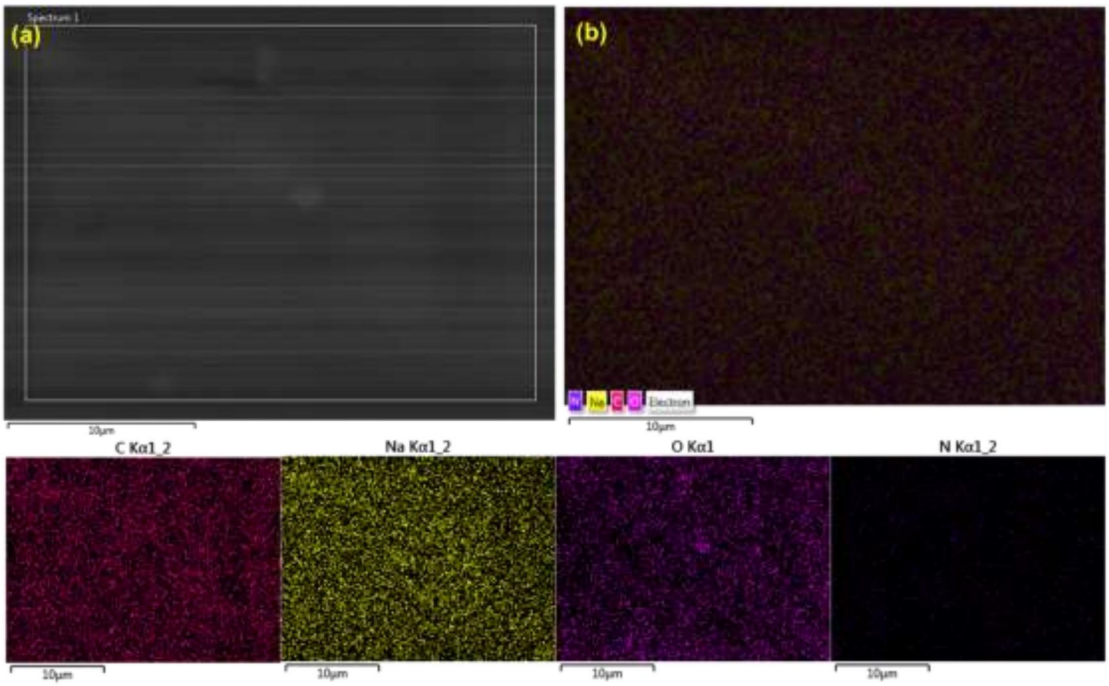

Figure 6.3 FESEM and EDX mapping on the top surface of CMC membrane (a) FESEM image (10kX) (b) elemental mapping.

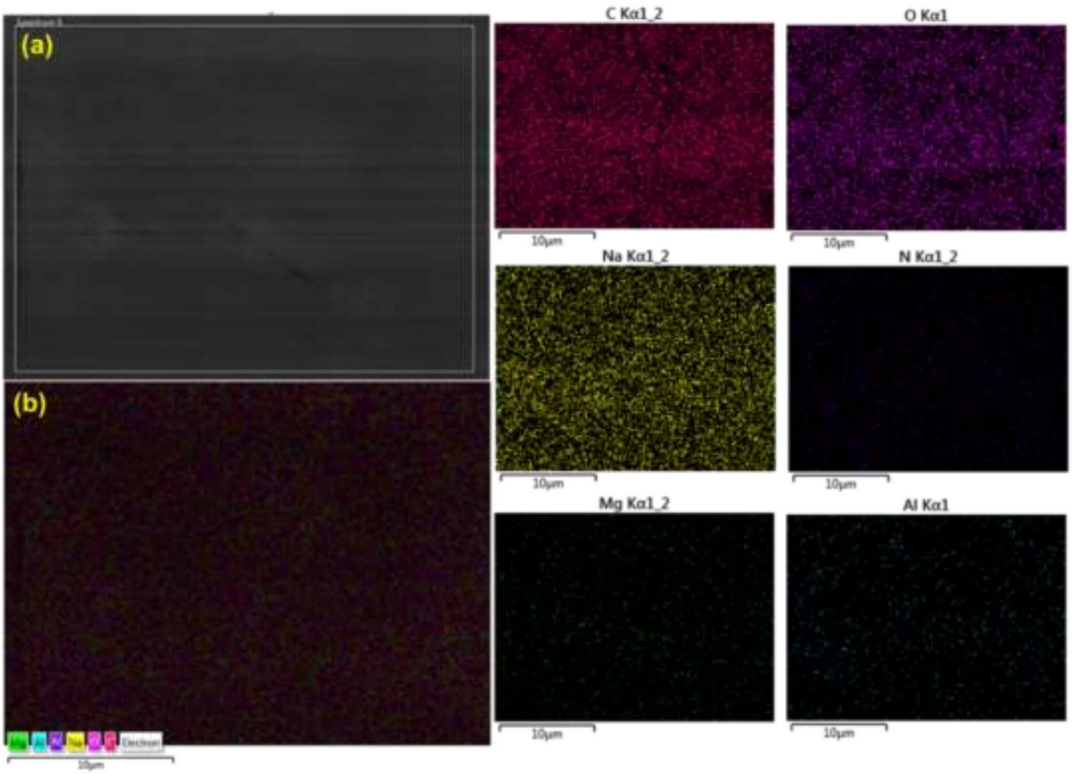

Figure 6.4 FESEM and EDX mapping on the top surface of CMC/HT membrane (a) FESEM image (10kX) (b) elemental mapping.

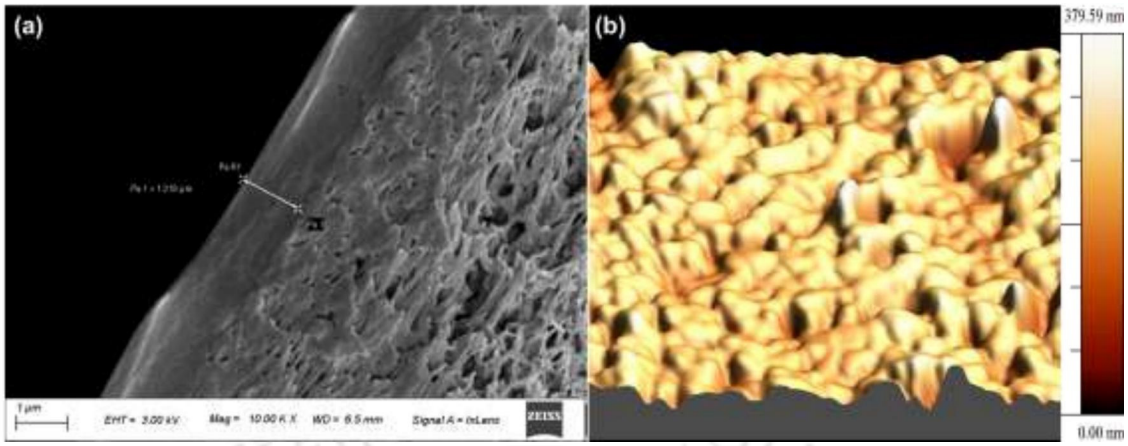

Figure 6.5 (a) FESEM cross section and (b) AFM image (3D) of CMC/HT membrane.

6.3.2 Thermal Stability

The better understanding of the thermal behavior of CMC/HT membrane has been assessed with the help of TGA. The thermogram presented in **Figure 6.6a** indicated that the CMC/HT membrane undergoes four mass loss stages. The first stage weight loss up to 100 °C represented the evaporation of free moisture held by the active layer. The major weight loss was observed in the range of 247- 318 °C which indicated the decomposition of polysaccharide ring and breakage of the glycosidic bond of CMC. The slight downturn observed after 400 °C corresponds to the loss of molecular water present in the system. The fourth stage of weight loss was attributed to CO_2 loss and dihydroxylation. The isothermal analysis performed at a different temperature is shown in **Figure 6.6b**. The CMC/HT membranes showed a huge mass loss of ~12 % when the membrane was heated from 30 to 80 °C. This loss was probably due to the removal of moisture from the active layer that was absorbed by the sample from the environment while loading into the TGA instrument. Then the membrane was held at 80 °C for 30 minutes and witnessed a weight loss of 1.54 %. Later, the same sample was detained at 90, 100 and 110 °C for 30 minutes and obtained a weight loss of 0.17, 0.11 and 0.02 %, respectively. The TGA isothermal data evidenced the temperature stability of the membrane at the experimental temperature conditions (80, 90, 100 and 110 °C).

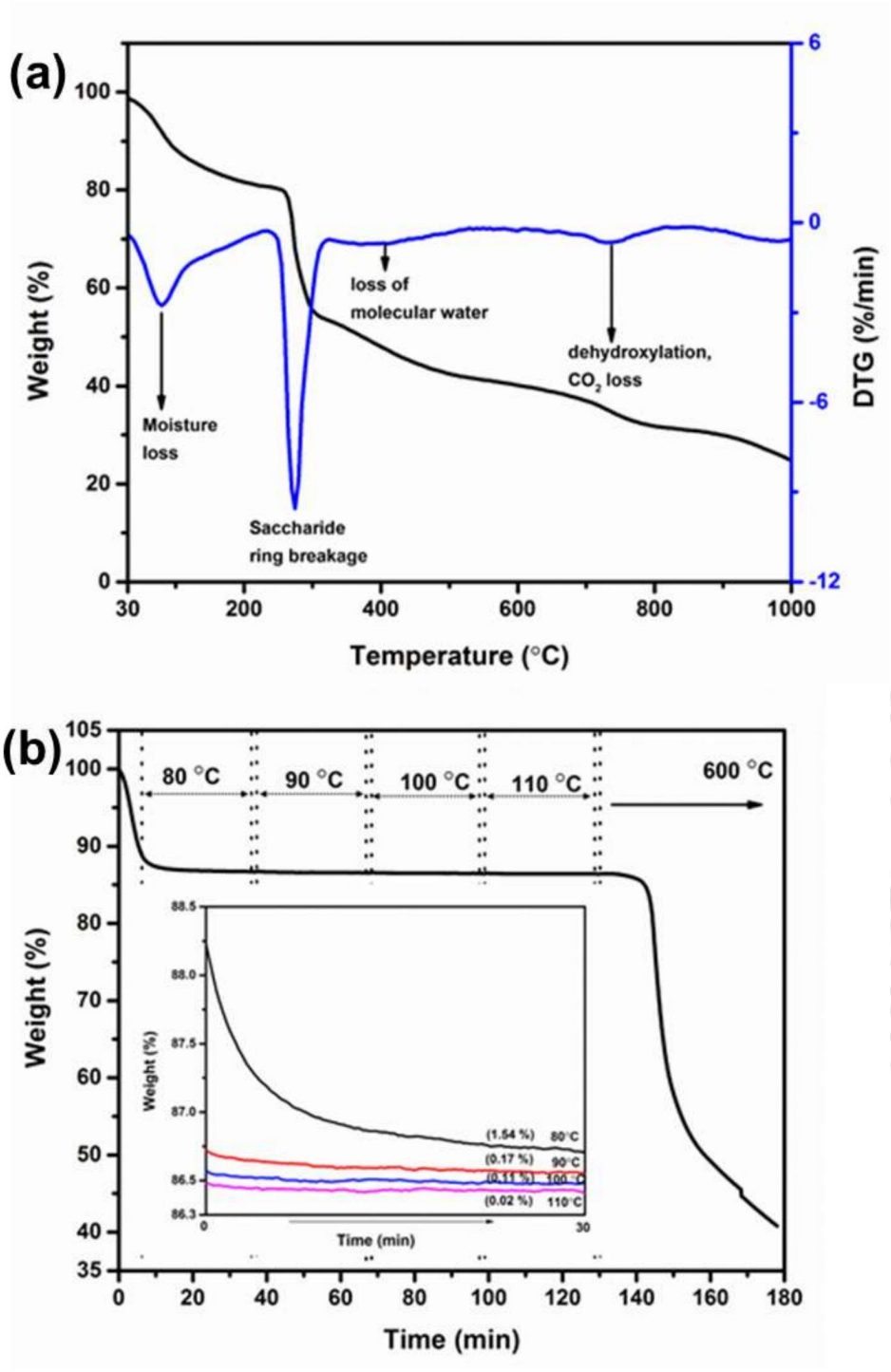

Figure 6.6 TGA graph obtained for CMC/HT active layer (a) dynamic (b) isotherm.

6.3.3 Moisture Retention Ability

The moisture holding behaviour of CMC/HT active layer was monitored under the environment prepared at different relative humidity percentage (RH %) as mentioned in **Table 6.1**. The moisture retention (W_R) ability of the membrane enhanced with increased

RH % and ultimately the membrane showed W_R % of ~ 293 % at 100 % RH. However, W_R % was lower than the pristine CMC active layer [105]. The electrostatic interaction between negatively charged CMC and positively charged cations of HT form cross-linked network.[147] As a result of this, the membrane attains stable morphology under a moisture environment and reduced the W_R %.

Table 6.1 Moisture retention behaviour of CMC/HT membrane at different RH %

RH %	20	40	60	80	100
MR %	10.1 ± 1.2	17.3 ± 1.5	24 ±1	45.3 ± 2.5	293 ± 4.5

6.3.4 CO_2 Separation Study

The steady state CO_2 permeation data was obtained within 5 hours for CMC/HT membrane whereas CMC and other CMC/amine membranes take almost 8 hours to stabilize its permeation. The end result of CO_2 permeance and CO_2/N_2 selectivity at varied temperature has been represented by **Figure 6.7a**. During this experiment, the sweep/feed water to the saturator ratio was maintained at 1.67 and other operating conditions were same as described in section 2.3. The CO_2 permeance was obtained as 41 GPU at operating temperature 60 °C which was increased gradually as the temperature was raised up to 90 °C. The CO_2 permeance becomes 63 GPU at 90 °C. This increase might be due to the increased rate of facilitated transport reaction between CO_2 and amine of CMC with increase in temperature. A drastic reduction of CO_2 permeance was detected when the temperature reaches 100 °C and 110 °C. This decreasing trend corresponded to the huge loss of moisture at a higher temperature which provides stiffness to the membrane. However, the CO_2 permeance showed by CMC/HT membrane at 100 °C and 110 °C was relatively more than that of pure CMC membrane as described in our earlier work [105]. This might be due to the increased free volume of CMC after HT loading and thereby promoting gas transport through the membrane. Here, the alternate pathways provided by HT predominantly worked for CO_2 transportation. Although, the high - speed gas channels allow N_2 passage along with CO_2. Consequently, low CO_2/N_2 selectivity was achieved for CMC/HT membrane. Now, fixing the operating temperature at 90 °C, the sweep/feed water supply was varied to study the effect of moisture. The results obtained from this experiment are presented in **Figure 6.7b**. The CO_2 permeance was 30 GPU at sweep/feed

water flow ratio of 0.33 which became 70 GPU as the ratio was increased to 2.33. This might be due to basically two reasons (a) the membrane became flexible with increase in moisture supply rate and (b) the facilitated transport was increased in presence of more water molecules. Further increase in the water flow ratio showed a very negligible decrease in CO_2 permeance. At the same time, the CO_2/N_2 selectivity increased from 7 to 13 as the water flow ration increased from 0.33 to 2.33, respectively. Later, at water flow ratio of 3, the CO_2/N_2 selectivity decreased which may be due to the competitive sorption among CO_2, water and N_2 molecules. The performance stability of CMC/HT membrane was investigated up to 10 days at a constant temperature 90 °C and sweep/feed water flow ratio of 2.33. The membrane exhibited a consistent CO_2 permeance and CO_2/N_2 selectivity as shown in **Figure 6.8**.

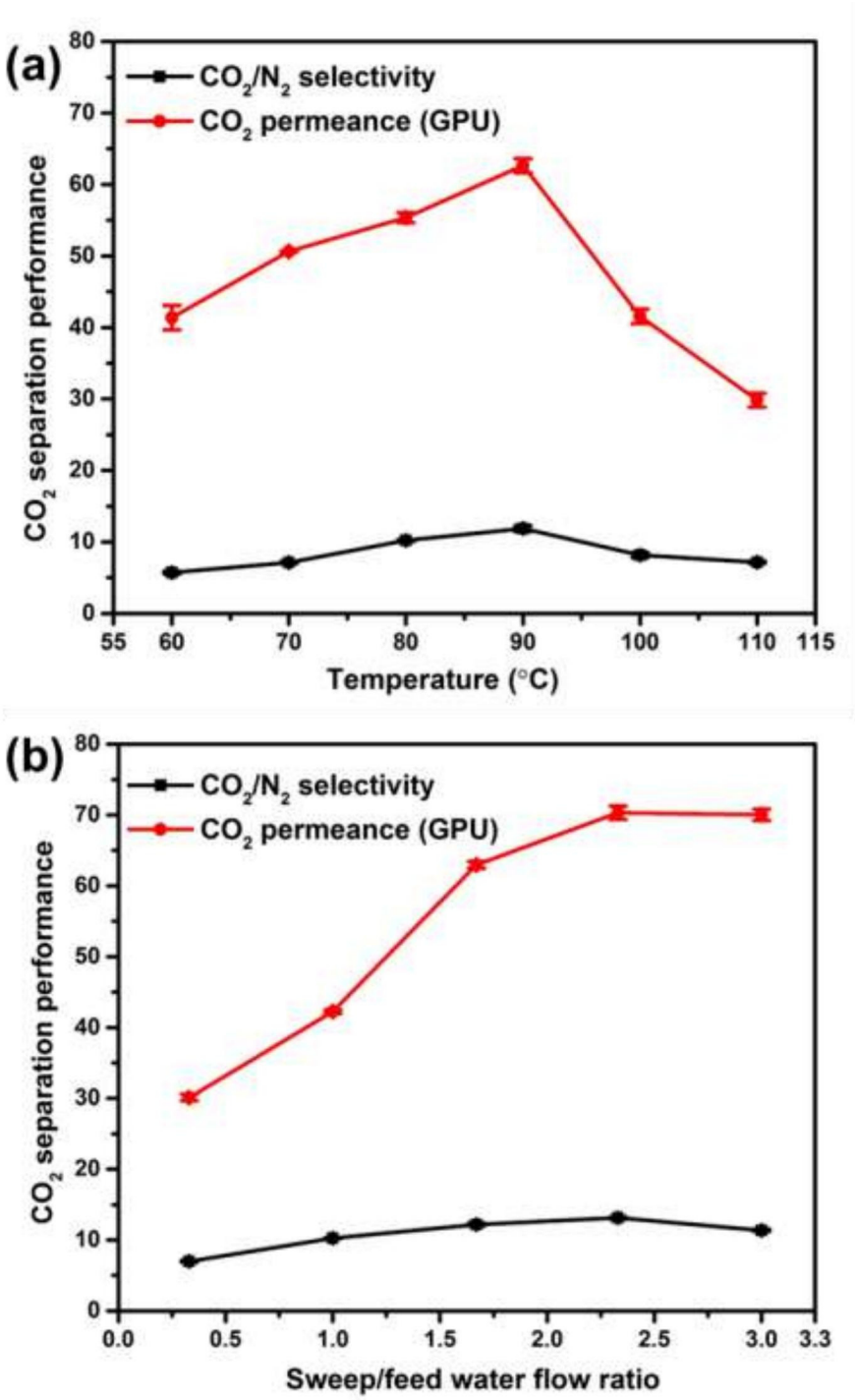

Figure 6.7 Effect of (a) temperature (b) water flow ratio on CO_2 separation performance of CMC/HT membrane.

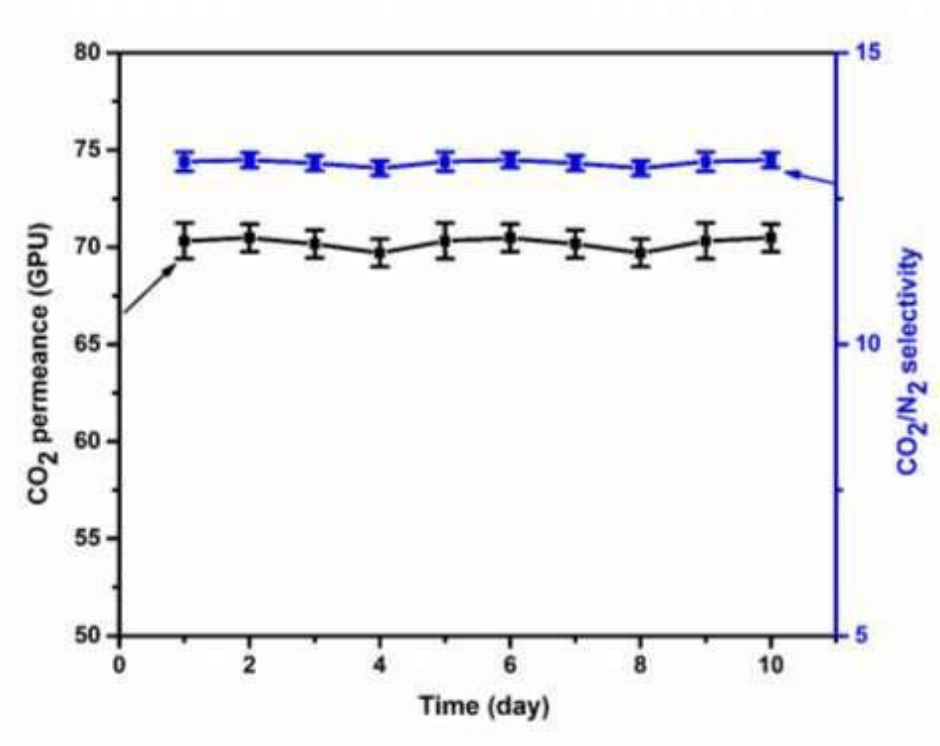

Figure 6.8 Performance stability of CMC/HT membrane at temperature = 90 °C, sweep/feed water flow ratio = 2.33.

6.3.5 Characterization of the Membrane After Gas Permeation

The presence of functional groups on the membranes after gas permeation study was investigated by FTIR analysis as presented in **Figure 6.9**. The CMC/HT membrane was dried before inserting into the FTIR instrument so that external moisture absorbed during permeation experiment can be minimized. The spectra obtained for CMC/HT before and after gas permeation test are similar which indicated that the membrane didn't lose its integrity during permeation study.

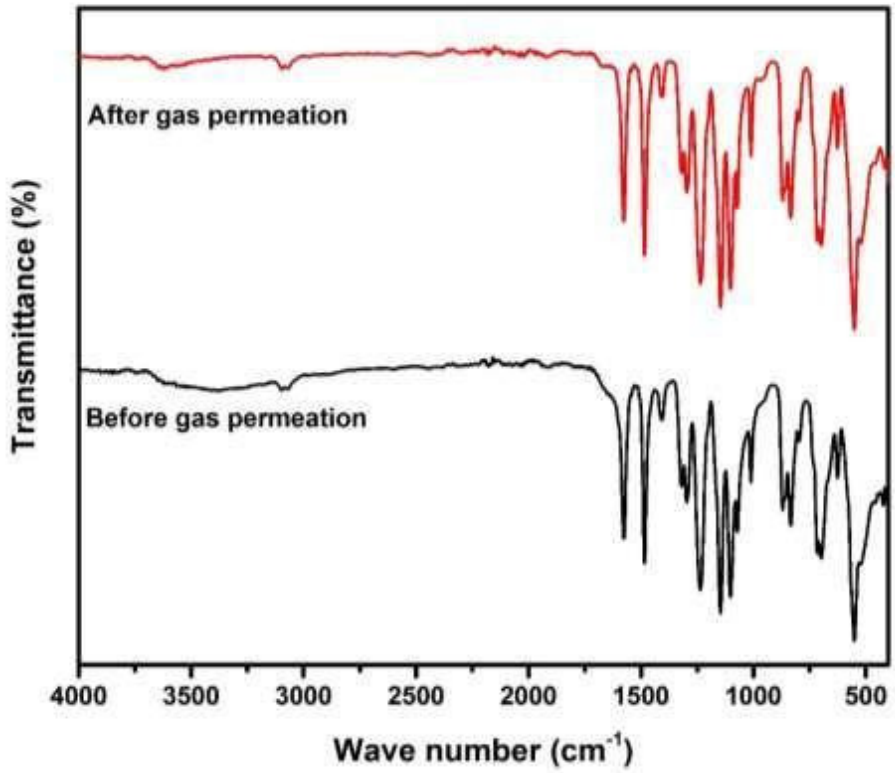

Figure 6.9 FTIR of CMC/HT membrane (with PES support) before and after gas permeation study.

6.3.6 Comparative Study

A comparative study has been carried out on very recent CO_2/N_2 separation works performed with the help of mixed matrix membranes as tabulated in **Table 6.2**. Before 2019 also, various CO_2/N_2 separation experiments have been accomplished using mixed matrix membranes. The membrane composing of 4,4-(hexafluoroisopropylidene) diphthalic anhydride-durene/ zeolitic imidazolate frameworks -8 showed CO_2 permeance of 43 with CO_2/N_2 selectivity 17 [148]. Another work performed by our group used poly (vinyl alcohol)/ poly (ethylene glycol)/ silica nanoparticle to prepare CO_2- selective mixed matrix membrane. This membrane exhibited CO_2 permeance of 26 GPU with CO_2/N_2 selectivity 300 [149]. Thus, it is clear that all the discussed membranes showed

comparatively high CO_2/N_2 selectivity than CMC/HT membrane due to the higher thickness of the membrane. However, in terms of CO_2 permeance performance, CMC/HT membrane is quite better than those membrane systems. Besides, the gas separation performance of CMC/HT membrane was compared with other HT incorporated membranes. The membrane composed of poly (PEA-HT-TMC)/PS exhibited the CO_2 permeance of 90 GPU along with the CO_2/N_2 selectivity of 40. In this case, a crosslinking reaction was taking place between PEA and TMC. On the other hand, CMC/HT membrane showed closer CO_2 permeance without crosslinking which may create a probable space for the CMC/HT in the membrane based CO_2 separation field.

Table 6.2 Gas separation performance of recently developed various membranes systems

Membrane system [ref]	Temperature (°C)	Feed pressure (Bar)	Thickness (μm)	CO_2 permeance (GPU)	CO_2/N_2 selectivity
Pebax-1657/COF-5 **[150]**	30	1	55*	~8.9	~ 49.3
Pebax- DA-PEI-TiO_2 **[151]**	20	3	10**	~6.8	~101
PVA/PEG/alumina **[152]**	25	1.5	175*	~2.3	~80
Pebax-1657/aminosilane functionalized GO **[153]**	35	2	80*	~11.6	~71
CMC/HT [this work]	90	2	1.22	~70	~13

*Average value is taken for CO_2 permeance calculation, **Thickness is taken from the SEM image

6.4 Conclusions

The high - speed CO_2 transport membrane has been developed by loading 1 % HT in the CMC matrix. The FTIR, XRD and EDX mapping analysis verified the successful fabrication of CMC/HT membrane. The FESEM image proved the formation of dense active layer of a 1.21 µm over a PES substrate and the surface roughness of 23.9 µm was determined by AFM analysis. The membrane showed thermal stability at the higher operating temperature range 80 - 110 °C. Additionally, the moisture retention ability of the membrane helped in reducing the gas transfer resistance and enhanced CO_2 permeance. Finally, the CO_2 separation study performed on CMC/HT membrane estimated optimum CO_2 permeance of 70 GPU at 90 °C with a separation factor of 13.

CHAPTER 7

Thermally Stable and Moisture Responsive Carboxymethyl Chitosan/Dendrimer/Hydrotalcite Membrane for CO_2 Separation

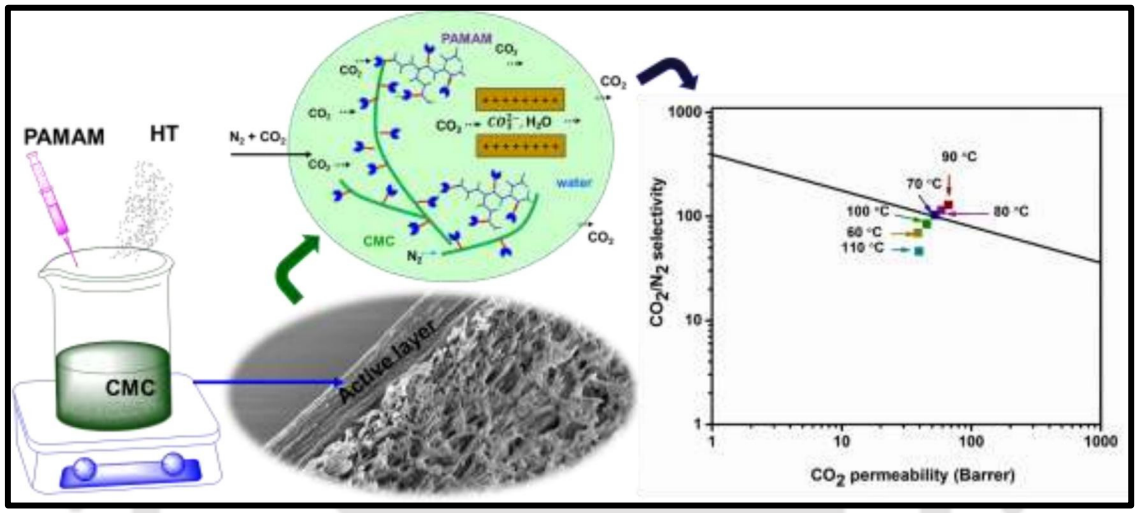

Overall graphical representation of CMC/PAMAM/HT system in terms of CO_2 separation.

CHAPTER 7

Thermally Stable and Moisture Responsive Carboxymethyl Chitosan/Dendrimer/Hydrotalcite Membrane for CO_2 Separation

This chapter encompasses the preparation of mixed matrix membrane (MMM) by incorporation of hydrotalcite (HT) into the CMC/PAMAM matrix which is thermally stable and moisture receptive. In Chapter 4 and 6, we have already discussed the novelty and quality improvement in CMC/PAMAM and CMC/HT membranes for CO_2 separation. In this study, the presence of both materials bestow some unique properties to the membrane which work for the betterment of separation performance.

7.1. Introduction

To date, different kinds of filler and carrier combinations have endeavoured. However, the fillers in most MMMs can only swing in a restricted position which makes it difficult to attain substantial gas selectivity [154]. On this context, we have proposed the fabrication of a more efficient MMM comprising high-speed facilitated transport channels provided by HT and dendrimer. It is worth mentioning that due to the presence of abundant amino and amido groups in PAMAM structure, PAMAM has coordination capability with metal ions. Therefore, it is highly expected that HT and PAMAM will be very compatible entities inside the CMC matrix [155]. In this work, we have anticipated that PAMAM and HT will be in favour of improved CO_2 permeability and CO_2/N_2 selectivity presumably due to three reasons - (1) the mobility of PAMAM can expedite the CO_2 facilitated transport, (2) the large number of carrier sites in PAMAM can offer a continuous CO_2 transport channel resulting the increase in CO_2 permeability and (3) the cations, Mg^{2+} and Al^{3+}, present in HT can act as CO_2 absorption sites [156]. Meanwhile, CMC was picked as a matrix for the membrane fabrication due to its comprehensive performance offered by the inherent amine group in its structure. Moreover, the HT channel can increase the polymer chain spacing which enhances the gas permeance [157]. Keeping these points in mind, we have presumed that the novel combination of dendrimer and hydrotalcite supposedly will enhance both CO_2/N_2 selectivity and CO_2 permeance of the CMC membranes.

7.2. Experimental section

7.2.1. Materials

Carboxymethyl chitosan (CMC) has been synthesized in our laboratory as discussed in **Chapter 2**. PAMAM with ethylenediamine core (generation 0.0, 20% solution in methanol) was obtained from Sigma Aldrich. HT was synthesized in our laboratory following an already existing procedure [79]. The materials used for HT synthesis i.e. Na_2CO_3, Al $(NO_3)_3.9H_2O$, NaOH and Mg $(NO_3)_2.6H_2O$ were purchased from Merck. Sterlitech, USA has supplied the porous support consisting of polyethersulfone (PES) membrane with a pore diameter of 0.1µm. Millipore water® was used during the experiment. CO_2/N_2 (20/80), the feed stream was brought from Vadilal Chemicals Ltd. The sweep gas argon (99.99% purity) and helium required for gas chromatography were procured from Jainex Gases Company, India.

7.2.2. Membrane Fabrication

Aqueous CMC solution was stirred at room temperature and bubble - free homogeneous solution has been achieved after centrifugation. Adding calculated amount of PAMAM and HT to CMC solution, CMC/PAMAM/HT (89% CMC + 10% PAMAM + 1% HT) casting solution has been obtained. The uniform and viscous solution were poured onto a PES support and cast using GARDCO micron film applicator (Paul N. Gardner, USA). The casting knife opening was set as 2 mils intending an active layer thickness of 1 µm over the porous support. Later, the cast membrane was kept inside a laminar fume hood for slow solvent evaporation (12 hours) and lastly dried at 100 °C (6 hours). The dried flat sheet membrane was then cut into a circular size of dimension 45 mm diameter and fixed in a permeation cell for CO_2 separation test.

7.2.3. Characterization Techniques and Gas Permeation Set Up

The instruments used for FTIR, XPS, FESEM, AFM and TGA analysis are same as mentioned in **Chapter 2**. Similarly, the moisture retention test set up and gas permeation set up have been elaborated in the same chapter. The amine leaching from the membrane has been confirmed with the help of UV Visible Spectrophotometer (Model No.: UV-2600, Make: Shimadzu, Singapore). The water collected from the knock out of gas permeation set up was taken for this analysis.

7.3 Results and discussion

7.3.1. Morphological Analysis

The FESEM images represented the morphology of the prepared membrane. CMC/PAMAM/HT membrane presented a dense surface (**Figure 7.1a)** formed over porous support. The appropriate percentage of HT and PAMAM resolved the problem of particle agglomeration mostly occurs during MMM fabrication. The cluster formation of fillers may cause defective membrane surface. The use of highly viscous polymer solutions generally helps in slowing down of particle sedimentation. Accordingly, we have fixed the casting solution viscosity as >1200 cp and achieved the defect - free active layer with thickness 979 nm as shown in **Figure 7.1b**. The AFM image provided the average roughness of the membrane surface as 9.33 nm which is almost similar to the control polymer membrane, i.e. CMC (10.78 nm) as mentioned in our previous work [105]. The minor reduction in average roughness is may be due to the settlement of HT in the valley region of CMC or due to the proper distribution of PAMAM and HT in CMC matrix [158].

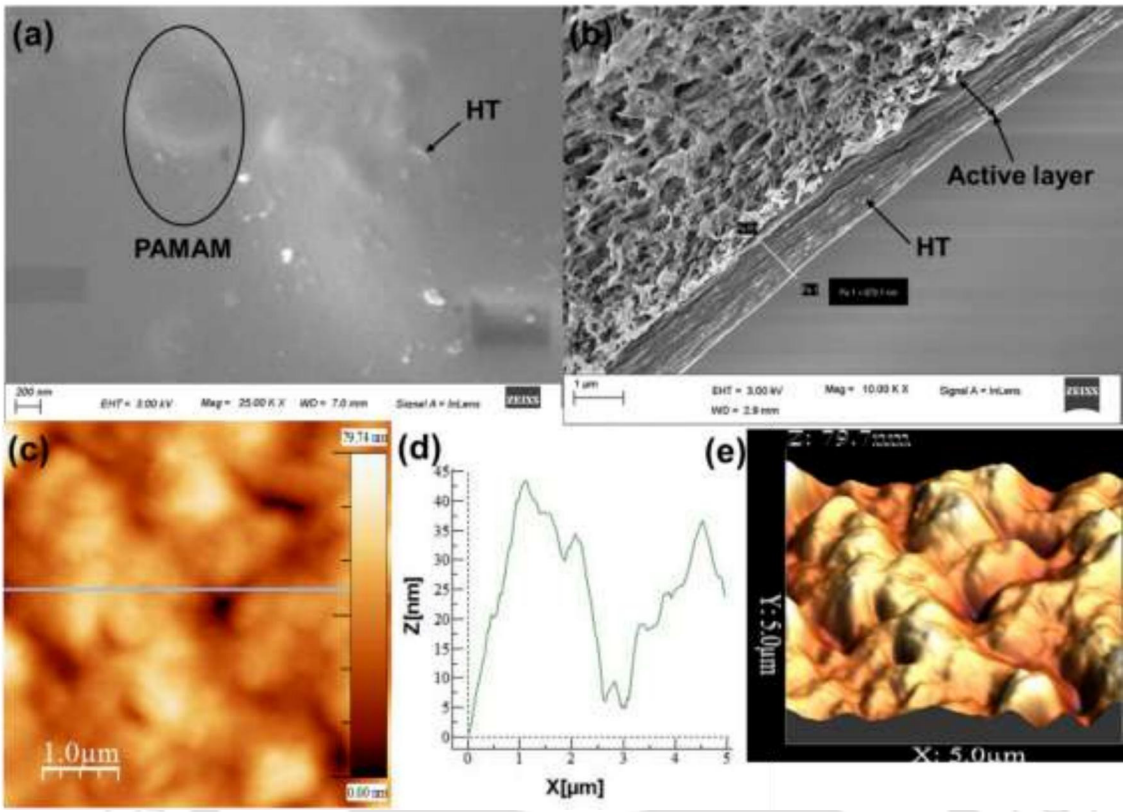

Figure 7.1 FESEM (a) top surface (b) cross section and AFM image (c) 2D view (d) height profiling (e) 3D view of CMC/PAMAM/HT membrane.

7.3.2. Structural Aspect

The ATR-FTIR spectrum of the active layer of CMC/PAMAM/HT membrane have been shown in **Figure 7.2a**. The spectrum for CMC was taken from our previous work performed under the same conditions using the same instrument [105]. The broad and strong peak observed at 3200-3500 cm^{-1} is due to the cumulative effect of the hydroxyl stretch of HT host layers, H_2O molecules of the HT interlayer, N-H stretch of CMC and PAMAM [107, 159]. The symmetrical stretching band of the CH_2 group in polymer has been perceived at 2888 cm^{-1}. The peak noticed at 1410 cm^{-1} attributed to the C=O of –COONa symmetric stretching of CMC. The vibrational absorption of interlayer CO_3^{2-} of HT has been observed at 1384 cm^{-1} [160]. Meanwhile, the bands around 600–900 cm^{-1} has been assigned to metals (Mg, Al). The dominant band appeared in the range 1550-1665 cm^{-1} corresponds to N-H bending of the amine and amide group of PAMAM [161, 162]. Also, the broad band formation indicated the H-bonding between the NH_2 of CMC and OH of the HT brucite layer [163]. Another significant peak was observed at 2168 which attributed the formation of amine salt by the carboxylate of CMC and primary amine

of PAMAM. The C-N stretch occurred in the range 1145-1005 cm^{-1} indicated the presence of PAMAM in the CMC/PAMAM/HT active layer. Similarly, the XPS survey scan and narrow scan (**Figure 7.2b, Figure 7.3a-f**) performed on CMC/PAMAM/HT active layer also indicated the presence of required elements (C, O, N, Na, Mg, Al). The binding energies found at 1070.4 eV, 74.4 eV and 49.5 eV are specific to Na of CMC, Al^{3+} and Mg^{2+} ions present in HT filler, respectively [164]. The peak obtained at 530.7 eV and 532.5 eV (**Figure 7.3a**) may be due to hydroxide and crystallized water content of HT, respectively [165]. However, the O1s deconvoluted peak observed at 531 eV could be due to the presence of carbonate ions of HT, amide group of PAMAM or carboxylate group of CMC matrix. The narrow scan spectra drawn for N1s (**Figure 7.3b**) indicates the presence of primary (400.04 eV), secondary (398.29 eV) and tertiary amines (401.46 eV) in the membrane directing the loading of PAMAM. In **Figure 7.3c**, the high-resolution C1s spectra showed peaks at 284.85 eV, 286.58 eV and 288.4 eV attributed to adventitious C of the polymer backbone, C of the amide group of PAMAM and carbonate ions of HT, respectively. Thus, XPS spectra support the FTIR data and confirmed the successful blending of PAMAM with CMC and loading of HT in the membrane matrix. The uniform distribution of PAMAM and HT in the CMC matrix has been established from the FESEM coupled EDX analysis as shown in **Figure 7.4**. The mapping accomplished on the skin layer of the CMC/PAMAM/HT membrane indicates the presence of N, Al and Mg which have come from PAMAM and HT.

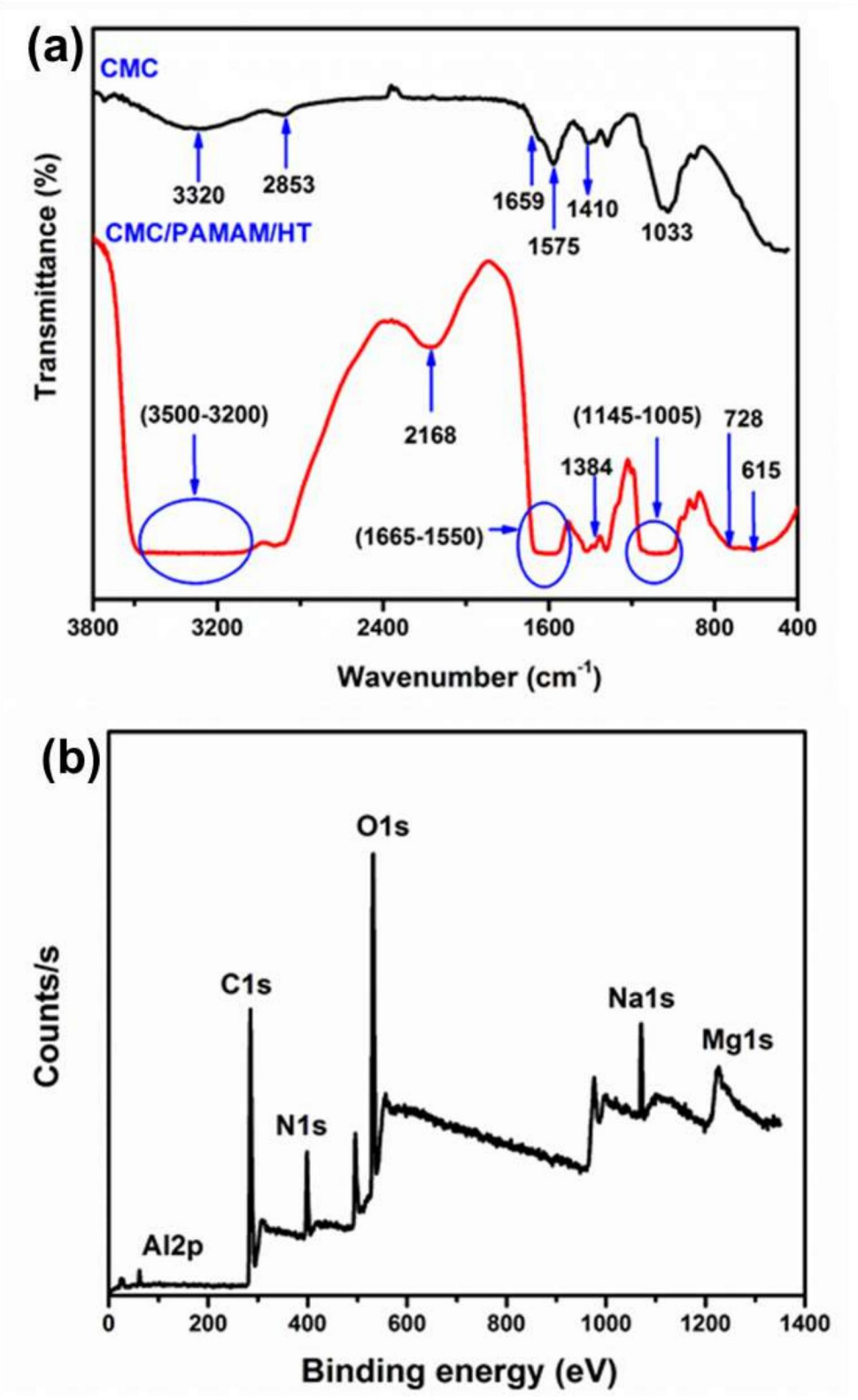

Figure 7.2 (a) FTIR spectrum (b) XPS survey spectrum of CMC/PAMAM/HT active layer.

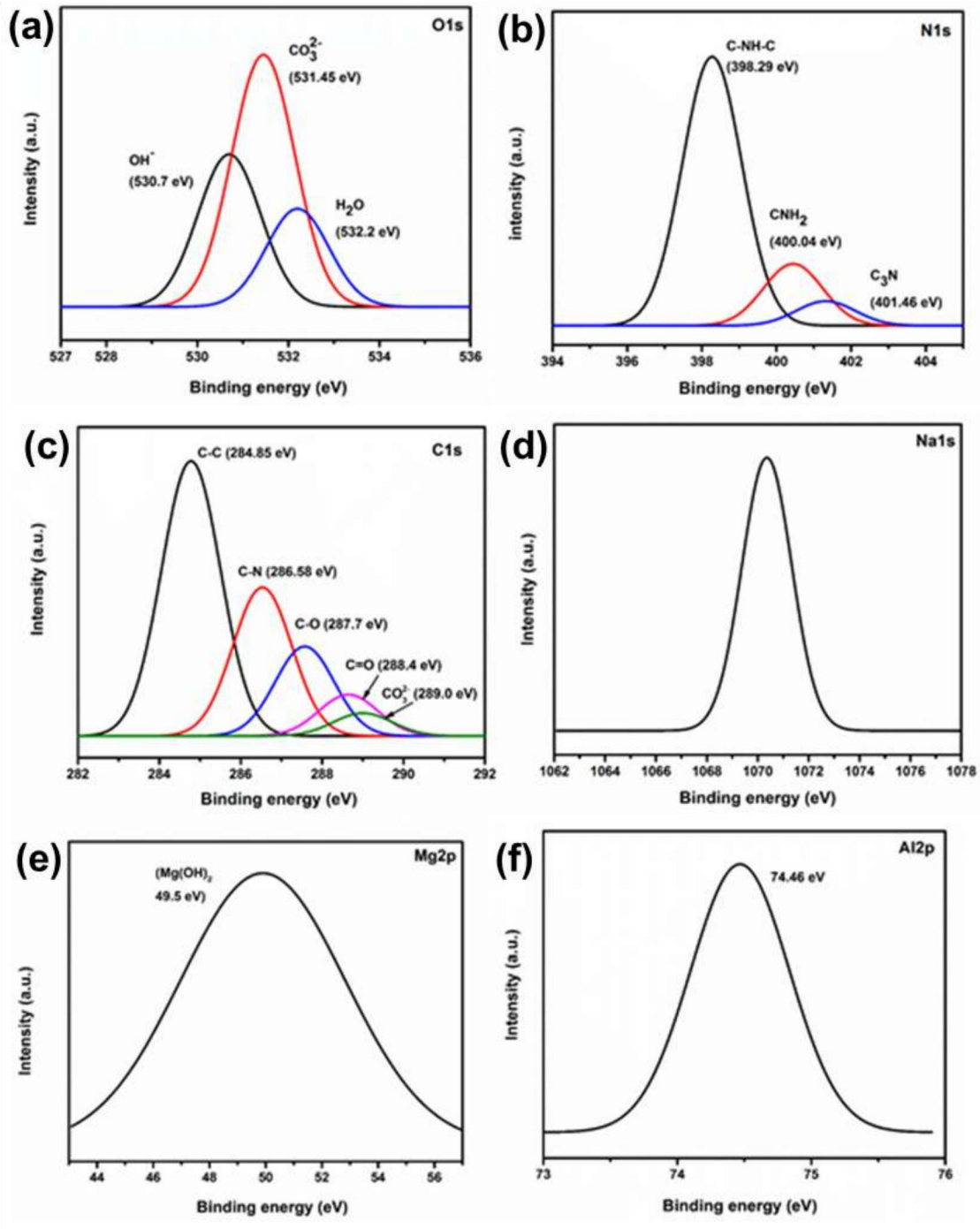

Figure 7.3 XPS narrow scan of CMC/PAMAM/HT for (a) O1s, (b) N1s, (c) C1s, (d) Na1s, (e) Mg2p and (f) Al2p.

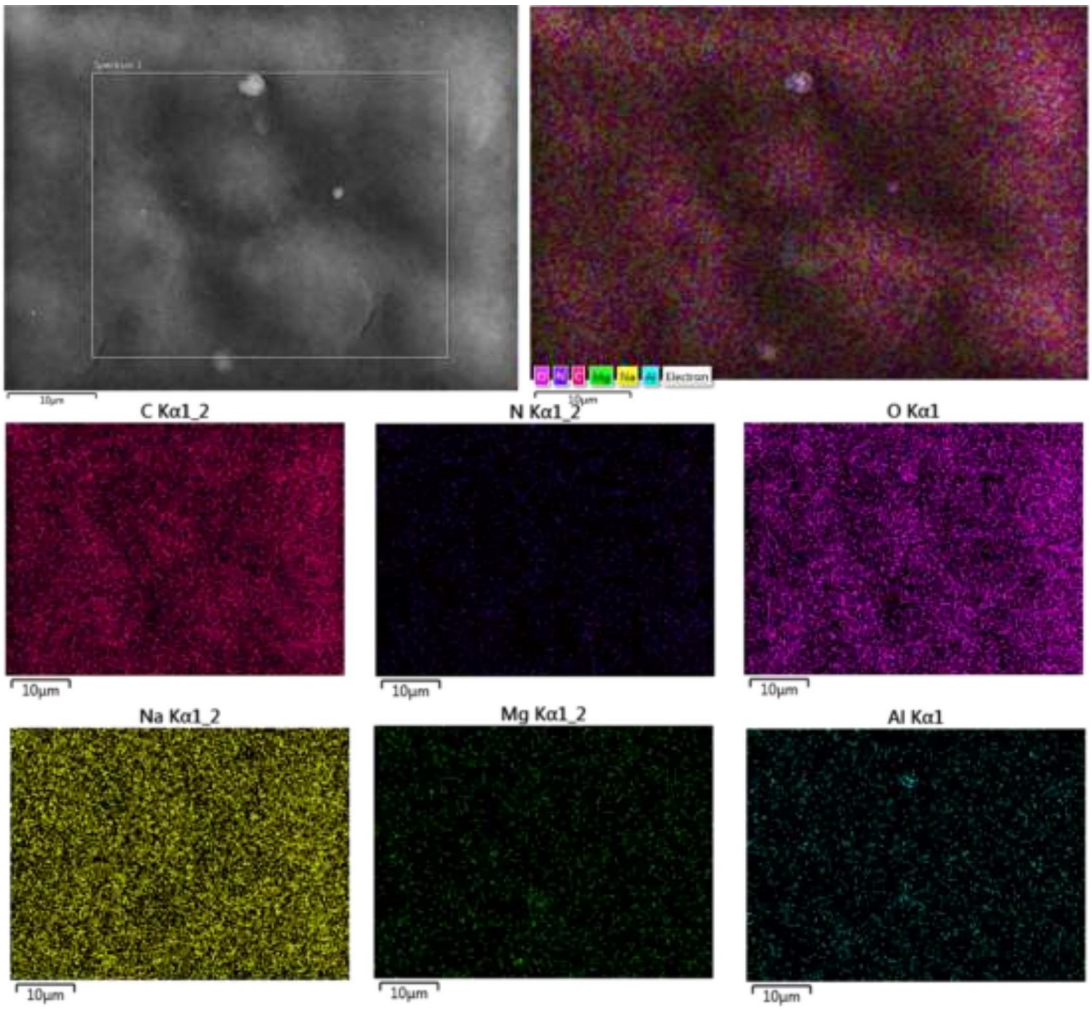

Figure 7.4 EDX mapping analysis of the top surface CMC/PAMAM/HT membrane.

7.3.3 Thermal Stability

The TGA isotherm profile for CMC/PAMAM/HT membrane has been demonstrated in **Figure 7.5**. The membrane was held for 30 min at temperatures 80 °C, 90 °C, 100 °C and 110 °C to evaluate its thermal stability for a long term gas permeation operation. Though, a loss of ~3.2 wt% was observed for the isotherm performed at 80 °C can be presumed on account of moisture removal. Later, minor losses of 0.6, 0.45 and 0.25 % has been observed for the isotherm performed at 90 °C, 100 °C and 110 °C, respectively. This loss is may be due to the removal of leftover moisture after 80 °C isotherm. This indicates the temperature stability of the prepared membrane up to 100 ºC which has been further verified with temperature assisted XPS analysis as shown in **Figure 7.6**. The survey spectra obtained for CMC/PAMAM/HT membrane at room temperature and higher temperature indicated the intact structure of the membrane. Although, the decrease in the

atomic percentage of oxygen at higher temperatures has been witnessed in **Table 7.1** which may be interrelated to the moisture loss event perceived in **Figure 7.5**. Also, the deconvoluted O1s spectra corresponding to water molecules present in the membrane supported the above-mentioned result.

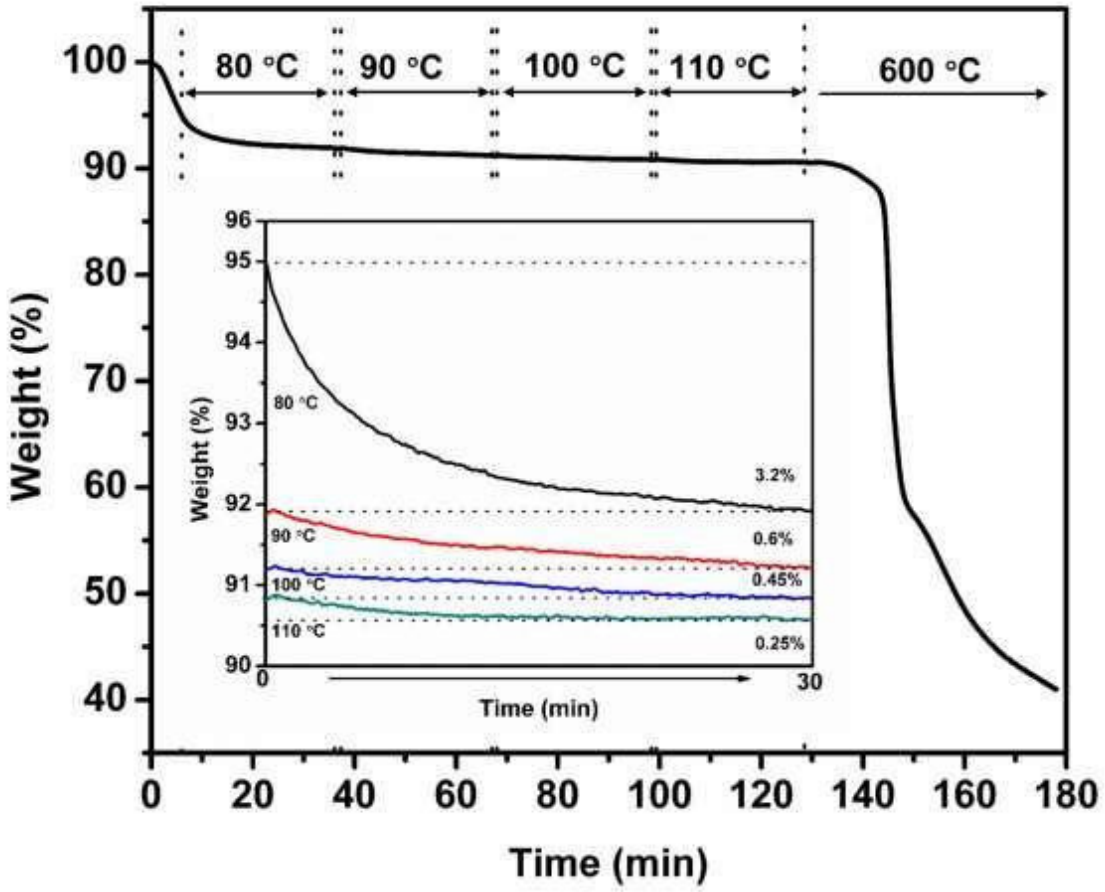

Figure 7.5 TGA isotherm for CMC/PAMAM/HT membrane at 80 °C, 90 °C, 100 °C and 110 °C.

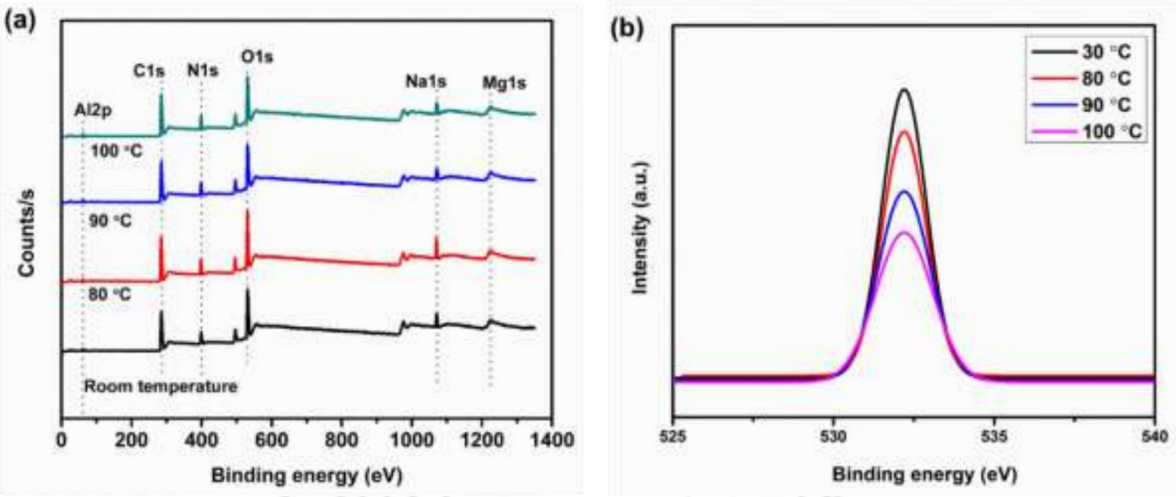

Figure 7.6 XPS analysis of CMC/PAMAM/HT membrane at different temperatures (a) survey spectra (b) deconvulated O1s spectra corresponding to H_2O molecule.

Table 7.1 Elemental analysis of CMC/PAMAM/HT active layer at different temperatures

Elements	Room temperature (Atomic %)	80 °C (Atomic %)	90 °C (Atomic %)	100 °C (Atomic %)
O1s	28.35	26.88	26.87	26.34
C1s	57.34	59.38	59.56	60
N1s	10.17	9.5	9.52	9.89
Na1s	3.09	3.53	3.43	3.36
Mg2s	0.1	0.12	0.08	0.04
Mg2p	0.68	0.47	0.32	0.08
Al2p	0.27	0.12	0.21	0.29

7.3.4 Moisture Retention Ability

The moisture uptake percentage of CMC/PAMAM/HT active layer has been obtained under different temperature and humid conditions as shown in the bar diagram (**Figure 7.7**). The moisture uptake percentage has been decreased with the increase in temperature. At 60 °C the moisture uptake was ~135 % which has been reduced to ~129 % as the temperature raised to 70 °C. Later, the moisture uptake % was obtained as ~104%, ~61%,

~44% under the temperature environment of 80 °C, 90 °C and 100 °C, respectively. Generally, the incorporation of HT offers excellent hydrophilicity to the membrane due to the hydroxyl groups present in the layered structure [166]. Also, PAMAM creates a hydrophillic environment inside the polymer matrix. This is reasonably accepted that the presence of moisture regulates the facilitated reaction and provides greater inter-chain space in the polymer matrix which induces the transport of gas molecules [52]. However, sometimes the excess flexibility encourages the passage of N_2 gas molecules along with CO_2 which adversely affects CO_2/N_2 selectivity of the membrane.

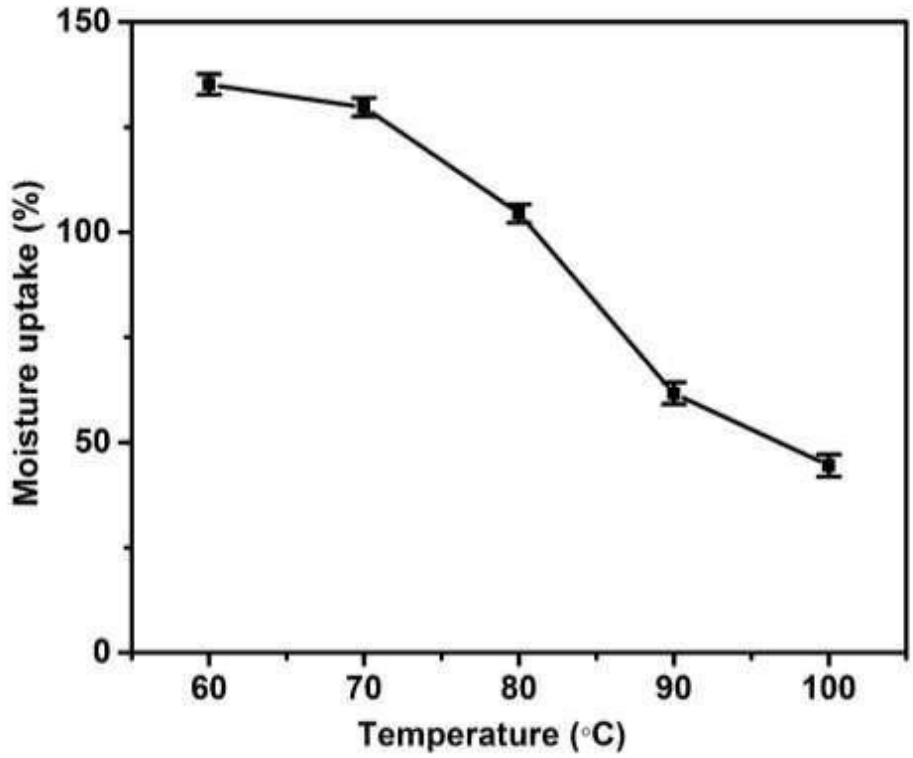

Figure 7.7 Moisture uptake behavior of CMC/PAMAM/HT membrane at different temperatures.

7.3.5 CO_2 Separation Study

7.3.5.1. Influence of active layer thickness

The effects of active layer thickness on CO_2 permeability and CO_2/N_2 selectivity were studied using CMC/PAMAM/HT membrane. Three different thickness of active layer has been fabricated using the following relation [41]:

$$T_2 \times D_2 = 0.5 \times C_1 \times T_{gap} \times D_1 \quad (7.1)$$

Where, T_2 and T_{gap} are the dry membrane thickness and the gap setting of the casting knife, respectively (μm), D_2 , D_1 are the density of the dry membrane and casting solution, respectively (g/cm^3) and C_1 is the total solid concentration of the casting solution in gm. The FESEM image obtained for the cross - section of all membranes has been shown in **Figure 7.8.**

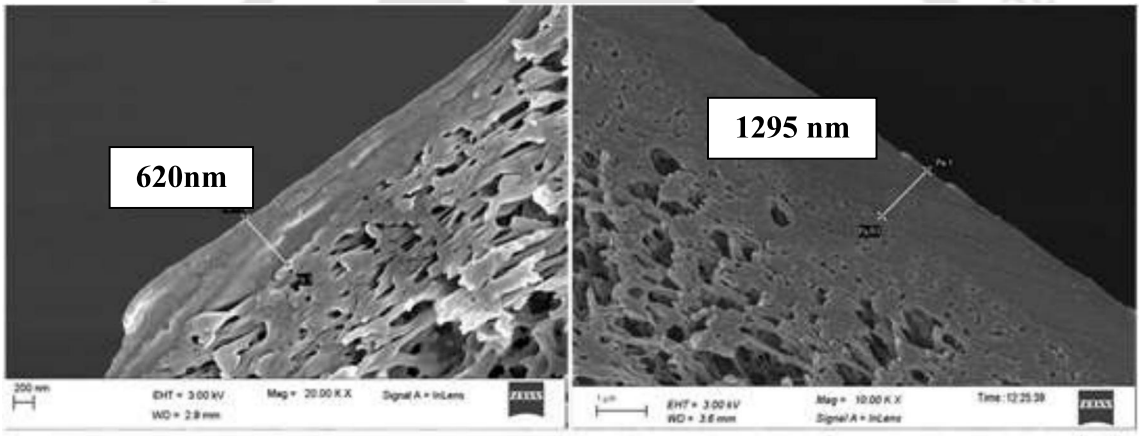

Figure 7.8 FESEM image (cross section) of CMC/PAMAM/HT with different active layer thickness.

The separation performance shown by the variable active layer thicknesses is given in **Table 7.2**. It has noticed that the membrane with an active layer thickness of ~ 600 nm showed higher CO_2 permeance value but very less CO_2/N_2 selectivity. On the other hand, when the membrane thickness was ~1200 nm, the CO_2/N_2 selectivity was higher although the permeance was not up to mark. The membrane with approximately 1μm thickness showed CO_2/N_2 selectivity of 67 and CO_2 permeance 123 GPU which is somewhat considerable. The increasing CO_2 permeance with lower active layer thickness refers that CMC/PAMAM/HT membrane follows the solution - diffusion mechanism and facilitated

transport. A similar selectivity and membrane thickness relation was reported by Khalilinejadand and co-workers [167].

Table 7.2 Influence of active layer thickness on CO_2 separation with feed absolute pressure = 2 bar and operating temperature = 90 °C

Active layer thickness (nm)	Sweep/feed water flow ratio	CO_2 Permeance (GPU)	CO_2/N_2 Selectivity
~500-600	2.33	~137	~10
	1.67	~121	~18
~900-1000	2.33	~123	~67
	1.67	~113	~86
~1250-1300	2.33	~112	~93
	1.67	~105	~128

7.3.5.2 Influence of temperature

A study has been carried out to investigate the behaviour of CO_2 separation performance for CMC/PAMAM/HT MMM at different temperatures (60-110 °C) and water flow ratio (sweep/feed) 2.33. The absolute feed side and sweep side pressure have been maintained at 2 bar and 1.21 bar, respectively. **Figure 7.9a** showed that the CO_2 permeance persistently increased from 60 to 90 °C. The CO_2 permeance obtained at 60 °C was 66 GPU which was later increased more than 50 % with raised temperature up to 90 °C and achieved permeance of 123 GPU. This may be caused by the fact that the increase in temperature augments the rate of reaction between amines and CO_2 under moisture environment, resulted in stimulated CO_2 facilitated transport. A decrease in CO_2 permeance was observed (81 GPU) as the temperature reached 100 °C. A similar trend has been witnessed for CO_2/N_2 selectivity with the increase in temperature. The CO_2/N_2 selectivity obtained at 60 °C was ~30 which become better (52) as the temperature raised to 70 °C. Afterward, the CO_2/N_2 selectivity reached up to 59 and 66 at 80 °C and 90 °C, respectively. Also, the separation performance at 80 °C and 90 °C has been located above the Robson upper bound curve (2008) as shown in **Figure 7.9b**. Similar to CO_2 permeance, as the temperature stretched to 100 °C the CO_2/N_2 selectivity also got reduced to 45. The rise in temperature beyond 100 °C significantly abridged the CO_2 separation performance

as the water preservation capacity of CMC/PAMAM/HT membrane has been reduced diminishing the facilitated transport. Also, the membrane loses flexibility as evaporation of water molecules from the active layer takes place at higher temperatures. The stiffness of the MMM obstructs the passage of the gas molecules ensuing the drop in overall CO_2 separation permeance. Other than the moisture loss, CMC/PAMAM/HT membrane is thermally stable at the operating temperatures which can be understood from the earlier discussion in **Section 7.3.2**. It is worth mentioning that CMC/PAMAM/HT membrane was tested for 15 days at a similar operating condition to understand its performance stability and obtained a stable CO_2 permeance and CO_2/N_2 selectivity.

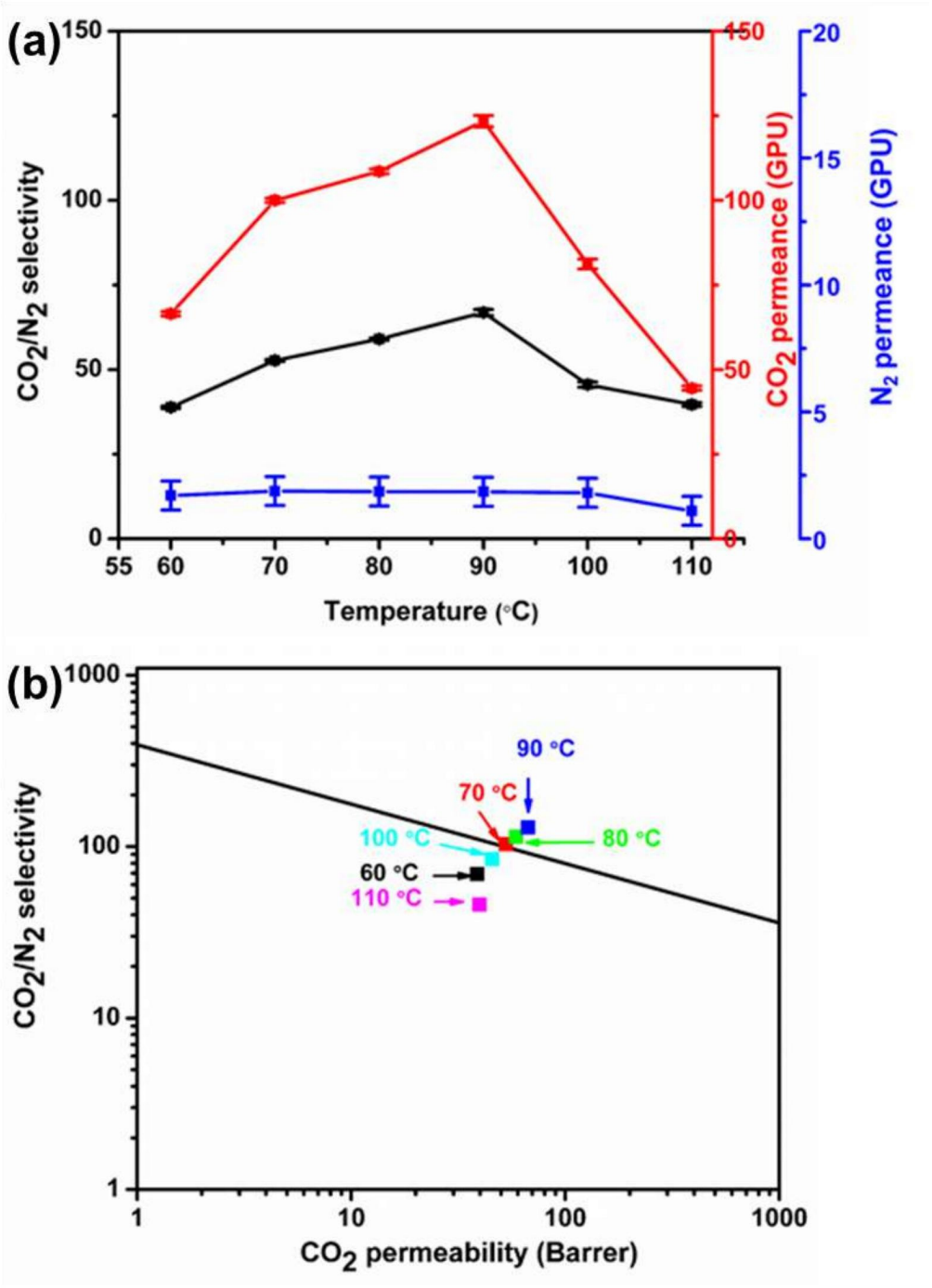

Figure 7.9 (a) Effect of temperature on CO_2 separation performance of CMC/PAMAM/HT membrane (b) Robson upper bound (2008) plot for CO_2/N_2 separation at different temperature.

7.3.6 Characterization of The Membrane After Gas Permeation

The FTIR characterization performed on the membrane before and after gas permeation study indicated the unchanged functional groups present in the membrane (**Figure 7.10a**). The absorbance band obtained at 3440 cm^{-1} corresponds to the NH stretch of the primary amine group of PAMAM which was observed merged with OH stretch band for the membrane before permeation test. Since the gas permeation test was performed until 110 °C, most of the water molecules may get evaporated during the experiment. Therefore, the cumulative effect of OH and NH stretch is not visible in the spectrum obtained after gas permeation test. The UV Vis analysis was performed on the water knock out obtained from the feed and sweep side outlet. **Figure 7.10b** signposted the absence of amines in the feed and sweep side water knock out. Therefore, the probability of leaching out of amines can be assumed as zero or negligible. Also, the AFM image showed a roughness factor of 10.34 nm (**Figure 7.11**) which is almost alike to the value attained for the membrane before permeation test (**Figure 7.2**). The EDX mapping performed for the membrane after gas permeation experiment also shows the presence of same elements in the membrane physique as before (**Figure 7.12**).

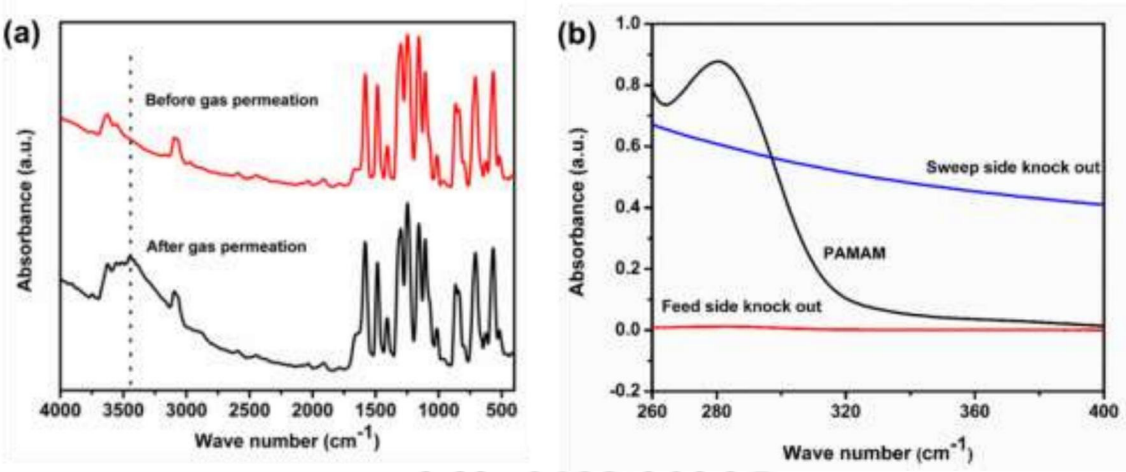

Figure 7.10 (a) FTIR analysis of the membrane before and after gas permeation (b) UV analysis of the water knockout obtained from feed and sweep side.

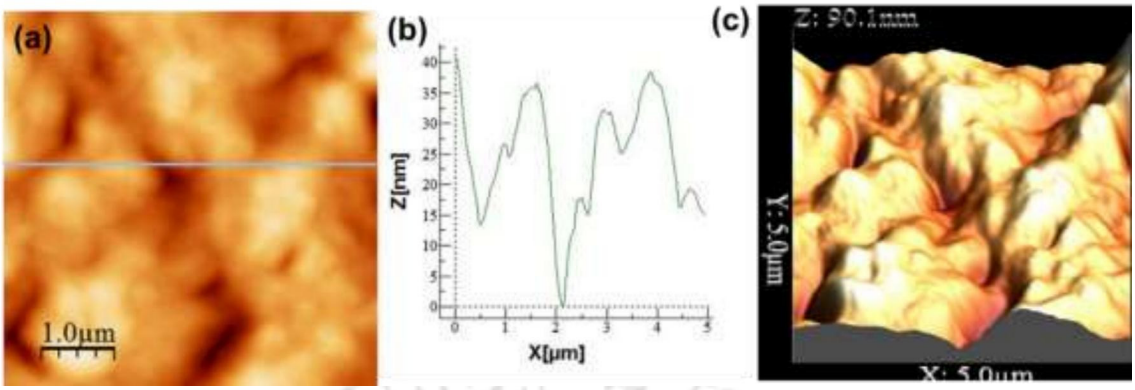

Figure 7.11 AFM analysis of the membrane after gas permeation test.

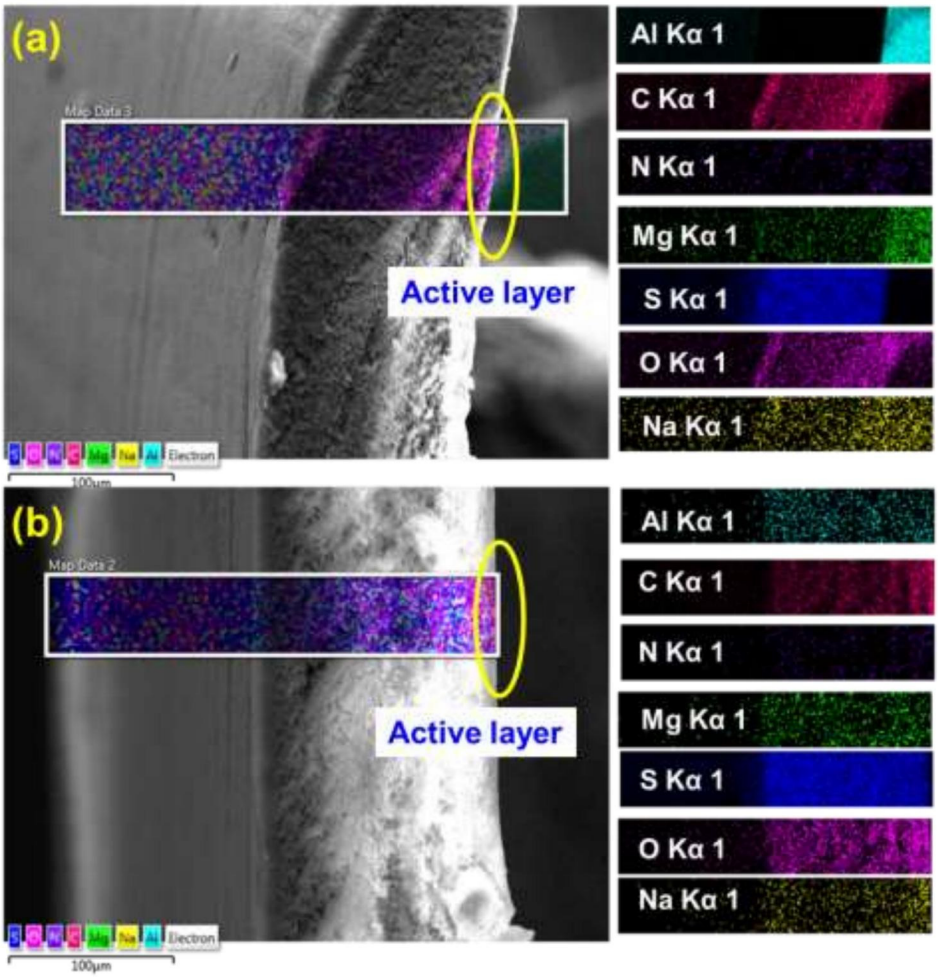

Figure 7.12 EDX mapping for the cross section of CMC/PAMAM/HT membrane (a) before gas permeation (b) after gas permeation.

7.3.7 Comparative Study

The result gained from this work has been thoroughly compared with the recent studies in MMMs for CO_2/N_2 separation. Although most of the MMMs are based on Pebax [71, 168] and poly(vinyl amine) [80, 169, 170], various membrane matrices have been tested for CO_2/N_2 separation application [171-173]. Casado-Coterillo's group reported few chitosan based MMMs for CO_2/N_2 separation where they incorporated ionic liquid and metal-organic framework to improve the separation performance [94, 95, 174, 175]. The membrane system consists of (copper(II)-benzene-1,3,5-tricarboxylate)/1-ethyl-3-methylimidazolium acetate/chitosan (HKUST-1/IL–CS) was experimented above room temperature and obtained the CO_2 permeance ~ 40 GPU with the CO_2/N_2 selectivity ~19 at 50 °C [95]. In a similar work performed on chitosan/ silk fibroin/graphene nanoparticle MMM exhibited the optimum CO_2 permeance of ~159 GPU with the CO_2/N_2 selectivity ~ 93 at 90 °C [136]. Likewise, the present membrane system (CMC/PAMAM/HT) showed a comparable CO_2/N_2 separation performance at 90 °C along with fabrication simplicity and nanometre ranged thickness. Therefore, considering both CO_2 permeance and CO_2/N_2 selectivity, CMC/PAMAM/HT membrane can be considered as a potential flue gas separation membrane.

7.4 Conclusions

Availing the advantages and overcoming the respective deficiencies of fillers, amine and matrix, CMC/PAMAM/HT membrane has been developed. The XPS, FTIR and EDX mapping analysis verified the successful fabrication of CMC/PAMAM/HT membrane. The microscopic analyses have proven the development of flawless active layer supported by PES. The moisture - holding test showed the remarkable moisture retention ability of the membrane which emphatically improves the CO_2 separation. Later, the thermally stable hydrophilic membrane was employed in a gas permeation cell for CO_2 separation study. Estimable performance for CO_2 separation was achieved for the prepared membrane at 90 °C with water flow ratio of 2.33 (sweep side/feed side) and absolute pressure of 2/1.2 bar (feed side/sweep side).

CHAPTER 8

Overall Conclusions and Recommendation for Future Work

CHAPTER 8

Overall Conclusions and Recommendation for Future Work

This chapter draws appropriate conclusions based on the investigations carried out in the present study. This chapter also provides some useful recommendations for future research in the relevant field.

8.1. Major Conclusions

The major conclusions are summarized below:

- The successful synthesis of CMC has been established by the spectroscopic analyses. The defect free gas separation membrane has been fabricated and characterized with the help of microscopic analysis. The moisture retention and thermal behavior shown by CMC active layer imply that it can be an effective CO_2 selective membrane. The optimum performance of CO_2 separation was obtained for CMC membrane at 80 °C with supplied sweep/feed water flow ratio of 1.67 and feed pressure of 2/1.2 bar (feed/sweep) presenting a significant increase of CO_2 permeance (~35 GPU) and CO_2/N_2 selectivity (~39) as compared to that of chitosan membrane.

- The thermally stable hydrophilic membranes of PZ20, PZ30 and PZ40 were successfully prepared and implemented in the GC set up for CO_2 separation. The XPS analysis confirmed the successful synthesis of PZ20 membranes. The microscopic analysis established the formation of defect free active layer over the porous support. The water retention test revealed the high moisture holding capacity of the PZ blended membranes over the CMC membrane, which positively influenced the CO_2 separation. Excellent performance of CO_2 separation was obtained for PZ20 membrane at 80 °C with supplied sweep/feed water flow ratio of 1.67 and feed pressure of 2/1.2 bar (feed/sweep) exhibiting a remarkable increase of CO_2 permeance (89 GPU) and CO_2/N_2 selectivity (103) as compared to that of pure CMC membrane.

- PAMAM can be conjectured as the very effective CO_2 selective molecular gate after blending with CMC owing to its various tunable properties. The spectroscopic and microscopic analyses have established the formation of flawless thin layered CMC/PAMAM composite membrane. The increased percentages of PAMAM contribute aggregated molecules on the membrane surface which hinder gas permeation. Temperature stability and the moisture retention ability of the CMC/PAMAM have driven the membrane towards high temperature CO_2 separation application. The detailed study on mixed gas permeation have recognized the engagement of the membrane in facilitated transport, solution diffusion and salting out phenomena. In conclusion, the membrane exposed an overall CO_2 permeance of ~98 GPU with the CO_2/N_2 selectivity ~149 on maintenance of sweep/feed water flow ratio 1.67 at 90 °C. Thus, CMC/PAMAM membrane set forth itself to be an impending candidate for large scale CO_2 separation application.

- The CNTs are dispersed in CMC successfully and a series of CMC membranes with different CNTs content were prepared using solution casting method. The Raman and FETEM techniques verified the formation of CMC wrapped CNTs on application of wet grinding assisted sonication. The development of defect-free thin layer of CMC/CNTs over the porous support has been spotted in the FESEM images. The AFM images signposted the surface roughness of the membranes increases with increased percentage of CNTs. The XPS and FTIR analyses confirmed the development of CNTs incorporated membranes. The water uptake ability of the matrix layers was also investigated under different humid environment and the moisture holding capacity was decreased with the increasing of CNTs loading in the CMC membrane. Optimal CO_2 permeance (~ 43 GPU) and CO_2/N_2 selectivity (~ 45) were achieved with the incorporation of 1 wt. % CNTs at water flow ratio 3 and temperature 80 °C.

- The limitation of getting lower CO_2 permeance in CMC/CNTs membrane was taken into account and high - speed CO_2 transport membrane was developed by loading HT in the CMC matrix. The FTIR, XRD and EDX mapping analysis verified the successful fabrication of CMC/HT membrane. The FESEM image proved the formation of dense active layer of a 1.21 μm over a PES substrate and the surface roughness of 23.9 μm was determined by AFM analysis. The membrane showed thermal stability at the higher operating temperature range 80 - 110 °C. Additionally, the moisture retention

ability of the membrane helped in reducing the gas transfer resistance and enhanced CO_2 permeance. Finally, the CO_2 separation study performed on CMC/HT membrane estimated optimum CO_2 permeance of 70 GPU at 90 °C with a separation factor of 13.

- Availing the advantages and overcoming the respective deficiencies of fillers, amine and matrix, CMC/PAMAM/HT membrane has been developed. The XPS, FTIR and EDX mapping analysis verified the successful fabrication of CMC/PAMAM/HT membrane. The microscopic analyses proven the development of flawless active layer supported by PES. The moisture holding test showed the remarkable moisture retention ability of the membrane which emphatically improves the CO_2 separation. Later, the thermally stable hydrophilic membrane was employed in a gas permeation cell for CO_2 separation study. Estimable performance for CO_2 separation was achieved for the prepared membrane at 90 °C with water flow ratio of 0.6 (feed side/sweep side) and absolute pressure of 2/1.2 bar (feed side/sweep side).

- *Comparative Study:* The comparative study on the basis of highest CO_2 permeance shown by the membranes conducted under this research study at different operating temperature, sweep/feed water flow ratio and absolute pressure = 2/1.21 bar (feed/sweep) is shown in **Table 8.1**. CMC has been identified as competent CO_2 selective membrane owing to its inherent amine group in its structure and its polyionic salt nature. The CO_2 permeance and CO_2/N_2 selectivity have improved after the loading of PZ. However, CMC/PZ membrane showed very fast CO_2 transport performance but the performance stability retained up to 3 days. On the contrary, PAMAM blended system exhibited long term CO_2 separation performance even after 6 days. In the meantime, the CO_2 permeance and CO_2/N_2 selectivity of CMC/PAMAM were also improved ~ 2.8 and ~ 3.5 times than CMC. Later, the study performed on filler (CNTs and HT) incorporated CMC membrane revealed two different consequences. CNTs incorporated CMC membrane (CMC/CNTs) offered better CO_2 permeance and CO_2/N_2 selectivity concurrently as compared to CMC. Conversely, the membrane loaded with HT in CMC (CMC/HT) displayed remarkable CO_2 permeance but inferior CO_2/N_2 selectivity than that of CMC. However, both the membranes were stable during the course of the experiment. Well ahead, based on the abovementioned studies a goal has set to work on the improvement of CO_2/N_2 selectivity of CMC/HT

membrane. In view of that, CMC/PAMAM/HT membrane was fabricated and obtained the significant augmentation of CO_2 permeance and CO_2/N_2 selectivity than the other tested membranes (CMC, CMC/PZ, CMC/PAMAM, CMC/CNT and CMC/HT) as tabulated in **Table 8.1**. Moreover, CMC/PAMAM/HT membrane was found thermally stable and possessed long term performance stability. This substantiated the efficiency of the membrane for CO_2 separation application.

Table 8.1 Optimum CO_2 separation performance exhibited by the membranes studied in this research work.

Membrane system (in Wt. %)	CO_2 permeance (GPU)	CO_2/N_2 selectivity	Operating temperature (°C)	Sweep/feed water flow ratio
100 % CMC	35	39	80	1.67
20 % PZ+ 80% CMC	89	103	80	1.67
10 % PAMAM + 90 % CMC	101	137	90	2.33
1 % CNTs + 99 % CMC	45	43	80	3
1 % HT + 99 % CMC	70	13	90	2.33
1 % HT + 10 % PAMAM + 89 % CMC	123	67	90	2.33

8.2 Recommendation for Future Research

This work presents a systematic and detailed investigation to understand the water swellable membrane based CO_2 separation featured with different amine carriers and fillers. Undoubtedly there are several areas which merit further research attention.

- All the gas permeation studies were performed at a constant feed absolute pressure i.e., at flue gas condition. The effect of feed side pressure on the separation performance

can be studied to know the potentiality of the membranes for other CO_2 separation applications.

- The gas permeation test was performed using 20 % CO_2 and 80 % N_2 gas mixture. Apart from these, the test can be performed with some percentage of H_2, O_2, SOx and NOx as impurities in the present feed gas.
- The performance stability of CMC/PAMAM/HT membrane was investigated up to 15 days and obtained the unaffected CO_2 permeance. However, the study of the effect of O_2 on the membrane will provide additional information as most of the amines are oxidized in the presence of O_2.
- Economic valuation of the prepared membranes can be appraised to endorse their applications for commercial usages in industries.
- The incorporation of pristine nanofillers (CNT and HT) leads to improvement in the overall CO_2 permeation. However, there is further scope for amine or other functionalization of the fillers to enhance CO_2 permeation activity.
- Other than CMC, there is a scope for alteration of chitosan structure to other derivatives which can be the probable membranes for CO_2 separation.

References

[1] I. Dincer, Renewable energy and sustainable development: a crucial review, Renewable and sustainable energy reviews, 4 (2000) 157-175.

[2] E.R. Lemon, CO_2 and plants: the response of plants to rising levels of atmospheric carbon dioxide, CRC Press, 2019.

[3] N. Panwar, S. Kaushik, S. Kothari, Role of renewable energy sources in environmental protection: A review, Renewable and Sustainable Energy Reviews, 15 (2011) 1513-1524.

[4] M.K. Mondal, H.K. Balsora, P. Varshney, Progress and trends in CO_2 capture/separation technologies: a review, Energy, 46 (2012) 431-441.

[5] M. Wang, A. Lawal, P. Stephenson, J. Sidders, C. Ramshaw, Post-combustion CO_2 capture with chemical absorption: a state-of-the-art review, Chemical engineering research and design, 89 (2011) 1609-1624.

[6] I. Hidalgo, L. Szabo, J.C. Ciscar, A. Soria, Technological prospects and CO_2 emission trading analyses in the iron and steel industry: A global model, Energy, 30 (2005) 583-610.

[7] H.J. Lee, J.D. Lee, P. Linga, P. Englezos, Y.S. Kim, M.S. Lee, Y. Do Kim, Gas hydrate formation process for pre-combustion capture of carbon dioxide, Energy, 35 (2010) 2729-2733.

[8] P. Linga, R. Kumar, P. Englezos, The clathrate hydrate process for post and pre-combustion capture of carbon dioxide, Journal of hazardous materials, 149 (2007) 625-629.

[9] M. Kanniche, R. Gros-Bonnivard, P. Jaud, J. Valle-Marcos, J.-M. Amann, C. Bouallou, Pre-combustion, post-combustion and oxy-combustion in thermal power plant for CO_2 capture, Applied Thermal Engineering, 30 (2010) 53-62.

[10] J. Adanez, A. Abad, F. Garcia-Labiano, P. Gayan, F. Luis, Progress in chemical-looping combustion and reforming technologies, Progress in energy and combustion science, 38 (2012) 215-282.

[11] Z.H. Lee, K.T. Lee, S. Bhatia, A.R. Mohamed, Post-combustion carbon dioxide capture: Evolution towards utilization of nanomaterials, Renewable and Sustainable Energy Reviews, 16 (2012) 2599-2609.

[12] B. Shimekit, H. Mukhtar, Natural gas purification technologies-major advances for CO_2 separation and future directions, in: Advances in natural gas technology, IntechOpen, 2012.

[13] R.W. Baker, K. Lokhandwala, Natural gas processing with membranes: an overview, Industrial & Engineering Chemistry Research, 47 (2008) 2109-2121.

[14] T.C. Merkel, H. Lin, X. Wei, R. Baker, Power plant post-combustion carbon dioxide capture: An opportunity for membranes, Journal of membrane science, 359 (2010) 126-139.

[15] D. Aaron, C. Tsouris, Separation of CO_2 from flue gas: a review, Separation Science and Technology, 40 (2005) 321-348.

[16] G. Xu, F. Liang, Y. Yang, Y. Hu, K. Zhang, W. Liu, An improved CO_2 separation and purification system based on cryogenic separation and distillation theory, Energies, 7 (2014) 3484-3502.

[17] J. Adewole, A. Ahmad, S. Ismail, C. Leo, Current challenges in membrane separation of CO_2 from natural gas: A review, International Journal of Greenhouse Gas Control, 17 (2013) 46-65.

[18] L. Zhao, E. Riensche, R. Menzer, L. Blum, D. Stolten, A parametric study of CO_2/N_2 gas separation membrane processes for post-combustion capture, Journal of Membrane Science, 325 (2008) 284-294.

[19] M.K. Barillas, R.M. Enick, M. O'Brien, R. Perry, D.R. Luebke, B.D. Morreale, The CO_2 permeability and mixed gas CO_2/H_2 selectivity of membranes composed of CO_2-philic polymers, Journal of membrane science, 372 (2011) 29-39.

[20] B.D. Freeman, Basis of permeability/selectivity tradeoff relations in polymeric gas separation membranes, Macromolecules, 32 (1999) 375-380.

[21] R.W. Baker, J. Wijmans, Y. Huang, Permeability, permeance and selectivity: A preferred way of reporting pervaporation performance data, Journal of Membrane Science, 348 (2010) 346-352.

[22] W. Yave, A. Car, S.S. Funari, S.P. Nunes, K.-V. Peinemann, CO_2-philic polymer membrane with extremely high separation performance, Macromolecules, 43 (2009) 326-333.

[23] S. Barma, B. Mandal, Synthesis and characterization of ordered mesoporous silica membrane: Role of porous support and gas permeation study, Microporous and Mesoporous Materials, 210 (2015) 10-19.

[24] Y. Dai, J. Johnson, O. Karvan, D.S. Sholl, W. Koros, Ultem®/ZIF-8 mixed matrix hollow fiber membranes for CO_2/N_2 separations, Journal of Membrane Science, 401 (2012) 76-82.

[25] S. Sridhar, S. Bee, S.K. Bhargava, Membrane-based gas separation: principle, applications and future potential, Chem. Eng. Dig, (2014) 1-25.

[26] C.A. Scholes, A. Qader, G.W. Stevens, S.E. Kentish, Membrane pilot plant trials of CO2 separation from flue gas, Greenhouse Gases: Science and Technology, 5 (2015) 229-237.

[27] C.A. Scholes, S.E. Kentish, G.W. Stevens, Effects of minor components in carbon dioxide capture using polymeric gas separation membranes, Separation & Purification Reviews, 38 (2009) 1-44.

[28] Z. Dai, S. Fabio, N.G. Marino, C. Riccardo, L. Deng, Field test of a pre-pilot scale hollow fiber facilitated transport membrane for CO_2 capture, International Journal of Greenhouse Gas Control, 86 (2019) 191-200.

[29] K. Ramasubramanian, W.W. Ho, Recent developments on membranes for post-combustion carbon capture, Current Opinion in Chemical Engineering, 1 (2011) 47-54.

[30] S. Kim, Y.M. Lee, High performance polymer membranes for CO_2 separation, Current Opinion in Chemical Engineering, 2 (2013) 238-244.

[31] L. Robeson, B. Freeman, D. Paul, B. Rowe, An empirical correlation of gas permeability and permselectivity in polymers and its theoretical basis, Journal of Membrane Science, 341 (2009) 178-185.

[32] D. Gottschlich, D. Roberts, J. Way, A theoretical comparison of facilitated transport and solution-diffusion membrane modules for gas separation, Gas Separation & Purification, 2 (1988) 65-71.

[33] B. Prasad, B. Mandal, Preparation and characterization of CO_2-selective facilitated transport membrane composed of chitosan and poly (allylamine) blend for CO_2/N_2 separation, Journal of Industrial and Engineering Chemistry, 66 (2018) 419-429.

[34] S. Kasahara, E. Kamio, T. Ishigami, H. Matsuyama, Effect of water in ionic liquids on CO_2 permeability in amino acid ionic liquid-based facilitated transport membranes, Journal of membrane science, 415 (2012) 168-175.

[35] J. Zou, W.W. Ho, CO_2-selective polymeric membranes containing amines in crosslinked poly (vinyl alcohol), Journal of Membrane Science, 286 (2006) 310-321.

[36] O.H. LeBlanc Jr, W.J. Ward, S.L. Matson, S.G. Kimura, Facilitated transport in ion-exchange membranes, Journal of Membrane science, 6 (1980) 339-343.

[37] T.J. Kim, B. Li, M.B. Hägg, Novel fixed-site–carrier polyvinylamine membrane for carbon dioxide capture, Journal of Polymer Science Part B: Polymer Physics, 42 (2004) 4326-4336.

[38] R.D. Noble, Analysis of facilitated transport with fixed site carrier membranes, Journal of Membrane Science, 50 (1990) 207-214.

[39] Y. Cai, Z. Wang, C. Yi, Y. Bai, J. Wang, S. Wang, Gas transport property of polyallylamine–poly (vinyl alcohol)/polysulfone composite membranes, Journal of Membrane Science, 310 (2008) 184-196.

[40] E.L. Cussler, R. Aris, A. Bhown, On the limits of facilitated diffusion, Journal of Membrane Science, 43 (1989) 149-164.

[41] Y. Chen, W.W. Ho, High-molecular-weight polyvinylamine/piperazine glycinate membranes for CO_2 capture from flue gas, Journal of Membrane Science, 514 (2016) 376-384.

[42] F. Zhou, H.N. Tien, W.L. Xu, J.-T. Chen, Q. Liu, E. Hicks, M. Fathizadeh, S. Li, M. Yu, Ultrathin graphene oxide-based hollow fiber membranes with brush-like CO_2-philic agent for highly efficient CO_2 capture, Nature communications, 8 (2017) 2107.

[43] Z. Idris, D.A. Eimer, Representation of CO_2 absorption in sterically hindered amines, Energy Procedia, 51 (2014) 247-252.

[44] H. Matsuyama, M. Teramoto, H. Sakakura, Selective permeation of CO_2 through poly 2-(N, N-dimethyl) aminoethyl methacrylate membrane prepared by plasma-graft polymerization technique, Journal of Membrane Science, 114 (1996) 193-200.

[45] G.J. Francisco, A. Chakma, X. Feng, Membranes comprising of alkanolamines incorporated into poly (vinyl alcohol) matrix for CO_2/N_2 separation, Journal of Membrane Science, 303 (2007) 54-63.

[46] S. Wang, X. Li, H. Wu, Z. Tian, Q. Xin, G. He, D. Peng, S. Chen, Y. Yin, Z. Jiang, Advances in high permeability polymer-based membrane materials for CO_2 separations, Energy & Environmental Science, 9 (2016) 1863-1890.

[47] C. Nagel, K. Günther-Schade, D. Fritsch, T. Strunskus, F. Faupel, Free volume and transport properties in highly selective polymer membranes, Macromolecules, 35 (2002) 2071-2077.

[48] Z. Tong, W.W. Ho, Facilitated transport membranes for CO_2 separation and capture, Separation Science and Technology, 52 (2017) 156-167.

[49] L. Deng, T.-J. Kim, M.-B. Hägg, Facilitated transport of CO_2 in novel PVAm/PVA blend membrane, Journal of Membrane Science, 340 (2009) 154-163.

[50] L. Zhang, R. Wang, Salting-out effect on facilitated transport membranes for CO_2 separation: From fluoride salt to polyoxometalates, RSC Advances, 2 (2012) 9551-9554.

[51] Y. Li, Q. Xin, H. Wu, R. Guo, Z. Tian, Y. Liu, S. Wang, G. He, F. Pan, Z. Jiang, Efficient CO_2 capture by humidified polymer electrolyte membranes with tunable water state, Energy & Environmental Science, 7 (2014) 1489-1499.

[52] L. Liu, A. Chakma, X. Feng, Gas permeation through water-swollen hydrogel membranes, Journal of Membrane Science, 310 (2008) 66-75.

[53] J. Wang, S. Wang, Q. Xin, Y. Li, Perspectives on water-facilitated CO_2 capture materials, Journal of Materials Chemistry A, 5 (2017) 6794-6816.

[54] A. Mondal, B. Mandal, Synthesis and characterization of crosslinked poly (vinyl alcohol)/poly (allylamine)/2-amino-2-hydroxymethyl-1, 3-propanediol/polysulfone composite membrane for CO_2/N_2 separation, Journal of membrane science, 446 (2013) 383-394.

[55] H. Matsuyama, A. Terada, T. Nakagawara, Y. Kitamura, M. Teramoto, Facilitated transport of CO_2 through polyethylenimine/poly (vinyl alcohol) blend membrane, Journal of Membrane Science, 163 (1999) 221-227.

[56] A. Ito, M. Sato, T. Anma, Permeability of CO_2 through chitosan membrane swollen by water vapor in feed gas, Die Angewandte Makromolekulare Chemie: Applied Macromolecular Chemistry and Physics, 248 (1997) 85-94.

[57] L.A. El-Azzami, E.A. Grulke, Parametric study of CO_2 fixed carrier facilitated transport through swollen chitosan membranes, Industrial & Engineering Chemistry Research, 48 (2009) 894-902.

[58] Y. Liu, S. Yu, H. Wu, Y. Li, S. Wang, Z. Tian, Z. Jiang, High permeability hydrogel membranes of chitosan/poly ether-block-amide blends for CO_2 separation, Journal of Membrane Science, 469 (2014) 198-208.

[59] B. Prasad, B. Mandal, CO_2 separation performance by chitosan/tetraethylenepentamine/poly (ether sulfone) composite membrane, Journal of Applied Polymer Science, 134 (2017) 45206.

[60] M. Yu, Y. Dai, K. Yang, H. Li, H. Guo, G. He, TEA incorporated CS blend composite membrane for high CO_2 separation performance, RSC advances, 6 (2016) 27016-27019.

[61] J.-N. Shen, C.-C. Yu, G.-N. Zeng, B. Van der Bruggen, Preparation of a facilitated transport membrane composed of carboxymethyl chitosan and polyethylenimine for CO_2/N_2 separation, International journal of molecular sciences, 14 (2013) 3621-3638.

[62] M. Inoue, M. Ueda, T. Higashi, T. Anno, K. Fujisawa, K. Motoyama, M. Mizuguchi, Y. Ando, H. Jono, H. Arima, Therapeutic Potential of Polyamidoamine Dendrimer for Amyloidogenic Transthyretin Amyloidosis, ACS chemical neuroscience, (2019).

[63] A. Asandei, A. Ciuca, A. Apetrei, I. Schiopu, L. Mereuta, C.H. Seo, Y. Park, T. Luchian, Nanoscale investigation of generation 1 PAMAM dendrimers interaction with a protein nanopore, Scientific reports, 7 (2017) 6167.

[64] K. Kono, Dendrimer-based bionanomaterials produced by surface modification, assembly and hybrid formation, Polymer journal, 44 (2012) 531.

[65] A.S. Kovvali, H. Chen, K.K. Sirkar, Dendrimer membranes: a CO_2-selective molecular gate, Journal of the American Chemical Society, 122 (2000) 7594-7595.

[66] S. Duan, I. Taniguchi, T. Kai, S. Kazama, Poly (amidoamine) dendrimer/poly (vinyl alcohol) hybrid membranes for CO_2 capture, Journal of membrane science, 423 (2012) 107-112.

[67] S. Duan, T. Kouketsu, S. Kazama, K. Yamada, Development of PAMAM dendrimer composite membranes for CO_2 separation, Journal of membrane science, 283 (2006) 2-6.

[68] O.G. Nik, X.Y. Chen, S. Kaliaguine, Functionalized metal organic framework-polyimide mixed matrix membranes for CO_2/CH_4 separation, Journal of Membrane Science, 413 (2012) 48-61.

[69] A. Ismail, P. Goh, S. Sanip, M. Aziz, Transport and separation properties of carbon nanotube-mixed matrix membrane, Separation and Purification Technology, 70 (2009) 12-26.

[70] C. Lu, H. Bai, B. Wu, F. Su, J.F. Hwang, Comparative study of CO_2 capture by carbon nanotubes, activated carbons, and zeolites, Energy & Fuels, 22 (2008) 3050-3056.

[71] H. Zhang, R. Guo, J. Hou, Z. Wei, X. Li, Mixed-Matrix Membranes Containing Carbon Nanotubes Composite with Hydrogel for Efficient CO_2 Separation, ACS Applied Materials & Interfaces, 8 (2016) 29044-29051.

[72] L. Deng, M.-B. Hägg, Carbon nanotube reinforced PVAm/PVA blend FSC nanocomposite membrane for CO_2/CH_4 separation, International Journal of Greenhouse Gas Control, 26 (2014) 127-134.

[73] S. Kim, T.W. Pechar, E. Marand, Poly(imide siloxane) and carbon nanotube mixed matrix membranes for gas separation, Desalination, 192 (2006) 330-339.

[74] L. Ansaloni, Y. Zhao, B.T. Jung, K. Ramasubramanian, M.G. Baschetti, W.W. Ho, Facilitated transport membranes containing amino-functionalized multi-walled carbon nanotubes for high-pressure CO_2 separations, Journal of Membrane Science, 490 (2015) 18–28.

[75] A. Ahmad, Z. Jawad, S. Low, S. Zein, A cellulose acetate/multi-walled carbon nanotube mixed matrix membrane for CO_2/N_2 separation, Journal of Membrane Science, 451 (2014) 55-66.

[76] E. Van Selow, P. Cobden, P. Verbraeken, J. Hufton, R. Van den Brink, Carbon capture by sorption-enhanced water− gas shift reaction process using hydrotalcite-based material, Industrial & Engineering Chemistry Research, 48 (2009) 4184-4193.

[77] M. Ram Reddy, Z. Xu, G. Lu, J. Diniz da Costa, Layered double hydroxides for CO_2 capture: structure evolution and regeneration, Industrial & engineering chemistry research, 45 (2006) 7504-7509.

[78] X. Cao, Z. Wang, Z. Qiao, S. Zhao, J. Wang, Penetrated COF channels: amino environment and suitable size for CO_2 preferential adsorption and transport in mixed matrix membranes, ACS applied materials & interfaces, 11 (2019) 5306-5315.

[79] J. Liao, Z. Wang, C. Gao, M. Wang, K. Yan, X. Xie, S. Zhao, J. Wang, S. Wang, A high performance PVAm–HT membrane containing high-speed facilitated transport channels for CO_2 separation, Journal of Materials Chemistry A, 3 (2015) 16746-16761.

[80] Y. Shen, H. Wang, J. Liu, Y. Zhang, Enhanced performance of a novel polyvinyl amine/chitosan/graphene oxide mixed matrix membrane for CO_2 capture, ACS Sustainable Chemistry & Engineering, 3 (2015) 1819-1829.

[81] M. Barooah, B. Mandal, Synthesis, characterization and CO_2 separation performance of novel PVA/PG/ZIF-8 mixed matrix membrane, Journal of membrane science, 572 (2019) 198-209.

[82] B. Krajewska, Membrane-based processes performed with use of chitin/chitosan materials, Separation and purification technology, 41 (2005) 305-312.

[83] S. Islam, M.R. Bhuiyan, M. Islam, Chitin and chitosan: structure, properties and applications in biomedical engineering, Journal of Polymers and the Environment, 25 (2017) 854-866.

[84] S. Kalliola, E. Repo, V. Srivastava, F. Zhao, J.P. Heiskanen, J.A. Sirviö, H. Liimatainen, M. Sillanpää, Carboxymethyl chitosan and its hydrophobically modified derivative as pH-switchable emulsifiers, Langmuir, 34 (2018) 2800-2806.

[85] R. Jayakumar, M. Prabaharan, S. Nair, S. Tokura, H. Tamura, N. Selvamurugan, Novel carboxymethyl derivatives of chitin and chitosan materials and their biomedical applications, Progress in Materials Science, 55 (2010) 675-709.

[86] A. Jimtaisong, N. Saewan, Utilization of carboxymethyl chitosan in cosmetics, International journal of cosmetic science, 36 (2014) 12-21.

[87] A.A. Shamsabadi, F. Seidi, E. Salehi, M. Nozari, A. Rahimpour, M. Soroush, Efficient CO_2-removal using novel mixed-matrix membranes with modified TiO_2 nanoparticles, Journal of Materials Chemistry A, 5 (2017) 4011-4025.

[88] H.-C. Ge, D.-K. Luo, Preparation of carboxymethyl chitosan in aqueous solution under microwave irradiation, Carbohydrate research, 340 (2005) 1351-1356.

[89] M.R. Kasaai, Calculation of Mark–Houwink–Sakurada (MHS) equation viscometric constants for chitosan in any solvent–temperature system using experimental reported viscometric constants data, Carbohydrate polymers, 68 (2007) 477-488.

[90] J. Huang, J. Zou, W.W. Ho, Carbon dioxide capture using a CO_2-selective facilitated transport membrane, Industrial & Engineering Chemistry Research, 47 (2008) 1261-1267.

[91] M. Omidkhah, M.Z. Pedram, A.E. Amooghin, Facilitated transport of CO_2 through DEA-mediated poly (vinyl alcohol) membrane cross-linked by formaldehyde, Journal of Membrane Science & Technology, 3 (2013).

[92] S. Yuan, Z. Wang, Z. Qiao, M. Wang, J. Wang, S. Wang, Improvement of CO_2/N_2 separation characteristics of polyvinylamine by modifying with ethylenediamine, Journal of membrane science, 378 (2011) 425-437.

[93] Z. Qiao, Z. Wang, C. Zhang, S. Yuan, Y. Zhu, J. Wang, S. Wang, PVAm–PIP/PS composite membrane with high performance for CO_2/N_2 separation, AIChE Journal, 59 (2013) 215-228.

[94] E. Santos, E. Rodríguez-Fernández, C. Casado-Coterillo, Á. Irabien, Hybrid ionic liquid-chitosan membranes for CO_2 separation: mechanical and thermal behavior, International Journal of Chemical Reactor Engineering, 14 (2016) 713-718.

[95] C. Casado-Coterillo, A. Fernández-Barquín, B. Zornoza, C. Téllez, J. Coronas, Á. Irabien, Synthesis and characterisation of MOF/ionic liquid/chitosan mixed matrix membranes for CO_2/N_2 separation, RSC Advances, 5 (2015) 102350-102361.

[96] G. Versteeg, W.P.M. van Swaaij, On the kinetics between CO_2 and alkanolamines both in aqueous and non-aqueous solutions—II. Tertiary amines, Chemical engineering science, 43 (1988) 587-591.

[97] I. Taniguchi, H. Urai, T. Kai, S. Duan, S. Kazama, A CO_2-selective molecular gate of poly (amidoamine) dendrimer immobilized in a poly (ethylene glycol) network, Journal of membrane science, 444 (2013) 96-100.

[98] G. He, Y. Kong, H. Zheng, W. Ke, X. Chen, Y. Yin, Y. Yi, Preparation and Properties of Poly (amidoamine) Dendrimer/Quaternary Ammonium Chitosan Hydrogels, Journal of Wuhan University of Technology-Mater. Sci. Ed., 33 (2018) 736-743.

[99] D.L. Pavia, G.M. Lampman, G.S. Kriz, J.A. Vyvyan, Introduction to spectroscopy, Cengage Learning, 2008.

[100] X. Qi, J. Qin, Y. Fan, X. Qin, Y. Jiang, Z. Wu, Carboxymethyl chitosan-modified polyamidoamine dendrimer enables progressive drug targeting of tumors via pH-sensitive charge inversion, Journal of biomedical nanotechnology, 12 (2016) 667-678.

[101] J.M. Joshi, V.K. Sinha, Ceric ammonium nitrate induced grafting of polyacrylamide onto carboxymethyl chitosan, Carbohydrate polymers, 67 (2007) 427-435.

[102] Y. Wen, F. Yao, F. Sun, Z. Tan, L. Tian, L. Xie, Q. Song, Antibacterial action mode of quaternized carboxymethyl chitosan/poly (amidoamine) dendrimer core–shell nanoparticles against Escherichia coli correlated with molecular chain conformation, Materials Science and Engineering: C, 48 (2015) 220-227.

[103] L. Deng, M.-B. Hägg, Swelling behavior and gas permeation performance of PVAm/PVA blend FSC membrane, Journal of membrane science, 363 (2010) 295-301.

[104] W.-P. Zhu, J. Gao, S.-P. Sun, S. Zhang, T.-S. Chung, Poly (amidoamine) dendrimer (PAMAM) grafted on thin film composite (TFC) nanofiltration (NF) hollow fiber membranes for heavy metal removal, Journal of Membrane Science, 487 (2015) 117-126.

[105] R. Borgohain, B. Prasad, B. Mandal, Synthesis and characterization of water-soluble chitosan membrane blended with a mobile carrier for CO_2 separation, Separation and Purification Technology, 222 (2019) 177-187.

[106] B. Prasad, B. Mandal, Moisture responsive and CO_2 selective biopolymer membrane containing silk fibroin as a green carrier for facilitated transport of CO_2, Journal of membrane science, 550 (2018) 416-426.

[107] H.-R. Kim, J.-W. Jang, J.-W. Park, Carboxymethyl chitosan-modified magnetic-cored dendrimer as an amphoteric adsorbent, Journal of hazardous materials, 317 (2016) 608-616.

[108] L.A. El-Azzami, E.A. Grulke, Carbon dioxide separation from hydrogen and nitrogen by fixed facilitated transport in swollen chitosan membranes, Journal of Membrane Science, 323 (2008) 225-234.

[109] A. Mondal, B. Mandal, CO_2 separation using thermally stable crosslinked poly (vinyl alcohol) membrane blended with polyvinylpyrrolidone/polyethyleneimine/tetraethylenepentamine, Journal of membrane science, 460 (2014) 126-138.

[110] C. Yi, Z. Wang, M. Li, J. Wang, S. Wang, Facilitated transport of CO_2 through polyvinylamine/polyethlene glycol blend membranes, Desalination, 193 (2006) 90-96.

[111] L.A. El-Azzami, E.A. Grulke, Carbon dioxide separation from hydrogen and nitrogen: Facilitated transport in arginine salt–chitosan membranes, Journal of Membrane Science, 328 (2009) 15-22.

[112] S. Xiao, X. Feng, R.Y. Huang, Trimesoyl chloride crosslinked chitosan membranes for CO_2/N_2 separation and pervaporation dehydration of isopropanol, Journal of Membrane Science, 306 (2007) 36-46.

[113] S. Chatterjee, M.W. Lee, S.H. Woo, Enhanced mechanical strength of chitosan hydrogel beads by impregnation with carbon nanotubes, Carbon, 47 (2009) 2933-2936.

[114] S. Mallakpour, A. Zadehnazari, Synthesis, morphology investigation and thermal mechanical properties of dopamine-functionalized multi-walled carbon nanotube/poly (amide-imide) composites, Reactive and Functional Polymers, 106 (2016) 112-119.

[115] H.-X. Wu, X.-Q. Qiu, W.-M. Cao, Y.-H. Lin, R.-F. Cai, S.-X. Qian, Polymer-wrapped multiwalled carbon nanotubes synthesized via microwave-assisted in situ emulsion polymerization and their optical limiting properties, Carbon, 45 (2007) 2866-2872.

[116] F. Peng, F. Pan, H. Sun, L. Lu, Z. Jiang, Novel nanocomposite pervaporation membranes composed of poly (vinyl alcohol) and chitosan-wrapped carbon nanotube, Journal of Membrane Science, 300 (2007) 13-19.

[117] W. Yang, Y. Wang, J. Li, X. Yang, Polymer wrapping technique: an effective route to prepare Pt nanoflower/carbon nanotube hybrids and application in oxygen reduction, Energy & Environmental Science, 3 (2010) 144-149.

[118] Z.A. Mohammadi, S.F. Aghamiri, A. Zarrabi, M.R. Talaie, A comparative study on non-covalent functionalization of carbon nanotubes by chitosan and its derivatives for delivery of doxorubicin, Chemical Physics Letters, 642 (2015) 22-28.

[119] C. Tang, T. Zhou, J. Yang, Q. Zhang, F. Chen, Q. Fu, L. Yang, Wet-grinding assisted ultrasonic dispersion of pristine multi-walled carbon nanotubes (MWCNTs) in chitosan solution, Colloids and Surfaces B: Biointerfaces, 86 (2011) 189-197.

[120] P. Liu, Modifications of carbon nanotubes with polymers, European Polymer Journal, 41 (2005) 2693-2703.

[121] Y. Liu, P. Liang, H.Y. Zhang, D.S. Guo, Cation-controlled aqueous dispersions of alginic-acid-wrapped multi-walled carbon nanotubes, Small, 2 (2006) 874-878.

[122] Y. Zhou, H. Yang, H.-Y. Chen, Direct electrochemistry and reagentless biosensing of glucose oxidase immobilized on chitosan wrapped single-walled carbon nanotubes, Talanta, 76 (2008) 419-423.

[123] Q. Yang, L. Shuai, X. Pan, Synthesis of fluorescent chitosan and its application in noncovalent functionalization of carbon nanotubes, Biomacromolecules, 9 (2008) 3422-3426.

[124] M.A. Salam, R. Burk, Synthesis and characterization of multi-walled carbon nanotubes modified with octadecylamine and polyethylene glycol, Arabian Journal of Chemistry, 10 (2017) S921-S927.

[125] F.R. de Abreu, S.P. Campana-Filho, Characteristics and properties of carboxymethylchitosan, Carbohydrate Polymers, 75 (2009) 214-221.

[126] M.F. Jimenez-Solomon, P. Gorgojo, M. Munoz-Ibanez, A.G. Livingston, Beneath the surface: Influence of supports on thin film composite membranes by interfacial polymerization for organic solvent nanofiltration, Journal of membrane science, 448 (2013) 102-113.

[127] H. Bidgoli, A. Zamani, M.J. Taherzadeh, Effect of carboxymethylation conditions on the water-binding capacity of chitosan-based superabsorbents, Carbohydrate research, 345 (2010) 2683-2689.

[128] T.-Y. Liu, S.-Y. Chen, Y.-L. Lin, D.-M. Liu, Synthesis and characterization of amphiphatic carboxymethyl-hexanoyl chitosan hydrogel: water-retention ability and drug encapsulation, Langmuir, 22 (2006) 9740-9745.

[129] S. Bibi, T. Yasin, S. Hassan, M. Riaz, M. Nawaz, Chitosan/CNTs green nanocomposite membrane: Synthesis, swelling and polyaromatic hydrocarbons removal, Materials Science and Engineering: C, 46 (2015) 359-365.

[130] R. Narducci, J.F. Chailan, A. Fahs, L. Pasquini, M.L. Di Vona, P. Knauth, Mechanical properties of anion exchange membranes by combination of tensile stress–strain tests and dynamic mechanical analysis, Journal of Polymer Science Part B: Polymer Physics, 54 (2016) 1180-1187.

[131] J.B. Marroquin, K. Rhee, S. Park, Chitosan nanocomposite films: enhanced electrical conductivity, thermal stability, and mechanical properties, Carbohydrate polymers, 92 (2013) 1783-1791.

[132] S.C. Barros, A.A. da Silva, D.B. Costa, C.M. Costa, S. Lanceros-Méndez, M.T. Maciavello, J.G. Ribelles, F. Sentanin, A. Pawlicka, M.M. Silva, Thermal–mechanical

behaviour of chitosan–cellulose derivative thermoreversible hydrogel films, Cellulose, 22 (2015) 1911-1929.

[133] D.F. Sanders, Z.P. Smith, R. Guo, L.M. Robeson, J.E. McGrath, D.R. Paul, B.D. Freeman, Energy-efficient polymeric gas separation membranes for a sustainable future: a review, Polymer, 54 (2013) 4729-4761.

[134] J.C. Poshusta, R.D. Noble, J.L. Falconer, Temperature and pressure effects on CO_2 and CH_4 permeation through MFI zeolite membranes, Journal of membrane science, 160 (1999) 115-125.

[135] Y. Zhao, W.W. Ho, CO_2-selective membranes containing sterically hindered amines for CO_2/H_2 separation, Industrial & Engineering Chemistry Research, 52 (2012) 8774-8782.

[136] B. Prasad, B. Mandal, Graphene-Incorporated Biopolymeric Mixed-Matrix Membrane for Enhanced CO_2 Separation by Regulating the Support Pore Filling, ACS applied materials & interfaces, 10 (2018) 27810-27820.

[137] Y.I. Matveev, V.Y. Grinberg, V. Tolstoguzov, The plasticizing effect of water on proteins, polysaccharides and their mixtures. Glassy state of biopolymers, food and seeds, Food Hydrocolloids, 14 (2000) 425-437.

[138] H. Zhang, H. Tian, J. Zhang, R. Guo, X. Li, Facilitated transport membranes with an amino acid salt for highly efficient CO_2 separation, International Journal of Greenhouse Gas Control, 78 (2018) 85-93.

[139] R.S. Murali, S. Sridhar, T. Sankarshana, Y. Ravikumar, Gas permeation behavior of Pebax-1657 nanocomposite membrane incorporated with multiwalled carbon nanotubes, Industrial & Engineering Chemistry Research, 49 (2010) 6530-6538.

[140] H. Cong, J. Zhang, M. Radosz, Y. Shen, Carbon nanotube composite membranes of brominated poly (2, 6-diphenyl-1, 4-phenylene oxide) for gas separation, Journal of Membrane Science, 294 (2007) 178-185.

[141] H.-H. Tseng, I.A. Kumar, T.-H. Weng, C.-Y. Lu, M.-Y. Wey, Preparation and characterization of carbon molecular sieve membranes for gas separation—the effect of incorporated multi-wall carbon nanotubes, Desalination, 240 (2009) 40-45.

[142] S. Wang, Y. Liu, S. Huang, H. Wu, Y. Li, Z. Tian, Z. Jiang, Pebax–PEG–MWCNT hybrid membranes with enhanced CO_2 capture properties, Journal of Membrane Science, 460 (2014) 62-70.

[143] Y. Han, W.W. Ho, Recent advances in polymeric membranes for CO_2 capture, Chinese Journal of Chemical Engineering, (2018).

[144] M. Mokhtar, T.S. Saleh, S.N. Basahel, Mg–Al hydrotalcites as efficient catalysts for aza-Michael addition reaction: a green protocol, Journal of Molecular Catalysis A: Chemical, 353 (2012) 122-131.

[145] H.-y. Zeng, Z. Feng, X. Deng, Y.-q. Li, Activation of Mg–Al hydrotalcite catalysts for transesterification of rape oil, Fuel, 87 (2008) 3071-3076.

[146] S. Wang, L. Chen, Y. Tong, Structure–property relationship in chitosan-based biopolymer/montmorillonite nanocomposites, Journal of Polymer Science Part A: Polymer Chemistry, 44 (2006) 686-696.

[147] S. Barkhordari, M. Yadollahi, H. Namazi, pH sensitive nanocomposite hydrogel beads based on carboxymethyl cellulose/layered double hydroxide as drug delivery systems, Journal of Polymer Research, 21 (2014) 454.

[148] V. Nafisi, M.-B. Hägg, Gas separation properties of ZIF-8/6FDA-durene diamine mixed matrix membrane, Separation and Purification Technology, 128 (2014) 31-38.

[149] M. Barooah, B. Mandal, Enhanced CO_2 separation performance by PVA/PEG/silica mixed matrix membrane, Journal of Applied Polymer Science, 135 (2018) 46481.

[150] K. Duan, J. Wang, Y. Zhang, J. Liu, Covalent organic frameworks (COFs) functionalized mixed matrix membrane for effective CO_2/N_2 separation, Journal of Membrane Science, 572 (2019) 588-595.

[151] H. Zhu, J. Yuan, J. Zhao, G. Liu, W. Jin, Enhanced CO_2/N_2 separation performance by using dopamine/polyethyleneimine-grafted TiO_2 nanoparticles filled PEBA mixed-matrix membranes, Separation and Purification Technology, 214 (2019) 78-86.

[152] M.R. Dilshad, A. Islam, U. Hamidullah, F. Jamshaid, A. Ahmad, M.T.Z. Butt, A. Ijaz, Effect of alumina on the performance and characterization of cross-linked PVA/PEG 600 blended membranes for CO_2/N_2 separation, Separation and Purification Technology, 210 (2019) 627-635.

[153] J. Zhang, Q. Xin, X. Li, M. Yun, R. Xu, S. Wang, Y. Li, L. Lin, X. Ding, H. Ye, Mixed matrix membranes comprising aminosilane-functionalized graphene oxide for enhanced CO_2 separation, Journal of Membrane Science, 570 (2019) 343-354.

[154] L. Dong, C. Zhang, Y. Bai, D. Shi, X. Li, H. Zhang, M. Chen, High-performance PEBA2533-functional MMT mixed matrix membrane containing high-speed facilitated transport channels for CO_2/N_2 separation, ACS Sustainable Chemistry & Engineering, 4 (2016) 3486-3496.

[155] A. Varma, S. Deshpande, J. Kennedy, Metal complexation by chitosan and its derivatives: a review, Carbohydrate Polymers, 55 (2004) 77-93.

[156] Z. Yong, A.r.E. Rodrigues, Hydrotalcite-like compounds as adsorbents for carbon dioxide, Energy conversion and management, 43 (2002) 1865-1876.

[157] J. Liao, Z. Wang, C. Gao, S. Li, Z. Qiao, M. Wang, S. Zhao, X. Xie, J. Wang, S. Wang, Fabrication of high-performance facilitated transport membranes for CO_2 separation, Chemical Science, 5 (2014) 2843-2849.

[158] B. Pilch-Pitera, M. Kędzierski, E. Olejnik, S. Zapotoczny, Structure and properties of polyurethane-based powder clear coatings systems modified with hydrotalcites, Progress in Organic Coatings, 95 (2016) 120-126.

[159] M.M. Rao, B.R. Reddy, M. Jayalakshmi, V.S. Jaya, B. Sridhar, Hydrothermal synthesis of Mg–Al hydrotalcites by urea hydrolysis, Materials Research Bulletin, 40 (2005) 347-359.

[160] O.P. Ferreira, S.G. De Moraes, N. Duran, L. Cornejo, O.L. Alves, Evaluation of boron removal from water by hydrotalcite-like compounds, Chemosphere, 62 (2006) 80-88.

[161] P. Fernandez-Saiz, J. Lagaron, M. Ocio, Optimization of the film-forming and storage conditions of chitosan as an antimicrobial agent, Journal of agricultural and food chemistry, 57 (2009) 3298-3307.

[162] K. Sarkar, P. Kundu, Preparation of low molecular weight N-maleated chitosan-graft-PAMAM copolymer for enhanced DNA complexation, International journal of biological macromolecules, 51 (2012) 859-867.

[163] Y. Wang, D. Zhang, Bioinspired assembly of layered double hydroxide/carboxymethyl chitosan bionanocomposite hydrogel films, Journal of Materials Chemistry B, 2 (2014) 1024-1030.

[164] J.-C. Dupin, H. Martinez, C. Guimon, E. Dumitriu, I. Fechete, Intercalation compounds of Mg–Al layered double hydroxides with dichlophenac: different methods of preparation and physico-chemical characterization, Applied Clay Science, 27 (2004) 95-106.

[165] J. Chen, Y. Song, D. Shan, E.-H. Han, In situ growth of Mg–Al hydrotalcite conversion film on AZ31 magnesium alloy, Corrosion Science, 53 (2011) 3281-3288.

[166] I. Nicotera, K. Angjeli, L. Coppola, A. Enotiadis, R. Pedicini, A. Carbone, D. Gournis, Composite polymer electrolyte membranes based on Mg–Al layered double hydroxide (LDH) platelets for H2/air-fed fuel cells, Solid State Ionics, 276 (2015) 40-46.

[167] I. Khalilinejad, H. Sanaeepur, A. Kargari, Preparation of poly (ether-6-block amide)/PVC thin film composite membrane for CO_2 separation: effect of top layer thickness and operating parameters, Journal of Membrane Science and Research, 1 (2015) 124-129.

[168] V. Nafisi, M.-B. Hägg, Development of dual layer of ZIF-8/PEBAX-2533 mixed matrix membrane for CO_2 capture, Journal of Membrane Science, 459 (2014) 244-255.

[169] S. Zhao, X. Cao, Z. Ma, Z. Wang, Z. Qiao, J. Wang, S. Wang, Mixed-matrix membranes for CO_2/N_2 separation comprising a poly (vinylamine) matrix and metal–organic frameworks, Industrial & Engineering Chemistry Research, 54 (2015) 5139-5148.

[170] Y. Chen, L. Zhao, B. Wang, P. Dutta, W.W. Ho, Amine-containing polymer/zeolite Y composite membranes for CO_2/N_2 separation, Journal of Membrane Science, 497 (2016) 21-28.

[171] A. Fernández-Barquín, C. Casado-Coterillo, M. Etxeberria-Benavides, J. Zuñiga, A. Irabien, Comparison of flat and hollow-fiber mixed-matrix composite membranes for CO_2 separation with temperature, Chemical Engineering & Technology, 40 (2017) 997-1007.

[172] L. Xiang, Y. Pan, G. Zeng, J. Jiang, J. Chen, C. Wang, Preparation of poly (ether-block-amide)/attapulgite mixed matrix membranes for CO_2/N_2 separation, Journal of Membrane Science, 500 (2016) 66-75.

[173] H. Sanaeepur, A. Kargari, B. Nasernejad, A.E. Amooghin, M. Omidkhah, A novel Co^{2+} exchanged zeolite Y/cellulose acetate mixed matrix membrane for CO_2/N_2 separation, Journal of the Taiwan Institute of Chemical Engineers, 60 (2016) 403-413.

[174] C. Casado-Coterillo, M. del Mar López-Guerrero, Á. Irabien, Synthesis and characterisation of ETS-10/acetate-based ionic liquid/chitosan mixed matrix membranes for CO_2/N_2 permeation, Membranes, 4 (2014) 287-301.

[175] M.D.M.L. Guerrero, C. Casado-Coterillo, A. Irabien, Synergistic Effect of Combining Titanosilicate and 1-Ethyl-3-Methylimidazolium Acetate in Mixed Matrix Membranes for Efficient CO_2 Separation, European Journal of Sustainable Development, 4 (2015) 103-112.

Appendix 1

Structure of various polymers and amines used in this study

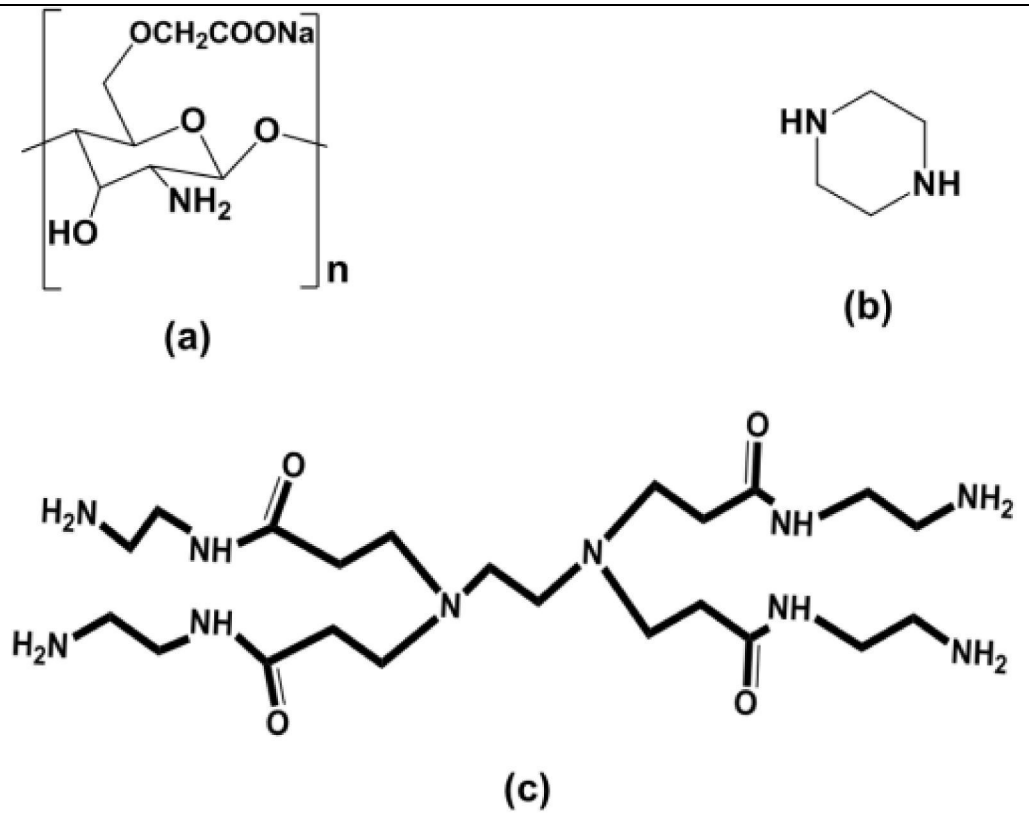

Figure A1.1 Chemical structure of (a) CMC, (b) PZ and (c) PAMAM.

Structure of various fillers used in this study

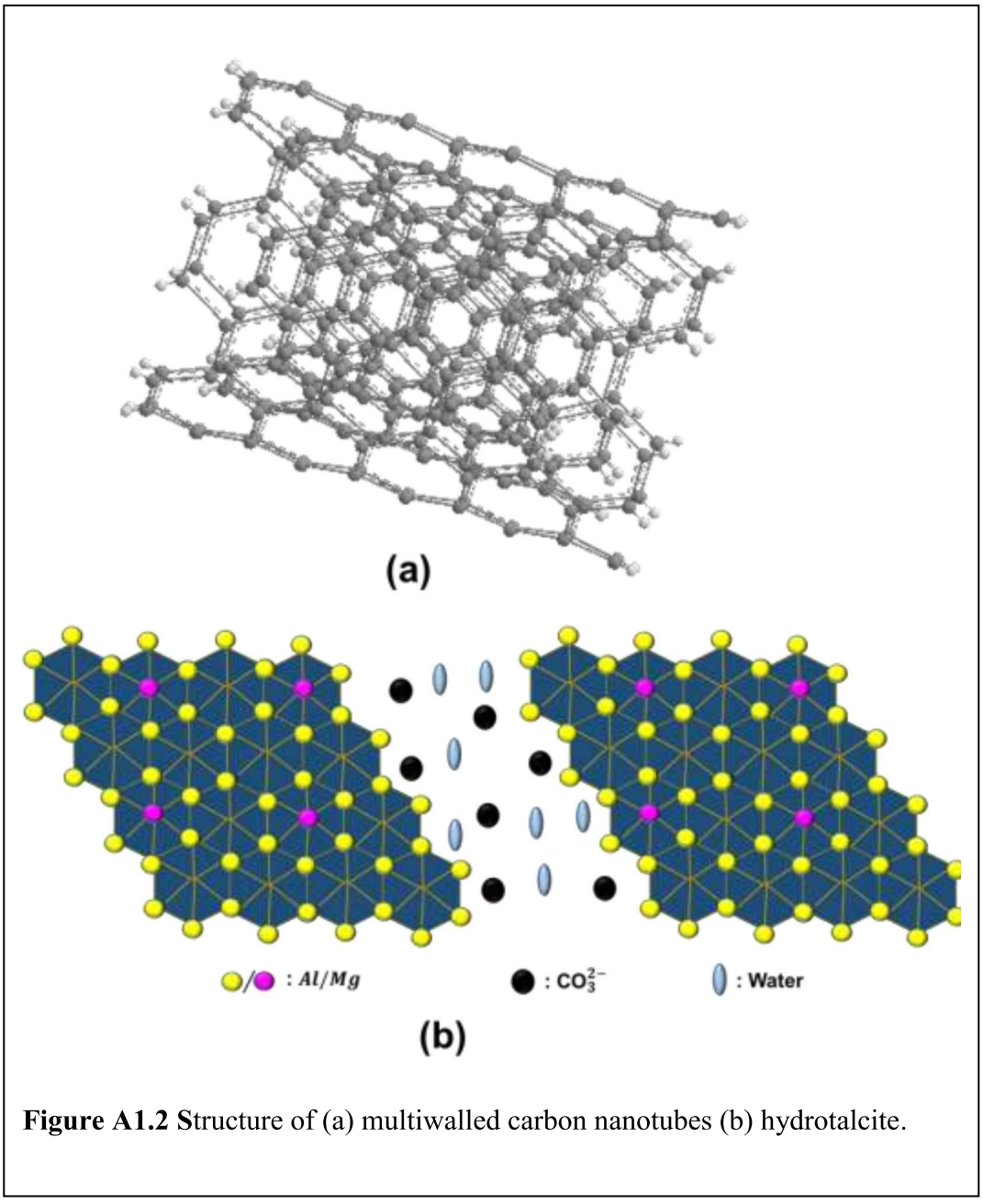

Figure A1.2 Structure of (a) multiwalled carbon nanotubes (b) hydrotalcite.

Appendix 2

A2.1 Gas Transport Parameters Calculation and Gas Chromatography Data

Gas transport parameters (CO_2 and N_2 fluxes, CO_2 and N_2 permeability, CO_2/N_2 selectivity) calculation (The calculation procedure adapted here was originally taken from PhD thesis of Arijit Mondal, reference given at the end of the Appendix**)**

η_R (mol/min) = retentate molar flow rate = $\frac{PV}{RT}$

Where,

P (atmospheric pressure at which the retentate gas is emitting) = 1 atm.

V (volumetric flow rate of mixed gas at retentate side) = 38 cc/min = 38 $\times 10^{-6}$ m^3/min.

T (room temperature at °K) = 298.15 °K.

R (universal gas constant) = 8.205746 × 10^{-5} m^3 atm /°K mol.

$$\boldsymbol{\eta_R}\ \textbf{(Mole/min)} = \frac{1 \times 38 \times 10^{-6}}{8.205746 \times 10^{-5} \times 298.15} = \textbf{1.53} \times \textbf{10}^{-3}\ \textbf{mole /min.}$$

η_{Ar} (Mole/min) = argon (carrier gas) molar flow rate = $\frac{PV}{RT}$

P (atmospheric pressure at which the carrier gas is emitting) = 1 atm

V (volumetric flow rate of carrier gas at permeate side) = 34 cc/min = 34 × 10^{-6} m^3/min.

T (room temperature at °K) = 298.15 °K.

R (universal gas constant) = 8.205746 × 10^{-5} m^3 atm /°K mol.

$$\boldsymbol{\eta_{Ar}}\ \textbf{(mol/min)} = \frac{\mathbf{1 \times 34 \times 10^{-6}}}{\mathbf{8.205746 \times 10^{-5} \times 298.15}} = \textbf{1.37} \times \textbf{10}^{-3}\ \textbf{mol /min.}$$

η_P (mol/min) = permeate molar flow rate =

$$[(CO_2 \text{ mole fraction} \times \frac{CO_2}{CO_2}\frac{(P)_{G.C}}{(F)_{G.C}} + (N_2 \text{ mole fraction} \times \frac{N_2}{N_2}\frac{(P)_{G.C}}{(F)_{G.C}})]$$

$$\times \frac{Ar\ molar\ flow\ rate\ (mol/min)}{[1-(CO_2 \text{ mole fraction} \times \frac{CO_2(P)_{G.C}}{CO_2(F)_{G.C}} - (N_2 \text{ mole fraction} \times \frac{N_2(P)_{G.C}}{N_2(F)_{G.C}})]}$$

Where.

$CO_2(P)_{G.C}$ = CO_2 mole fraction at permeate side from G.C analysis (**Figure A2.1**)

$CO_2(F)_{G.C}$ = CO_2 mole fraction at feed side from G.C analysis (**Figure A2.1**)

$N_2(P)_{G.C}$ = N_2 mole fraction at permeate side from G.C analysis (**Figure A2.1**)

$N_2(F)_{G.C}$ = N_2 mole fraction at feed side from G.C analysis (**Figure A2.1**)

CO_2 mole fraction = 0.2

N_2 mole fraction = 0.8

Ar molar flow rate = 1.37×10^{-3} mol /min.

η_P (mol/min) = permeate molar flow rate = 2.66×10^{-5} mol/min.

p_{CO_2} (R,psi) = CO_2 partial pressure at retentate side =

$$[BP_F \text{ (psig)} + P_{ambient} \text{ (kPa)} \times \frac{14.7}{101.325}] \times$$

$$\frac{[\eta_R - 0.5 \times \eta_P]\ (mol/min) \times CO_2\ mole\ fraction \times [0.5 + 0.5 \times \frac{CO_2(R)_{G.C}}{CO_2(F)_{G.C}}]}{[\eta_R - 0.5 \times \eta_P]\ (mol/min) + \frac{[(0.5 \times H_2O_F) + (0.5 \times H_2O_{distribution} \times (H_2O_F + H_2O_S))]\ (ml/min)}{18\ (ml/mol)}}$$

Where,

BP_F =Back pressure (psig) at feed side of the membrane = 14.7 psig.

$P_{ambient}$ = Ambient pressure (kPa) =101.6 kPa

$CO_2(R)_{G.C}$ = CO_2 mole fraction at retentate side from G.C analysis (**Figure A2.1**)

$CO_2(F)_{G.C}$ = CO_2 mole fraction at feed side from G.C analysis (**Figure A2.1**)

H_2O_F = Feed side water flow rate (ml/min) = 0.03 ml /min

H_2O_S = Sweep side water flow rate (ml/min) = 0.05 ml/min

$H_2O_{distribution}$ = Total water distribution =

$$\frac{\text{Retentate } side\ water\ knockout\ volume}{\text{Retentate } side\ water\ knockout\ volume + Sweep\ side\ water\ knockout\ volume} = 0.3$$

η_R = 1.84×10^{-3} mole /min

η_P = 7.65×10^{-5} mol/min

CO_2 mole fraction = 0.2

p_{CO_2} (R,psi) = CO_2 partial pressure at retentate side = 3.04 psi

p_{CO_2} (P, psi) = CO_2 partial pressure at permeate side =

$$[BP_S\,(psig) + P_{ambient}\,(kPa) \times \frac{14.7}{101.325}] \times \frac{[(\eta_{Ar} + 0.5 \times \eta_P)(mol/min) \times CO_2\ mole\ fraction \times 0.5 \times \frac{CO_2(P)_{G.C}}{CO_2(F)_{G.C}}]}{[\eta_{Ar} + 0.5 \times \eta_P](mol/min) + \frac{[(0.5 \times H_2O_S) + (0.5 \times (1 - H_2O_{distribution}) \times (H_2O_F + H_2O_S))]\,(ml/min)}{18\ (ml/mol)}}$$

BP_S = Back pressure at Sweep side of the membrane module = 4 psig.

$P_{ambient}$ = Ambient pressure (kPa) =101.6 k Pa

$CO_2(P)_{G.C}$ = CO_2 mole fraction at permeate side from G.C analysis (**Figure A2.1**)

$CO_2(R)_{G.C}$ = CO_2 mole fraction at feed side from G.C analysis (**Figure A2.1**)

H_2O_F = Feed side water flow rate (ml/min) = 0.03 ml /min

H_2O_S = Sweep side water flow rate (ml/min) = 0.05 ml/min

$H_2O_{distribution}$ = Total water distribution = 0.3

η_{Ar} = 1.53 × 10^{-3} mole /min

η_P = 2.66 × 10^{-5} mol/min

CO_2 mole fraction = 0.2

p_{CO_2} (P,psi) = CO_2 partial pressure at permeate side = 0.14 psi

p_{N_2}(R,psi) = N_2 partial pressure at retentate side =

$$[BP_F\,(psig) + P_{ambient}\,(kPa) \times \frac{14.7}{101.325}] \times$$

$$\times \frac{[\eta_R - 0.5 \times \eta_P]\,(mol/min) \times N_2\ mole\ fraction \times [0.5 + 0.5 \times \frac{N_2(R)_{G.C}}{N_2(F)_{G.C}}]}{[\eta_R - 0.5 \times \eta_P]\,(mol/min) + \frac{[(0.5 \times H_2O_F) + (0.5 \times H_2O_{distribution} \times (H_2O_F + H_2O_S))]\,(ml/min)}{18\,(ml/mol)}}$$

Where,

BP_F = Back pressure (psig) at feed side of the membrane module = 14.7 psig

$P_{ambient}$ = Ambient pressure (kPa) =101.6kPa

$N_2(R)_{G.C}$ = N_2 mole fraction at retentate side from G.C analysis (**Figure A2.1**)

$N_2(F)_{G.C}$= N_2 mole fraction at feed side from G.C analysis (**Figure A2.1**)

H_2O_F = Feed side water flow rate (ml/min) = 0.03 ml/min

H_2O_S = Sweep side water flow rate (ml/min) = 0.05 ml/min

$H_2O_{distribution}$= Total water distribution = 0.3

Molecular weight of water = 18 g/mol = 18 ml/min (if density of water is 1)

η_{Ar} = 1.37 × 10^{-3} mole /min

η_P = 2.66 × 10^{-5} mol/min

N_2 mole fraction = 0.8

p_{N_2}(R,psi) = N_2 partial pressure at retentate side = 13.6 psi

p_{N_2}(P,psi) = N_2 partial pressure at permeate side =

$$[\mathrm{BP_S\,(psig)} + \mathrm{P_{ambient}\,(kPa)} \times \frac{14.7}{101.325}\,] \times$$

$$\frac{[\eta_{Ar} + 0.5 \times \eta_P](mol/min) \times N_2\ mole\ fraction \times 0.5 \times \frac{N_2(P)_{G.C}}{N_2(F)_{G.C}}\,]}{[\eta_{Ar} + 0.5 \times \eta_P](mol/min) + \frac{[(0.5 \times H_2O_S) + (0.5 \times (1 - H_2O_{distribution}) \times (H_2O_F + H_2O_S))]\,(ml/min)}{18\,(ml/mol)}}$$

Where,

BP_S = Back pressure (psig) at sweep side of the membrane module = 4 psig

$P_{ambient}$ = Ambient pressure (kPa) =101.6kPa

$N_2(P)_{G.C}$ = N_2 mole fraction at permeate side from G.C analysis (**Figure A2.1**)

$N_2(F)_{G.C}$ = N_2 mole fraction at feed side from G.C analysis (**Figure A2.1**)

H_2O_F = Feed side water flow rate (ml/min) = 0.03 ml/min

H_2O_S = Sweep side water flow rate (ml/min) = 0.05 ml/min

$H_2O_{distribution}$ = Total water distribution = 0.3

η_{Ar} = 1.37×10^{-3} mol /min

η_P = 2.66×10^{-5} mol/min

N_2 mole fraction = 0.8

p_{N_2}(P,psi)= **N_2 partial pressure at permeate side = 0.0027 psi**

Volumetric flow rates calculations:

V_{CO_2}(cm^3/sec) = permeate side volumetric flow rate of CO_2 at STP =

$$\frac{\eta_{Ar} \times CO_2(P)_{G.C} \times CO_2\ mole\ fraction \times 8.314 \times 273.15 \times 1000000}{CO_2(F)_{G.C} \times 101325 \times 60 \times [1 - (CO_2\ mol\ fraction \times \frac{CO_2(P)_{G.C}}{CO_2(F)_{G.C}}) - (N_2\ mol\ fraction \times \frac{N_2(P)_{G.C}}{N_2(F)_{G.C}})]}$$

$V_{CO_2}(cm^3/sec)$ = permeate volumetric gas flow rate of CO_2 = 9.62×10^{-03} cm^3/sec

$V_{N_2}(cm^3/sec)$ = permeate volumetric gas flow rate of N_2= $$\frac{\eta_{Ar} \times N_2(P)_{G.C} \times N_2\ mole\ fraction \times 8.314 \times 273.15 \times 1000000}{N_2(F)_{G.C} \times 101325 \times 60 \times [1 - (CO_2\ mol\ fraction \times \frac{CO_2(P)_{G.C}}{CO_2(F)_{G.C}}) - (N_2\ mol\ fraction \times \frac{N_2(P)_{G.C}}{N_2(F)_{G.C}})]}$$

V_{N_2}(cm^3/sec) = permeate volumetric gas flow rate of N_2= 3.13 ×10^{-04}cm^3/sec

CO_2 Flux (10^{-6} cm^3(STP)/cm^{2}sec), CO_2 Permeability (Barrer), CO_2 Permeance (GPU) and CO_2/NO_2 Selectivity

$(\Delta p)_{CO_2}$ at psi = partial pressure difference at psi = p_{CO_2}(R, psi) - p_{CO_2} (P, psi)

$(\Delta p)_{CO_2}$ at psi = 2.91 psi

$(\Delta p)_{CO_2}$ at cmHg = partial pressure difference at cm Hg = $\frac{(\Delta p)_{CO_2}\ \text{at psi}}{14.7} \times 76$

$(\Delta p)_{CO_2}$ = 15.04 cm Hg

CO_2 flux = $\frac{V_{CO_2}\ cm^3/sec}{\text{area of membrane } (cm^2)}$

Where,

V_{CO_2} (cm^3/sec) = **9.62×10^{-03}** (cm^3/sec)

Area of membrane = 7.5 cm^2

CO_2 flux = 1282 × 10^{-6} cm^3 (STP)/cm^{2}s

CO_2 permeability = $\frac{V_{CO_2}\ (cm^3/sec) \times \text{thickness(cm)}}{\text{area of membrane } (cm^2) \times (\Delta p)_{CO_2}\ \text{at cm Hg}}$

Where,

V_{CO_2} (cm^3/sec) = **2.80 × 10^{-2}** cm^3/sec

Area of membrane = 7.5cm^2

Thickness = 0.00026 cm = 2.6 micron

$(\Delta p)_{CO_2}$ at cm Hg = 15.04 cm Hg

CO_2 Permeability = ~221.7 × 10^{-10} cm^3 (STP) cm/cm^2s cmHg = 222 Barrer

CO_2 permeance = $\frac{CO_2 \text{ Permeability}}{thickness} = \frac{222\ (Barrer)}{2.6}$ = ~ 85 GPU

1 GPU = 10^{-6} cm^3 (STP)/cm^2s cmHg

$\frac{CO_2}{N_2}$ Selectivity = $\frac{\frac{CO_2\ (P)_{G.C.}}{N_2\ (P)_{G.C.}}}{\frac{CO_2\ (R)_{G.C.}}{N_2\ (R)_{G.C.}}} = \frac{\frac{0.0186}{0.0006}}{\frac{0.1981}{0.8096}}$ = ~ 126

N_2 Flux (10^{-6} cm^3 (STP)/cm^2sec), N_2 Permeability (Barrer), and N_2 Permeance (GPU).

$(\Delta p)_{N_2}$ (psi) = partial pressure difference at psi = p_{N_2}(R, psi) - p_{N_2} (P, psi)

$(\Delta p)_{CO_2}$ (psi) = 12.042 psi

$(\Delta p)_{N_2}$ (cm Hg) = partial pressure difference at cm Hg = $\frac{(\Delta p)_{N_2} \text{at psi}}{14.7}$ × 76

$(\Delta p)_{N_2}$ = 62.25 cm Hg

N_2 flux = $\frac{V_{N_2}\ (cm^3/\text{sec})}{area\ of\ membrane\ (cm^2)}$

V_{N_2} (cm^3/sec) = 3.13 ×10^{-04} (cm^3/sec)

Area of membrane = 7.5 cm^2

N_2 flux = ~ 41.78 × 10^{-6} cm^3(STP)/cm^2s

N_2 permeability = $\frac{V_{N_2}\ (cm^3/\text{sec}) \times \text{thickness(cm)}}{\text{area of membrane } (cm^2) \times (\Delta p)_{N_2} \text{ at cm Hg}}$

Where

V_{N_2} (cm^3/sec) = 3.13 × 10^{-04} (cm^3/sec)

Area of membrane = 7.5 cm^2

Thickness = 0.00026cm = 2.6 micron

$(\Delta p)_{N_2}$ at cm Hg = 62.258 cm Hg

N_2 Permeability = 1.7 × 10^{-10} cm^3 (STP) cm/cm^2s cmHg = 1.7 Barrer

N_2 permeance = $\frac{N_2 \text{ Permeability}}{\text{thickness}} = \frac{1.7}{2.6}$ = **0.67 GPU**

1 GPU = 10^{-6} cm^3(STP)/cm^2s cmHg

A2.2 Gas Chromatography Operating Protocol

Here, we have used Varian-450 G.C for all the permeation experiments. The detail G.C operating protocols are mentioned below:

Injector programing: Heater (ON) at 120 °C

Tine (min)	**Split state**	**Split ratio**
Initial	ON	1
0.00	ON	1
1.00	ON	1

Oven programing:

Column oven (ON) and Rear oven (ON) at 100 °C

Rate (°C /**min**)	**Temperature** (°C)	**Time (min)**	**Total time (min)**
Initial	40	2.00	2.00
10	70	5.00	10.00
			Total time 10.00

Column pneumatics: (pressure program)

Rate (psi/min)	Pressure (psi)	Time (min)	Total time (min)
Initial	15	10.00	10.00
			Total time 10.00

Detector (TCD) programing:

Heater (ON) at 95 °C

Electronics (ON)

Filament temperature at 235 °C

Filament temperature limit at 390 °C

TCD event table

Time (min)	Range	Auto zero	Polarity
Initial	0.05	YES	Negative

Gas sampling valve (GSV) programing:

Time (min)	Gas sampling valve
Initial	Fill
0.02	Inject

A2.3 Detail Purity Percentage of all Calibration Gases

Name	**Purity compositions**
4 % CO_2 + 4 % N_2, balance Argon	CO_2 (99.999 %), N_2 (99.999 %), Ar (99.999 %), H_2O (< 2 ppm) and CO (< 0.5 ppm)
8 % CO_2 + 8 % N_2, balance Argon	CO_2 (99.999 %), N_2 (99.999 %), Ar (99.999 %), H_2O (< 2 ppm) and CO (< 0.5 ppm)
12 % CO_2 + 12 % N_2, balance Argon	CO_2 (99.999 %), N_2 (99.999), Ar (99.999 %), H_2O (< 2 ppm) and CO (< 0.5 ppm)
20 % CO_2, balance N_2	CO_2 (99.999 %), N_2 (99.999 %), H_2O (< 2 ppm) and CO (< 0.5 ppm)
40 % CO_2, balance N_2	CO_2 (99.999 %), N_2 (99.999 %), H_2O (< 2 ppm) and CO (< 0.5 ppm)
Pure CO_2	CO_2 (99.999 %)
Pure N_2	N_2 (99.999 %)

Feed side

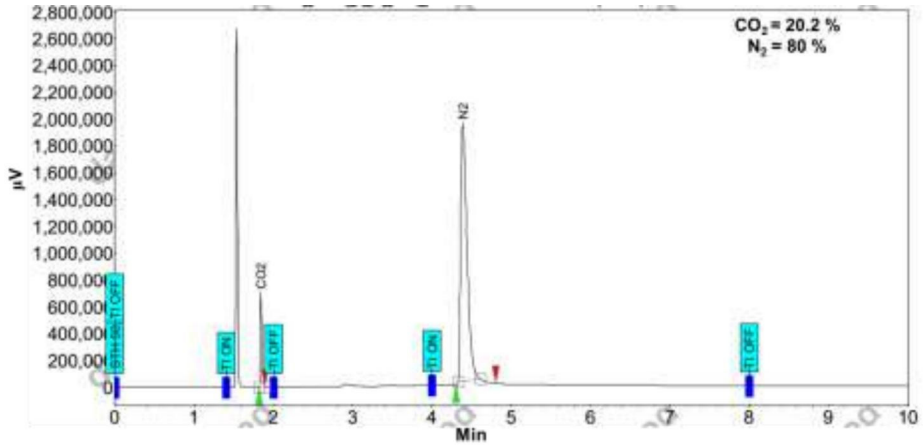

Retentate side

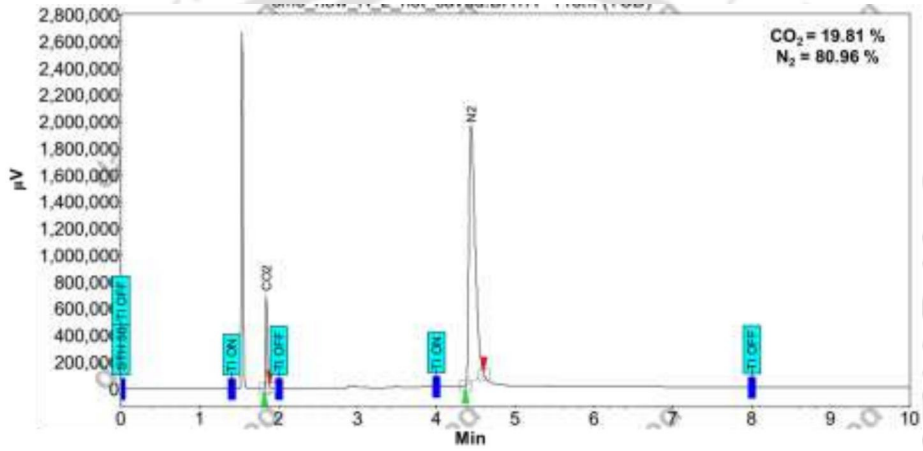

Permeate side

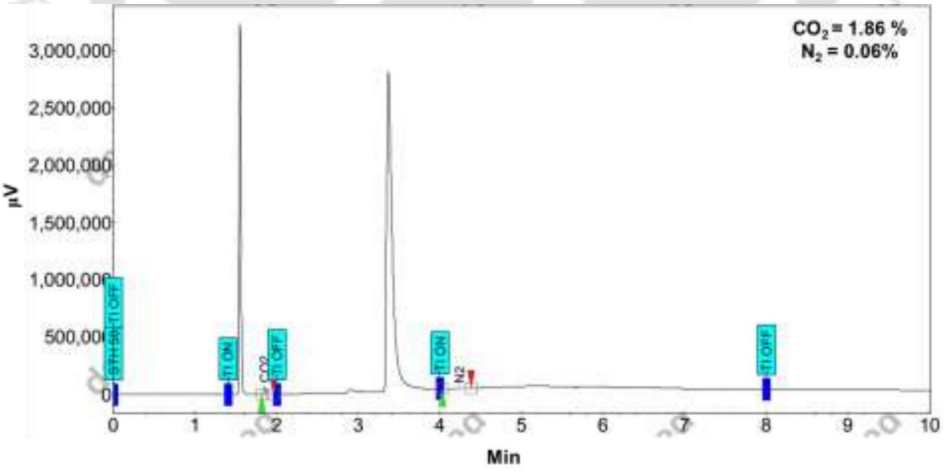

Figure A2.1 GC peaks of PAMAM10 membrane at 80 °C and absolute pressure = 2/1.21 bar (feed/sweep) having sweep/feed water flow ratio of 1.67.

Reference (Appendix 2)

Mondal, A. CO_2-Selective Thin-Film Polymer Composite Membranes: Improvement of Thermal Stability and Role of Amine Carriers. PhD dissertation, Indian Institute of Technology, Guwahati, 2014.

Research Output

Book Chapter

1. B. Prasad, **R. Borgohain**, B. Mandal. Advances in bio-based polymer membranes for CO_2 separation, Advances in Sustainable polymer: Synthesis, Fabrication and Characterization under in the series Materials Horizons: From Nature to Nanomaterials, Editor: V. Katiyar, R. Gupta, T. Ghosh (2019) 277-307 (**Springer India Pvt. Ltd**)

Journal publications

1. R. Borgohain, B. Mandal. "pH Responsive Carboxymethyl Chitosan/Poly (amidoamine) Molecular Gate Membrane for CO_2/N_2 Separation", ACS Applied Materials & Interfaces (2019) 11, 42616-42628 (**ACS – 8.456**).
2. R. Borgohain, Prasad, B., Mandal, B., Synthesis and Characterization of water soluble chitosan membrane for CO_2 separation, Separation and purification technology (2019) 222 (177-187) (**Elsevier-5.107**)
3. R. Borgohain, N. Jain, B. Prasad, B. Mandal, B. Su. "Carboxymethyl chitosan /carbon nanotubes mixed matrix membranes for CO_2 separation", Reactive and Functional Polymers (2019) 143, 104331 (**Elsevier -3.07**)
4. R. Borgohain, B. Mandal. "High-Speed CO_2 Transport Channel Containing Carboxymethyl Chitosan /Hydrotalcite Membrane for CO_2 Separation", Journal of Applied Polymer Science (2019) 137, 48715 (**Wiley – 2.18**).
5. R. Borgohain, B. Mandal. "Thermally Stable and Moisture Responsive Carboxymethyl Chitosan/Dendrimer/Hydrotalcite Membrane for CO_2 Separation", Journal of Membrane Science(2020) (**Elsevier – 7.015**) (Minor revision received on 13/03/2020)
6. R. Borgohain, U. Pattnaik, B. Prasad, B. Mandal. "Chitosan- Based Membranes for Sustainable CO_2 Separation applications: Structure- Property Relationships, Issues, and the way Forward ", Energy & Environmental Science (2020) (**RSC- 33.2**) (Communicated)

Conference proceedings

1. R. Borgohain, B. Prasad, M. Barooah, B. Mandal, (2016) cellulose acetate/ carbon nanotube mixed matrix membrane for CO_2 separation, ASP 2016, GIFU, Japan, December (2016) (**Poster**).

2. R. Borgohain, P. Madu, B. Mandal, Cellulose Acetate/diethyl amine Functionalized Carbon Nanotube Mixed Matrix Membrane for CO_2 Separation. NCWECCS 2017, National Institute of Technology Rourkela, August 3-5 (2017) (**Oral**).

3. R. Borgohain, B. Prasad, B. Mandal. Chitosan/ Carbon Nanotube Mixed Matrix Membrane for CO_2 Separation, Chemcon 2017, Haldia Institute of Technology, December (2017) (**Oral**).

4. R. Borgohain, B. Mandal. Carboxymethyl chitosan mixed matrix membrane for CO_2 separation, Research conclave, Indian Institute of Technology Guwahati, March (2018) (**Poster**).

5. R. Borgohain, B. Prasad, B. Mandal. Amine functionalized zinc oxide based mixed matrix membrane for CO_2 separation, Conference on Carbon Capture, Storage and Re-use in India, Indian Institute of Technology Bombay, October (2018) (**Poster**).

6. R. Borgohain, B. Mandal. Enhanced CO_2 separation by carboxymethyl chitosan mixed matrix membrane, Conference on Carbon Capture and Its Utilization, National Chemical Laboratory Pune, December (2018) (**Oral**).

7. R. Borgohain, P. Das, B. Mandal. Metal Organic Framework Incorporated Water Swellable Polymer Membrane for Enhanced CO_2 Separation, 1st Euro Asia Conference on Carbon capture and Utilisation, Sunway University, Malaysia, August (2019) (**Oral**).

Awards and Achievements

1. **Best poster presentation (3rd position)**, *The Indian Chemical Engineering Congress (CHEMCON 2016)*, Dec. 27-30, 2016, Anna University, Chennai, India.

2. **Best oral presentation,** *1st Euro Asia Conference on Carbon capture and Utilisation*, August 6-7, 2019, Sunway University, Malaysia.

Front Page of the Papers Published in Various Reputed International Journals

JOURNAL OF Applied Polymer SCIENCE

High-speed CO_2 transport channel containing carboxymethyl chitosan/hydrotalcite membrane for CO_2 separation

Rajashree Borgohain, Bishnupada Mandal
Department of Chemical Engineering, Indian Institute of Technology Guwahati, Guwahati, Assam 781039, India
Correspondence to: B. Mandal (E-mail: bpmandal@iitg.ac.in)

ABSTRACT: A comprehensive understanding of carboxymethyl chitosan (CMC)-based mixed matrix membrane (MMM) has been critically investigated. The present work elaborates the compatibility of hydrotalcite (HT) and CMC in terms of CO_2 separation application. Various spectroscopic and microscopic techniques have been utilized to characterize the respective properties of the prepared membrane. The temperature stability and moisture retention behavior of the membrane recognized itself as the flue gas separation membrane. The CO_2/N_2 separation experiment was performed on the MMM at different temperature (60–110 °C) and sweep/feed water flow to the saturator ratio (0.33 to 3). The membrane exhibited the optimum CO_2 permeance of 70 GPU at 90°C pertaining to water flow ratio of 2.33 (sweep/feed). The CO_2/N_2 selectivity observed at that same operating condition was 13. © 2019 Wiley Periodicals, Inc. J. Appl. Polym. Sci. **2019**, *137*, 48715.

KEYWORDS: carboxymethyl chitosan; CO_2 separation; hydrotalcite

Received 10 July 2019; accepted 22 October 2019
DOI: 10.1002/app.48715

INTRODUCTION

The advancements in the field of membrane technology are leading the researchers toward an economic CO_2 capture approach. However, the polymeric and inorganic membranes individually are not able to meet the demand. Therefore, another category of membrane called mixed matrix membrane (MMM) is studied, which possesses both the properties of polymeric and inorganic materials.[1,2] Extensive works have been performed on MMMs using various nanosheets, nanotubes, and nanoparticles.[3–9] Hydrotalcite (HT) has been found to excel in terms of efficient CO_2 capture ability due to carrier availability and memory effect characteristic.[8,10,11] HT is a layered double hydroxide (LDH) with the ideal formula $[M^{2+}_{(1-x)}M^{3+}_{x}(OH)_2]^{x+}(A_{x/n})^{n-}\cdot yH_2O$; where M^{2+} and M^{3+} are the octahedrally coordinated cations, A^{n-} is the counter anion residing in the interlayer space of the hydroxide layers and $0.25 < x < 0.44$.[12] Various works have been accomplished in the field of CO_2 capture, utilizing different layered double hydroxides.[13,14] Most of these works are based on the adsorption technology.[15–17] The limitations offered by the adsorption technology encouraged researchers to move toward membrane-based separation. In this context, some remarkable works can be cited, which have been performed by loading layered doubled hydroxides in membrane matrix.[11,18] The hydrated carbonate anions sailing in the interlayer of HT as shown in Figure 1(a) works as the carrier for CO_2 facilitation, which can be described by the following reaction.[19]

$$CO_2 + CO_3^{2-} + H_2O \rightleftharpoons 2HCO_3^-$$

Meanwhile, the incorporation of HT may interrupt the polymer chain coiling, thus increasing the free volume for higher gas permeability. In this perspective, the CO_2 separation experiment performed on Poly(polyetheramine-hydrotalcite-trimesoyl chloride)/polysulfone (poly[PEA-HT-TMC]/PS) can be cited.[20] The poly (PEA-HT-TMC)/PS composite membrane showed CO_2 permeance of 90 GPU and the CO_2/N_2 selectivity of 40 at 1 bar when the HT concentration was 0.25 wt%. This membrane was formed by the crosslinking reaction between PEA and TMC. Generally, the chemical crosslinking methods are considered to be time consuming and complex process.[21] Therefore, it is very necessary to identify a compatible polymer matrix for the development of a MMM. Carboxymethyl chitosan (CMC), a water-soluble derivative of chitosan is one of the versatile polymers, which has been widely accepted as the matrix for MMMs as it comprises of ample carboxyl, hydroxyl, and amine groups in the skeletal [Figure 1(b)], which offers possible sites for metal ion interaction.[22–24] CMC already has attracted a large number of researchers from the field of biomedical application due to its exceptional physical and chemical properties.[25–27] Lately, CMC has been proven to be an effective CO_2 selective membrane as experimented in our previous work.[28] In addition, as an anionic biopolymer, CMC may be intercalated into the HT interlayer as a

Additional Supporting Information may be found in the online version of this article.

ACS APPLIED MATERIALS & INTERFACES

Research Article

Cite This: ACS Appl. Mater. Interfaces 2019, 11, 42616−42628

www.acsami.org

pH Responsive Carboxymethyl Chitosan/Poly(amidoamine) Molecular Gate Membrane for CO_2/N_2 Separation

Rajashree Borgohain and Bishnupada Mandal*

Department of Chemical Engineering, Indian Institute of Technology, Guwahati India, 781039

Supporting Information

ABSTRACT: Efficient carbon dioxide separation is an emerging field of interest in the era of energy scarcity and environmental calamity. The present study focuses on the versatile aspects of carboxymethyl chitosan and dendrimer in terms of CO_2 separation. A comprehensive study has been accomplished to inspect the physicochemical properties of the prepared membrane. The mixed gas (CO_2/N_2) separation performances have been measured varying the temperature (60−110 °C) and sweep/feedwater flow ratio (0.33−3). The blend membrane containing 10 weight (wt.)% dendrimer presented highest CO_2 permeance of ∼100 GPU and CO_2/N_2 selectivity ∼149 on maintenance of sweep/feedwater flow ratio 2.33 and 1.67, respectively, at an operating temperature of 90 °C. The remarkable performance displayed by the membrane has been explained with reference to the dendrimer molecular gate mechanism and the salting out effect offered by carboxymethyl chitosan matrix.

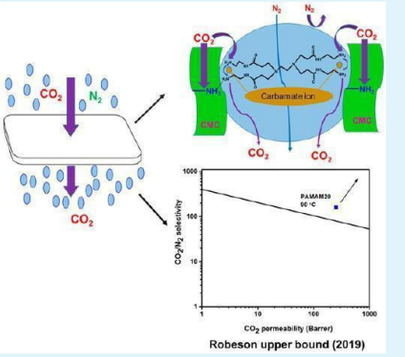

KEYWORDS: *carboxymethyl chitosan, membranes, CO_2 separation, dendrimer, facilitated transport*

1. INTRODUCTION

The membrane based CO_2 capture technology has extensively fascinated researchers. This is due to its reasonable capital and operational budget, energy efficiency, operational ease, consistency, compactness, and most importantly, environmental safety.[1−6] Based on different applications, the matrix materials have been chosen from ceramic, polymeric, and mixed matrix groups. The flexibility offered by the polymeric membranes extends its practice over other membranes. Most of the CO_2 transport polymeric membranes follow either solution−diffusion or facilitated transport mechanism. In postcombustion CO_2 capture, the solution−diffusion mechanism exhibits reduced performance due to low CO_2 partial pressure in flue gas and alteration in membrane structure because of plasticization by water vapor.[7−9] These membranes show low selectivity governed by Robeson's upper bound, suffering a trade-off between permeability and selectivity.[10−13] To overcome these limitations, researchers welcomed facilitated transport membranes as they offer improved CO_2 performance beyond the upper bound limit.[14] Facilitated transport membranes are described by the selective and reversible reaction of CO_2,[10] with the reactive carriers forming complexes, which facilitate the transport of CO_2 through the membrane. These carriers can be either mobile or fixed. Mobile carriers react with CO_2 on the upstream side, forming complexes which freely move through the membrane, releasing CO_2 on the downstream side. Although they offer high separation performance, they lack stability due to carrier loss and degradation.[15−17] The use of fixed carriers, which are covalently bonded to the membrane polymer chains, thereby having limited mobility around the equilibrium position, overcomes these problems.[18,19] CO_2 reacts with the fixed carrier forming the complex, from which it hops to the adjacent carrier along the direction of the driving force to the downstream side, where it is released.[20,21]

Recently, a number of fixed carriers containing polymeric membranes have been studied, aiming for CO_2 separation. Chitosan is one of the trending biopolymers which possesses primary amine in its unit structure. Also, its abundance, good film-forming ability, and thermal stability of the membrane without cross-linking draws the attention of scholars.[14,22−25] However, the limited solubility (pH < 6.5) of chitosan and presence of unconverted chitin retained in chitosan adversely affects the gas separation performance.[26,27] Besides, chitosan precipitates upon the addition of amine to the solution. Carboxymethylation of chitosan resolves this inadequacy and presents a water-soluble chitosan derivative, namely, carboxymethylchitosan (CMC) (Figure 1a).[28] CMC is a natural polyelectrolyte which becomes positive under acidic conditions, balanced in neutral conditions, and negatively charged in alkaline medium.[29−31] The inherent primary amines and water retention ability of CMC membrane directly take part in amine mediated CO_2 transport. However, the excessive swelling of the membrane may decline the expected CO_2 permeance. Thereby, the addition of external amines has been encouraged to acquire improved CO_2 selectivity over other gases. Lately, the addition of dendrimers as a carrier for CO_2 facilitation proves to be a potential method to enhance the

Received: August 21, 2019
Accepted: October 21, 2019
Published: October 21, 2019

Separation and Purification Technology 222 (2019) 177–187

Contents lists available at ScienceDirect

Separation and Purification Technology

journal homepage: www.elsevier.com/locate/seppur

Synthesis and characterization of water-soluble chitosan membrane blended with a mobile carrier for CO_2 separation

Rajashree Borgohain, Babul Prasad, Bishnupada Mandal*

Department of Chemical Engineering, Indian Institute of Technology Guwahati, Guwahati 781039, India

ARTICLE INFO

Keywords:
Carboxymethyl chitosan
Membranes
CO_2 separation
Piperazine

ABSTRACT

The present study demonstrates the alteration of chitosan to carboxymethyl chitosan (CMC). Further, this CMC has been blended with a mobile carrier, piperazine (PZ), to prepare a membrane for CO_2 separation. Various instruments like nuclear magnetic resonance spectroscopy (NMR), X-ray photoelectron spectroscopy (XPS), Fourier transform infrared spectroscopy (FTIR), thermo gravimetric analysis (TGA) and field emission scanning electron microscopy (FESEM) have been used to characterize the prepared membranes. The moisture holding behavior of the membranes at different relative humidity has been assessed by water retention test. The CO_2 separation study was executed at different temperatures (60–120 °C) and sweep side water flow rate (0.01–0.09 ml/min). The blend membrane containing 20 wt (wt.) % PZ exhibited optimum CO_2 permeance of 89 GPU and CO_2/N_2 selectivity of 103 at 80 °C and sweep side water flow rate of 0.05 ml/min.

1. Introduction

The global warming problem seems to be a matter of great concern due to the continuous escalation of CO_2 in the atmosphere [1]. There are various natural and anthropogenic sources responsible for the CO_2 emission of which power plants contribute a major share of CO_2 emission in the atmosphere [2]. The absorption, adsorption, cryogenic distillation and membrane technology have been used to reduce CO_2 [3–6]. Amongst all, CO_2 separation via membranes look promising due to its operational simplicity, easy handling, low cost and corrosion free nature [7]. The membranes used to isolate CO_2 either follow the solution-diffusion mechanism or facilitated transport mechanism [8]. After the desulfurization step the flue gas retains 10–15% of CO_2 along with N_2 on wet basis [9]. Although, both the gases have similar kinetic diameters (CO_2 = 0.330 nm and N_2 = 0.364 nm), CO_2 possess an electron-deficient carbon atom which is favorable for interactions with electronegative species [10]. This leads to strong acid-base interactions that conduces facilitated transport of CO_2, whereas N_2 is not affected [11]. The membranes following facilitated transport mechanism offers scope for improvement in the CO_2 permeance and selectivity via the reversible reactions between reactive carriers (amine, carbonate and carboxylate) and CO_2 [12]. The carriers responsible for facilitated transport can be categorized as mobile and fixed carriers. The mobile carriers which can freely move across the membrane is a desirable choice for assisting CO_2 facilitation as compared to the fixed carriers with limited mobility around its equilibrium position [13–15]. Mobile carriers like monoethanolamine (MEA), diethanolamine (DEA), ethylenediamine (EDA) etc. were introduced in the CO_2 selective membranes [16–18]. However, these membranes were found to be unstable due to the high volatility of the amines [19]. In contrast, piperazine (PZ) has lower volatility and it acts as amine promoter. Later, Wang et al. studied the effect of EDA and PZ incorporated to polyvinyl amine matrix separately and observed the superior performance of PZ over EDA [20]. They suggested that the presence of two secondary amine groups reduce the crystallinity of these membranes and improves permeation performance.

Other than the carriers, the matrix material also contributes significantly towards CO_2 separation. Various polymer matrices chosen for gas separation activities includes polysulfone, polyethersulfone, cellulose acetate, polyvinyl alcohol, chitosan, polycarbonate, etc. [21–26]. The biopolymer chitosan has recently captivated researchers due to its film-forming ability, temperature stability, and a fixed carrier site to interact with CO_2 [27]. Ito et al. studied on swollen chitosan membrane for CO_2/N_2 separation at room temperature and achieved CO_2 permeance of 35.71 GPU and CO_2/N_2 selectivity of 70 [28]. Further, El-Azami group worked on swollen chitosan membrane varying the temperature from 20 to 150 °C and attained a permeance of 7.4 GPU at 110 °C [29]. However, certain downsides of chitosan limits the application of chitosan as a membrane matrix for CO_2 separation. The chitosan dissolves only in moderately acidic solution (pH < 6.5) and it

* Corresponding author.
E-mail address: bpmandal@iitg.ac.in (B. Mandal).

https://doi.org/10.1016/j.seppur.2019.04.038
Received 5 January 2019; Received in revised form 12 April 2019; Accepted 12 April 2019
Available online 13 April 2019

Reactive and Functional Polymers 143 (2019) 104331

Contents lists available at ScienceDirect

Reactive and Functional Polymers

journal homepage: www.elsevier.com/locate/react

Carboxymethyl chitosan/carbon nanotubes mixed matrix membranes for CO_2 separation

Rajashree Borgohain[a], Nimesh Jain[b], Babul Prasad[c], Bishnupada Mandal[a,*], Baowei Su[d,*]

[a] Department of Chemical Engineering, Indian Institute of Technology, Guwahati 781039, India
[b] Department of Chemical Engineering, Indian Institute of Technology (BHU), Varanasi 221005, India
[c] William G. Lowrie Department of Chemical and Biomolecular Engineering, The Ohio State University, Columbus, OH 43210-1350, USA
[d] Key Laboratory of Marine Chemistry Theory and Technology (Ocean University of China), Ministry of Education, Qingdao 266100, China

ARTICLE INFO

Keywords:
Carboxymethyl chitosan
CO_2 separation
Multiwalled carbon nanotube
Mixed matrix membranes

ABSTRACT

The separation of CO_2 using membranes has grabbed vast attention of researchers in the recent years. In this study, a thermally stable carboxymethyl chitosan (CMC)/multiwalled carbon nanotubes (CNTs) mixed matrix membrane (MMM) has been proposed for separation of CO_2 from CO_2/N_2 gas mixture. Herein, the amine groups present in CMC serve as CO_2 carrier and CNTs provide alternate pathway to the gas molecules. Various spectroscopic and microscopic analyses have been performed to confirm the successful wrapping of CNTs. Further, the prepared mixed matrix membranes were characterized using field emission scanning electron microscopy, atomic force microscopy, X-ray photoelectron spectroscopy and dynamic mechanical analyzer. The wrapping of CNT improves the dispersion of CNT in CMC matrix. The moisture holding ability of the membranes which is essential for the facilitated transport reaction has been measured at different humid conditions. The CMC/CNTs MMM exhibited CO_2 permeance and CO_2/N_2 selectivity of 43 GPU and 45, respectively, at sweep/feed water supply ratio of 3 and at 80 °C temperature.

1. Introduction

Energy consumption is indispensable to the growth of economic development, but at the same time massive use of non-renewable fossil fuels as the primary source of energy contributes largely to the global warming due to the emission of CO_2 [1]. Therefore, the capture of CO_2 is a significant solution to control the global warming and the related environmental deterioration. CO_2-selective membrane technology is preferred over other conventional technologies, i.e. absorption, adsorption or cryogenic distillation, owing to its numerous advantages like minimum energy requirement, less capital investment, and low operational cost [2–5]. However, it is very much desirable to prepare a membrane ensuring both high CO_2 permeance and selectivity [6].

Mixed matrix membranes (MMMs) are the promising membranes having significant potential in gas separation applications [7–10]. Various filler materials such as zeolite, silica nanoparticle, graphene oxide, etc. have been studied so far [11–13]. However, the study of carbon nanotubes (CNTs) (Fig. 1) have been of a special interest [14,15]. CNTs fused in membranes basically provides one-dimensional nano-channels that act as alternate paths for CO_2 transport through membranes [16]. However, the pristine CNTs cannot disperse in polymeric matrix due to hydrophobic nature of the CNT surface. Therefore, functionalization of CNTs is required either by chemical or physical treatment. Chemical treatment process might lead to degradation of the walls of CNTs [17]. The dispersion of CNTs can be improved without chemical treatment through substantial wrapping by polymers such as carboxymethyl chitosan (CMC), which has emulsifying capacity and unique solubility [18]. The CNTs wrapping method not only preserves the inherent sp2 structure of CNTs, but also sustains the electronic structure of CNTs in a nondestructive manner [19]. The CMC wrapped CNTs (CMC-w-CNT) also show homogeneous dispersion in the membrane matrix due to the intermolecular interaction between matrix and the wrapping material [20].

Generally the polar groups of polymer can positively interact with CO_2, providing greater solubility in the membrane [21]. However, these polar groups often cause high polymer cohesion energy and low free volume that restrict the fast transportation of gas molecules across the membrane. The water swellable polymer (WSP) membranes overcome the aforesaid limitation by increasing the free volume [22]. A WSP membrane was prepared using polydopamine (PDA) nano-aggregates

* Corresponding authors.
E-mail addresses: r.borgohain@iitg.ac.in (R. Borgohain), nimesh.jain.che16@iitbhu.ac.in (N. Jain), bpmandal@iitg.ac.in (B. Mandal), subaowei@ouc.edu.cn (B. Su).

https://doi.org/10.1016/j.reactfunctpolym.2019.104331
Received 10 June 2019; Received in revised form 10 July 2019; Accepted 2 August 2019
Available online 05 August 2019
1381-5148/